PNNL-14604

Pacific Northwest
National Laboratory
Operated by Battelle for the
U.S. Department of Energy

2004 Initial Assessments of Closure for the S-SX Tank Farm: Numerical Simulations

Z. F. Zhang
V. L. Freedman
S. R. Waichler
M. D. White

April 2004

Prepared for the U.S. Department of Energy
under Contract DE-AC06-76RL01830

DISCLAIMER

PACIFIC NORTHWEST NATIONAL LABORATORY
operated by
BATTELLE
for the
UNITED STATES DEPARTMENT OF ENERGY
under Contract DE-ACO6-76RLO183O

Printed in the United States of America

Available to DOE and DOE contractors from the
Office of Scientific and Technical Information,
P.O. Box 62, Oak Ridge, TN 37831-0062;
ph: (865) 576-8401
fax: (865) 576-5728
email: reports@adonis.osti.gov

Available to the public from the National Technical Information Service,
U.S. Department of Commerce, 5285 Port Royal Rd., Springfield, VA 22161
ph: (800) 553-6847
fax: (703) 605-6900
email: orders@ntis.fedworld.gov
online ordering: http://www.ntis.gov/ordering.htm

This document was printed on recycled paper.
(8/00)

PNNL-14604

2004 Initial Assessments of Closure for the S-SX Tank Farm: Numerical Simulations

Z. F. Zhang
V. L. Freedman
S. R. Waichler
M. D. White

April 2004

Prepared for
the U.S. Department of Energy
under Contract DE-AC06-76RL01830

Pacific Northwest National Laboratory
Richland, WA 99352

Summary

In support of CH2M HILL Hanford Group, Inc.'s (CHG) preparation of a Field Investigative Report (FIR) for the closure of the Hanford Site Single-Shell Tank (SST) Waste Management Area (WMA) tank farms, a set of numerical simulations of flow and solute transport was executed to investigate potential contaminant source scenarios that may pose long-term risks to groundwater from the closure of the S-SX Tank Farm. This report documents the simulation of seven cases (plus two verification cases) involving two-dimensional cross sections through the S Tank Farm (Tanks S-101, S102, and S-103) and one case for a three-dimensional cross section of the S Tank Farm. Using a unit release scenario at Tank S-103, three types of leaks were simulated. These simulations assessed the effect of leaks during retrieval as well as residual wastes and ancillary equipment after closure. Two transported solutes were considered: uranium-238 (U-238) and technetium-99 (Tc-99). To evaluate the effect of sorption on contaminant transport, six sorption coefficients were simulated for U-238. Overall, simulation results for the S Tank Farm showed that only a small fraction (< 0.4%) of the U-238 with sorption coefficients ≥ 0.6 mL/g migrated from the vadose zone in all of the cases. For the conservative solute, Tc-99, the simulations investigating leaks during retrieval demonstrated the highest peak concentrations and the earliest arrival times due to the high infiltration rate from meteoric recharge before surface barriers were installed. Residual leaks were investigated with different release rate models, including a uniform, advection-dominated, diffusion-dominated, and saltcake (solubility-controlled) release models. Of the four models, peak concentrations were lowest and arrival times latest for the uniform release model due to the lower release rate of the residual tank waste solids. Similar peak concentrations occurred for the advection-dominated and saltcake models due to the higher release rate. For the tank ancillary equipment leak case, the diffusion-dominated release rate model yielded peak concentrations and arrival times that were similar to the majority of the past leak cases for residual tank wastes. Comparisons of the results of the two- and three-dimensional simulations show that the two-dimensional simulation overestimated peak concentrations of the contaminants by a factor of 41.1 for Tc-99 and 36.6 for U-238 with a sorption coefficient of 0.03 mL/g.

Acronyms

ASCII	American Standard Code for Information Interchange
bgs	below ground surface
BTC	Break Through Curve
CA	Composite Analysis
CFEST	Coupled Fluid, Energy, and Solute Transport
CHG	CH2M HILL Hanford Group, Inc.
CR	Configuration report
DOE	The U.S. Department of Energy
DST	Double Shell Tank
EPA	The US Environmental Protection Agency
FIR	Field Investigation Report
FY	Fiscal Year
ILAW	Immobilized Low-Activity Waste
MDP	Modeling Data Package
ORP	Office of River Protection, U.S. Department of Energy
PNNL	Pacific Northwest National Laboratory
PNWD	Pacific Northwest Division
RCRA	Resource Conservation and Recovery Act
RPP	River Protection Project
SGM	Site-Wide Groundwater Model
SPLIB	A Library of Iterative Methods for Sparse Linear Systems
SST	Single-Shell Tank
STOMP	**S**ubsurface **T**ransport **O**ver **M**ultiple **P**hases
TPA	The Tri-Party Agreement
WAC	Washington Administrative Code
WMA	Waste Management Area

Contents

Figures

Tables

1.0 Introduction

The U.S. Department of Energy (DOE) is charged with evaluating the impacts associated with closure of the single shell tanks (SSTs) and double shell tanks (DSTs) at the Hanford tank farms. In keeping with this charge, DOE has begun a series of field investigations at the S-SX Tank Farm in the 200 West Area that was made necessary by the Tri-Party Agreement (TPA) (TPA M-45-98-03) (Ecology et al. 1989). Under the TPA, the SSTs and DSTs are Resource Conservation and Recovery Act (RCRA) hazardous waste management units that will eventually be closed under State Dangerous Waste regulations (WAC 173-303). To evaluate the risks associated with these closure activities, this report documents numerical simulations that investigated the effects closure of S-SX Tank Farm will have on groundwater resources. In these analyses, it is assumed that the S-SX Tank Farm will be closed as a landfill. The potential waste sources include spills, retrieval leaks, and residual tank waste from tanks and tank ancillary equipment.

The modeling approach used in this study at the S-SX Tank Farm is similar to the S-SX field investigation report (FIR) (White et al. 2001), B-BX-BY (Freedman et al. 2002) and C Tank farm modeling reports (Zhang et al. 2003). The specific objectives of the numerical assessment are to quantify the risks posed by tank closure. The assessments of this investigation focus specifically on impacts to groundwater resources (i.e., concentration of contaminants in the groundwater). By providing quantitative comparisons of the different potential contaminant sources, the results from this evaluation may affect current operations or future decisions on retrieval of tank waste and closure of the S-SX Tank Farm.

This report documents initial investigations performed via numerical simulation of contaminant migration beneath the S-SX Tank Farm and the calculation of peak concentrations and arrival times at points of compliance. The report is divided into sections that generally follow the overall simulation procedures. First the objectives are summarized and then the numerical simulations that were executed are listed. Next the process of converting the data provided in the Modeling Data Package (MDP) (Khaleel and Connelly 2003) into input files for the STOMP simulator is described. Much of this discussion relies on the reader having access to the STOMP guide documents and focuses on the correlation between the MDP and STOMP input cards. This is followed by a description of the extent of contamination within the vadose zone, movement of contaminants through the vadose zone to the groundwater, and movement of contaminants through the groundwater to points of compliance.

The principal objective for these investigations was executing the simulations specified in the MDP, using widely accepted, scientifically based computational software and reporting the generated results. To promote an open exchange of scientific knowledge and ideas, the software used in this study will be made available upon request to the U.S. Government and its contractors. To ensure that these simulations can be repeated in the future, the source coding, input files, and output files have been stored in electronic form and are also available to the U.S. Government and its contractors. Although Battelle – Pacific Northwest Division maintains a copyright on the STOMP simulator, the U.S. Government retains a paid-up, non-exclusive, irrevocable worldwide license to reproduce, prepare derivative works, and perform and display publicly by or for the U.S. Government, including the right to distribute to other government contractors. Numerical simulation of contaminant migration through the vadose zone and unconfined aquifer beneath the S-SX Tank Farm required converting information in the MDP into electronic input that could be interpreted by the STOMP simulator, executing the software, and translating the simulation output into graphical form for reporting. This procedure is described in the final section of the report.

1.1 Modeling Approach

The scope and data required to perform the numerical simulations are documented in the MDP (Khaleel and Connelly 2003) provided by CH2M HILL Hanford Group, Inc. The numerical simulations were executed with the STOMP simulator (White and Oostrom 2000, 2004), which modeled the vadose zone as an aqueous-gas porous media system where transport through the gas phase was neglected. All simulations used the infinite dilution assumption for coupling fluid flow and contaminant transport.

Fluid flow within the vadose zone was described using Richard's equation, whereas contaminant transport was described using the conventional advective-dispersive transport equation with an equilibrium linear sorption coefficient (K_d) formulation. Stratigraphic information for the cross sections was based on the studies of Lindsey and Reynolds (2001) and the MDP (Khaleel and Connelly 2003). These cross sections include dipping strata and, when combined with the Polmann (1990) model for anisotropy in relative permeability for unsaturated soils, allow the simulator to model the enhanced spreading at the fine- to coarse-grained interfaces and the increased downslope movement of water along these interfaces.

Modeling parameters used to describe soil-moisture retention, phase relative permeability, saturated hydraulic conductivity (intrinsic permeability), and bulk density (porosity) for individual strata were based on data collected from 200 Area soils (Khaleel and Connelly 2003). For each stratum (soil type) defined on the cross-section stratigraphy, the small-scale laboratory measurements were scaled spatially upward using the Polmann (1990) model to obtain equivalent horizontal and vertical unsaturated hydraulic conductivities as a function of mean tension. This scaling technique yielded a mathematical expression describing macroscopic anisotropy in the unsaturated hydraulic conductivity as a function of mean tension for each stratum. When multiple soil samples were available for a given stratum, arithmetic averaging of van Genuchten parameters (van Genuchten 1980) was used to define the soil-moisture retention function for each stratum. When multiple soil samples were unavailable for a given stratum, data were used from soil samples taken from the same stratum. Hydraulic properties were determined from laboratory measurements of soil moisture retention and unsaturated hydraulic conductivity when available. This approach avoided extrapolating unsaturated hydraulic conductivities (van Genuchten 1980; Mualem 1976) to dry conditions based on a saturated conductivity estimate (Khaleel et al. 1995). To reflect field conditions, laboratory data were corrected for the presence of any gravel fraction in the sediment samples (Khaleel and Relyea 1997).

1.2 Model Application

A steady flow simulation was run to establish flow conditions for the S-SX Tank Farm before the tank farm was in place. Steady flow conditions for the preconstruction period were established using a constant surface recharge of meteoric water and fixing the aquifer flux across the cross section. No solute transport was considered during the steady flow simulations. Transient simulations involved both fluid flow and solute transport and were simulated in two stages. In the first stage, flow and solute transport were simulated while the tanks were still intact. The second stage of the simulation predicted flow and solute transport after tank integrity was lost. The transient simulations started with the flow conditions from the previous simulation and responded to changes in meteoric recharge caused by barrier emplacements and/or tank degradation. Two simulations also considered retrieval leaks. The incoming aquifer water flux remained fixed throughout the transient simulation.

Initial conditions for solute concentrations were based on the source type and assumed lateral extent for U-238 and Tc-99 (Khaleel and Connelly 2003). As specified by the data package, two contaminant species (Tc-99 and U-238) were used to represent a range of constituent mobility in these analyses. A two-dimensional (2-D) west-to-east cross section through the S-SX Tank Farm, traversing three SSTs, was used to model fluid flow and solute transport. Hence, concentrations do not account for spreading or dilution of solutes in the third dimension. To evaluate the averaging scheme to be used in deriving the tank farm fence line contaminant breakthrough curve on the basis of 2-D modeling results, a three-dimensional (3-D) simulation over the full S Tank farm was carried out.

Several potential contaminant sources were considered, including retrieval leaks (spills) and residual tank waste from tanks and tank ancillary equipment. Each source was simulated as a unit inventory release. Unit inventory releases of the contaminants were used for solute transport so that inventories could be scaled eventually to the estimated leak inventory for the S-SX Tank Farm independently of the applied water. All unit releases in the simulations originated from S-103, the tank farthest from the exit boundary. Releases from this tank were considered so that contaminant transport behavior beneath each of the tanks could be analyzed. To test whether contaminant transport originating from other tanks is similar, two verification cases were run that considered unit releases from each of the three tanks in the cross section.

For all of the simulation cases, results from vadose zone-aquifer simulations were then transported using streamtube modeling to its downstream compliance points. The streamtube model is an analytical model with the assumption that the aquifer is homogeneous and the flow is one-dimensional (1-D) while the transport is 3-D. The results from the streamtube model were examined by comparing them with the results of simulations by the Hanford Site-Wide Groundwater Model (SGM). The SGM is a 3-D finite element model based on the Coupled Fluid, Energy, and Solute Transport (CFEST-96) code (Gupta et al. 1987; Gupta 1996).

In keeping with the approach taken for modeling fluid flow, solute transport properties for bulk density, diffusivity, and dispersivity were specified for each stratum. Contaminant mobility was defined through an equilibrium linear sorption coefficient (K_d). Uncertainty remains about the linear sorption coefficient and the applicability of a linear-sorption model for U-238. For example, Kaplan et al. (1996) found that, when uranium was in the form of uranyl, the K_d values were functions of pH and soil moisture content and remained nearly constant in solution concentrations of 3.3 and 100 μg/L. Consequently, Kaplan et al. (1996) concluded that a more complicated sorption model did not necessarily warrant a better performance. As a result, a linear-sorption model was used in S-SX Tank Farm simulations, and a range of linear sorption coefficients was used in the modeling to assess the migration behavior of U-238 (e.g., K_d = 0.01, 0.03, 0.1, 0.3, 0.6, and 1.0 mL/g). There is little doubt, however, that the linear sorption coefficient (K_d) for Tc-99 is close to zero in Hanford sediments. This low K_d, coupled with its long half-life (2.03×10^5 yr), allows Tc-99 to migrate long distances in both the vadose zone and groundwater, posing a threat to groundwater quality for a long time.

2.0 Case Descriptions

The flow and solute transport simulations executed in this report were specified in the MDP (Khaleel and Connelly 2003). This suite of simulations investigated the impacts on groundwater resources from potential contaminant sources, which included retrieval leaks (spills), and residual tank waste from tanks and tank ancillary equipment. Also investigated in this study was the effect of contaminant release rates, sorption, and initial inventory placement and flow dimensionality on solute transport. A 2-D cross section representing a northwest-southeast transect through the S-SX Tank Farm was used for the computational domain for seven cases. No scaling of concentrations and water sources was performed to convert the reported concentrations to an effective concentration in three dimensions. A 3-D simulation was run to determine a conversion factor for concentrations in two dimensions to concentrations in three dimensions. The entire S Tank farm domain was used in the 3-D simulation.

The following simulations were conducted for the cross section that included Tanks S-101, S-102, and S-103:

- Inventory leaks during retrieval using a unit release at Tank S-103 (Cases 1 and 2)
- Residual waste leachates from tanks following closure using a unit release at Tank S-103 (Cases 3-6)
- Residual waste leachates from tank ancillary equipment following closure using a unit release at Tank S-103 (Case 7)

Data from verification simulations were provided to test the principal of superposition with respect to contaminant transport:

- Inventory leaks during retrieval using a unit release at Tanks S-101, S-102 and S-103 (Case 2 verification)
- Residual waste leachates from tanks following closure using a unit release at Tank S-101, S-102 and S-103 (Case 5 verification)

In addition to the seven cases, data from a 3-D flow and transport simulation were provided to determine a dilution factor for converting concentrations in two dimensions to concentrations in three dimensions at the tank farm fence line. As in Case 1, this closure scenario involved inventory leaks during retrieval using a unit release at Tank S-103. The cases are summarized in Table 2.1 and described in Sections 2.1 through 2.7.

2.1 Retrieval Leak (4,000 gallons)

This scenario (Case 1) investigated a retrieval leak of 4,000 gallons that was in the lower-right corner of Tank S-103 and began on the first day of the year 2000. The leak lasted for 14 days and contained a unit release of each of the contaminant species (Tc-99 and U-238). The U-238 contaminant was simulated with six different linear sorption coefficients (K_d = 0.01, 0.03, 0.1, 0.3, 0.6, and 1.0 mL/g).

2.2 Retrieval Leak (8,000 gallons)

This scenario (Case 2) investigated a retrieval leak of 8,000 gallons that was in the lower-right corner of Tank S-103 and began on the first day of the year 2000. The leak lasted 14 days and contained a unit release of each of the contaminant species (Tc-99 and U-238). The U-238 contaminant was simulated with six different linear sorption coefficients (K_d = 0.01, 0.03, 0.1, 0.3, 0.6, and 1.0 mL/g).

Table 2.1. Case Descriptions

Case	Description	Specialized Model	Waste Form Diffusion Coefficient[(a)] (cm^2/s)
1	Retrieval Leaks (4,000 gal)		
2	Retrieval Leaks (8,000 gal)		
3	Residual Tank Wastes (release rate R_0) [(b)]		
4	Residual Tank Wastes	Advection-dominated	
5	Residual Tank Wastes	Diffusion-dominated	6.0×10^{-7}
6	Residual Tank Wastes	Saltcake	
7	Residual Ancillary Equipment Wastes	Diffusion-dominated	6.0×10^{-7}

(a) Refers to diffusion within the waste source, which differs from the molecular diffusion coefficient in pore water.
(b) $R_0 = 10^{-6}$ Ci/yr for 500 yr and 10^{-4} for 9995 yr.

2.3 Residual Tank Waste

This scenario (Case 3) investigated a residual tank waste source with release rate defined as 10^{-6} Ci/yr for 500 years, followed by 10^{-4} Ci/yr for 9,995 years. The release occurred over the bottom width of Tank S-103. The leak began on the first day of the year 2050, the date when tank integrity was lost. This was the only case in which a full unit release of each contaminant species (Tc-99 and U-238) was not simulated. This occurred because the full release was to last 10,495 years. Because the release began in the year 2050, and flow and transport was simulated to the year 12000, 545 years of the planned release did not occur. The U-238 contaminant was simulated with six linear sorption coefficients (K_d = 0.01, 0.03, 0.1, 0.3, 0.6, and 1.0 mL/g).

2.4 Residual Tank Waste (advection dominated)

This scenario (Case 4) investigated a residual tank waste source using an advection-dominated release model. The release occurred over the bottom width of Tank S-103, with a source thickness of 0.825 m. The leak began on the first day of the year 2050, the date when tank integrity was lost. A unit release of each of the contaminant species (Tc-99 and U-238) was simulated. The U-238 contaminant was simulated with six different linear sorption coefficients (K_d = 0.01, 0.03, 0.1, 0.3, 0.6, and 1.0 mL/g).

2.5 Residual Tank Waste (diffusion dominated)

This scenario (Case 5) investigated a residual tank waste source using a diffusion-dominated release model and a diffusion coefficient of 6×10^{-7} cm^2/s. The release occurred over the bottom width of Tank S-103 with a source thickness of 0.825 m. The leak began on the first day of the year 2050, the date tank integrity was lost. Grout was used as tank fill material beginning in the year 2050. A unit release of each of the contaminant species (Tc-99 and U-238) was simulated. The U-238 contaminant was simulated with six different linear sorption coefficients (K_d = 0.01, 0.03, 0.1, 0.3, 0.6, and 1.0 mL/g).

2.6 Residual Tank Waste (saltcake)

This scenario (Case 6) investigated a residual tank waste source using a saltcake release model that assumed an aqueous solubility of 650 g/L for the residual waste. The release occurred over the bottom width of Tank S-103 with a surface area of 453 m^3 and a volume of 10.2 m^3 (360 ft^3). The leak began on the first day in the year 2050, the date when tank integrity was lost. A unit release of each of the contaminant species (Tc-99 and U-238) was simulated. The U-238 contaminant was simulated with six linear sorption coefficients (K_d = 0.01, 0.03, 0.1, 0.3, 0.6, and 1.0 mL/g).

2.7 Residual Ancillary Equipment Waste (diffusion dominated)

This scenario (Case 7) investigated a residual ancillary equipment waste source using a diffusion-dominated release model and a diffusion coefficient of 6×10^{-7} cm^2/s. The waste source originated between Tanks S-103 and S-102 at a depth of 20 ft (6.1 m) below ground surface with an inventory diameter of 24.4 ft (8.0 m). Grout was used as tank fill material. The leak began on the first day of the year 2050, the date when tank integrity was lost. A unit release of each of the contaminant species (Tc-99 and U-238) was simulated. The U-238 contaminant was simulated with six different linear sorption coefficients (K_d = 0.01, 0.03, 0.1, 0.3, 0.6, and 1.0 mL/g).

3.0 Technical Approach

A multistep approach was used to execute the simulations described in the modeling data package (MDP) (Khaleel and Connelly 2003). In brief, the approach involved converting information in the data package to a suite of input files, executing the STOMP simulator, determining solute concentrations at the compliance points using a streamtube model, and translating the simulation results into graphical form. This section provides an overview, followed by a more extensive review of these steps.

3.1 Overview

Two types of input are defined in a STOMP simulation: 1) a simulation control and material definition file, and 2) a soil zonation file. Model input data stored in these files were developed from the modeling data package in conjunction with the discretization of the physical domain. The physical domain was a west-east 2-D cross section through Tanks S-101, S-102, and S-103. The physical domain was discretized using a Cartesian grid with uniform horizontal and vertical spacing of 1 m.

Graphical representations of geologic interpretations and engineered structures in the S-SX Tank Farm subsurface (Khaleel and Connelly 2003, Appendix B) were converted to zonation maps based on the Cartesian discretization of the physical domain. Hydrologic properties, as defined in the MDP, for each of six identified soil types were converted to input in the form of STOMP input cards. Transport property data for the two contaminants and six soil-type combinations were converted to input in the form of STOMP input cards. The conceptual model was then completed by converting boundary conditions and sources, as specified in the MDP, into input in the form of STOMP input cards, specifying execution controls and requesting output data.

Time-varying surface recharge and tank leaks required a transient flow solution to be executed with the solute transport calculations. The transient flow and transport simulations were initiated using a steady flow solution to the boundary value problem using the initial boundary values. This approach neglects time variations in surface recharge prior to the start of simulation. The steady flow initial condition was generated with a simulation to steady flow conditions. The same steady-state flow solution was used for each of the seven cases executed in this work. This represented the preconstruction time period for the S-SX Tank Farm. This simulation did not involve solute transport and was executed as a transient simulation from a uniform initial condition to a steady flow condition that honored the surface recharge and unconfined aquifer flux. The steady flow and transient simulations were executed on a Linux workstation. For compatibility between platforms, the input, zonation, and inventory files were maintained as ASCII formatted files.

The steady flow solution was then used as an initial condition for the seven transient flow and solute transport cases executed in this work. Because in all cases tank integrity was eventually lost, the transient simulations were simulated in two stages. In the first stage, flow and solute transport were simulated while the tanks were still intact. In this stage, nodes representing the tanks were inactive, hence impermeable to flow and transport. In the second stage, once tank integrity was lost, these nodes were converted to active nodes with a material type identical to that surrounding the tanks in the S-SX Tank Farm.

Simulation results were written to three types of output files: 1) a reflected input and reference node file, 2) a series of plot files, and 3) a series of surface-flux files. The reflected input and reference node file contains a translation of the input files as interpreted by the simulator (e.g., with unit conversions) and a time sequence of the simulation history and chosen variables (e.g., aqueous pressure, moisture content, solute concentrations, Darcy fluxes) at selected grid locations. Plot files contain variable data for all grid points at selected simulation times. These files are used to generate color-scaled plots and animations through Tecplot.[(a)] A utility program called *PlotTec* is used to translate STOMP plot files into Tecplot-formatted input files. Surface-flux files contain rate and integral information about fluxes crossing user-defined internal or external boundaries. Solute fluxes and aqueous fluxes at the downgradient domain boundary within the groundwater are used to calculate average solute concentrations and source rates. Surface-flux files are also used to generate rate and integral plots of solutes exiting the computational domain and entering the groundwater. A utility program, *Surfcalc*, was used to translate STOMP surface-flux files into formatted input files suitable for plotting.

Solute breakthrough curves for the aquifer, or solute concentrations as a function of time at the compliance points outside the S-SX Tank Farm, were computed by extrapolating solute concentrations exiting the STOMP computational domain. An analytical solution to the advection-dispersion equation for solute transport through a saturated porous media in three dimensions was used, following the approach described by Baetslé (1969) and documented in Domenico and Schwartz (1990). This approach assumed that the solute originated at a point source as a series of slugs released over time. The method of superposition was used to integrate the slug releases. The solute mass from each slug migrated from the point source by advective-dispersive transport in a steady, uniform flow field. As the solute mass was transported advectively with the flow, it spread longitudinally and transversely via hydrodynamic dispersion and molecular diffusion. The mass flux of solute used as input was computed from the STOMP surface file output for mass flux exiting the 15-m-thick aquifer at the east side of the domain. Aquifer recharge along the groundwater flow path was neglected in translating solute concentrations to the compliance points. To check the analytical groundwater transport results, simulations were run using the 3-D SGM for two cases.

3.2 Modeling Data Package

Meteoric recharge and parameters for vadose zone flow and transport were provided in the MDP. Selected data are repeated in this section.

3.2.1 Recharge Estimates

Portions of the S-SX Tank Farm surfaces are covered with gravel to prevent vegetative growth and provide radiation shielding for site workers. Bare gravel surfaces, however, enhance net infiltration of meteoric water compared with undisturbed, naturally vegetated surfaces. Between tanks, infiltration is further enhanced by the effect of percolating water being diverted by the impermeable sloping surface of the tank domes.

(a) Amtec Engineering, Inc. 2003. Tecplot, Version 10.0. Bellevue, WA.

Recharge rates for all seven cases were varied to represent various stages of tank and barrier construction. For example, the beginning of the simulation represents the tank preconstruction period, and recharge is estimated at 3.5 mm/yr. Once the tanks are in place in the year 1952, recharge rates increase to their current estimate of 100 mm/yr. In the year 2050, a protective barrier is installed at the surface, and the recharge rate estimate decreases to 0.5 mm/yr. The recharge rate is increased again to 3.5 mm/yr when degradation of the barrier occurs in the year 2550. These values are summarized in Table 3.1 (Khaleel and Connelly 2003).

Table 3.1. Recharge Estimates (mm/yr)

Pre-1952	1952–2050	2050–2550	2550–12000
3.5	100.0	0.5	3.5

3.2.2 Vadose Zone Flow and Transport Properties

Upscaled values of parameters for fluid flow and solute transport for the vadose zone were used in these investigations. Details for computing upscaled parameters are provided in Khaleel and Connelly (2003). Fluid flow parameters for the vadose zone include soil moisture retention characteristics and saturated hydraulic conductivity. Solute transport parameters include bulk density, diffusivity, sorption coefficients, and macrodispersivity. Table 3.2 lists the composite, fitted van Genuchten-Mualem parameters (van Genuchten 1980) for various strata at the S-SX Tank Farm. Note that the material type numbers are identical to those indicated in the MDP Section 4.2.

Table 3.2. Composite van Genuchten-Mualem Parameters for Various Strata at the S-SX Tank Farm (Khaleel and Connelly 2003, Appendix C)

Strata/Material Type	Number of Samples	θ_s	θ_r	α 1/cm	n	l	K_s cm/s
Backfill (1)	10	0.1380	0.0100	0.0210	1.3740	0.5	5.60E-04
Sand H2 (2)	12	0.3819	0.0443	0.117	1.6162	0.5	9.88E-05
Gravelly Sand H1 (3)	11	0.2126	0.0032	0.0141	1.3730	0.5	2.62E-04
Plio-Pleistocene (4)	4	0.4349	0.0665	0.0085	1.8512	0.5	2.40E-04
Sandy Gravel (5)	10	0.1380	0.0100	0.0210	1.3740	0.5	2.89E-02
Grout	-	0.5781	0.0	1.05E-5	1.6500	0.5	4.47E-08

3.2.3 Stochastic Model for Macroscopic Anisotropy

Variable tension-dependent anisotropy provides a framework for upscaling small-scale laboratory measurements to the effective (i.e., upscaled) properties for the large-scale tank farm vadose zone. A stochastic model (Polmann 1990) was used to evaluate tension-dependent anisotropy for sediments at the S-SX Tank Farm; details are in Khaleel and Connelly (2003, Appendix D). The following is a brief description of the variable anisotropy model used in this investigation.

Yeh et al. (1985) analyzed steady unsaturated flow through heterogeneous porous media using a stochastic model. Parameters such as hydraulic conductivity were treated as random variables rather than as deterministic quantities. The Gardner (1958) relationship was used by Yeh et al. to describe unsaturated hydraulic conductivity as a function of saturated hydraulic conductivity and tension according to Equation (3.1)

$$K(\psi) = K_s \exp(-\beta\psi) \tag{3.1}$$

where K is the unsaturated hydraulic conductivity, K_s is the saturated hydraulic conductivity, ψ is the tension, and β is a fitting parameter. Equation (3.1) can be written as shown in Equation (3.2). This form is referred to as the log-linear model,

$$\ln K(\psi) = \ln K_s - \beta\psi \tag{3.2}$$

because the log of the hydraulic conductivity is linearly related to the tension through a constant slope, β. A constant slope, however, is often inadequate for describing $\ln K(\psi)$ over the range of tension of interest for field applications. As an alterative, β can be approximated locally by straight lines over a range of tensions. The lnKs term can then be derived by extrapolating the local slopes to zero tension.

Using a linear correlation model between the zero-tension intercept and β, Polmann (1990) presented a generalized model that accounts for the cross-correlation of the local soil property (i.e., $\ln K_s$ and β) residual fluctuations. Compared against the uncorrelated $\ln K_s$ and β model, partial correlation of the properties was shown to have a significant impact on the magnitude of the effective parameters derived from the stochastic theory. The Polmann [1990] equations for deriving the effective parameters are as shown in Equations (3.3) through (3.6)

$$\langle \mathrm{LnK} \rangle = \langle \mathrm{LnK_s} \rangle - A\langle\psi\rangle - \frac{\sigma^2_{\mathrm{LnKs}} \lambda \left[p - p^2 \langle\psi\rangle - \zeta^2 \langle\psi\rangle \right]}{(1 + A\lambda)} \tag{3.3}$$

$$\sigma^2_{\mathrm{LnK}} = \frac{\sigma^2_{\mathrm{LnKs}} \left[(1 - p\langle\psi\rangle)^2 + \zeta^2 \langle\psi\rangle^2 \right]}{(1 + A\lambda)} \tag{3.4}$$

$$K_h^{eq} = \exp\left[\langle \mathrm{LnK} \rangle + \frac{\sigma^2_{\mathrm{LnK}}}{2} \right] \tag{3.5}$$

$$K_v^{eq} = \exp\left[\langle \mathrm{LnK} \rangle - \frac{\sigma^2_{\mathrm{LnK}}}{2} \right] \tag{3.6}$$

where

σ^2_{LnK} = the variance of log unsaturated conductivity

$\langle \psi \rangle$ = the mean tension

σ^2_{LnKs} = the variance of $\ln K_s$

$\langle \mathrm{LnK_s} \rangle$ = the mean of $\ln K_s$

p = the slope of the β versus $\ln K_s$ regression line

$\zeta = \dfrac{\sigma_\delta}{\sigma_{LnKs}}$

σ_δ = the standard deviation of the residuals in the β versus $\ln K_s$ regression

A = the mean slope, β, for $\ln K_s$ versus ψ

λ = the vertical correlation length for $\ln K_s$

K_h^{eq} = the equivalent unsaturated horizontal hydraulic conductivity

K_v^{eq} = the equivalent unsaturated vertical hydraulic conductivity.

Macroscopic anisotropy parameter estimates for the strata at the S-SX WMA are listed in Table 3.3. Details on the derivation of these parameter estimates are included in Khaleel and Connelly (2003, Appendix D).

Table 3.3. Macroscopic Anisotropy Parameters Based on Polmann Equations for Strata at the S-SX Tank Farm (Khaleel and Connelly 2003, Section 4.2)

Strata/Material Type	No. of Samples	$\langle LnK_s \rangle$	σ^2_{LnKs}	p	ζ	λ (cm)	A
Backfill (1)	10	-15.76	3.56	-1.1e-4	1.84e-4	30	0.00371
Sand H2 (2)	12	-14.59	1.50	-7.2e-4	6.55e-4	50	0.00620
Gravelly Sand H1 (3)	11	-14.85	1.94	-2.6e-4	2.50e-4	30	0.00368
Plio-Pleistocene (4)	4	-10.43	1.01	-2.4e-3	9.34e-4	50	0.00104
Sandy Gravel (5)	10	-15.76	3.56	-1.1E-4	1.84E-4	30	0.00371

3.2.4 Bulk Density and Sorption Coefficient

Both bulk density (ρ_b) and the sorption coefficient (K_d) estimates were needed to calculate retardation factors for different solute species. Effective large-scale estimates of bulk density, distribution coefficient, and their product for U-238 for a K_d of 0.6 mL/g are listed in Table 3.4 for the five strata samples.

Table 3.4. Effective Parameter Estimates for the Product of Bulk Density and Retardation Coefficient for U-238 at the S-SX Tank Farm

Strata/Material	K_d (mL/g)	$E[\rho_b]$ (g/mL)
Backfill (1)	0.6	2.13
Sand H2 (2)	0.6	1.76
Gravelly Sand H1 (3)	0.6	1.94
Plio-Pleistocene (4)	0.6	2.13
Sandy Gravel/Ringold (5)	0.6	2.13

The average ρ_b, $E[\rho_b]$ estimates were based on data in Tables D-1a through D-1d of Khaleel and Connelly (2003). The K_d estimates for U-238 were based on Kaplan and Serne (2000) data for undisturbed sediments. The distribution coefficient for Tc-99 was estimated to be zero.

3.2.5 Diffusivity

It was assumed that the effective, large-scale diffusion coefficients for all strata at the S-SX Tank Farm were a function of volumetric moisture content and could be expressed using the Millington and Quirk (1961) empirical relation, as shown in Eq. 3.7:

$$D_e(\theta) = D_o \frac{\theta^{10/3}}{\theta_s^2} \tag{3.7}$$

where D_e is the effective diffusion coefficient of an ionic species, D_o is the molecular diffusion coefficient for the species in water, θ is the water content, and θ_s is the saturated water content. The molecular diffusion coefficient for all species in pore water was assumed to be 2.5×10^{-5} cm^2/s (Kincaid et al. 1995).

3.2.6 Macrodispersivity

Field-scale dispersivities are referred to as macrodispersivities. The heterogeneities that exist at various length scales result in a scale dependence of macrodispersivities. An extended review is provided in Appendix D of Khaleel and Connelly (2003) on the rationale for vadose zone macrodispersivity estimates. Macrodispersivity estimates were needed for both reactive (U-238) and nonreactive (Tc-99) species. Estimates for the nonreactive species are listed in Table 3.5.

The net effect of species sorption is to retard the migration through geologic media. Soil sorption is a function of the species and soil properties and varies spatially with soil properties (Gelhar 1993; Talbott and Gelhar 1994). Stochastic analysis results for macrodispersivity enhancement for the five strata are presented in Appendix D of Khaleel and Connelly (2003) for the reactive species (U-238). In this analysis, the unsaturated hydraulic conductivities were evaluated at a tension of 100 cm via the fitted

Table 3.5. Nonreactive Macrodispersivity Estimates for Strata at the S-SX Tank Farm

Strata/Material	σ^2_{lnK}	Correlation Length λ, cm	A_L, cm	A_T, cm
Backfill (1)	4.54	30	~150	15
Sand H2 (2)	4.60	30	~150	15
Gravelly Sand H1 (3)	3.19	30	~100	10
Plio-Pleistocene (4)	0.92	30	~50	5
Sandy Gravel (5)	4.54	30	~150	15

van Genuchten-Mualem relation. The macrodispersivity enhancement ranged from 1.06 for sandy sediments to about 2.24 for Plio-Pleistocene (silty) sediments. The aquifer thickness in the STOMP simulation was assumed to be 15 m. Other parameters used to characterize are summarized in Table 3.6.

Table 3.6. Cross-Section Aquifer Geometry and Properties

Parameter	Value	Reference
Aquifer Hydraulic Conductivity	25 m/day	MDP (Khaleel and Connelly 2003)
Effective Porosity	0.138	
Hydraulic Gradient	0.0011 m/m	
Aquifer Thickness	15 m	

3.3 STOMP Input File Generation

Two types of input files were used to drive the STOMP simulator: 1) a simulation control file and material definition (input) and 2) a soil zonation file (zonation). All input files were written and stored in ASCII text format. The simulation control and material definition input files were assembled using a conventional text editor, whereas the zonation file was generated with a utility program.

3.3.1 Input File

As described in the STOMP User's Guide (White and Oostrom 2004), the input file is divided into cards that group common data (e.g., solution control, hydraulic properties, output control, boundary conditions). The input files for the simulated cases will be provided in electronic form (see Section 6).

3.3.2 Zonation File

The zonation file is an ordered listing (i.e., I,J,K indexing) of integers that identify the rock/soil type for every grid cell in the computational domain. Inactive nodes are assigned an integer value of zero, and rock/soil types are assigned numbers in accordance with the ordered listing of rock/soil types in the rock/soil zonation card. For example, an integer value of one in the zonation file refers to backfill, and a value of three refers to gravelly sand H1. Zonation files for the executed simulations were generated for the cross section through S-101, S-102, and S-103 of the S Tank Farm, which is shown in Appendix C of the MDP. Color delineated images of the zonation files for the S-SX Tank Farm cross sections are shown in

Figure 3.1. In Figure 3.1a, the preconstruction period for the tank farm is shown. Figure 3.1b shows the post-construction tank farm cross section, where the H1 gravelly sand unit has been replaced with backfill material surrounding the tanks. These files were generated from digitized versions of the geologic cross sections for the S-SX Tank Farm.

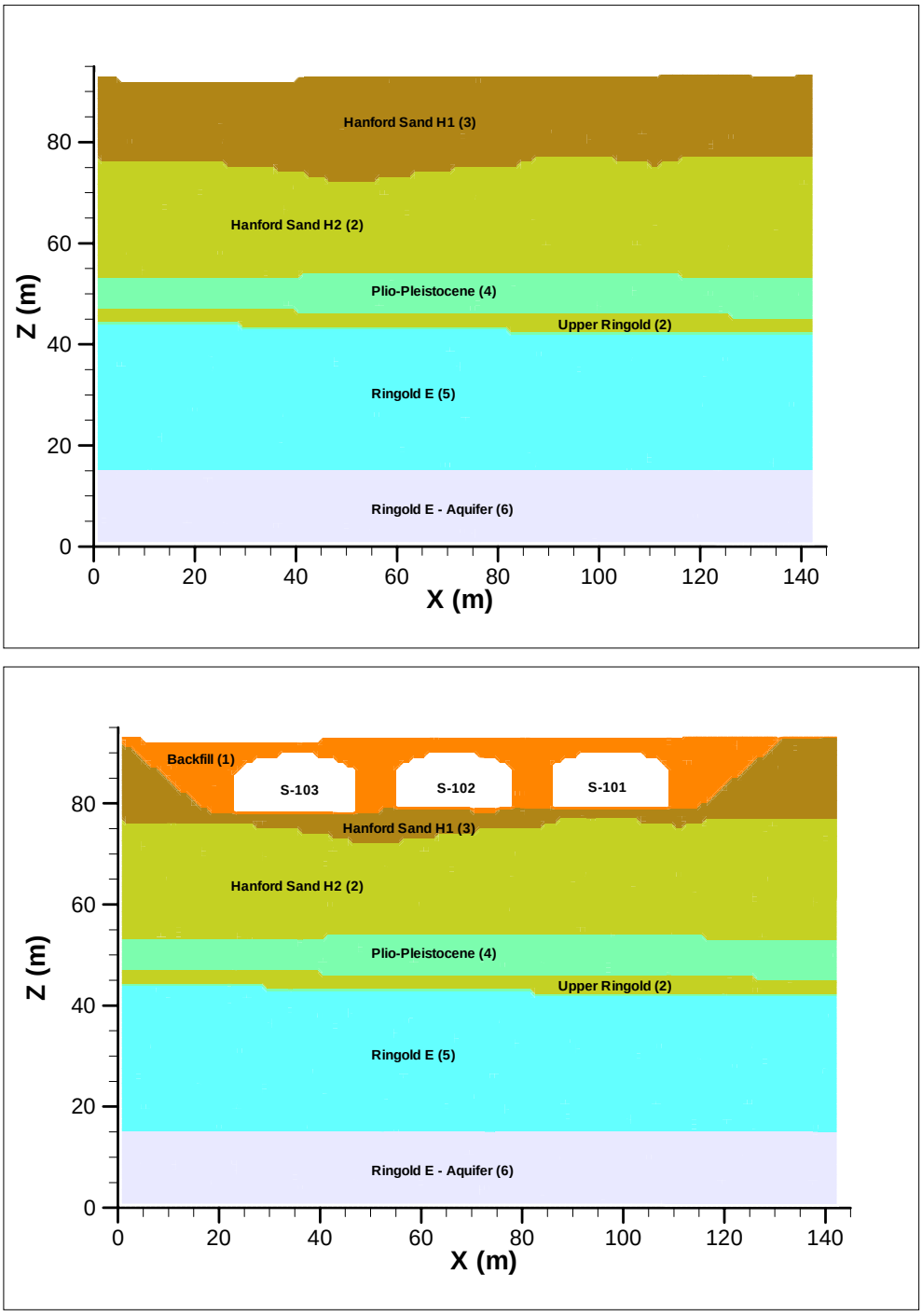

Figure 3.1. Rock/Soil Zonation for the Pre- and Post-Construction Periods of the S-SX Tank Farm

The cross section containing Tanks S-101, S-102 and S-103 (Figure 3.1b) was modeled using a computational domain with a horizontal (west-east) extent of 143 m, a vertical extent of 93 m, and a unit width. From the ground surface, the simulation domain extended vertically to 15 m below the water table. Spacing of 1 m was used for the computational grid in both the horizontal and vertical directions. The 3-D simulation domain had a west-east extent of 144 m, and a vertical extent of 93 m as the 2-D cases. Instead of a unit width, the 3-D domain had a south-north extent of 153 m. Grid resolutions for the 3-D simulations were 3 m in the horizontal and 1 m in the vertical, which is why the 3-D simulation is 1 m longer in the horizontal. The geology is a primarily layered system created by alluvial deposition, with a more permeable gravely sand stratum that forms the foundation for the tank bottoms.

3.4 Implemented Features

For the S-SX field investigation (White et al. 2001), the STOMP simulator, as documented in White and Oostrom (2000, 2004) and Nichols et al. (2000), was modified to extend its capabilities for modeling saturation dependent anisotropy, enhanced macrodispersivity, and specialized Courant number control. These features were also implemented for the S-SX Tank Farm simulations. For a detailed description of these features, refer to White et al. (2001).

In addition to these features, three different release models were implemented in the STOMP simulator for describing radionuclide releases from the tank wastes, as documented in Zhang et al. (2003). These include advection-dominated, diffusion-dominated and saltcake release models and were used to account for different release mechanisms in the tank wastes. In the C Closure investigation (Zhang et al. 2003), the saltcake release model was implemented in STOMP kinetically. However, in this investigation, the saltcake model was modified so that the release rate is constant until all of the tank wastes are released.

For all three of the models, the average release rate for the current time step was determined by integrating the rate equations at the beginning and end of each time step. The release rate was then determined by differencing the integrated rates over the time step. The modified saltcake release model is described below. The advection- and diffusion-dominated release models are discussed again here.

3.4.1 Advection-Dominated Release Model

The advection-dominated release model, also known as the mixing-cell cascade model, was used to simulate releases from stabilized (grouted tank or tank ancillary) waste. For stabilized waste, the contaminants were released into the subsurface at a rate determined by both the rate of infiltrating water and the amount of dispersion occurring within the source. In the mixing-cell cascade model of Kozak et al. (1990), the tank interior was considered to comprise a series of cascading, N equal-sized, well-stirred cells, where the total volume of the N cells was equal to the volume of the tank residual waste. The mixing-cell cascade model for N equal-sized cells is defined as

$$Q(t) = qAC_0 \exp(-\gamma_N t) \sum_{i=1}^{N} \frac{(\gamma_N t)^{i-1}}{(i-1)!} \tag{3.8}$$

where Q is the release rate, t is time, q is the vertical Darcy flux, A is the horizontal (planar) area of the tank interior, γ is equal to $q/(\theta R)$, θ is the volumetric moisture content in the residual waste, and R is the retardation factor, which is assumed to be equal to 1. The initial concentration of contaminant (C_o) in the interstitial water is determined as

$$C_0 = \frac{m}{\theta V R} \tag{3.9}$$

where m is the total inventory, which is unity in these analyses, and V represents the total volume of the residual waste. By defining a source thickness for the residual wastes as $d = V/A$ and substituting Eq. 3.9 and $q = \gamma\theta R$ into Eq. 3.8, the advection-dominated release model can be written as

$$Q(t) = \frac{\gamma}{d} exp(-\gamma N t) \sum_{i=1}^{N} \frac{(\gamma N t)^{i-1}}{(i-1)!} \tag{3.10}$$

Two values, the number of mixing cells (N) and the source thickness (d), were required as inputs to the STOMP simulator. Values used in this analysis are shown in Table 3.7.

The advection-dominated release rate for a given time step was determined by differencing the integral of Eq. (3.10) with respect to time at the beginning and end of the time step and dividing this difference by the time step. As a closed-form solution for the integral of Equation (3.10) with respect to time is dependent on N (the number of mixing cells), STOMP solves Eq. 3.10 using Romberg integration (Press et al. 1992). Romberg integration is a recursive method that uses the extended trapezoidal rule for integration, which progressively increases the number of trapezoids under the curve to reduce the error term to a previously set tolerance.

Table 3.7. Input Parameters for the Three Release Models

Advection-Dominated		**Diffusion-Dominated**		**Saltcake**	
Parameter	Value	Parameter	Value	Parameter	Value
Source Thickness (d)	0.825 m	Source Thickness (d)	0.825 m	Source Volume (V)	10.2 m^3
Number of Mixing Cells (N)	10	Diffusion Coefficient (D_e)	6.0×10^{-7} cm^2/s	Surface area (A)	453 m^2
				Aqueous Solubility (s)	650 g/L
				Waste Density (ρ_m)	1.7 g/cm^3

3.4.2 Diffusion-Dominated Release Model

The diffusion-dominated release model is used to simulate the release of contaminants from stabilized (e.g., grouted tank or tank ancillary) wastes. With little or no advection through the waste container, the release can be modeled as a diffusion-limited process given as (Khaleel and Connelly 2003)

$$Q(t) = \frac{I}{d}\sqrt{\frac{D_e}{\pi t}} \tag{3.11}$$

where D_e is the effective diffusion coefficient. I is the total inventory defined as

$$I = C_0 \sum_i V_i = C_0 V_T \tag{3.12}$$

where V_T is the total volume of all cells.

Two values, the diffusion coefficient within the waste source (D_e) and the source thickness (d), were required as inputs to the STOMP simulator. Values used in this analysis are shown in Table 3.7.

As with the advection-dominated release model, the release rate for a given time step was determined by differencing the integral of Eq. 3.11 over the time step. A closed-form integral solution was used to determine the average release rate for the diffusion-dominated model. The total amount of mass released is given as

$$M(t) = \frac{2I}{d}\sqrt{\frac{D_e t}{\pi}} \tag{3.13}$$

where M is the current quantity of the contaminant (in Ci) at time t.

3.4.3 Saltcake Release Model

Solubility-controlled release (saltcake) model assumes that a solid controls the solution concentration in the aqueous phase of the constituents being released. Solubility models are thermodynamic equilibrium models and do not consider kinetics. The saltcake release model presented here is a modification of the release model in Zhang et al. (2003) so that the release rate is a constant rather than a variable dependent on the total mass at the source. When applied to residual tank wastes, the term “cake” applies to the sludge and hard heel residual in the tanks that compose the structural matrix.

The saltcake model considered in this analysis consisted of a very simple mathematical formulation containing a water flux, waste source thickness, and waste solid solubility term. The contaminant release mechanism of the cake model was the dissolution of the “structural matrix.” As the matrix dissolved, all of the contaminants were assumed to leach congruently at the same rate. The release rate model implemented in STOMP was given as

$$Q(t) = \frac{\Delta M}{\Delta t} = \frac{M_0 Aqs}{V\rho_m} \tag{3.14}$$

where M_0 is the original quantity of the contaminant in Ci embedded in the cake, A is the surface area of the salt cake exposed to the release mechanism, q is the recharge rate, s is the aqueous solubility of the saltcake, V is tank waste volume, and ρ_m is the density of the waste. The amount of contaminant remaining in the salt cake is given as

$$M = M_0\left[1 - \frac{Aqst}{V\rho_m}\right] \tag{3.15}$$

Three values, the solubility (s), surface area (A), waste volume (V), and the density of the waste (ρ_m) were required as inputs to the STOMP simulator. Values used in this analysis are shown in Table 3.7.

3.5 Source Terms

The source terms in these analyses consisted of three different source types, including 1) leaks during retrieval, 2) residual waste leachate from tanks following closure, and 3) residual waste leachate from tank ancillary equipment following closure. For the retrieval leakage scenarios, this source type represents leaks that might occur during waste retrieval operations using water-based sluicing. Releases from the residual wastes (from both tank and tank ancillary equipment) may occur over an extended period following the closure of the tank farm. Contaminant migration would occur when infiltrating water comes into contact with the tanks or tank ancillary equipment. Dissolved contaminants then have the potential to mobilize in the vadose zone and enter the groundwater table.

For all of the cases presented in this report, sources are located near or at S-103, the tank farthest from the exit boundary. All sources are simulated as a unit curie so that results can be scaled when actual source inventories are known. Two additional cases were run with a unit source at each of the three tanks in the cross section. These cases are presented to compare the transport behavior of the contaminants in the various tanks.

3.6 STOMP Execution

The reported simulations were executed on Linux workstations. All executables were generated from a single source code that is readable and available in electronic form (Section 6). Executing the simulator required two steps: 1) compiling the source code with a parameters definition file and 2) executing the compiled code on a workstation or personal computer. The executable forms of the STOMP simulator were generated for these investigations using the default level of optimization for each compiler. STOMP was coded following ASCII FORTRAN 77 protocols and yielded no warning or error messages during compilation. The size of the computational domains (~18,000 nodes) necessitates the use of a conjugate gradient linear system solver with a compact storage scheme for the Jacobian matrix. The STOMP simulator uses the SPLIB solver (Bramley and Wang 1995) for sparse linear systems for solutions implementing conjugate gradient solvers. The SPLIB solver is a collection of libraries that must be assembled on the executing computer and linked to the STOMP simulator during compilation. The SPLIB files and

instructions necessary to complete the compilation and execution of the STOMP simulator will be available in electronic form (Section 6).

3.7 Result Translation

For these investigations, the STOMP simulator read a series of input files and generated an output file, surface flux files, and a series of plot files. As described previously, the STOMP output file contains reflected data from the input files, simulation progression information, and reference-node output. The output files were used only for verification and simulation tracking. Input, output, plot, and surface-flux files are located in the simulation case directories and will be available in electronic format (Section 6).

For the 2-D simulations, because a 2-D cross section through the S-SX Tank Farm was used, reported concentrations are for 2-D flow within the soil slice. No scaling of concentrations and water sources was performed to convert the reported concentrations to a three-dimensional plume.

Concentration calculations for the breakthrough curves presented in Appendix B were made using STOMP output values for solute mass and water mass fluxes at the fence line. These data were recorded in STOMP surface files and used to calculate average groundwater concentrations and average fence line concentrations. Both concentration calculations were scaled using the water flux at the fence line rather than aquifer thickness. For example, average concentrations at the fence line (C_{fl}) were computed as

$$C_{fl} = \frac{Solute\ Flux\ at\ Fence\ Line\ (Ci/day)}{Water\ Flux\ at\ Fenceline\ (L/day)} \tag{3.16}$$

Similarly, average concentrations at the water table (C_{wt}) were calculated as

$$C_{wt} = \frac{Solute\ Flux\ at\ Water\ Table\ (Ci/day)}{Water\ Flux\ at\ Fenceline\ (L/day)} \tag{3.17}$$

Fence line concentrations were then used as sources in the analytic aquifer streamtube model described in the next section to predict concentrations at the distal compliance points.

Note that the concentrations calculated using Eq. 3.16 and 3.17 were average concentrations for a plane at the water table and the fence line. For the 3-D simulation, the simulation extent at the south-north direction, the direction perpendicular to the groundwater flow direction was 153 m. Consequently, an average concentration underestimates the peak solute concentration because 1) the solute flux is not uniformly distributed at the south-north direction and 2) the total volume of water through the fence line is much larger than the corresponding 2-D case. To correctly reflect the solute peak concentrations at the fence line, the 153-m-long surface was divided into 51 subsurfaces. The peak concentration occurs at the subsurface that coincides with the center line of Tanks S-101, S-102, and S-103. The concentrations were calculated using Eq. 3.16 and 3.17 and the solute and water fluxes through the subsurface.

3.8 Analytical Groundwater Transport Modeling

The instantaneous point source model (Baetslé 1969) for a three dimensional space, as reported by Domenico and Schwartz (1990), is shown in Eq. (3.18):

$$C(x,y,z,t) = \left[\frac{C_0 V_0}{\left(8(\pi t)^{3/2}\left(D_x D_y D_z\right)^{1/2}\right)} \right] exp\left[-\frac{(x-vt)^2}{4D_x t} - \frac{y^2}{4D_y t} - \frac{z^2}{4D_z t} - \lambda t \right] \quad (3.18)$$

where C is the solute concentration as a function of position and time (pCi/L or µg/L), C_0V_0 is the instantaneous source of solute mass (pCi or µg), D_x, D_y, D_z are spatial components of the hydrodynamic dispersion coefficient (m^2/yr), x, y, z are spatial distances from the solute source (m), t is the time (yr), λ is the solute species radioactive decay half-life (yr), and v is the pore-water velocity (m/yr). The spatial components of hydrodynamic dispersion coefficients include dispersive and diffusive elements, according to Eq. (3.19):

$$D_i = \alpha_i v + D_m \quad for \quad i = x, y, z \quad (3.19)$$

where α_i is the dispersivity (m), and D_m is the molecular diffusion coefficient (m^2/yr).

If the soil sorption of solute is assumed to be linear, the transport of a reactive solute can also be described by Eq. (3.18). The dispersivities, D*, and the pore-water velocity, v*, of a reactive solute relate to those, D and v, of a conservative solute as

$$D^* = D/R \text{ and } v^* = v/R \quad (3.20)$$

where R is the retardation factor and is defined as

$$R = 1 + \rho_b K_d/\theta \quad (3.21)$$

and θ is volumetric soil water content.

The instantaneous point source model (Eq. 3.18) was used to calculate the concentration of contaminant species originating at the S-SX Tank Farm and traveling to two remote compliance points along groundwater flow path southeast of the gap. The two compliance points along the southeast pathway are 1) the 200 Area exclusion boundary, and 2) the Columbia River.

The streamtube model considered longitudinal and transverse dispersion, as well as molecular diffusion. To simulate the transport of solutes from temporally dispersed source, the analytical groundwater model assumed transport from a series of solute slugs. The method of superposition was used to integrate the individual slug sources.

The concentration at compliance points is calculated by a FORTRAN code (*point_3d.f*) that implements the instantaneous pulse equation. The distance to each compliance point along the groundwater flow path was based on streamlines derived from the CFEST site-wide groundwater model as described in Section 5. Values for the y and z directions are assigned values of zero signifying that the point of observation was along the longitudinal center line.

Input into the streamtube model includes STOMP mass fluxes (as a file read) as well as velocity, distance and dispersivities (as a screen prompt). Parameter values and filenames were input into the model using the R-scripting language (see Section 6). The 10,000-year period for the S-SX tank analysis, between years 2000 and 12000, was modeled using 10,000 (about 3,500 for Case 1_3d) uniformly spaced solute release events. Radiological decay of the species was not considered.

4.0 Simulation Results

This section reports key fluid flow and solute transport behavior, breakthrough curves, and mass balances for the S-SX Tank Farm simulations at the groundwater table, fence line, and two downgradient compliance points. Two-dimensional simulations in STOMP were used to determine fluid flow and solute transport behavior at the groundwater table and fence line for the S-101, S-102, and S-103 cross section. Resulting concentrations from the 2-D simulations were not scaled to account for spreading and dilution associated with a three-dimensional plume. However, results of 2-D and 3-D simulations were compared to determine a dilution factor for the 2-D concentrations. An analytical, 1-D streamtube model that accounts for 3-D diffusion and dispersion was used to predict solute transport behavior at the downstream compliance points.

4.1 Summary Description of the Simulations

As described in Section 2, using a unit release at Tank S-103 and a 2-D cross section through Tank S-101, S-102 and S-103, seven scenarios were simulated to investigate the effect of different source types, for instance, leaks during retrieval (Cases 1 and 2), residual waste leachates from tanks after closure (Cases 3–6), and residual waste leachates from tank ancillary equipment following closure (Case 7). Two cases (Cases 2v and 5v, the verification cases) simulated contaminant transport from all three of the tanks in the cross section. One case (Case 1_3d) investigated effects of flow dimensionality on solute transport.

Six different sorption coefficients (K_d = 0.01, 0.03, 0.1, 0.3, 0.6, and 1.0 mL/g) were used to investigate a wide range of retardation for the U-238 species. The conservative species, Tc-99, was assumed to have a $K_d = 0$. In the results presented in this report, the notation "U_K_d" is used to represent each of the uranium contaminant species from Tank S-103. For example, U_0.01 represents the uranium contaminant with K_d = 0.01 mL/g. If the contaminant source was located at multiple tanks (as in Cases 2v and 5v), the notation "Tc_tank#" or "U_tank#_K_d" is used. For example, Tc_S102 represents the technetium from Tank S-102 and U_S101_0.03 the uranium species from Tank S-101 with K_d = 0.03 mL/g.

As discussed in Section 2, because tank integrity was presumably lost in January 2050, the simulation of flow and transport of each case has been carried out in two stages, one from 1952 to 2050 and the other from 2050 to 12000. Initial flow conditions for the first stages of the simulation were established with a steady-state flow simulation that assumed a natural infiltration rate of 3.5 mm/yr.

For the analytical (streamtube) groundwater transport model, concentration decreases occurred through longitudinal, transverse horizontal, and transverse vertical dispersion as well as molecular diffusion. Radioactive decay was not considered because Tc-99 and U-238 have long half-lives. Data on the potential flow path to the southeast of the gap are presented for the exclusion boundary and the Columbia River compliance points. The streamtube model is discussed in more detail in Section 5.

4.2 Section Organization

Saturations and inventory profiles are shown in Appendix A. The mass flux, cumulative activity, and breakthrough curves (BTC) for the various cases are presented in Appendix B. Because solute concentra-

tions at the groundwater table were scaled by the water flux at the fence line (see Eq. 3.17, Section 3.7), BTCs at the groundwater and fence line compliance points demonstrated similar behavior. Though contaminant concentrations are reported in curies, for the sake of simplicity, the term "mass" is substituted for "activity." The peak mass fluxes and arrival times at the groundwater table and the fence line are summarized in Tables 4.2 through 4.8. The peak concentrations and arrival times at the groundwater table, the fence line, the exclusion boundary, and the Columbia River are summarized in Tables 4.9 through 4.15. The mass balance for each contaminant in each case is summarized in Tables 4.16 through 4.22.

Saturation and concentration distribution profiles shown in Appendix A also show interfaces between the material types. Before year 2050, the tanks were impermeable and are shown in white in these figures. After the year 2050, tank outlines are shown in these figures, even though tank integrity was lost. Because tanks were assumed to be filled with backfill or grout after losing their integrity, the tank outlines exist in these figures only as points of reference. Although the transport of seven solutes was simulated, only the results of selected solutes, e.g., Tc, U_0.10 and U_0.60, are shown in the appendixes to represent the zero-retarded, weakly retarded and strongly retarded species. Plot-file outputs for all the simulations were generated at years 2500 (or 2550), 3000, 4000, 5000, 6000, 8000, 10000, 12000, and the years that Tc and U_0.10 concentrations at the fence line reached their peak values. Additional output does exist for individual cases. Each plot file includes values for saturation, aqueous pressure, moisture content, and concentration of the seven solute species.

In the sections that follow, results are reported for each case organized by source type. A summary description and comparison of results follows the individual case descriptions. Case 1 was considered as a base case and is referenced in terms of relative peak concentrations for the other cases. The saturation distribution without any tank leak is termed the baseline saturation.

4.3 Initial Conditions and Baseline Saturation Distributions

The saturation field was dependent on the surface recharge, hydrologic parameters, soil distribution, and impermeable structures (e.g., SSTs). The initial moisture condition in 1952 for all cases was achieved by running a simulation for the cross section using a recharge rate of 3.5 mm/yr for 1000 years (see Figure A.1a). Because this period represents the preconstruction period of the S-SX Tank Farm, the simulation was run without the three tanks in place. These conditions yielded a mean saturation of 0.387 in the vadose zone.

Recharge rates were varied to represent various stages of tank and barrier construction; for example, the beginning of the simulation represented the tank preconstruction period. After the tanks were in place in 1952, recharge rates increased—and then decreased once a protective barrier was in place in 2050. The recharge rate increased again when degradation of the barrier occurred in the year 2550. As outlined below, overall moisture content in the vadose zone was mainly affected by the change in recharge rates.

Because the recharge rates for all seven cases were the same, the saturation distribution within the domain did not vary much among the cases. From 1952 to 2050, the recharge was assumed to increase from the preconstruction estimate of 3.5 mm/yr to the current value of 100 mm/yr. This change was due to the replacement of the gravel-sand layer at the top of the domain (unit H1, see Figure 3.1) with a

porous backfill material, which increased the mean vadose zone saturation by 42% to 0.551 in the year 2050 if the tanks were filled with backfill material (Figure A.2a).

From 2050 to 2550, the annual recharge rate was decreased to the barrier design value of 0.5 mm/yr, causing a subsequent decrease in the soil water content. In 2550 the mean saturation in the vadose zone was 0.333, which was a decrease of 40% from the year 2050 (Figure A.2b). The barrier began to degrade in 2550, increasing the recharge rate to 3.5 mm/yr. By the end of the simulations at year 12000, the mean saturation at the vadose zone was 0.377 (Figure A.3), which was close to the average saturation of 0.387 in the preconstruction period. Even with the flux of water entering the domain in Cases 1 and 2 (15.2 and 30.3 m^3, respectively), the overall moisture content in the vadose zone in the year 12000 was the same as that for the other cases that did not simulate water leaks during retrieval (see Figure A.3).

During the simulation period from 1952 to 12000, the water table level showed little variation with changes in the surface recharge rate.

4.4 Retrieval Leaks

Two simulation cases, Cases 1 and 2, investigated transport behavior for contaminants originating from leaks that might occur during waste retrieval operations using water-based sluicing. Two retrieval rates were simulated: Case 1 with a unit release of each contaminant in 4,000 gallons of water, and Case 2 with a unit release of each contaminant in 8,000 gallons of water. Both cases simulated the source at Tank S-103. A third case, a verification case for Case 2, simulated unit releases of contaminants in 8,000 gallons of water at each of the three tanks, S-101, S-102, and S-103, in the simulation domain.

4.4.1 Case 1: 4000-Gallon Leak at S-103 (base case)

Case 1 was a retrieval leak of 4,000 gallons at the lower-right corner of Tank S-103 that began on the first day of the year 2000. The leak lasted for 14 days and contained a unit release of each of the contaminant species (Tc-99 and U-238). Additional plot-file output for this simulation was generated at the beginning (year 2000) and the end (14 days after January 1, 2000) of the leak and the years 2001, 2010, 2050, and 2100.

The aqueous saturation field for the S-103 to S-101 cross section at the time the leakage ended is shown in Figure A.4, which shows the effects of the tank leak on the moisture content distribution in the subsurface. For example, the soil at the leak location was completely saturated at the end of the 14-day leak. Saturations near the leak were much higher than anywhere else in the vadose zone. This effect, however, disappeared by the year 2050 because the volume of the leak was small compared with the total recharge entering the system at 100 mm/yr.

The distribution of the aqueous concentration of the contaminants at the time of peak concentration at fence line is shown as color images in Figures A.5 through A.7 in logarithmic scale for the years when the peak concentration occurred, i.e., year 2062 for Tc, 5550 for U_0.10, and 12000 for U_0.60. Tc-99 moved faster than the other contaminants because it did not sorb to subsurface materials. For U-238, the species with larger K_d values transported slower than the U-238 contaminant with lower K_d values.

Figures B.1 through B.6 plot the mass flux, cumulative mass, and BTCs for each of the contaminants. Figure B.1 shows mass flux and cumulative activity for Tc-99 at the groundwater table and fence line, which display double peaks (Figure B.1) due to variations in the recharge rate. For U-238 double peaks also occurred, although the peaks progressively lowered and flattened as K_d values increased. For example, the first peak was higher than the second for Tc-99 (Figure B.1); for K_d = 0.10 mL/g (Figure B.3), the second peak on the mass flux curve was higher than the first. For K_d = 0.60 mL/g (Figure B.5), the peak flux had not appeared by the year 12000. By 12000, the percentage of contaminants that had transported past the fence line boundary was 100% for Tc-99, U_0.01, U_0.03, and U_0.10; 48% for U_0.30; 0.4% for U_0.60; and 0.0% for U_1.00.

Peak concentrations and arrival times at the fence line for the base case (Case 1) are summarized in Table 4.1. The peak concentration of Tc-99 at the fence line (C_{fl}) was 5.46×10^{-8} Ci/L. Relative to Tc-99, peak concentrations at the fence line for U-238 species with different K_d values were 52.4% for U_0.01, 11.4% for U_0.03, 3.8% for U_0.10, 1.8% for U_0.30, 0.1% for U_0.60, and 0.0% for U_1.00.

Table 4.1. Predicted Peak Concentrations (Ci/L) and Arrival Times at the Fence Line for the Base Case (Case 1)

Species	Peak Concentration (Ci/L)	Peak Concentration Arrival Time (yr)
Tc	5.46E-08	2062
U_0.01	2.86E-08	2066
U_0.03	6.22E-09	2082
U_0.10	2.07E-09	5550
U_0.30	1.00E-09	11574
U_0.60	2.80E-11	12000
U_1.00	1.10E-14	12000

4.4.2 Case 2: 8000-Gallon Leak at S-103

Case 2 simulation investigated a retrieval leak of 8,000 gallons at the lower right corner of Tank S-103 that started on the first day of the year 2000. The leak lasted 14 days and contained a unit release of each of the contaminant species (Tc-99 and U-238). Additional plot-file output for this simulation was generated at the beginning (year 2000) and the end (14 days after January 1, 2000) of the leak and the years 2001, 2010, 2050, and 2100.

The saturation distribution on 1/15/2000 is shown in Figure A.8. The distribution of the aqueous concentration of the contaminants at the time of peak concentration at fence line is shown in Figures A.9 through A.11 in logarithmic scale for the years when the peak concentration occurred, i.e., year 2060 for Tc, 5452 for U_0.10, and 12000 for U_0.60. The mass flux, cumulative activity, and BTCs of each contaminant are shown in Figures B.7–B.12. As in Case 1, mass flux curves demonstrated double peaks due to variations in recharge. By 12000, the percentage of contaminants that had transported past the fence line boundary was 100% for Tc-99, U_0.01, U_0.03, and U_0.10; 48.6% for U_0.30; 0.4% for U_0.60; and 0.0% for U_1.00.

The peak concentration of Tc-99 at the fence line was 6.50×10^{-8} Ci/L (Table 4.9), a 19% increase over the peak concentration in Case 1. Relative to Tc-99, peak concentrations for the U-238 compounds were 57.3% for U_0.01, 14.4% for U_0.03, 3.2% for U_0.10, 1.5% for U_0.30, and 0.0% for U_0.60 and U_1.00.

4.4.3 Case 2v: 8000 Gallons at S-103, S-102 and S-101

As a verification of Case 2, Case 2v was a retrieval leak of 8,000 gallons at the lower-right corner of each of the three tanks in the domain. All of the leaks began on the first day of the year 2000 and continued for 14 days. Each retrieval leak contained a unit release of Tc-99 and U-238 with a K_d of 0.03 mL/g. No other K_d values were used in this simulation. Figure A.12 depicts soil water distribution at the end of the leakage, showing that the four plumes were similar in shape. However, due to the sloped interface between materials H1 and H2, flow from the middle tank (S-102) had slightly stronger lateral movement. After 10,000 years of simulation, however, the saturation distribution at the year 12000 was the same as the baseline (Figure A.3).

After 61 to 62 years since the start of the leak, the Tc-99 concentrations at the fence line reached their peak values. All three of the Tc-99 plumes (Figure A.13) were similar to the single-leak case at Tank S-103 (Figure A.9) in shape and concentration distribution. All three Tc-99 plumes from three different tanks also migrated at nearly the same velocity. The U-238 concentrations at the fence line reached their peak values 72 to 76 years after the start of the leak. All three of the U-238 (K_d = 0.03 mL/g) plumes (Figure A.14) were similar to the single-leak case at Tank S-103 in shape and concentration distribution (Figure A.10). Similar to Tc-99, the U-238 plumes from the three tanks also migrated at nearly the same velocity. By the year 12000, 100% of the contaminants had traveled past the fence line boundary.

Figures B.13 through B.24 plot the mass flux, cumulative mass, and BTCs of each contaminant. The peak fluxes, concentrations, and arrival times of the same contaminant released from different tanks were similar. For example, peak concentrations at the fence line were 3.80×10^{-8}, 6.08×10^{-8}, and 6.54×10^{-8} Ci/L for the Tc-99 released from Tanks S-101 (Figure B.14), S-102 (Figure B.16), and S-103 (Figure B.18), respectively. The corresponding peak arrival times were 2062, 2062, and 2061. The peak concentrations were nearly the same as those when there was only one retrieval leak at Tank S-103 (6.50×10^{-8} Ci/L). The peak concentration of Tc-99 from Tank S-101 was lower than those from S-102 or S-103; this may be due to the change of the thickness of soil layers.

4.4.4 Leak Volume Effects: Comparison of Cases 1 and 2

A comparison of results of Cases 1 and 2 shows that, when the leak volume was doubled, the Tc-99 peak concentrations at all the compliance points increased by 15~19% and arrival times were 1~5 years earlier. The peak concentrations of U-238 with K_d = 0.01 mL/g increased by 22~30%, and the arrival times were 2~6 years earlier. The peak concentrations of U-238 with K_d = 0.03 mL/g increased by 37~52%, and the arrival times were 7~11 years earlier. These results suggest that larger leak volumes will lead to higher peak concentrations and earlier arrival times.

However, for $K_d \geq 0.10$ mL/g, the second peak in the breakthrough curves was higher than the first in both cases. The BTCs of solutes with $K_d \geq 0.10$ mL/g had much flatter peaks than those of solutes with

$K_d \leq 0.03$ mL/g. Consequently, the difference in peak concentrations in the two cases became smaller. Peak concentrations of U-238 with K_d between 0.1 and 0.3 mL/g differed no more than 2% in the two cases.

The differences in mass flux between Cases 1 and 2 were similar to differences in concentration. For example, when the leak volume doubled, the Tc-99 peak mass flux at the water table and the fence line increased 18~19% and arrival times were 1~2 years earlier. However, the cumulative mass migrating out of the fence line did not show any difference between cases. At year 12000, the percentage of contaminants that had exited the fence line was nearly identical in both cases. Because the leak volume was small (and short in duration) relative to meteoric recharge, recharge rates largely controlled the amount of mass exiting the domain for the 10,000 year simulation.

4.5 Residual Tank Wastes with Different Controlling Processes

Cases 3–6 simulated contaminant transport behavior from residual tank wastes. This type of release occurs when water infiltrates residual tank wastes and mobilizes contaminants. Case 3 assumed constant release rates over specified time periods, and Cases 4–6 assumed that different physical processes such as advection, diffusion, and dissolution controlled the release rates. In Case 4, an advection-dominated release model (Eq. 3.10) was used to predict contaminant transport behavior and considered mixing processes occurring within the residual wastes. For stabilized waste, contaminants were released into the subsurface at a rate determined by both the rate of infiltrating water and the amount of dispersion occurring within the source. Case 5 assumed that little or no advection occurred in the residual tank waste source; thus the release was modeled as a diffusion-limited process (Eq. 3.13). In Case 6, it was assumed that the solid residual tank wastes release rate was controlled by solubility. The saltcake release model used in the Case 6 analysis is presented in (Eq. 3.15).

4.5.1 Case 3: Release Rate R_0 at S-103 (10^{-6} Ci/yr for 500 yr and 10^{-4} Ci/yr for 9995 yr)

Case 3 investigated a residual tank waste source with release rate R_0 defined as 10^{-6} Ci/yr for 500 years followed by a rate of 10^{-4} Ci/yr for 9,995 years. The release occurred over the bottom width of Tank S-103. The leak began on the first day of the year 2050, the date when tank integrity was lost.

The saturation distributions at years 2050 and 12000 were the same as the baseline (Figures A.1 to A.3). The distribution of the aqueous concentration of the contaminants at fence line is shown as color images in Figures A.15 to A.17 in logarithmic scale for the years when the peak concentration occurred, i.e., 8068 for Tc and 12000 for U_0.10 and U_0.60. Mass flux, cumulative mass, and BTCs for each contaminant are shown in Figures B.25–B.30. By the year 12000, the percentage of contaminant that had migrated past the fence line boundary was 76.7% for Tc-99, 73.3% for U_0.01, 66.4% for U_0.03, 42.2% for U_0.10, 1.7% for U_0.30, and 0.0% for both U_0.60 and U_1.00.

The peak concentration of Tc-99 at the fence line was 6.57×10^{-10} Ci/L (Table 4.9), 1.2% of the peak concentration predicted in Case 1. At the fence line, relative to Tc, peak concentrations of U-238 compounds with different K_d values were 100% for U_0.01 and U_0.03 and 99.7% for U_0.10, 16.3% for U_0.30, and 0.0% for U_0.60 and U_1.00. The arrival times for the peak fence line concentrations were years 8608 for Tc-99, 9729 for U_0.01, 11691 for U_0.03, and 12000 for U_0.10.

4.5.2 Case 4: Advection-Dominated Release

Case 4 investigated a residual tank waste source using an advection-dominated release model. The release occurred over the bottom width of Tank S-103 with a source thickness of 0.825 m. The number of mixing cells used in the advection-dominated release model was 10. The leak began on the first day of the year 2050, the date when tank integrity was lost.

The saturation distributions at years 2050 and 12000 were the same as the baseline (Figures A.1 to A.3). The distribution of the aqueous concentration of the contaminants at the time of peak concentration at fence line is shown as color images in Figures A.18 through A.20 in logarithmic scale for the years when the peak concentration occurred, i.e., year 4043 for Tc, 7242 for U_0.10, and 12000 for U_0.60. Mass flux, cumulative mass, and BTCs for each contaminant are shown in Figures B.31–B.36. By the year 12000, the percentage of contaminant that had migrated past the fence line boundary was 100% for Tc-99, U_0.01, and U_0.03; 99.8% for U_0.10; 18.1% for U_0.30; and 0.0% for U_0.60 and U_1.00.

In this scenario, the release rate was dependent on both water flow and the amount of dispersion occurring from the residual tank waste source, which was completely released in ~450 years. The peak concentration of Tc-99 at the fence line was 6.77×10^{-9} Ci/L (Table 4.9), 12.4% of the peak concentration predicted in Case 1. At the fence line, relative to Tc, peak concentrations for U-238 compounds with different K_d values were 83% for U_0.01, 63.7% for U_0.03, 34.3% for U_0.10, 11.7% for U_0.30, and 0.0% for U_0.60 and U_1.00. Arrival times for the peak fence line concentrations were years 4043 for Tc, 4360 for U_0.01, 5005 for U_0.03, and 7242 for U_0.10.

4.5.3 Case 5: Diffusion-Dominated Release ($D = 6\times10^{-7}$ cm^2s^{-1})

This case investigated a residual tank waste source using a diffusion-dominated release model and a diffusion coefficient of 6×10^{-7} cm^2/s. The release occurred over the bottom width of Tank S-103 with a source thickness of 0.825 m. The leak began on the first day of the year 2050, the date when tank integrity was lost. Grout was used as tank fill material beginning in the year 2050.

The saturation distributions at years 2050 and 12000 were the same as the baseline (Figures A.1 to A.3) except at the tank region (Figure A.21). This is due to the use of grout as the tank filling material, which has very high water-holding capacity. Consequently, the grout at the tank region was nearly saturated. The distribution of the aqueous concentration of the contaminants at the time of peak concentration at fence line is shown as color images in Figures A.22 through A.24 in logarithmic scale for the years when the peak concentration occurred, i.e., year 4899 for Tc, 9186 for U_0.10, and 12000 for U_0.60. Mass flux, cumulative mass, and BTCs for each contaminant are shown in Figures B.37–B.42. By the year 12000, the percentage of contaminants that had migrated past the fence line boundary was 90% for Tc-99, 88.8% for U_0.01, 84.8% for U_0.03, 62.5% for U_0.10, 2.2% for U_0.30; and 0.0% for U_0.60 and U_1.00.

The peak concentration of Tc-99 at the fence line was 1.47×10^{-9} Ci/L (Table 4.9), which was 2.7% of the peak concentration predicted in Case 1 (the other base case). At the fence line, relative to Tc, peak

concentrations of U-238 compounds with different K_d values were 95.2% for U_0.01, 85.7% for U_0.03, 63.7% for U_0.10, 9.5% for U_0.30, and 0.0% for U_0.60 and U_1.00.

4.5.4 Case 5v: Diffusion-Dominated Release at S-101, S-102, and S-103 ($D = 6\times10^{-7}$ cm^2s^{-1})

As a verification of Case 5, Case 5v simulated residual tank waste sources using a diffusion-dominated release model and a diffusion coefficient of 6×10^{-7} cm^2/s. The releases occurred over the bottom widths of each of the three tanks in the domain with source thickness of 0.825 m. The leak began on the first day of the year 2050, the date when tank integrity was lost. Grout was used as tank fill material beginning in the year 2050. Each residual tank waste source contained a unit release of Tc-99 and U-238 with a K_d = 0.03 mL/g. No other K_d values were used in this simulation. Figures A.25 and A.26 depict Tc-99 and U-238 concentration distributions, which show that the three plumes for each contaminant were similar in shape and migrated at nearly the same velocity. By the year 12000, all of the contaminants had exited the domain.

The saturation distributions at years 2050 and 12000 were the same as the baseline (Figures A.1 to A.3) except at the tank region (Figure A.21) because grout was used as the tank filling material. Figures B.43 through B.54 plot the mass flux, cumulative mass, and BTCs of each contaminant. The peak fluxes, concentrations, and arrival times of the contaminants released from different tanks were similar. For example, the peak concentrations of Tc-99 released from Tanks S-101 (Figure B.48), S-102 (Figure B.46), and S-103 (Figure B.44), respectively, at the fence line were 1.46×10^{-9}, 1.65×10^{-9}, and 1.46×10^{-9} Ci/L. The corresponding peak arrival times were 5106, 4883, and 4946. As in Case 2v, non-symmetrical transport behavior occurred due to asymmetry in stratigraphy and saturation distributions. Relative to the single residual waste source case (Case 5), peak concentrations and arrival times of the contaminants were nearly the same. For example, for Tc-99 released from only S-103, the peak concentration was 1.47×10^{-9} Ci/L and arrival time was year 4899 (Figure B.38). Note that peaks of the breakthrough curves of Cases 5 and 5v were very flat due to the slow source release.

4.5.5 Case 6: Saltcake (solubility-controlled) Release

This case investigated a residual tank waste source using a saltcake release model that assumed an aqueous solubility of 650 g/L for the residual waste. The dissolution process was expected to dominate in subsequent mobilization of the contaminants. Hence, the saltcake (solubility-controlled) release model (Eq. 3.15) was used to describe the transport behavior for residual waste sources. The release occurred over the bottom width of Tank S-103 with a volume of 10.2 m^3 (360 ft^3) and a surface area of 453 m^2, which represents the surface area of the bottom of the tank. The leak began on the first day of the year 2050, the date when tank integrity was lost.

The saturation distributions at years 2050 and 12000 were the same as the baseline (Figures A.1 to A.3). The distribution of the aqueous concentration of the contaminants at the time of peak concentration at fence line is shown as color images in Figures A.27 through A.29 in logarithmic scale for the years when the peak concentration occurred, i.e., year 4063 for Tc, 7334 for U_0.10, and 12000 for U_0.60. Mass flux, cumulative mass, and BTCs for each contaminant are shown in Figures B.55–B.60. By the year 12000, the percentage of contaminants that had migrated past the fence line boundary was 100% for Tc-99, U_0.01, and U_0.03; 99.7% for U_0.10; 15.7% for U_0.30; and 0.0% for U_0.60 and U_1.00.

The peak concentration of Tc-99 at the fence line was 6.78×10^{-9} Ci/L (Table 4.9), 12.4% of the peak concentration predicted in Case 1. At the fence line, relative to Tc, peak concentrations for U-238 compounds with different K_d values were 82.8% for U_0.01, 63.3% for U_0.03, 33.9% for U_0.10, 10.8% for U_0.30, and 0.0% for U_0.60 and U_1.00.

4.6 Residual Ancillary Equipment Wastes

This scenario investigated contaminant transport behavior from residual ancillary equipment wastes. These releases can occur when ancillary equipment left behind after closure activities comes into contact with water. Diffusive processes are expected to dominate in subsequent mobilization of the contaminants. Hence, the diffusion-dominated model used in Case 5 (Eq. 3.13) was used to describe the transport behavior for residual ancillary equipment waste sources.

4.6.1 Case 7: Diffusion-Dominated Release ($D = 6\times10^{-7}$ cm^2/s)

This case investigated a residual ancillary equipment waste source using a diffusion-dominated release model and a diffusion coefficient of 6×10^{-7} cm^2/s. The waste source originated between Tanks S-102 and S-103 at a depth of 20 ft (6.1 m) bgs with an inventory diameter of 24.4 ft (8 m). Grout was used as tank fill material. The leak began on the first day of the year 2050, the date when tank integrity was lost.

The saturation distributions at years 2050 and 12000 were the same as the baseline (Figures A.1 to A.3). The distribution of the aqueous concentration of the contaminants at the time of peak concentration at fence line is shown as color images in Figures A.30 through A.32 in logarithmic scale for the years when the peak concentration occurred, i.e., year 4186 for Tc, 7561 for U_0.10, and 12000 for U_0.60. Mass flux, cumulative mass, and BTCs for each contaminant are shown in Figures B.61–B.66. By the year 12000, the percentage of contaminants that had migrated past the fence line boundary was 96.3% for Tc-99, 95.9% for U_0.01, 94.7% for U_0.03, 87.0% for U_0.10, 9.7% for U_0.30, and 0.0% for U_0.60 and U_1.00.

The peak concentration of Tc-99 at the fence line was 4.28×10^{-9} Ci/L (Table 4.9), 7.8% of that predicted in Case 1. At the fence line, relative to Tc, peak concentrations for U-238 compounds with different K_d values were 85.5% for U_0.01, 69.2% for U_0.03, 40.7% for U_0.10, 11.8% for U_0.30, and 0.0% for U_0.60 and U_1.00. Arrival times for the peak fence line concentrations were years 4186 for Tc-99, 4523 for U_0.01, 5201 for U_0.03, and 7561 for U_0.10.

4.7 Relationship Between Two- and Three-Dimensional Simulations

Although the simulations in this report are 2-D, in reality, flow and transport from any source type will occur in three dimensions. Because of the long simulation times, simulating 3-D processes is not trivial; however, even though 2-D simulations have shorter run times, the absence of flow and transport in the third dimension translates into higher concentration predictions. Therefore, results from 2-D simulations need to be translated into equivalent values for a 3-D domain to better predict contaminant concentrations in the groundwater. However, this conversion relation is not known.

To determine a dilution factor for the 2-D simulations, Case 1 was simulated in 3-D. This base case scenario involved a retrieval leak of 4,000 gallons at the lower-right corner of Tank S-103 that began on the first day of the year 2000. The leak lasted for 14 days and contained a unit release of each of the contaminant species (Tc-99 and U-238). The main difference between the 2-D and 3-D simulations was the thickness of the simulation domain in the horizontal direction (y direction) perpendicular to the flow direction. In the 2-D simulation, a unit width (1 m) was used. In 3-D, the width was 153 m discretized into 3-m units. Hence, water and solute migration occurred in the y direction for the 3-D simulation whereas it was absent in 2-D.

To examine the relationship between the concentrations for the two simulations, the fence line aqueous concentrations of Tc-99 and U-238 with K_d = 0.03 mL/g are plotted along the y direction for the 3-D simulation when the peak concentrations occurred. Figure 4.1 shows that the highest concentrations occurred at the center line of Tanks S-101, S-102, and S-103 (y = 125 m), and as the distance from the tank center line increased, the concentrations decreased. Note that the concentration along the y direction was nearly symmetrical along the center line of the tank. Approximately 99.4% of Tc-99 and 98.3% of U-238 were within 40 m of the center line of the tank (from 105 to 145 m).

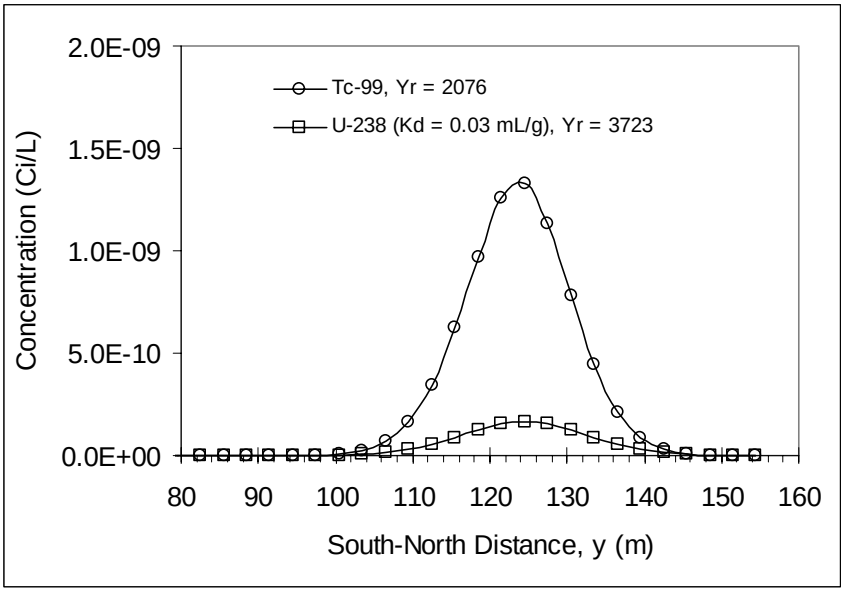

Figure 4.1. Fence Line Aqueous Concentration Along the Direction Perpendicular to the Flow Direction

Using the 3-D simulation, the distributions of the aqueous concentration of the contaminants at the center line of Tanks S-101, S-102, and S-103 at year 2100 are shown as color images in Figures 4.2a and 4.3a in logarithmic scale for Tc-99 and U_0.03. Results from the 2-D simulation of Case 1 (Figures 4.2b and 4.3b) demonstrate similar concentration distributions but higher concentration values than the 3-D simulation.

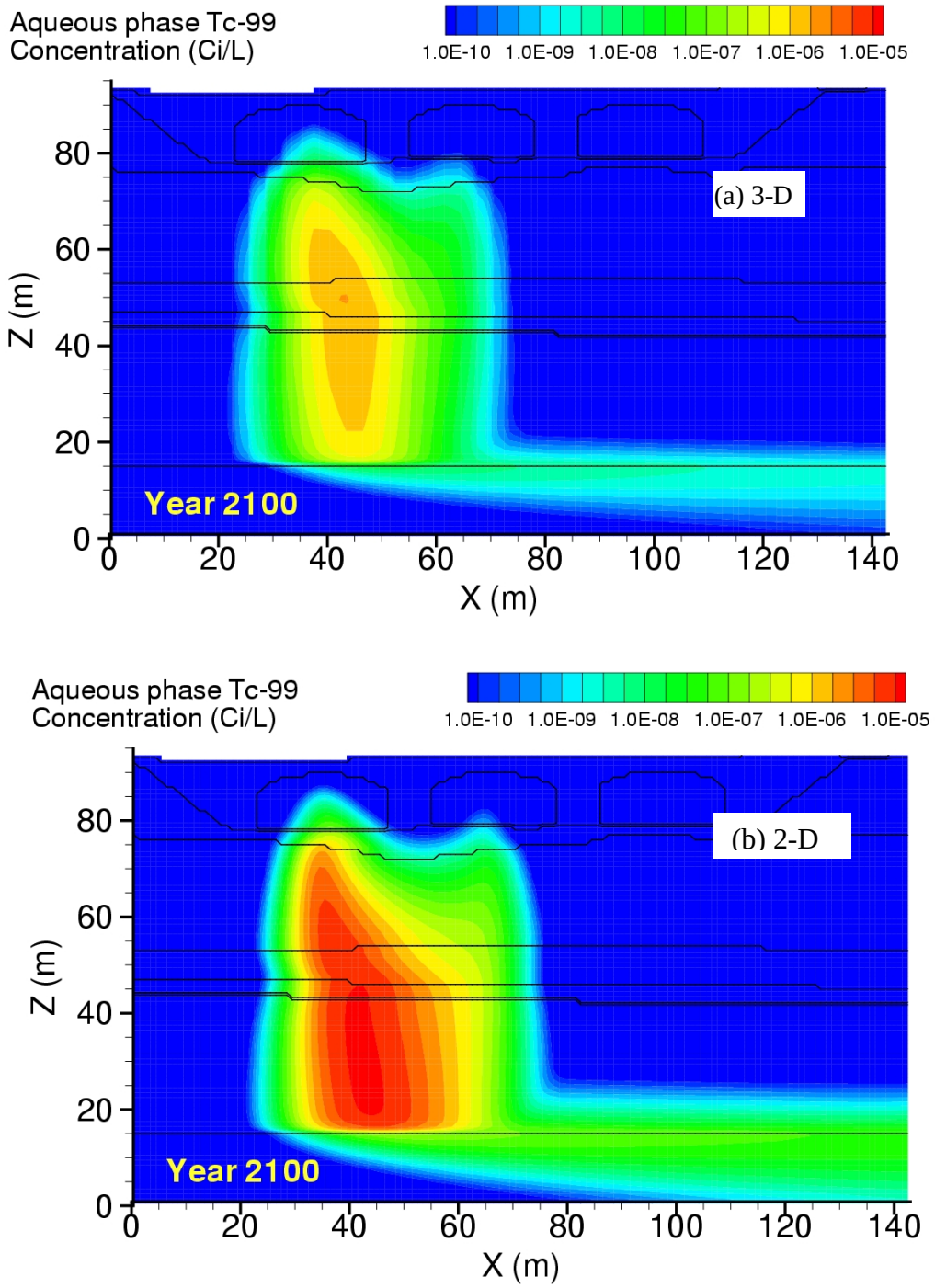

Figure 4.2. Tc-99 Aqueous Concentrations at Year 2100 at the Center Line of Tanks S-101, S-102, and S-103 Using Results of (a) 3-D Simulation and (b) 2-D Simulation

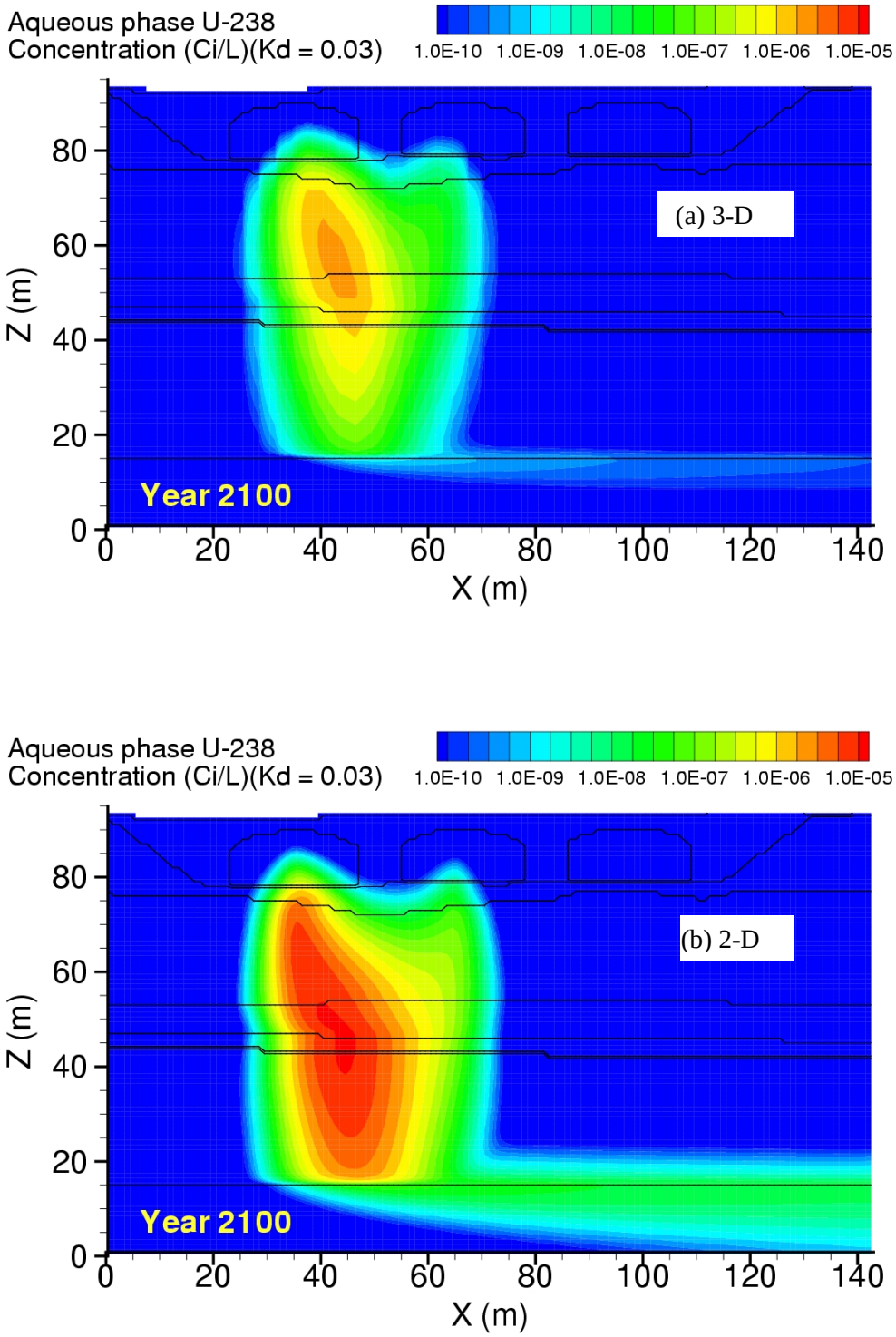

Figure 4.3. U-238 with K_d = 0.03 mL/g Aqueous Concentrations at Year 2100 at Center Line of Tanks S-101, S-102, and S-103 Using Results of (a) 3-D and (b) 2-D Simulations

Figure 4.4 compares the 2-D and 3-D breakthrough curves of Tc-99 and U-238 with K_d = 0.03 mL/g. For both Tc-99 and U-239, the shape of the breakthrough curves from the 2-D simulations were very similar to those from the 3-D simulations. The ratio of the 2-D and 3-D peak Tc-99 concentrations (C_{2d}/C_{3d}) was 41.1. The C_{2d}/C_{3d} ratio for U-238 with K_d = 0.03 mL/g was 36.6. The arrival time of the of the Tc-99 peak concentration from the 2-D simulation was 14 years earlier than that from the 3-D simulation. For U-238 with K_d = 0.03 mL/g, the arrival times of the first and seconds peak concentrations from the 2-D simulation were respectively 36 and 342 years earlier than that from the 3-D simulation.

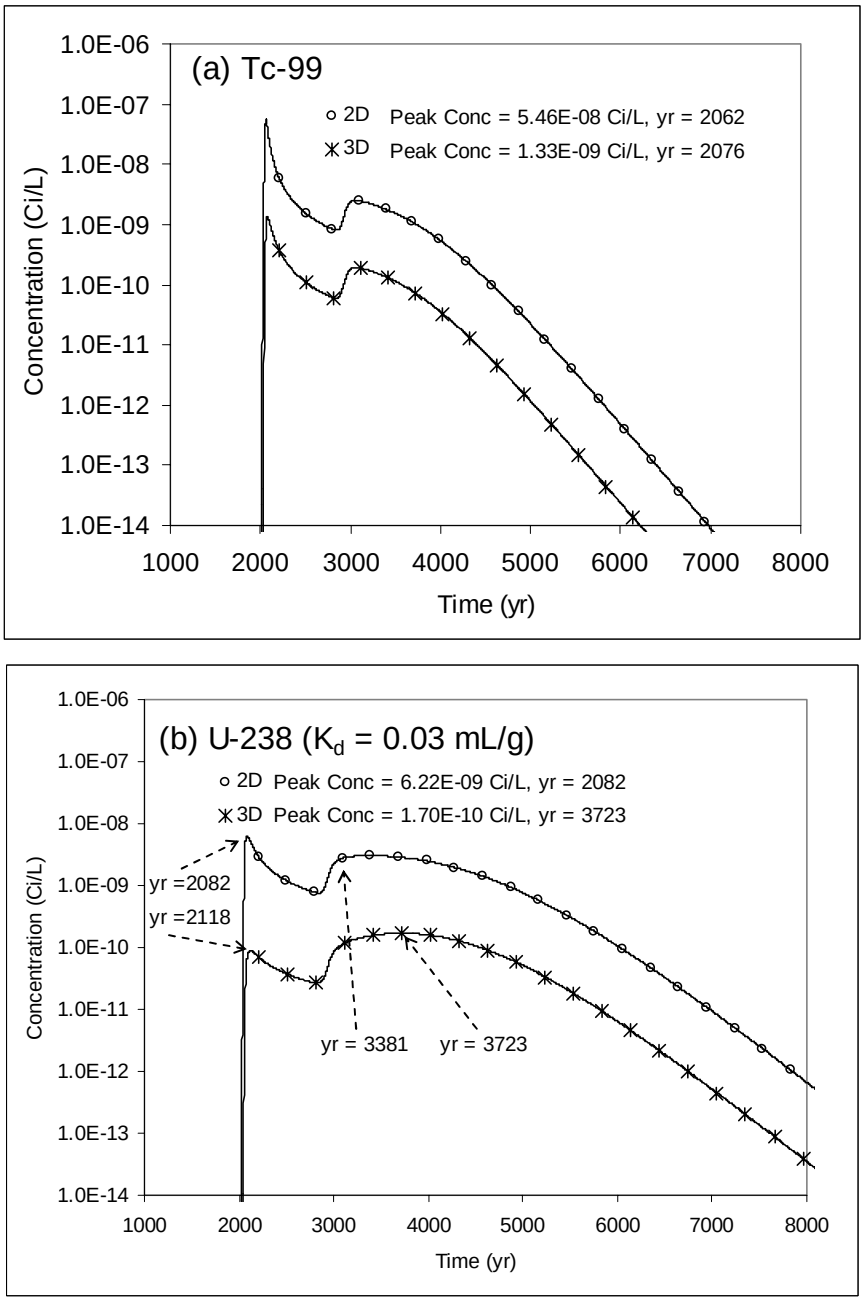

Figure 4.4. Comparison of BTCs of (a) Tc-99 and (b) U-238 with K_d = 0.03 mL/g Simulated with 2-D and 3-D

Table 4.2. Predicted Peak Tc-99 Flux (Ci/yr), Arrival Time, and Cumulative Mass (Ci)

Case	Groundwater Table			Fence Line		
	Flux (Ci/yr)	Arrival Time (yr)	Cumulative Mass (Ci)	Flux (Ci/yr)	Arrival Time (yr)	Cumulative Mass (Ci)
Case 1	9.14E-03	2060	1.0053	8.62E-03	2062	0.9999
Case 2	1.08E-02	2059	1.0057	1.03E-02	2060	1
Case 3	1.00E-04	8562	0.7677	1.00E-04	8608	0.7671
Case 4	1.03E-03	4037	1	1.03E-03	4043	1
Case 5	2.23E-04	4893	0.9	2.23E-04	4899	0.8999
Case 6	1.03E-03	4045	1	1.03E-03	4051	1
Case 7	6.52E-04	4181	0.9633	6.52E-04	4186	0.9632

Table 4.3. Predicted Peak U-238 (K_d = 0.01) Flux, Arrival Time, and Cumulative Mass

Case	Groundwater Table			Fence Line		
	Flux (Ci/yr)	Arrival Time (yr)	Cumulative Mass (Ci)	Flux (Ci/yr)	Arrival Time (yr)	Cumulative Mass (Ci)
Case 1	4.85E-03	2063	1.0036	4.48E-03	2066	1
Case 2	6.30E-03	2061	1.0041	5.87E-03	2063	1
Case 3	1.00E-04	9683	0.7333	1.00E-04	9729	0.7326
Case 4	8.56E-04	4353	1	8.56E-04	4360	1
Case 5	2.13E-04	5336	0.8883	2.13E-04	5342	0.8881
Case 6	8.56E-04	4368	1	8.56E-04	4375	1
Case 7	5.58E-04	4517	0.9594	5.58E-04	4523	0.9593

Table 4.4. Predicted Peak U-238 (K_d = 0.03) Flux, Arrival Time, and Cumulative Mass

Case	Groundwater Table			Fence Line		
	Flux (Ci/yr)	Arrival Time (yr)	Cumulative Mass (Ci)	Flux (Ci/yr)	Arrival Time (yr)	Cumulative Mass (Ci)
Case 1	1.06E-03	2075	1.0011	9.61E-04	2081	1
Case 2	1.62E-03	2067	1.0015	1.46E-03	2071	1
Case 3	1.00E-04	11636	0.6645	1.00E-04	11691	0.6637
Case 4	6.56E-04	4997	1	6.56E-04	5005	1
Case 5	1.92E-04	6208	0.8482	1.92E-04	6217	0.8479
Case 6	6.53E-04	5026	1	6.53E-04	5035	1
Case 7	4.50E-04	5192	0.947	4.50E-04	5201	0.9469

Table 4.5. Predicted Peak U-238 (K_d = 0.10) Flux, Arrival Time, and Cumulative Mass

Case	Groundwater Table			Fence Line		
	Flux (Ci/yr)	Arrival Time (yr)	Cumulative Mass (Ci)	Flux (Ci/yr)	Arrival Time (yr)	Cumulative Mass (Ci)
Case 1	3.16E-04	5533	0.9998	3.16E-04	5550	0.9997
Case 2	3.14E-04	5436	0.9998	3.14E-04	5452	0.9998
Case 3	9.97E-05	12000	0.4241	9.97E-05	12000	0.4224
Case 4	3.54E-04	7225	0.9976	3.54E-04	7242	0.9975
Case 5	1.42E-04	9169	0.6264	1.42E-04	9186	0.6248
Case 6	3.51E-04	7305	0.9971	3.51E-04	7322	0.9971
Case 7	2.65E-04	7544	0.871	2.65E-04	7561	0.8704

Table 4.6. Predicted Peak U-238 (K_d = 0.30) Flux, Arrival Time, and Cumulative Mass

Case	Groundwater Table			Fence Line		
	Flux (Ci/yr)	Arrival Time (yr)	Cumulative Mass (Ci)	Flux (Ci/yr)	Arrival Time (yr)	Cumulative Mass (Ci)
Case 1	1.53E-04	11533	0.4854	1.53E-04	11574	0.4795
Case 2	1.53E-04	11486	0.4921	1.53E-04	11525	0.4862
Case 3	1.68E-05	12000	0.0174	1.63E-05	12000	0.0167
Case 4	1.22E-04	12000	0.1855	1.21E-04	12000	0.1808
Case 5	2.18E-05	12000	0.0233	2.12E-05	12000	0.0224
Case 6	1.13E-04	12000	0.1618	1.11E-04	12000	0.1574
Case 7	7.86E-05	12000	0.0996	7.72E-05	12000	0.0966

Table 4.7. Predicted Peak U-238 (K_d = 0.60) Flux, Arrival Time, and Cumulative Mass

Case	Groundwater Table			Fence Line		
	Flux (Ci/yr)	Arrival Time (yr)	Cumulative Mass (Ci)	Flux (Ci/yr)	Arrival Time (yr)	Cumulative Mass (Ci)
Case 1	4.56E-06	12000	0.0041	4.26E-06	12000	0.0038
Case 2	4.42E-06	12000	0.0039	4.14E-06	12000	0.0036
Case 3	1.09E-08	12000	0	9.52E-09	12000	0
Case 4	2.60E-07	12000	0.0001	2.32E-07	12000	0.0001
Case 5	1.01E-08	12000	0	8.89E-09	12000	0
Case 6	1.67E-07	12000	0.0001	1.49E-07	12000	0.0001
Case 7	4.92E-08	12000	0	4.30E-08	12000	0

Table 4.8. Predicted Peak U-238 (K_d = 1.00) Flux, Arrival Time, and Cumulative Mass at Year 12000

Case	Groundwater Table			Fence Line		
	Flux (Ci/yr)	Arrival Time (yr)	Cumulative Mass (Ci)	Flux (Ci/yr)	Arrival Time (yr)	Cumulative Mass (Ci)
Case 1	2.03E-09	12000	0	1.67E-09	12000	0
Case 2	1.63E-09	12000	0	1.34E-09	12000	0
Case 3	8.83E-14	12000	0	0.00E+00	12000	0
Case 4	9.54E-12	12000	0	5.75E-12	12000	0
Case 5	2.60E-14	12000	0	0.00E+00	12000	0
Case 6	4.12E-12	12000	0	1.76E-12	12000	0
Case 7	2.58E-13	12000	0	0.00E+00	12000	0

Table 4.9. Predicted Peak Tc-99 Aqueous Concentrations (Ci/L) and Arrival Time (yr) Summary

Case	Groundwater		Fence Line		Exclusion Boundary (south)		Columbia River (south)	
	Conc.	Time	Conc.	Time	Conc.	Time	Conc.	Time
Case 1	5.78E-08	2060	5.46E-08	2062	4.64E-12	2352	1.33E-12	2432
Case 2	6.82E-08	2059	6.50E-08	2060	5.36E-12	2347	1.54E-12	2428
Case 3	6.57E-10	8562	6.57E-10	8608	1.04E-13	8399	2.65E-14	8968
Case 4	6.77E-09	4037	6.77E-09	4043	1.07E-12	4321	2.72E-13	4402
Case 5	1.47E-09	4893	1.47E-09	4899	2.32E-13	5178	5.90E-14	5259
Case 6	6.78E-09	4045	6.78E-09	4051	1.07E-12	4341	2.73E-13	4422
Case 7	4.28E-09	4181	4.28E-09	4186	6.76E-13	4465	1.72E-13	4546

Table 4.10. Predicted Peak U-238 (K_d = 0.01) Aqueous Concentrations (Ci/L) and Arrival Time (yr) Summary

Case	Groundwater		Fence Line		Exclusion Boundary (south)		Columbia River (south)	
	Conc.	Time	Conc.	Time	Conc.	Time	Conc.	Time
Case 1	3.08E-08	2063	2.86E-08	2066	2.85E-12	2384	8.05E-13	2470
Case 2	3.99E-08	2061	3.73E-08	2063	3.47E-12	2378	9.90E-13	2464
Case 3	6.57E-10	9683	6.57E-10	9729	1.08E-13	9252	2.77E-14	10083
Case 4	5.62E-09	4353	5.62E-09	4360	9.25E-13	4661	2.37E-13	4748
Case 5	1.40E-09	5336	1.40E-09	5343	2.31E-13	5645	5.90E-14	5732
Case 6	5.62E-09	4368	5.62E-09	4375	9.25E-13	4688	2.37E-13	4775
Case 7	3.66E-09	4517	3.66E-09	4523	6.03E-13	4824	1.54E-13	4912

Table 4.11. Predicted Peak U-238 (K_d = 0.03) Aqueous Concentrations (Ci/L) and Arrival Time (yr) Summary

Case	Groundwater		Fence Line		Exclusion Boundary (south)		Columbia River (south)	
	Conc.	Time	Conc.	Time	Conc.	Time	Conc.	Time
Case 1	6.82E-09	2075	6.22E-09	2082	8.48E-13	2454	2.34E-13	2550
Case 2	1.04E-08	2068	9.39E-09	2072	1.16E-12	2443	3.25E-13	2540
Case 3	6.57E-10	11636	6.57E-10	11691	1.17E-13	11015	3.00E-14	11408
Case 4	4.31E-09	4997	4.31E-09	5005	7.64E-13	5351	1.96E-13	5451
Case 5	1.26E-09	6208	1.26E-09	6217	2.24E-13	6562	5.75E-14	6663
Case 6	4.29E-09	5026	4.29E-09	5035	7.61E-13	5392	1.95E-13	5492
Case 7	2.96E-09	5192	2.96E-09	5201	5.25E-13	5546	1.35E-13	5646

Table 4.12. Predicted Peak U-238 (K_d = 0.10) Aqueous Concentrations (Ci/L) and Arrival Time (yr) Summary

Case	Groundwater		Fence Line		Exclusion Boundary (south)		Columbia River (south)	
	Conc.	Time	Conc.	Time	Conc.	Time	Conc.	Time
Case 1	2.07E-09	5533	2.07E-09	5550	4.48E-13	6050	1.16E-13	6196
Case 2	2.06E-09	5435	2.06E-09	5452	4.47E-13	5951	1.16E-13	6097
Case 3	6.55E-10	12000	6.55E-10	12000	1.41E-13	12000	3.66E-14	12000
Case 4	2.32E-09	7225	2.32E-09	7242	5.03E-13	7742	1.31E-13	7888
Case 5	9.36E-10	9170	9.36E-10	9186	2.03E-13	9687	5.26E-14	9833
Case 6	2.30E-09	7305	2.30E-09	7322	4.98E-13	7834	1.29E-13	7979
Case 7	1.74E-09	7543	1.74E-09	7561	3.77E-13	8061	9.78E-14	8206

Table 4.13. Predicted Peak U-238 (K_d = 0.30) Aqueous Concentrations (Ci/L) and Arrival Time (yr) Summary

Case	Groundwater		Fence Line		Exclusion Boundary (south)		Columbia River (south)	
	Conc.	Time	Conc.	Time	Conc.	Time	Conc.	Time
Case 1	1.00E-09	11534	1.00E-09	11574	2.96E-13	12000	7.54E-14	12000
Case 2	1.00E-09	11486	1.00E-09	11524	2.97E-13	12000	7.60E-14	12000
Case 3	1.10E-10	12000	1.07E-10	12000	1.48E-14	12000	2.92E-15	12000
Case 4	8.03E-10	12000	7.93E-10	12000	1.58E-13	12000	3.50E-14	12000
Case 5	1.43E-10	12000	1.39E-10	12000	1.98E-14	12000	3.96E-15	12000
Case 6	7.41E-10	12000	7.31E-10	12000	1.38E-13	12000	3.00E-14	12000
Case 7	5.16E-10	12000	5.07E-10	12000	8.71E-14	12000	1.83E-14	12000

Table 4.14. Predicted Peak U-238 (K_d = 0.60) Aqueous Concentrations (Ci/L) and Arrival Time (yr) Summary

Case	Groundwater		Fence Line		Exclusion Boundary (south)		Columbia River (south)	
	Conc.	Time	Conc.	Time	Conc.	Time	Conc.	Time
Case 1	2.99E-11	12000	2.80E-11	12000	1.84E-15	12000	2.47E-16	12000
Case 2	2.91E-11	12000	2.72E-11	12000	1.74E-15	12000	2.30E-16	12000
Case 3	7.15E-14	12000	6.25E-14	12000	6.58E-19	12000	4.08E-20	12000
Case 4	1.71E-12	12000	1.52E-12	12000	2.62E-17	12000	2.02E-18	12000
Case 5	6.66E-14	12000	5.84E-14	12000	6.52E-19	12000	4.15E-20	12000
Case 6	1.10E-12	12000	9.77E-13	12000	1.44E-17	12000	1.06E-18	12000
Case 7	3.23E-13	12000	2.82E-13	12000	2.70E-18	12000	1.64E-19	12000

Table 4.15. Predicted Peak U-238 (K_d = 1.00) Aqueous Concentrations (Ci/L) and Arrival Time (yr) Summary

Case	Groundwater		Fence Line		Exclusion Boundary (south)		Columbia River (south)	
	Conc.	Time	Conc.	Time	Conc.	Time	Conc.	Time
Case 1	1.33E-14	12000	1.10E-14	12000	2.35E-20	12000	1.90E-22	12000
Case 2	1.07E-14	12000	8.78E-15	12000	1.48E-20	12000	3.75E-23	12000
Case 3	5.80E-19	12000	0.00E+00	12000	0.00E+00	12000	0.00E+00	12000
Case 4	6.26E-17	12000	3.78E-17	12000	0.00E+00	12000	0.00E+00	12000
Case 5	1.71E-19	12000	0.00E+00	12000	0.00E+00	12000	0.00E+00	12000
Case 6	2.71E-17	12000	1.16E-17	12000	0.00E+00	12000	0.00E+00	12000
Case 7	1.70E-18	12000	0.00E+00	12000	0.00E+00	12000	0.00E+00	12000

4.8 Solute Mass Balance

Mass balance checks were performed on the seven solutes (Tc-99 and U-238 with different values of K_d) for each simulation case at year 12000 using this expression:

$$m_{error} = \frac{m_{released} - m_{domain} - m_{exit}}{m_{released}} \times 100\% \tag{4.1}$$

where m_{error} is the mass balance error in percent, $m_{released}$ is the total amount of solute released in the system, m_{domain} is the solute inventory in the domain computed from the STOMP plot-file output at year 12000, and m_{exit} is the integrated solute inventory, leaving the computational domain computed from the STOMP surface-flux output. The amount of each solute released into the system was one curie except for the case that involved slow releases (Case 3, with Tc-99 at 0.945 Ci). The solute mass leaving the computational domain through the aquifer was determined using surface-flux output on the eastern side of the domain. The surface-flux output provided both the solute-flux rate and cumulative mass. Other than solving the solute mass conservation equations, the STOMP simulator contains no algorithms for correcting local or global mass. Therefore, mass balance errors represent the actual mass balance errors from the conservation equations. Expressed as percent error, mass balance errors were small, no more than 0.0422%, as shown in Tables 4.16–4.22 for the seven contaminants.

Table 4.16. STOMP Mass Balance for Tc-99 at Year 12000

Case	Released	Domain	Exit	% Error
Case 1	1.000000E+00	0.000000E+00	9.999359E-01	6.407499E-03
Case 1_3d	1.000000E+00	0.000000E+00	9.995779E-01	4.221201E-02
Case 2	1.000000E+00	0.000000E+00	9.999604E-01	3.957748E-03
Case 3	9.455000E-01	1.784388E-01	7.671016E-01	-4.270983E-03
Case 4	1.000000E+00	0.000000E+00	9.999994E-01	5.960465E-05
Case 5	1.000000E+00	1.001591E-01	8.998527E-01	-1.178682E-03
Case 6	1.000000E+00	0.000000E+00	9.999995E-01	4.768372E-05
Case 7	1.000000E+00	3.678298E-02	9.632211E-01	-4.049391E-04

Table 4.17. STOMP Mass Balance for U-238 (K_d = 0.01) at Year 12000

Case	Released	Domain	Exit	% Error
Case 1	1.000000E+00	0.000000E+00	1.000021E+00	-2.098084E-03
Case 1_3d	1.000000E+00	0.000000E+00	9.998392E-01	1.608133E-02
Case 2	1.000000E+00	0.000000E+00	1.000010E+00	-1.001358E-03
Case 3	9.455000E-01	2.129143E-01	7.326260E-01	-4.266255E-03
Case 4	1.000000E+00	0.000000E+00	9.999995E-01	4.768372E-05
Case 5	1.000000E+00	1.119456E-01	8.880677E-01	-1.327694E-03
Case 6	1.000000E+00	0.000000E+00	9.999996E-01	4.172325E-05
Case 7	1.000000E+00	4.067994E-02	9.593245E-01	-4.421920E-04

Table 4.18. STOMP Mass Balance for U-238 (K_d = 0.03) at Year 12000

Case	Released	Domain	Exit	% Error
Case 1	1.000000E+00	4.952515E-10	1.000028E+00	-2.801468E-03
Case 1_3d	1.000000E+00	3.258163E-11	9.999461E-01	5.388257E-03
Case 2	1.000000E+00	3.816728E-10	1.000030E+00	-3.004112E-03
Case 3	9.455000E-01	2.818880E-01	6.636525E-01	-4.274135E-03
Case 4	1.000000E+00	1.613652E-08	9.999994E-01	5.799099E-05
Case 5	1.000000E+00	1.521518E-01	8.478648E-01	-1.658499E-03
Case 6	1.000000E+00	1.754794E-08	9.999994E-01	5.784985E-05
Case 7	1.000000E+00	5.310711E-02	9.468984E-01	-5.513430E-04

Table 4.19. STOMP Mass Balance for U-238 (K_d = 0.10) at Year 12000

Case	Released	Domain	Exit	% Error
Case 1	1.000000E+00	2.439826E-04	9.997479E-01	8.145071E-04
Case 1_3d	1.000000E+00	3.643207E-04	9.995986E-01	3.705695E-03
Case 2	1.000000E+00	2.136437E-04	9.997793E-01	7.072333E-04
Case 3	9.455000E-01	5.231187E-01	4.224195E-01	-4.040886E-03
Case 4	1.000000E+00	2.502217E-03	9.974986E-01	-7.883646E-05
Case 5	1.000000E+00	3.751994E-01	6.248353E-01	-3.466010E-03
Case 6	1.000000E+00	2.929200E-03	9.970719E-01	-1.121545E-04
Case 7	1.000000E+00	1.295975E-01	8.704160E-01	-1.345575E-03

Table 4.20. STOMP Mass Balance for U-238 (K_d = 0.30) at Year 12000

Case	Released	Domain	Exit	% Error
Case 1	1.000000E+00	5.205730E-01	4.794770E-01	-5.000830E-03
Case 1_3d	1.000000E+00	6.183521E-01	3.817684E-01	-1.204610E-02
Case 2	1.000000E+00	5.138358E-01	4.862137E-01	-4.950166E-03
Case 3	9.455000E-01	9.287739E-01	1.672949E-02	-3.547989E-04
Case 4	1.000000E+00	8.192483E-01	1.807939E-01	-4.221499E-03
Case 5	1.000000E+00	9.775604E-01	2.244459E-02	-4.991889E-04
Case 6	1.000000E+00	8.426248E-01	1.574140E-01	-3.884733E-03
Case 7	1.000000E+00	9.034491E-01	9.657618E-02	-2.529472E-03

Table 4.21. STOMP Mass Balance for U-238 (K_d = 0.60) at Year 12000

Case	Released	Domain	Exit	% Error
Case 1	1.000000E+00	9.962226E-01	3.775201E-03	2.183719E-04
Case 1_3d	1.000000E+00	9.987555E-01	1.216496E-03	2.804899E-03
Case 2	1.000000E+00	9.963777E-01	3.619050E-03	3.243564E-04
Case 3	9.455000E-01	9.454935E-01	4.497585E-06	2.114565E-04
Case 4	1.000000E+00	9.998716E-01	1.258133E-04	2.575107E-04
Case 5	1.000000E+00	9.999926E-01	4.263183E-06	3.127793E-04
Case 6	1.000000E+00	9.999191E-01	7.780117E-05	3.141940E-04
Case 7	1.000000E+00	9.999779E-01	1.990575E-05	2.207573E-04

Table 4.22. STOMP Mass Balance for U-238 (K_d = 1.00) at Year 12000

Case	Released	Domain	Exit	% Error
Case 1	1.000000E+00	9.999968E-01	8.748596E-07	2.284187E-04
Case 1_3d	1.000000E+00	9.999822E-01	5.670928E-08	1.776508E-03
Case 2	1.000000E+00	9.999970E-01	6.784610E-07	2.361376E-04
Case 3	9.455000E-01	9.454988E-01	0.000000E+00	1.323847E-04
Case 4	1.000000E+00	9.999992E-01	1.240519E-09	8.332245E-05
Case 5	1.000000E+00	9.999999E-01	0.000000E+00	5.960465E-06
Case 6	1.000000E+00	9.999986E-01	2.047563E-10	1.430307E-04
Case 7	1.000000E+00	9.999987E-01	0.000000E+00	1.311302E-04

5.0 Numerical Groundwater Transport Modeling Results

This section describes the two types of simulations performed with the 3-D numerical aquifer model of the Hanford Site. The first simulation was for a point source case that determined peak concentrations at the compliance boundaries and their respective travel times. This analysis was carried out to determine velocities needed as input to the analytical streamtube model (reported in Tables 4.9 through 4.15). A second set of simulations was performed to check the analytical groundwater transport results in Section 4. These simulations used a 3-D numerical aquifer model of the Hanford Site for two cases selected to represent two important closure assessment scenarios for the S-SX Tank Farm: 1) the 8,000-gal water line leak (Case 2) and 2) the residual waste source with a solubility-dominated release (Case 6). While the analytical model was used to predict concentrations of U-238 and Tc-99, the numerical model simulations were conducted only for Tc-99 to yield the most conservative concentration estimates. Model comparisons were made at two locations that included the exclusion and river boundaries.

The SGM is the 3-D numerical groundwater flow and contaminant transport process model used in this study for comparison with the analytical model results. The SGM is a 3-D finite element model based on the Coupled Fluid, Energy, and Solute Transport (CFEST-96) code (Gupta et al. 1987; Gupta 1996). This model and its conceptual basis are fully described in Wurstner et al. (1995) and Cole et al. (1997). They were most recently used in the Hanford Site Composite Analysis (Cole et al. 1997; Kincaid et al. 1998; Bergeron et al. 2001) and ILAW Performance Assessment (Bergeron and Wurstner 2000; Mann et al. 2001). Cole et al. (2001) contains a complete discussion of the uncertainties in the conceptual model as they are currently understood.

In the proceeding sections, the SGM that was implemented in this analysis is described. This is followed by a description of the point source simulation and how the results were used to obtain travel times (i.e., velocities) for the analytical streamtube model. In the final sections, numerical modeling results are presented and compared with the results obtained with the analytical streamtube model.

5.1 The Site-Wide Groundwater Model (SGM)

Although a CFEST SGM was also used in the S-SX FIR (White et al. 2001), major differences exist between S-SX FIR SGM and that used in the current analysis. First, the model in this work was calibrated within an uncertainty framework (Cole et al. 2001). Recalibrating the model enabled significant improvements to be made in simulating historical trends in water table changes over the entire site (Cole et al. 2001). This newer baseline model, which included a new interpretation of the top of basalt near Gable Butte and Gable Mountain, was also used in the B-BX-BY FIR (Freedman et al. 2002).

Another major difference between SGM used in the S-SX FIR and the one used in the current analysis is the grid that represents the Hanford Site. In the S-SX FIR, a progressive grid refinement procedure was used that began with a 375-m transport grid that was developed for the Composite Analysis (CA) (Kincaid et al. 1998). For this work, the new baseline model is implemented with a refined grid also based on the CA grid. This grid maintains a750 m spacing in the southern and western areas of the site (Figure 5.1), but the majority of the central plateau is discretized into 249 m units. The 200 West Area is further refined into 83 m nodal spacing.

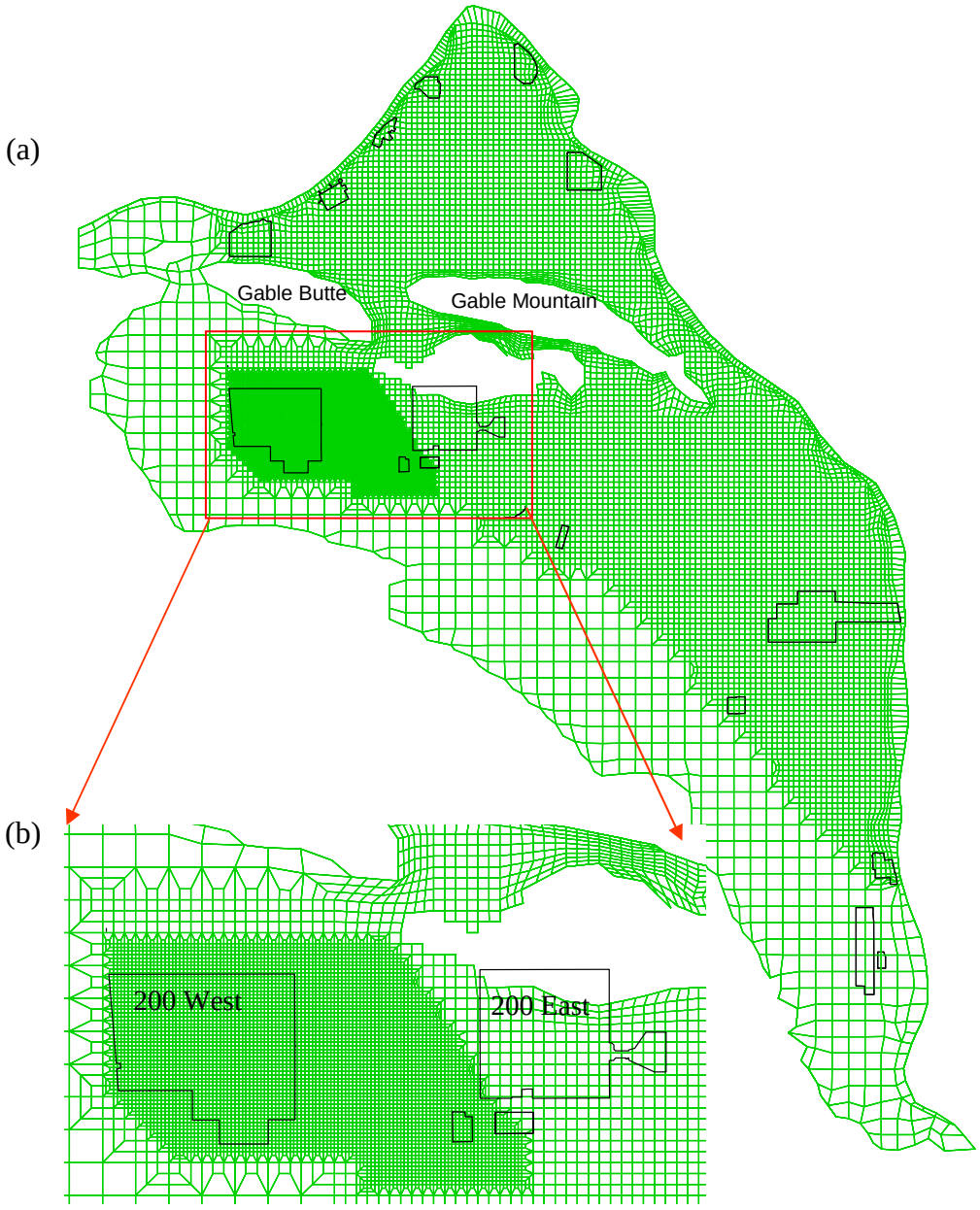

Figure 5.1. a) Refined Composite Analysis Grid (red square denotes area of smallest grid refinement); b) 200 Areas with 83 m Nodal Spacing in 200 West and 249 m in 200 East

Current field data indicate that for post-Hanford operations, the dissipation of the groundwater mounds in the 200 Areas causes flow to be cut off through the gap between Gable Butte and Gable Mountain. This reduction in flow is caused by basalt outcrops that impede flow when the water table is lowered. As a result, groundwater flows predominately in an easterly direction toward the Columbia River. To simulate this flow behavior in the S-SX FIR modeling, grid nodes were deleted that completely cut off northerly flow through the gap (White et al. 2001). In the current analysis, nodes were also deleted in the gap, but their removal was based on a new interpretation of the location of the basalt

outcrops for post-Hanford conditions (Figure 5.2). Although the deletion of grid nodes significantly reduced northward flow, a small amount of groundwater still trickled through the gap.

Despite differences in the description of flow between the models used in the S-SX FIR and the model used in this analysis, several important similarities still exist. For example, the nine major hydro-geologic units described in the prior model (Cole et al. 2001; White et al. 2001) are the same as those used in the current model. Seven of the primary units are illustrated in Figure 5.3 (Hartman 2000). Recharge and aquifer boundaries were also similar in the two models.

As in the S-SX FIR effort, this analysis involves steady-state flow with transient transport. This setup represents future "Post-Hanford" conditions with no artificial recharge, when the effects of the disposal mounds from Hanford operations have ceased.

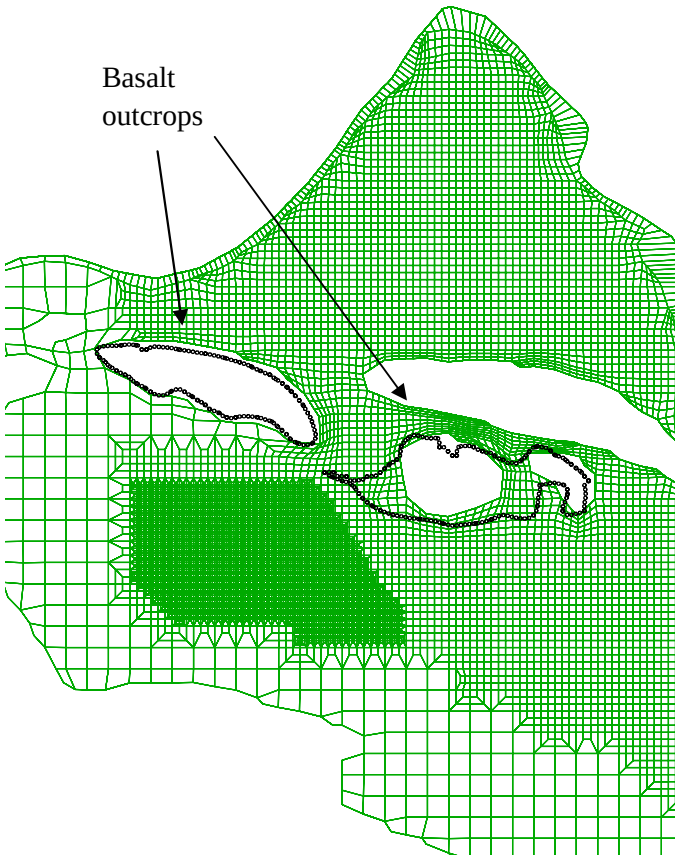

Figure 5.2. New Interpretation of Basalt Outcrop Locations for Post-Hanford Operation Flow Conditions (outlined in black) (nodes within black outlines were deleted from grid)

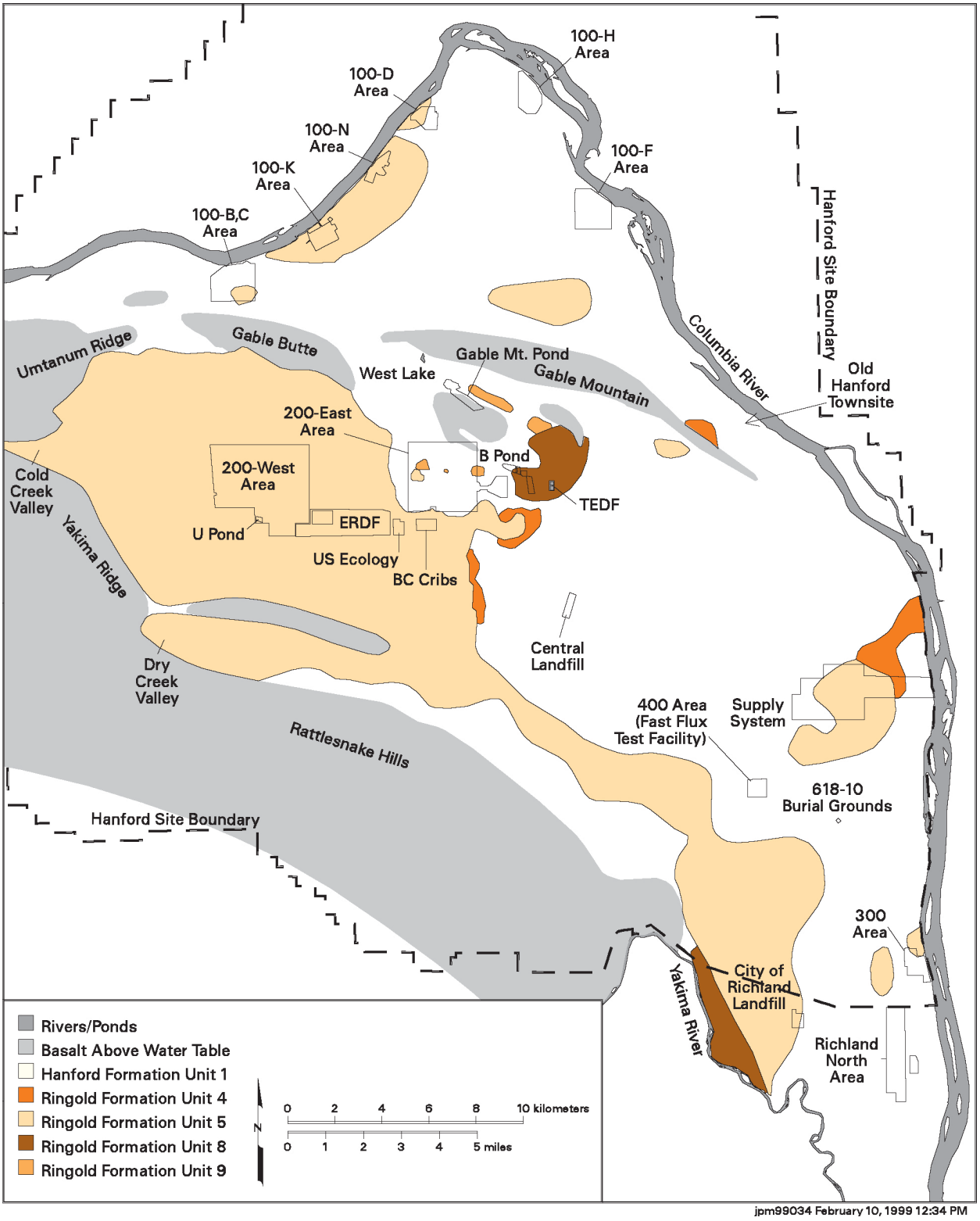

Figure 5.3. Map of SGM Hydrogeologic Units Containing the Water Table in March 1999 (Hartman 2000)

5.2 Flow and Transport Parameters for the SGM

To model groundwater flow, the distribution of hydraulic properties, including both horizontal and vertical hydraulic conductivity and porosity, were required for each hydrogeologic unit defined in the model. The procedure used to calibrate the current detailed process model is described in Cole et al. (2001). The resulting hydraulic conductivity distribution determined for the upper part of the aquifer is provided in Figure 5.4.

To simulate movement of contaminant plumes, the required transport properties include contaminant-specific distribution coefficients, bulk density, effective porosity, and the longitudinal and transverse dispersivities (α_l and α_t) that are the components of the dispersion tensor generally used to represent dispersion in a porous media that is isotropic with respect to dispersivity. As described in White et al. (2001), several difficulties are associated with determining appropriate values of dispersivity at the site-wide scale. Although dispersivity is often determined by inverse modeling of onsite tracer test break-through curves, no field tests have been conducted at the Hanford Site to develop an estimate for this parameter at the scale of transport appropriate for the SGM.

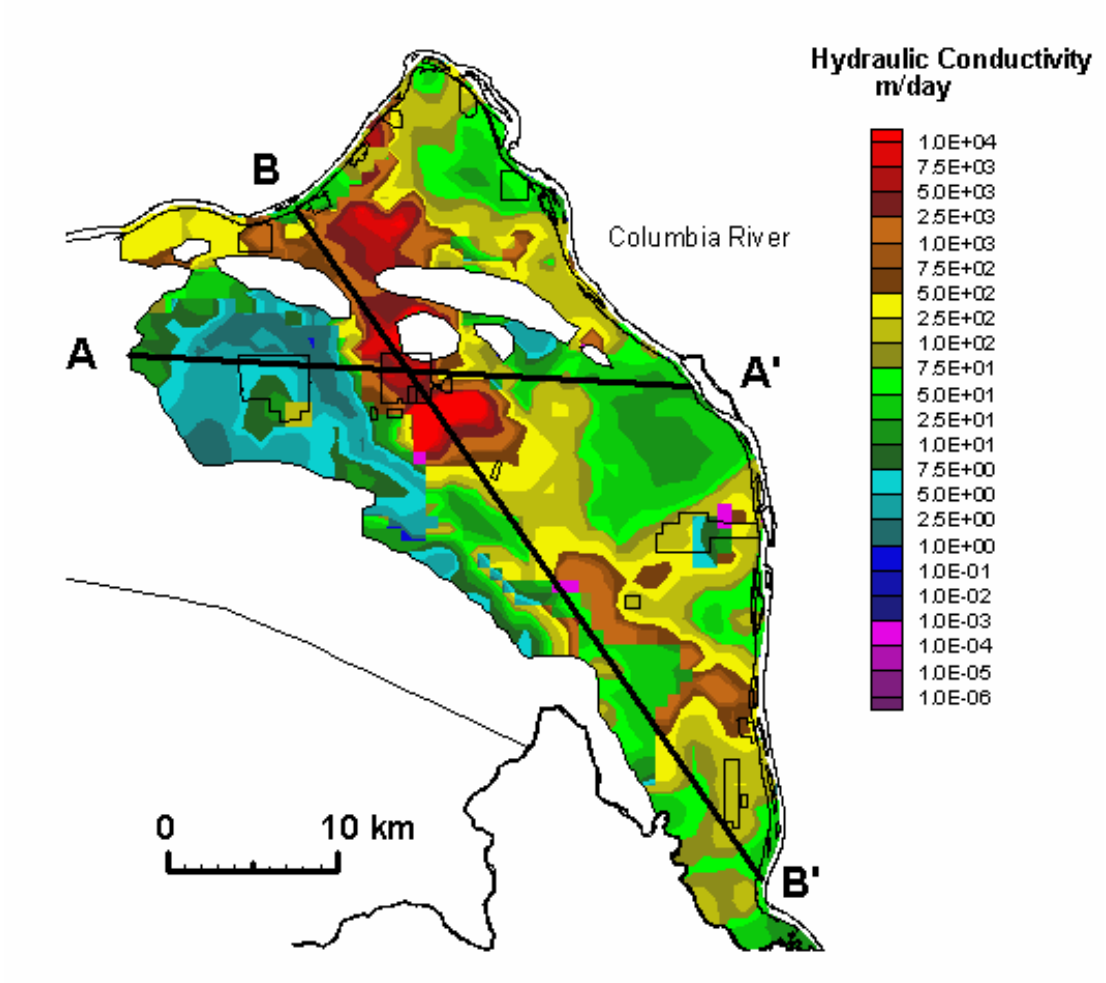

Figure 5.4. Hydraulic Conductivity Distribution (Cole et al. 2001)

Dispersivity is likely to vary across the Site depending on the degree of heterogeneity and the temporal variability of flow gradients. In the CA, uniform dispersivity values (e.g., longitudinal dispersivity, α_l = 95 m and transverse dispersivity, α_t = 19 m) were used. With the finer mesh used in the current model, dispersivities were reduced to satisfy the grid Peclet number. In the 200 West Area, the area of greatest refinement, a longitudinal dispersivity of 30 m and a transverse dispersivity of 6 m were used for the Ringold Formation. For the other units, a 62.5 m longitudinal dispersivity and a 12.5 m transverse dispersivity were implemented.

In the area of greatest grid refinement for the 200 West Area, dispersivities in the S-SX FIR were the same as those used in the current model. However, for areas outside the refinement area in 200 West, the S-SX FIR used the dispersivities implemented with the CA (White et al. 2001).

5.3 Flow and Transport Parameters for the Streamtube Model

A CFEST simulation of the SGM was used to determine solute transport velocities for the analytical streamtube model described in Section 3.8. To this end, a unit point source (1 Ci) simulation was performed to determine velocities, dispersivities, and travel distances to the downstream compliance points (the exclusion boundary and the Columbia River). Using a steady-state flow field to represent post-Hanford conditions, a unit source was injected as a pulse over a single time step into two surface nodes at the S Tank Farm (Figure 5.5). A 500-year transient transport simulation was carried out using one-year time steps.

To determine average flow velocities, the peak concentrations were determined at each of the downstream compliance boundaries. The arrival time of the peak concentrations at the compliance boundaries was assumed to be the travel time from the source. The travel distance was then determined using streamlines generated by Tecplot.[(a)] Figure 5.5 shows the red markers on the streamtrace that were used to calculate travel distances. Because of the circuitous nature of flow, the flow path distance was greater than the straight line distance. The flow velocity was then calculated using the time and distance data. Table 5.1 shows the peak concentrations and peak arrival times resulting from the unit source simulation. The travel distances and velocities determined from the unit source analysis are in Table 5.2. Also shown in Table 5.2 are the CFEST dispersivities that were used as inputs to the streamtube model.

As a test of the analytical model's ability to emulate the transport behavior of the CFEST-based SGM, Eq. 3.18 was also solved using a unit point source concentration and the dispersivities and average velocities shown in Table 5.2. MATHCAD[(b)] software was used to generate the breakthrough curves in Figure 5.6, which shows that the peak arrival times (276 years to the exclusion boundary and 358 years to the Columbia River) predicted by the SGM are also predicted by the analytical model (273 years to the exclusion boundary and 357 years to the Columbia River). However, peak concentrations using the analytical (MATHCAD) model relative to the CFEST SGM are 4.3 times higher at the exclusion boundary and 2.5 times higher at the Columbia River (Table 5.1). This result occurs because of

(a) Tecplot Version 10.0, Tecplot, Inc., Bellevue, WA.
(b) MATHCAD 2001i, Mathsoft Engineering & Education, Inc., Cambridge, MA.

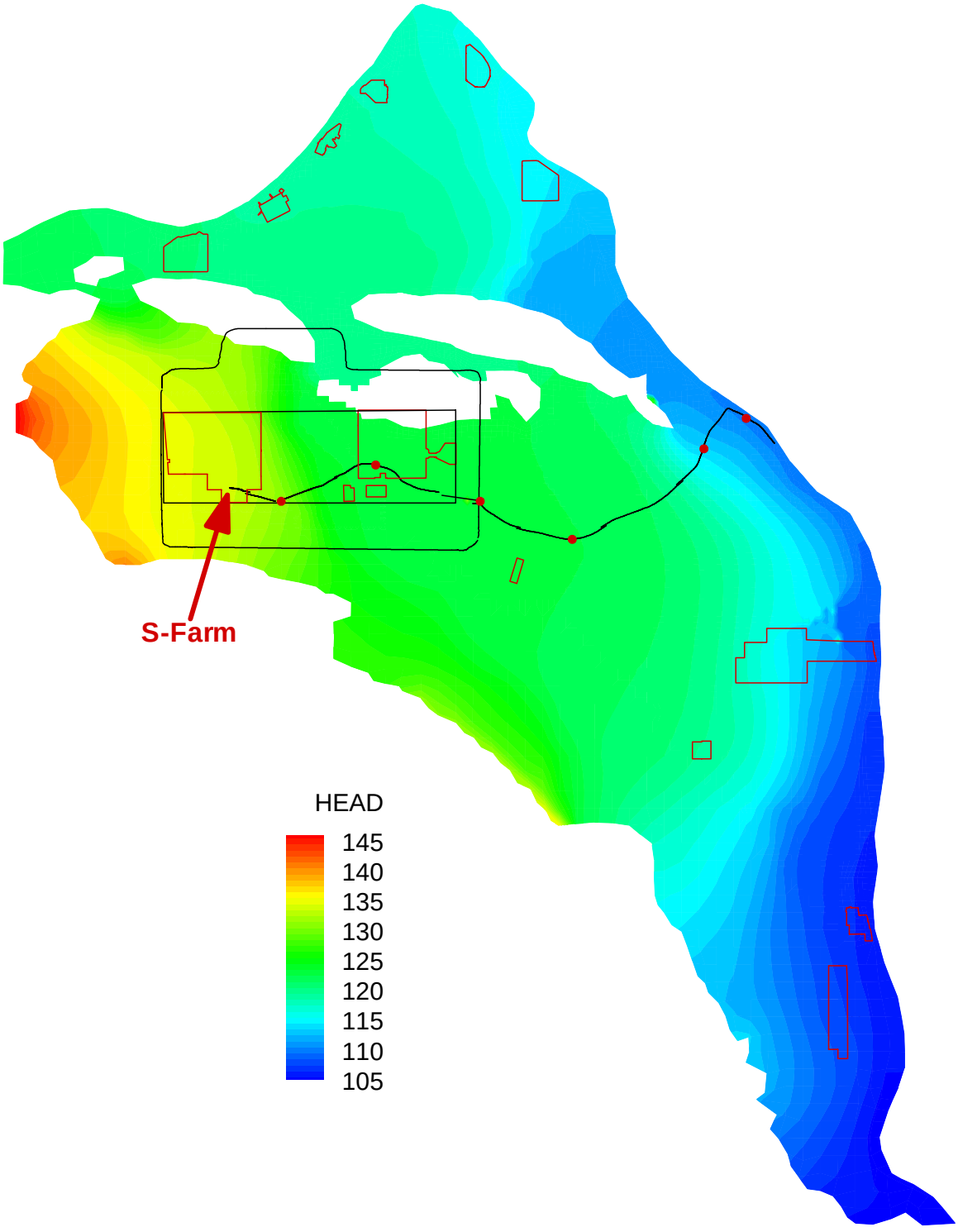

Figure 5.5. Post-Hanford Operations, Steady-State Potentiometric Surface for the SGM, and a Streamtrace Along the Peak Concentration Pathway. Red markers on streamtrace indicate points along which the travel distances were computed.

Table 5.1. Peak Concentrations and Arrival Times with a Unit Point Source for the CFEST-based SGM and the Analytical Model (MATHCAD)

Tc–99 Conc.	Exclusion Boundary		Columbia River	
	Time (yr)	Conc. (Ci/L)	Time (yr)	Conc. (Ci/L)
Analytical (MATHCAD)	273	1.50E-11	357	4.77E-12
SGM (CFEST)	276	3.51E-12	358	1.89E-12

Table 5.2 Travel Distances, Dispersivities, and Average Velocities for the Streamtube Model

Compliance Points	Distance (km)	Velocity (m/yr)	Longitudinal Dispersivity (m)	Transverse Dispersivity (m)	Vertical Dispersivity (m)
Exclusion Boundary	10.936	39.4	62.5	12.5	0.0002
Columbia River	32.723	90.4	62.5	12.5	0.0002

a)

b)

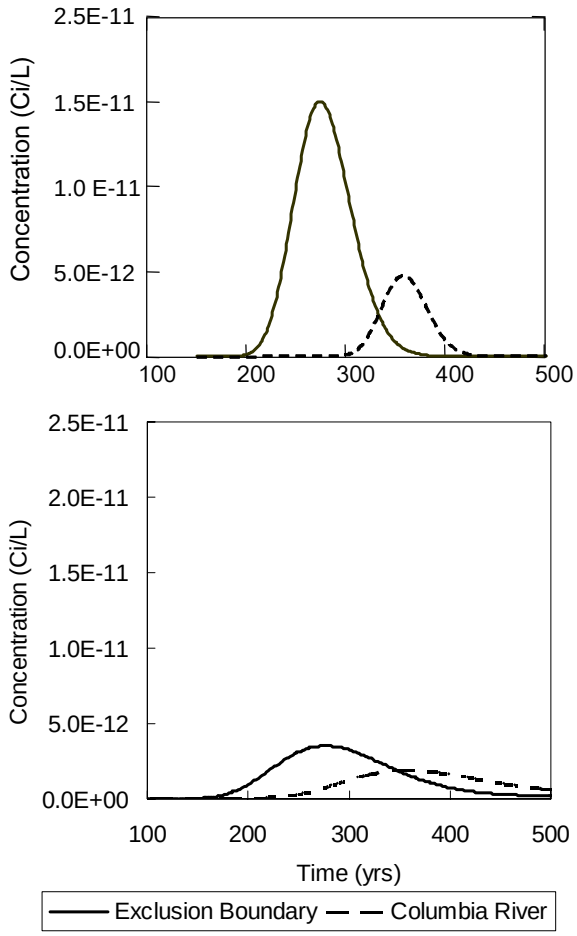

Figure 5.6. Breakthrough Curves for Unit Point Source Release (1 Ci) at Exclusion and Columbia River Boundaries Using a) Analytical Model (MATHCAD) and b) CFEST-Based SGM

differences in advective transport between the two models, and is observed in the wider peaks demonstrated by the SGM breakthrough curves in Figure 5.6 relative to those of the analytical model. For example, in the one-dimensional analytical model, advective transport occurred in only one direction, whereas in the SGM, it occurred in all three dimensions. Moreover, advective transport in the analytical model did not account for any heterogeneity. Hence, concentrations predicted by the SGM are more dilute than the concentrations predicted by the analytical model.

5.4 Modeling Results

The same 3-D transient groundwater flow system was used for Tc-99 transport modeling for both Cases 2 and 6. The only differences between these two cases were the release modes of the unit Tc-99 source. For Case 2, the Tc-99 was released over a period of 14 days with the water line leak of 8,000 gallons. For Case 6, no water line leak existed, and the release of Tc-99 was controlled by the solubility of the salt-cake in the tank.

5.4.1 Case 2: Water Line Leak

To simulate the contaminant release in the 8,000-gallon water line leak of Case 2, STOMP mass fluxes were used as input into the CFEST SGM beginning in the year 2000. Using a steady-state flow field to represent post-Hanford conditions, the annual mass fluxes from STOMP were injected as dry mass into two surface nodes at the S Tank Farm. Tc-99 transport was simulated for 600 years using 1-year timesteps.

Figure 5.7 shows the breakthrough curves predicted by the CFEST SGM at the exclusion and Columbia River boundaries. Figure 5.8 illustrates the plan view concentration contours at the water table

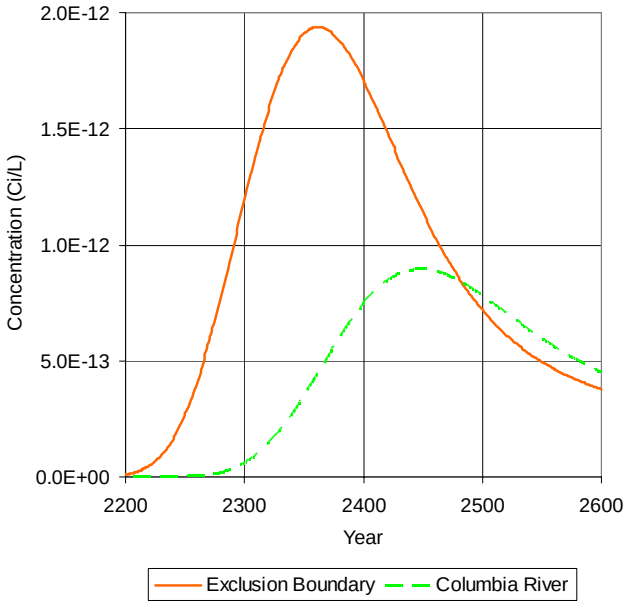

Figure 5.7. Breakthrough Curves Simulated by CFEST SGM for Case 2 at Both Exclusion and Columbia River Compliance Boundaries

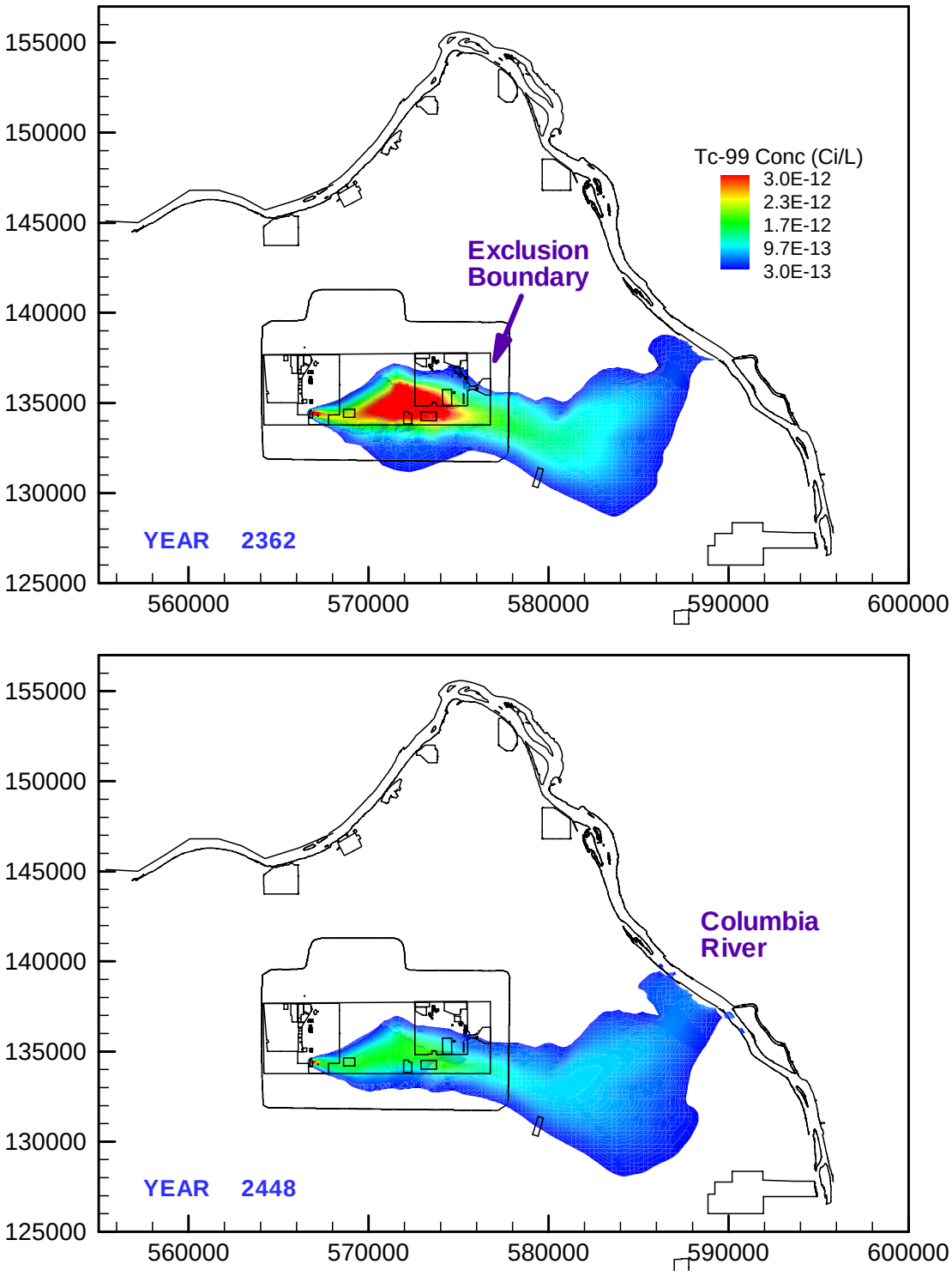

Figure 5.8. Composite SGM Results for Case 2, Illustrating Plan-View Concentration Contours when Concentrations Occurred at Exclusion Boundary (top) and Columbia River (bottom)

when the peak concentration occurred at the exclusion boundary and the Columbia River. At the downstream compliance points, dilution occurred for both models. As shown in Table 5.3, the peak concentration predicted by the analytical model was 2.8 times higher at the exclusion boundary than the peak predicted by the SGM. At the Columbia River, the SGM predicted a ~54% reduction in the peak concentration relative to its peak at the exclusion boundary, whereas the analytical model peak concentration decreased by ~71%. The peak concentration predicted by the analytical model was only 1.7 times higher than that predicted by the SGM at the Columbia River.

Because the streamtube model was calibrated with parameters from the SGM, its predictions of peak concentrations were fairly similar to those by CFEST but represented more conservative estimates of the peaks. Estimates of the arrival times were also more conservative in the streamtube model but differed only by 15 years at the exclusion boundary and 20 years at the Columbia River.

Table 5.3. Peak Tc-99 Concentrations (Ci/L) at Compliance Points for Case 2

Models	**Exclusion Boundary**		**Columbia River**	
	Time (yr)	Conc (Ci/L)	Time (yr)	Conc. (Ci/L)
Streamtube	2347	5.36E-12	2428	1.54E-12
SGM (CFEST)	2362	1.94E-12	2448	8.96E-13

5.4.2 Case 6: Residual Waste, Solubility-Release Model

To simulate the solubility-controlled release in Case 6, STOMP mass fluxes were used as input to the CFEST SGM beginning in the year 2127, when Tc-99 was predicted to arrive at the fence line. Because of the slow release, the Case 6 simulation was run for 2500 years, using five-year time steps that were subdivided into yearly increments for transport calculations. Hence, the annual mass fluxes from STOMP were averaged over five-year periods and injected as a dry mass into two surface nodes at the S Tank Farm. As in the previous simulations, a steady-state flow field was used to represent post-Hanford conditions.

Figure 5.9 shows BTCs predicted by the CFEST SGM at the exclusion and river boundaries. Figure 5.10 illustrates plan view concentration contours at the water table when the peak concentration occurred at the exclusion boundary and river. Although contaminant release was much slower than in Case 2, the behavior of the transport model followed similar trends. For example, as shown in Table 5.4, peak concentration predictions at the exclusion boundary simulated by the analytical model were ~1.7 times higher than those simulated by the CFEST model. The peak concentration by the analytical model was followed by a ~75% reduction in peak concentration at the Columbia River compliance boundary but only by ~39% by the CFEST SGM. Consequently, a lower peak concentration was predicted by the analytical streamtube model (~1.4 times) than by the SGM.

Differences in the predicted peak concentration arrival times for the two models were larger than in Case 2. For the exclusion boundary, the analytical model predicted the peak concentration arrival 36

years earlier than the SGM. At the Columbia River, the gap in peak arrival times is even wider, with the analytical streamtube model predicting breakthrough 113 years earlier than the CFEST-based SGM.

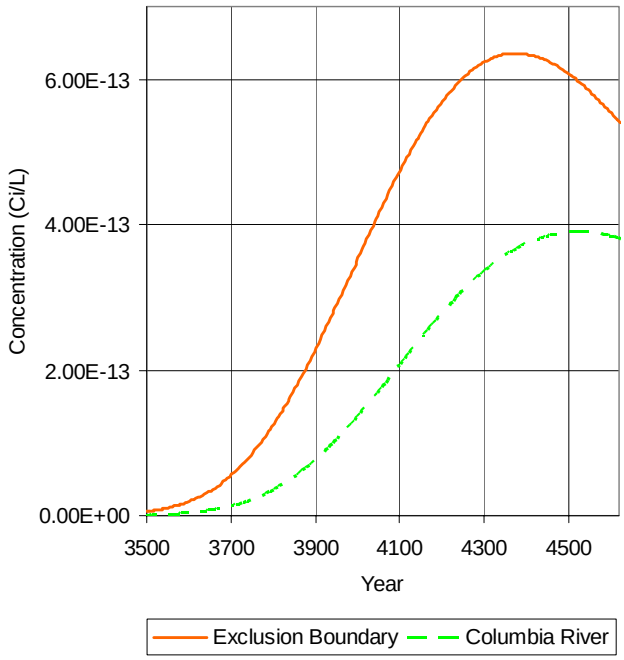

Figure 5.9. BTCs Simulated by CFEST SGM for Case 6 at Exclusion and River Compliance Boundaries

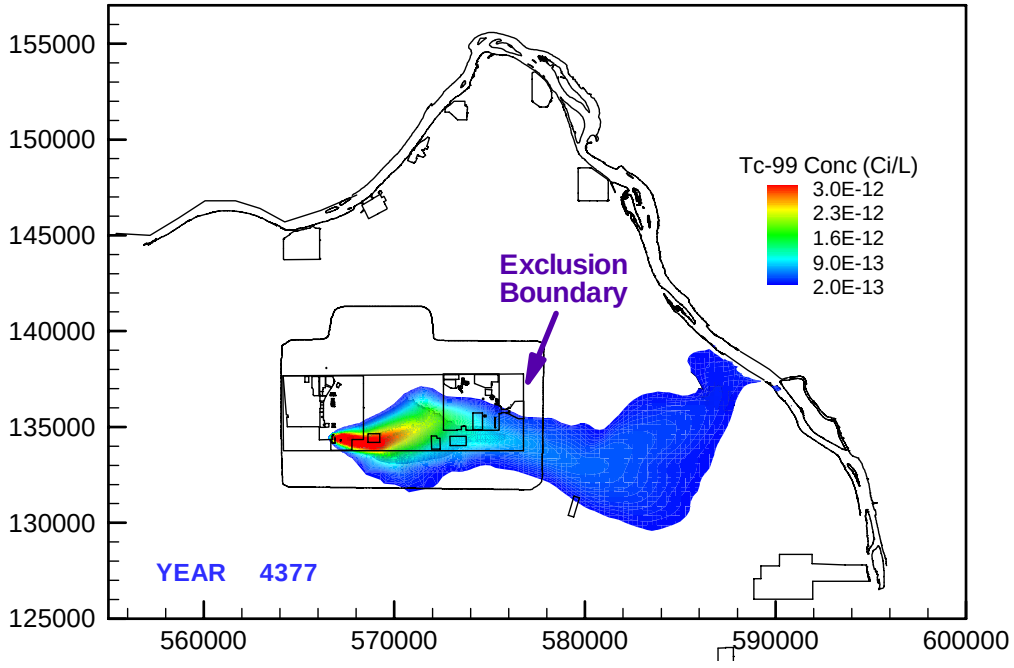

Figure 5.10. Composite SGM Results for Case 6, Illustrating Plan-View Concentration Contours at Times of Peak Concentrations for the Exclusion Boundary

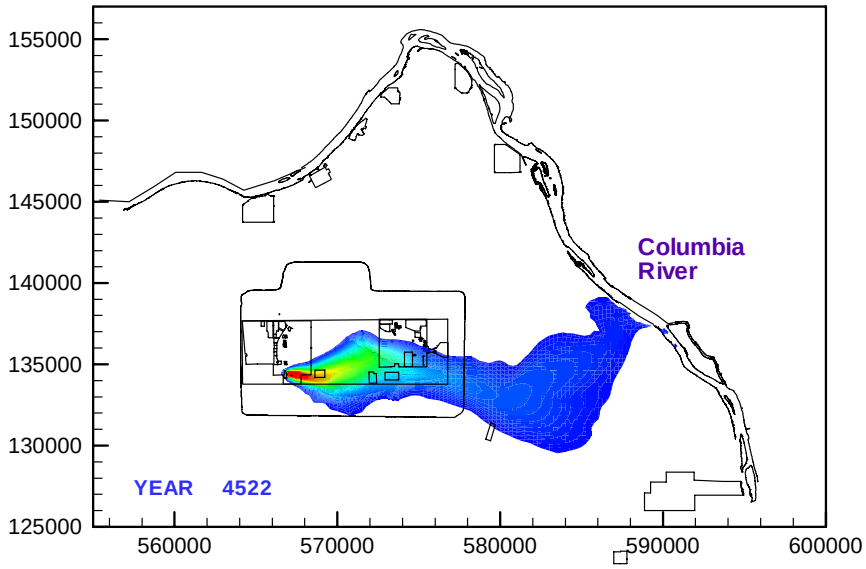

Figure 5.10 (contd). Composite SGM Results for Case 6, Illustrating Plan-View Concentration Contours at Times of Peak Concentrations for Columbia River

Table 5.4. Peak Tc-99 Concentration (Ci/L) at Compliance Points for Case 6

Models	**Exclusion Boundary**		**Columbia River**	
	Time (yr)	Conc (Ci/L)	Time (yr)	Conc. (Ci/L)
Streamtube	4341	1.07E-12	4422	2.73E-13
SGM (CFEST)	4377	6.36E-13	4535	3.90E-13

6.0 Electronic Files

The principal objectives of this investigation were to conduct the simulations and analyses using an open scientific approach and to provide modeling results that could be verified and repeated. In partial fulfillment of these objectives, the source coding for the STOMP simulator, ancillary utilities coding, input files, simulation output files, and converted result files are provided in electronic form with enough detail to enable the reported calculations to be repeated. This section describes the directory structure and contents of the files stored in electronic format.

6.1 Source Coding

Source code for the STOMP simulator is stored in the "stomp_src" directory. Ancillary utilities are stored in the "source" directory. The STOMP source code is in the file "*stomp1_sp.f*" and comprises a main calling routine and subroutines listed in alphabetical order. The STOMP source code was compiled with a FORTRAN 77 compiler and the files "parameters" and "commons." The "parameters" file was dimensioned for all of the simulations. Once compiled, the STOMP simulator must be linked with the "*splib.a*" library configured for a particular compiler. Files and instructions needed to create the "*splib.a*" library are included in the file "*splib.tar.gz*." Brief description of source coding for the various conversion and translations utilities used during these investigations is shown in Table 6.1.

Table 6.1. Source Code Directory

Program Name	Source Code File	Auxiliary Files	Functions
STOMP	stomp1_sp.f	commons, parameters	Simulate both flow and transport in the vadose zone and unconfined aquifer below the tank farm
Complinkit			Shell script to compile stomp1_sp.f and statically link it to splib.a, libblas.a
Total_flux	total_flux.f90		Modify STOMP surface file so that cumulative flux is continuous between stages 1 and 2
Surfcalc	surfcalc.c		Calculate solute concentration at the water table and fenceline
Plot_Tec	plot_tec.f		Convert the STOMP plot files to TecPlot readable format
Combobtcs	combobtcs.c		Combine the concentration data at different compliance points together
Point3d_disp	point3d_disp.f		Simulate transport in an aquifer, point3d_disp_slib.x.2d, point3d_disp_slib.x.3d
Mass_bal	mass_bal.f90		Calculate and tabularize mass balance of each simulation
Peak_conc	peak_conc.f90		Tabularize peak concentrations at each of the compliance points
Peak_flux	peak_flux.f90		Tabularize peak fluxes at each of the water table and the fence line

6.2 Geology

Zonation files to define the rock/soil-type and inactive-node distributions were provided with the MDP (Khaleel and Connelly 2003). These lithologic descriptions were based on inferences drawn from groundwater monitoring wells near the S-SX Tank Farm and from grain size data and supplemented by information from tank farm drywells and excavation (e.g., Price and Fecht 1976a, 1976b). Zonation files are stored in the individual case directories named as either "imperm_tanks.dat" or "perm_tanks.dat." Within the zonation file is information on the inactive nodes that define the tanks and cross-section boundaries. Rock/soil zonation files can be visualized as two-dimensional color-scaled images with Tecplot by opening the layout file for the cross section.

6.3 Steady Flow Simulations

A steady flow simulation was executed to generate initial condition flow fields for each of the transient solute transport simulations. This simulation is found in the "case00" directory and was executed with the STOMP simulator, which produced a "restart" file that described the steady flow field. The input, output, and restart files are catalogued in Table 6.2.

Table 6.2. Steady Flow Initial Condition Files

File Name	Description	File Type
input	STOMP input file	Text
output	STOMP reference-node output file	Text
plot	STOMP plot-file output file	Text
restart	STOMP restart file	Text

6.4 Coupled Vadose Zone and Unconfined Aquifer Modeling

Coupled vadose zone and unconfined aquifer modeling files are stored in directories named according to case number (e.g., directory case02 holds files associated with the Case 2 simulations). Verification case directories are identified with a "v" appended to the case number (e.g., case05v). The three-dimensional simulation case is identified with a "_3d" appended to the case number (i.e., case01_3d). Within all these directories are subdirectories for the three stages of the simulations, "1952to2050," "2050to12000," and "additional." These subdirectories hold input files, zonation files, reference-node output files, plot-file output files, and surface-flux output files. Also within the case directories are subdirectories containing converted plot-file output, Tecplot layout files, solute concentration and mass flux data files, and image files. The "btc" subdirectory contains files of timeseries output and the flux and concentration timeseries graph files in encapsulated postscript (*.eps) and portable network graphics (*.png) formats. The "tecplot" subdirectory contains Tecplot data files (*.plt), and *.eps, *.png files of the cross-section contour plots at the simulation domain.

Table 6.3. Coupled Vadose Zone and Unconfined Aquifer Modeling Files

File Name	Description	File Type
Input	STOMP simulator input	Text
Output	STOMP simulator reference-node output	Text
fn.srf	STOMP simulator surface-flux output	Text
*fn*_tot.srf	Modified STOMP simulator surface-flux output so that the cumulative flux is continuous between stages 1 and 2	Text
yr.plt	Tecplot data file at time *yr*	Tecplot binary
*yr_type_*.eps	Tecplot graph showing concentration or saturation profiles at distinct points in time	Text
*yr_type_*.png	Image file showing concentration or saturation profiles at distinct points in time (generated with convert – density 200x200 *eps *png)	Image
prepsurf_fenceline.csh, prepsurf_gwtable.csh	C-Shell script for computing BTCs at the fence line or groundwater table, respectively (executes Surfcalc for each contaminant)	Text
all_*_sgap.dat	Solute mass flux breakthrough data and concentration breakthrough data at the fence line and downgradient points	Text
*_*location*_mf.eps, *_*location*_c.eps	Mass flux and concentration breakthrough curves, respectively. Encapsulated postscript file generated using rungnu.csh	Text/Image
*_*location*_mf.png, *_*location*_c.png	Image file containing mass flux and concentration breakthrough curves, respectively (generated using convert – density 200x200 *eps *png)	Image

Notes:
is the plot file number indicator (e.g., plot.175, plot.3462, etc)
fn is the user-defined filename
yr represents the calendar year plotted in the image file
* is the plot variable [e.g., sat (saturation), ac_tc (aqueous conc tc), vc_U_0.10 (u total conc w/ K_d =0.10].
location represents the fence line or the gwtable (groundwater table) locations

Files for the regular simulation cases, where all releases were from the vicinity of tank S-103, were named with the contaminant and K_d value. For example, for files pertaining to U-238 with a K_d = 0.01 mL/g, "u_0.01" was used in the filename (see Table 6.3). In the verification cases, three tanks were involved in the release, and the notation included the tank number, as in "tc_S101_" or "u_S102_0.60_."

For each transient flow and solute transport simulation, the STOMP simulator read an input file, restart file, zonation file, and solute inventory file and generated one reference-node output file, one or more plot-file output files, and one or more surface-flux output files. The STOMP-generated plot-file output files were converted to Tecplot ASCII format using the PlotTec utility. These ASCII files were rendered with Tecplot to generate color-scaled images of saturation and solute concentration for selected points in time. The STOMP-generated surface flux output files were translated to ASCII mass flux and concentration timeseries *.dat files. The *.dat files were used as input to the analytical advection-dispersion ("streamtube") model to generate concentrations at downgradient points over time.

6.5 Analytical Groundwater Transport Modeling

Input and output files for the analytical groundwater transport ("streamtube") model were archived in the case BTC directories. C-Shell scripts for running the streamtube model and generating plots are included in a main folder called *2_btc_figs*. Execution of the streamtube model and subsequent post-processing creates output files for each species that contains the time and calculated concentrations at each compliance point in columns.

The scripts used to run the model and relevant utility programs are shown in Table 6.4. Script *runpoint.csh* contains the flow-path length, velocity, and hydraulic parameters, runs the streamtube model, and creates output files for each species that contain the time and calculated concentrations at each compliance point in columns. These scripts were executed for each case directory to generate the encapsulated postscript files for the plots used in this report.

Table 6.4. Analytical Groundwater Transport Modeling Files

File Name	Description	File Type
Run_allmodels.csh	C-Shell script for executing series of c-shell scripts used to generate breakthrough curves. .	Text
runpoint.csh	C-Shell script for executing the streamtube model (includes model parameters).	Text
runcombo.csh	C-Shell script for combining breakthrough data at the groundwater table, fence line, exclusion boundary, and Columbia River into one file	Text
run_gnu.csh	C-Shell script for generating breakthrough curve plot files	
riv_sgap_*.btc	Solute-concentration breakthrough data at the Columbia River for the flow path south of the gap	Text
exc_sgap_*.btc	Solute-concentration breakthrough data at the exclusion boundary for the flow path south of the gap	Text
all_*_sgap.dat	Solute-concentration breakthrough data at all compliance points for the groundwater flow path south of the gap	Text
*_sgap_c.eps	Image file containing concentration breakthrough curve data at the groundwater, fence line, exclusion boundary, and Columbia River for the flow path south of the gap	Text/Image
* Indicates the solute species (e.g., U_K_d, tc).		

6.6 STOMP Execution and Post-Processing

STOMP runs and all of the postprocessing steps can be executed using the shell scripts described previously in this section, and each of these steps may be executed individually at the command line to obtain the vadose zone and streamtube modeling results and their graphics. To provide further automation to the processing, R scripts were developed to provide a "wrapper" to the existing programs. R was used to simplify and generalize the selection of specific steps and cases for execution, and provide all necessary intermediate steps with a single command line execution. The actual computations at each of the processing steps described previously were accomplished with the existing C and Fortran programs, and shell, Tecplot, and Gnuplot scripts. A few additional processing steps were included in the

R scripts, such as graphics file format conversions, and finding the peak concentration years and then using that information to set up and execute the additional STOMP run to present concentrations at those years in cross-section plots. To execute certain processing steps for one or more case runs, options are set in the main R script *run_cases.r*, which is found in the sfarm root directory. For example, if only one case is needed to be run, then this option is set in the *run_cases.r* script. The actual postprocessing steps are coded in another R script, *template.r*. With a single command line execution, the following steps may be executed:

For each case:

1) Run STOMP for 1952-2050
2) Run STOMP for 2050-12000
3) Plot breakthrough curves with Gnuplot
4) Find years in which the peak concentration occurred at the fenceline for each contaminant
5) Do additional STOMP run to generate plot files for peak concentration years
6) Plot concentration distributions with Tecplot.

R is essentially an expanded and open source version of the commercially distributed S-plus, the statistics, graphing, and general purpose programming environment. R is a mature product that is well supported and documented, and is available at no cost for all of the usual operating systems (http://www.R-project.org). Help in using R can be found in the program and in Venables and Smith (2001), Krause and Olson (2000), and Venables and Ripley (1999, 2000). The R script can be executed two ways: 1) From the R shell, or 2) direct from the command line. For method 1, start R by entering R at the command line, then enter 'source ("run_cases.r").' For method 2, enter the following at the command line: 'R –slave –no-save < run_cases.r.'

7.0 References

Baetslé LH. 1969. "Migration of radionuclides in porous media." *Progress in Nuclear Energy Series XII, Health Physics*, AMF Duhamel, ed. Pergamon Press, Elmsford, NY, pp. 707–730.

Bergeron MP and SK Wurstner. 2000. *Groundwater Calculations Supporting the 2001 Immobilized Low-Activity Waste Disposal Facility Performance Assessment at the Hanford Site in Southeastern Washington*. PNNL-13400, Pacific Northwest National Laboratory, Richland, WA.

Bergeron MP, E Freeman, S Wurstner, CT Kincaid, FM Coony, D Strenge, R Aaberg, and P Eslinger. 2001. *Addendum to Composite Analysis for Low-Level Waste Disposal in the 200 Area Plateau of the Hanford Site*. PNNL-11800-Addendum 1, Pacific Northwest National Laboratory, Richland, WA.

Bramley R and X Wang. 1995. *SPLIB: A Library of Iterative Methods for Sparse Linear Systems.* Indiana University, Bloomington.

Cole CR, MP Bergeron, SK Wurstner, PD Thorne, S. Orr, and MI McKinley. 2001. *Transient Inverse Calibration of Hanford Site-Wide Groundwater Model to Hanford Operational Impacts—1943 to 1996.* PNNL-13447, Pacific Northwest National Laboratory, Richland, WA.

Cole CR, SK Wurstner, MP Bergeron, MD Williams, and PD Thorne. 1997. *Three-Dimensional Analysis of Future Groundwater Flow Conditions and Contaminant Plume Transport in the Hanford Site Unconfined Aquifer System: FY 1996 and 1997 Status Report.* PNNL-11801, Pacific Northwest National Laboratory, Richland, WA.

Domenico PA and FW Schwartz. 1990. *Physical and Chemical Hydrogeology*. John Wiley & Sons, New York, pp. 824.

Freedman VL, MW Williams, CR Cole , MD White, and MP Bergeron. 2002. *2002 Initial Assessments for B-BX-BY Field Investigation Report (FIR): Numerical Simulations*. PNNL-13949, Pacific Northwest National Laboratory, Richland, WA.

Gardner WR. 1958. "Some Steady-State Solutions of the Unsaturated Moisture Flow Equation with Applications to Evaporation From a Water Table." *Soil Science*, 85:228-232.

Gelhar LW. 1993. *Stochastic Subsurface Hydrology*. Prentice Hall, Englewood Cliffs, NJ.

Gupta SK, CR Cole, CT Kincaid, and AM Monti. 1987. *Coupled Fluid, Energy, and Solute Transport (CFEST) Model: Formulation and User's Manual.* BMI/ONWI-660, Battelle Memorial Institute, Columbus, OH.

Gupta SK. 1996. *Draft User's Manual, CFEST-96 Flow and Solute Transport, Constant/Variable Density, Computationally Efficient, and Low Disk PC/Unix Version*. Environmental System Technologies, Irvine, CA.

Hartman MJ. 2000. *Hanford Site Groundwater Monitoring: Setting, Sources and Methods*. PNNL-13080, Pacific Northwest National Laboratory, Richland, WA.

Kaplan DI, J Conca, RJ Serne, TW Wietsma, AT Owen, and TL Gervais. 1996. *Radionuclide Adsorption Distribution Coefficients Measured in Hanford Sediments for the Low Level Waste Performance Assessment Project*. PNNL-11485, Pacific Northwest National Laboratory, Richland, WA.

Kaplan DL and RJ Serne. 2000. *Geochemical Data Package for the Immobilized Low-Activity Waste Performance Assessment*. PNNL-13037, Pacific Northwest National Laboratory, Richland, WA.

Khaleel R and JF Relyea. 1997. "Correcting laboratory-measured moisture retention data for gravels." *Water Resources Research*, 33:1875-1878.

Khaleel R and MP Connelly. 2003. *Modeling Data Package for an Initial Assessment of Closure for S-SX Tank Farm.* RPP-17209 Rev. 0, CH2M HILL Hanford Group, Inc., Richland, WA.

Khaleel R, JF Relyea, and JL Conca. 1995. "Evaluation of van-Genuchten-Mualem relationships to estimate unsaturated conductivity at low water contents." *Water Resources Research*, 31:2659-2668.

Kincaid CT, JW Shade, GA Whyatt, MG Piepho, K Rhoads, JA Voogd, JH Westsik Jr, MD Freshley, KA Blanchard, and BG Lauzon. 1995. *Performance Assessment of Grouted Double-Shell Tank Waste Disposal at Hanford*. WHC-SD-WM-EE-004 Rev. 1, Westinghouse Hanford Company, Richland, WA.

Kincaid CT, MP Bergeron, CR Cole, MD Freshley, NL Hassig, VG Johnson, DI Kaplan, RJ Serne, GP Streile, DL Strenge, PD Thorne, LW Vail, GA Whyatt, and SK Wurstner. 1998. *Composite Analysis for Low-Level Waste Disposal in the 200-Area Plateau of the Hanford Site.* PNNL-11800, Pacific Northwest National Laboratory, Richland, WA.

Kozak MW, MSY Chu, PA Mattingly, JD Johnson, and JT McCord. 1990. *Background Information for the Development of a Low-Level Waste Performance Assessment Methodology*. NUREG/CR-453 (SAND90-0375) Vol. 5, U.S. Nuclear Regulatory Commission, Washington, DC.

Krause A and M Olson. 2000. *The Basics of S and S-plus*, 2nd edition. Springer, New York.

Lindsey KA and KD Reynolds. 2001. *Vadose Zone Geology of Boreholes 299-E33-45 and 299-E33-46 B-BX-BY Waste Management Area, Hanford Site, South-Central Washington.* RPP-8681 Rev. 0, CH2M HILL Hanford Group, Inc., Richland, WA.

Mann FM, RJ Puigh II, SH Finfrock, EJ Freeman, R Khaleel, DH Bacon, MP Bergeron, BP McGrail, and SK Wurstner. 2001. *Hanford Immobilized Low-Activity Tank Waste Performance Assessment, 2001 Version*. DOE/ORP-2000-24, U.S. Department of Energy Office of River Protection, Richland, WA.

Millington RJ and JP Quirk. 1961. "Permeability of Porous Media." *Nature* 183:387-388.

Mualem Y. 1976. "A New Model for Predicting the Hydraulic Conductivity of Unsaturated Porous Media." *Water Resources Research* 12:513-522.

Nichols WE, M Oostrom, and MD White. 2000. *STOMP Subsurface Transport Over Multiple Phases, Version 2.0, Application Guide.* PNNL-12028, Pacific Northwest National Laboratory, Richland, WA.

Polmann DJ. 1990. *Application of Stochastic Methods to Transient Flow and Transport in Heterogeneous Unsaturated Soils*. Ph.D. Thesis, Massachusetts Institute of Technology, Cambridge.

Press WH, BP Flannery, SA Teukolsky, and WT Vetterling. 1992. "Romberg Integration." *FORTRAN: The Art of Scientific Computing*, 2nd ed. Cambridge University Press, UK, pp. 134-135.

Price WH and KR Fecht. 1976a. *Geology of the 241-S Tank Farm*. ARH-LD-133, Atlantic Richfield Hanford Company, Richland, WA.

Price WH and KR Fecht. 1976b. *Geology of the 241-SX Tank Farm*. ARH-LD-134, Atlantic Richfield Hanford Company, Richland, WA.

Talbott ME and LW Gelhar. 1994. *Performance Assessment of a Hypothetical Low-Level Waste Facility: Groundwater Flow and Transport Simulation.* NUREG/CR-6114 Vol. 3, U.S. Nuclear Regulatory Commission, Washington, DC.

van Genuchten MT. 1980. "A Closed-Form Equation for Predicting the Hydraulic Conductivity of Unsaturated Soils." *Soil Science Society of America Journal* 44:892-898.

Venables W and B Ripley. 1999. *Modern Applied Statistics with S-plus*, 3rd edition. Springer, New York.

Venables W and B Ripley. 2000. *S Programming*. Springer, New York.

Venables W and D Smith. 2001. *An Introduction to R.* Network Theory Limited, Bristol, UK.

Washington State Department of Ecology, U.S. Environmental Protection Agency, and U.S. Department of Energy. 1989 and as Amended Through December 31, 1998. *Hanford Federal Facility Agreement and Consent Order*. 89-10 Rev. 5, Ecology, EPA, and DOE, Olympia, WA.

White MD and M Oostrom. 2000. *STOMP Subsurface Transport Over Multiple Phases, Version 2.0, Theory Guide.* PNNL-12030, Pacific Northwest National Laboratory, Richland, WA.

White MD and M Oostrom. 2004. *STOMP Subsurface Transport Over Multiple Phases, Version 3.1, User's Guide.* PNNL-14478, Pacific Northwest National Laboratory, Richland, WA.

White MD, M Oostrom, MD Williams, CR Cole and MP Bergeron. 2001. *FY00 Initial Assessments for S-SX Field Investigation Report (FIR): Simulations of Contaminant Migration with Surface Barriers*. PNWD-3111, Battelle – Pacific Northwest Division, Richland, WA.

Wurstner SK, PD Thorne, MA Chamness, MD Freshley, and MD Williams. 1995. *Development of a Three-Dimensional Groundwater Model of the Hanford Site Unconfined Aquifer System: FY 1995 Status Report.* PNL-10886, Pacific Northwest Laboratory, Richland, WA.

Yeh TCJ, LW Gelhar, and AL Gutjahr. 1985. "Stochastic Analysis of Unsaturated Flow in Heterogeneous Soils, 2. Statistically Anisotropic Media with Variable α." *Water Resources Research* 21:457-464.

Zhang ZF, VL Freedman, and MD White. 2003. *Initial Assessments of Closure for the C Tank Farm: Numerical Simulations*. PNNL-14334, Pacific Northwest National Laboratory, Richland, WA.

Appendix A: S Farm Saturation and Concentration Distributions

(a)

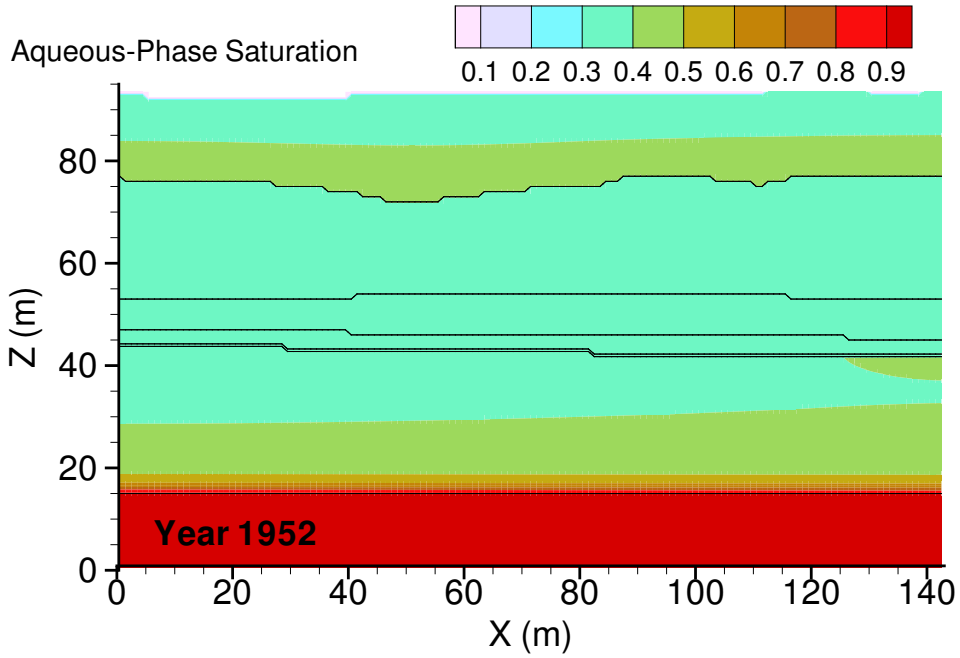

(b)

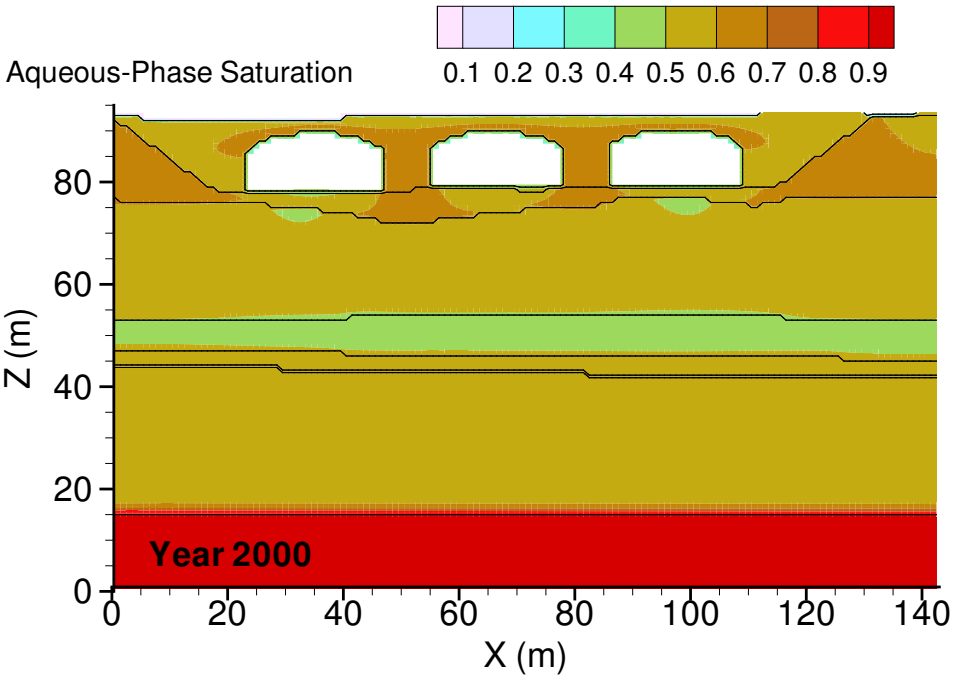

Figure A.1. Baseline aqueous saturation at (a) year 1952 and (b) 01/01/2000

(a)

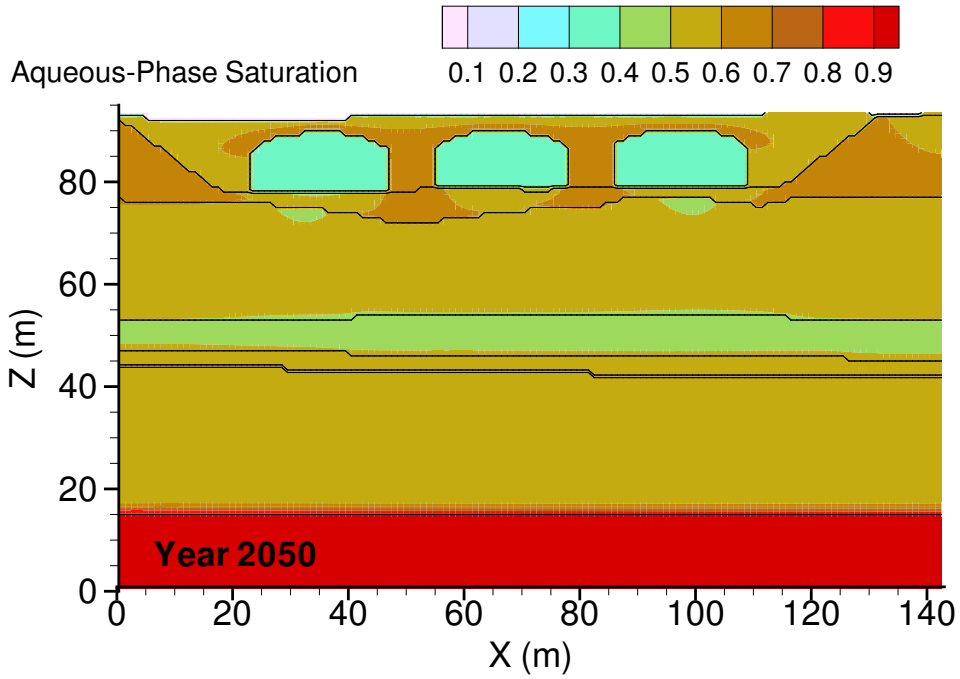

(b)

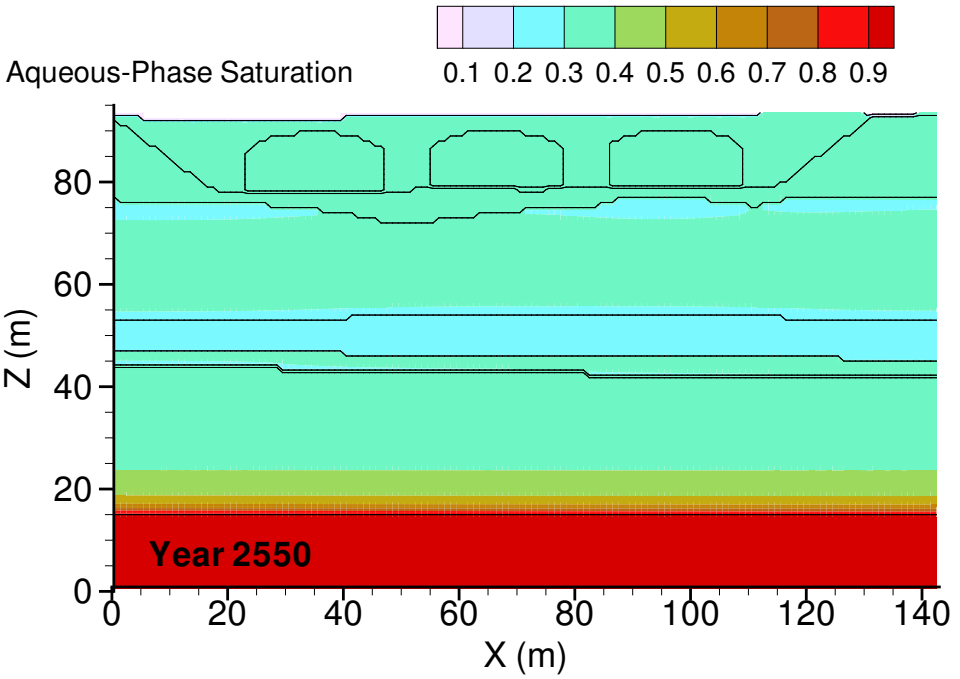

Figure A.2. Baseline aqueous saturation at (a) year 2050 and (b) year 2550

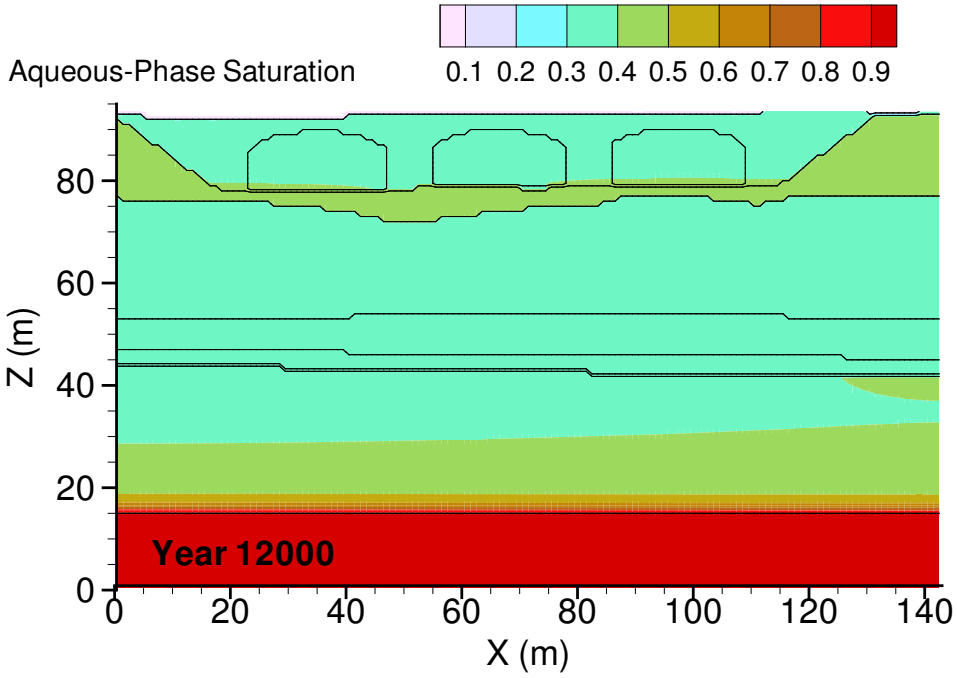

Figure A.3. Baseline aqueous saturation at year 12000

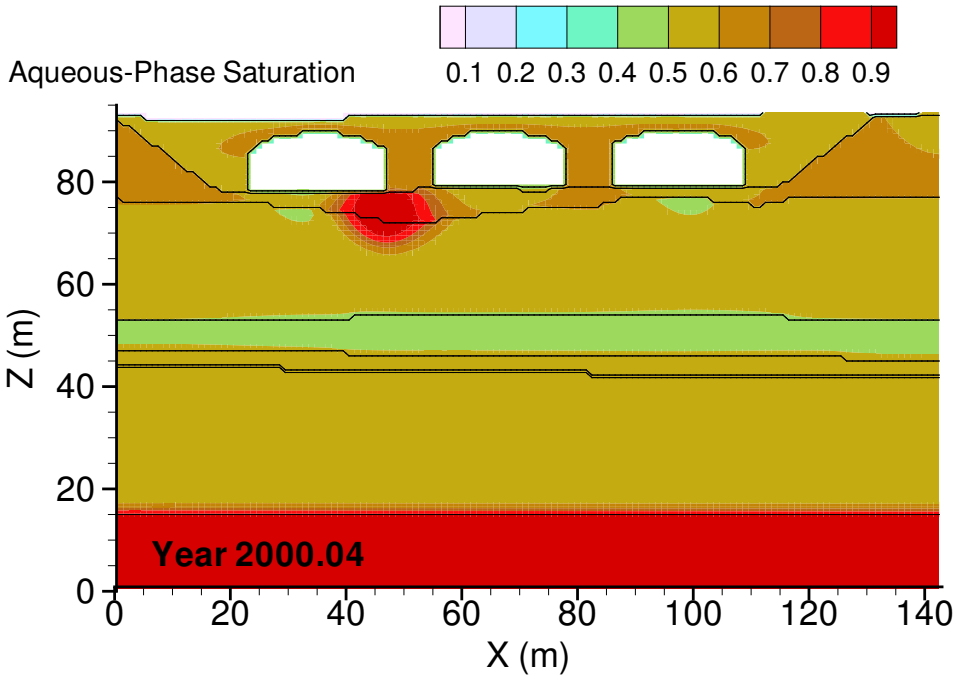

Figure A.4. Case 1, Aqueous saturation at 1/15/2000

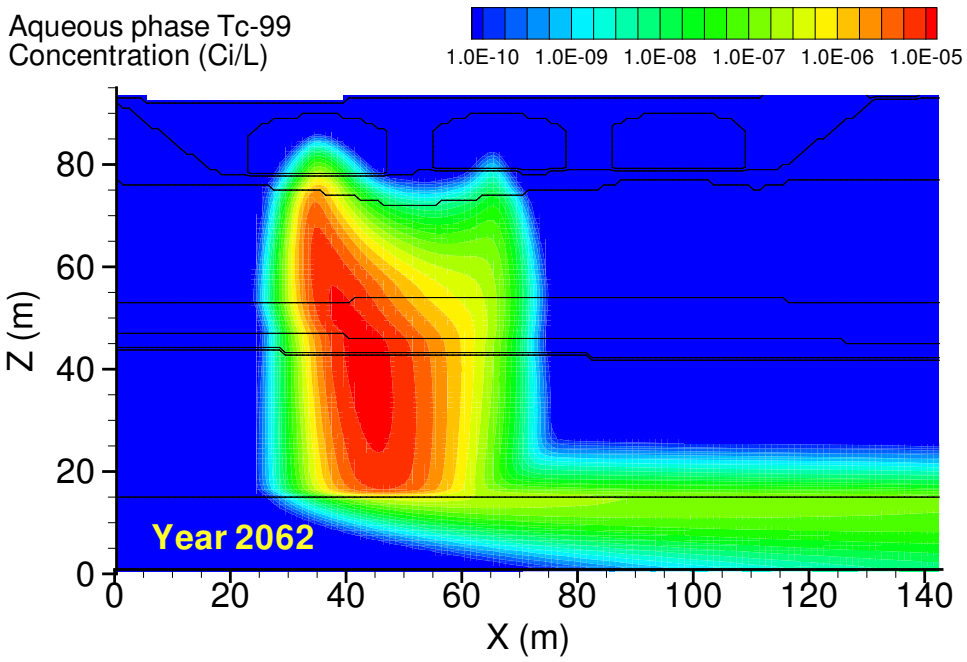

Figure A.5. Case 1, Tc-99 aqueous concentration at year 2062, time of peak concentration at fence line

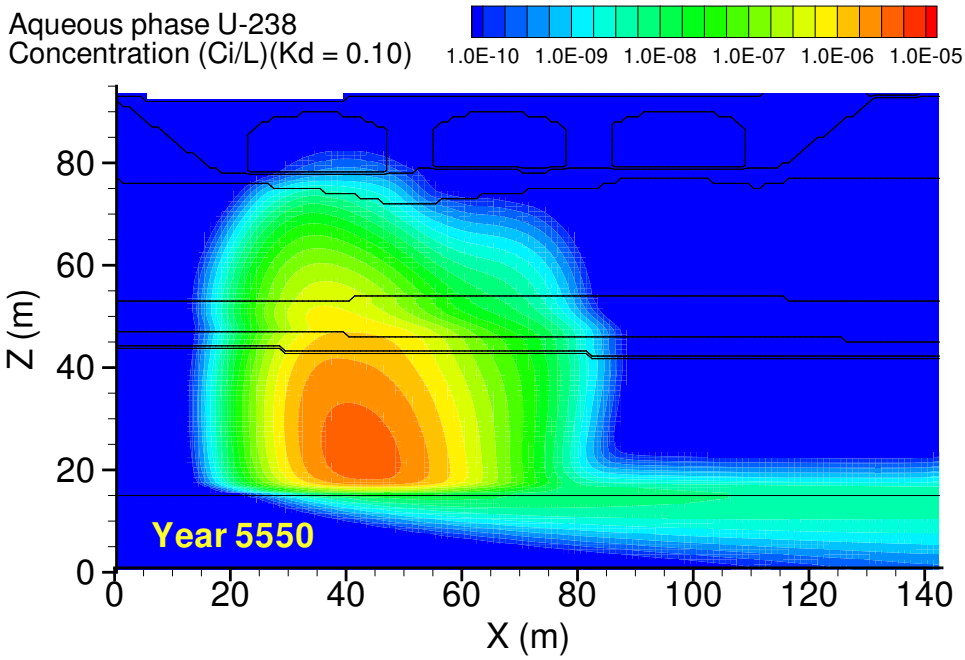

Figure A.6. Case 1, U-238 (K_d = 0.10) aqueous concentration at year 5550, time of peak concentration at fence line

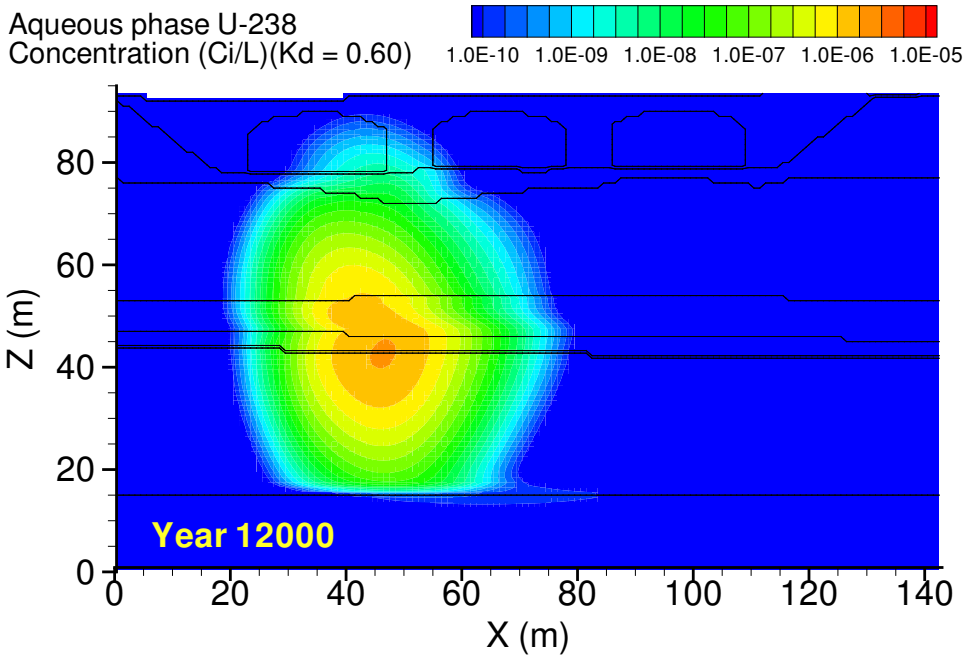

Figure A.7. Case 1, U-238 (K_d = 0.60) aqueous concentration at year 12000, time of maximum concentration at fence line

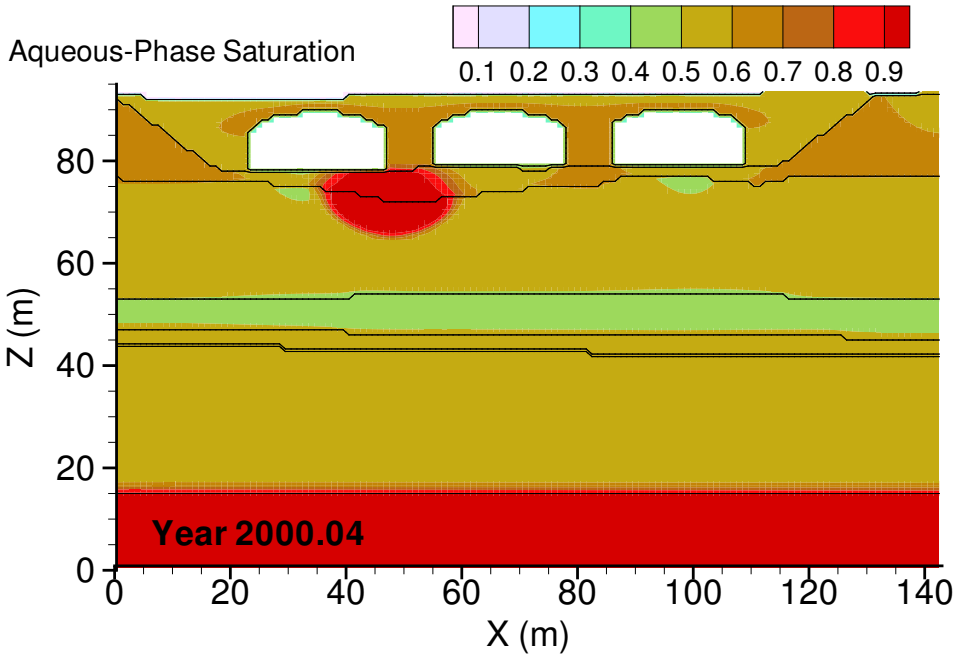

Figure A.8. Case 2, Aqueous saturation at 1/15/2000

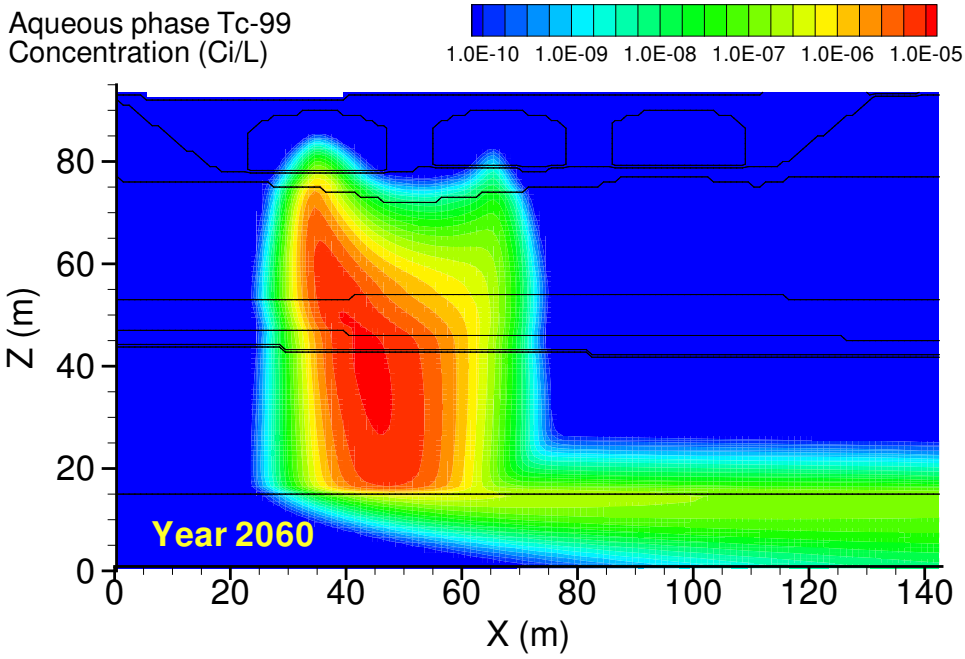

Figure A.9. Case 2, Tc-99 aqueous concentration at year 2060, time of peak concentration at fence line

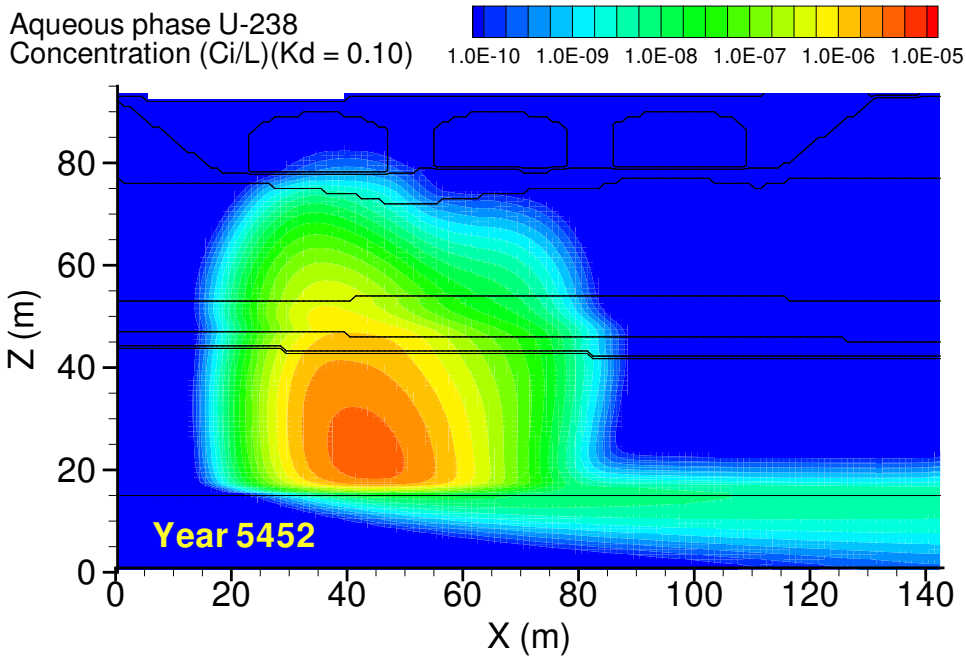

Figure A.10. Case 2, U-238 (K_d = 0.10) aqueous concentration at year 5452, time of peak concentration at fence line

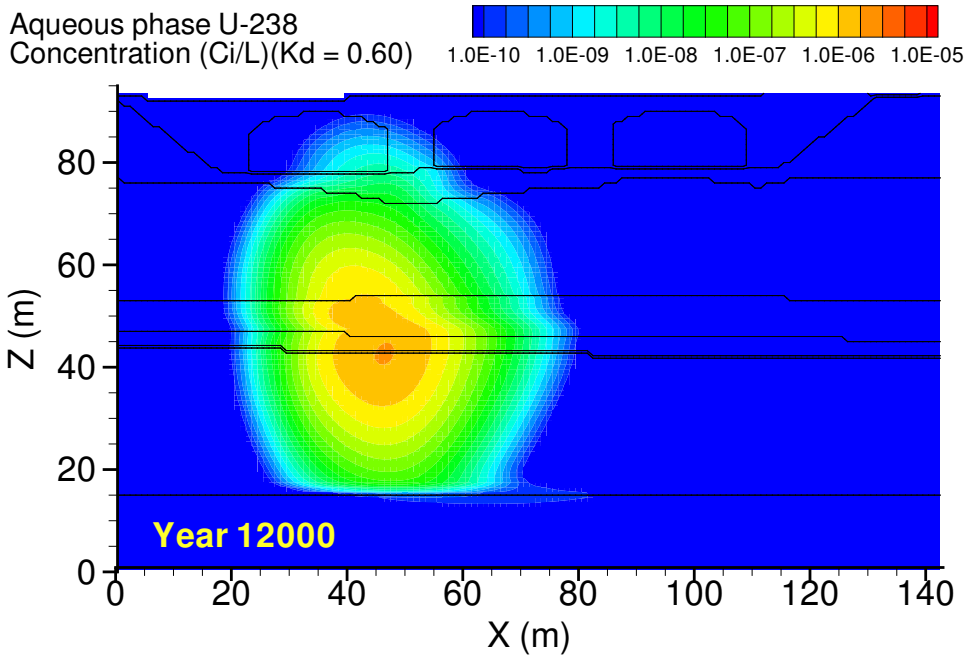

Figure A.11. Case 2, U-238 (K_d = 0.60) aqueous concentration at year 12000, time of maximum concentration at fence line

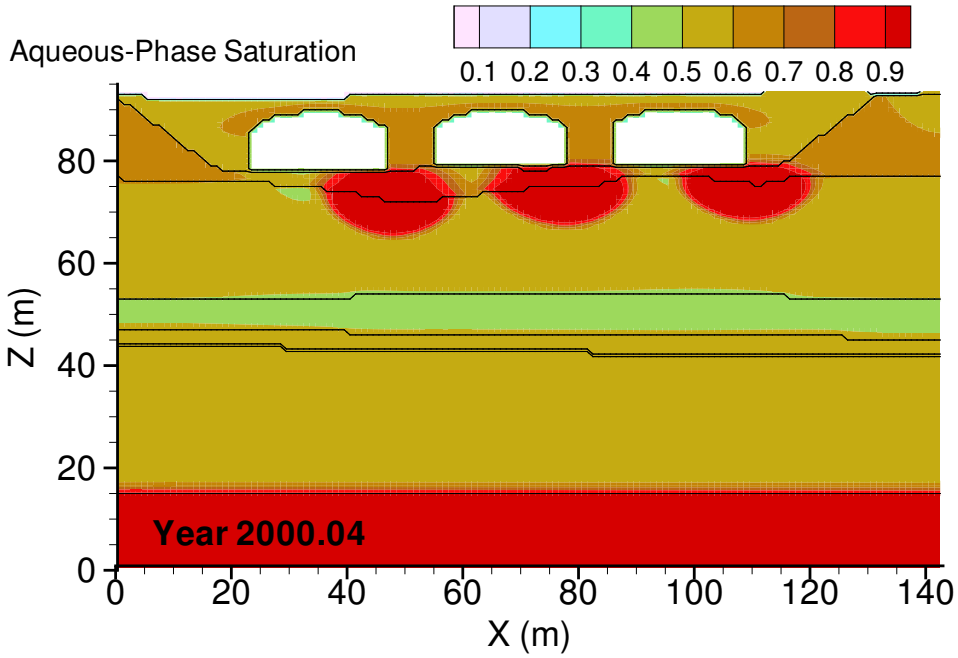

Figure A.12. Case 2v, Aqueous saturation at 1/15/2000

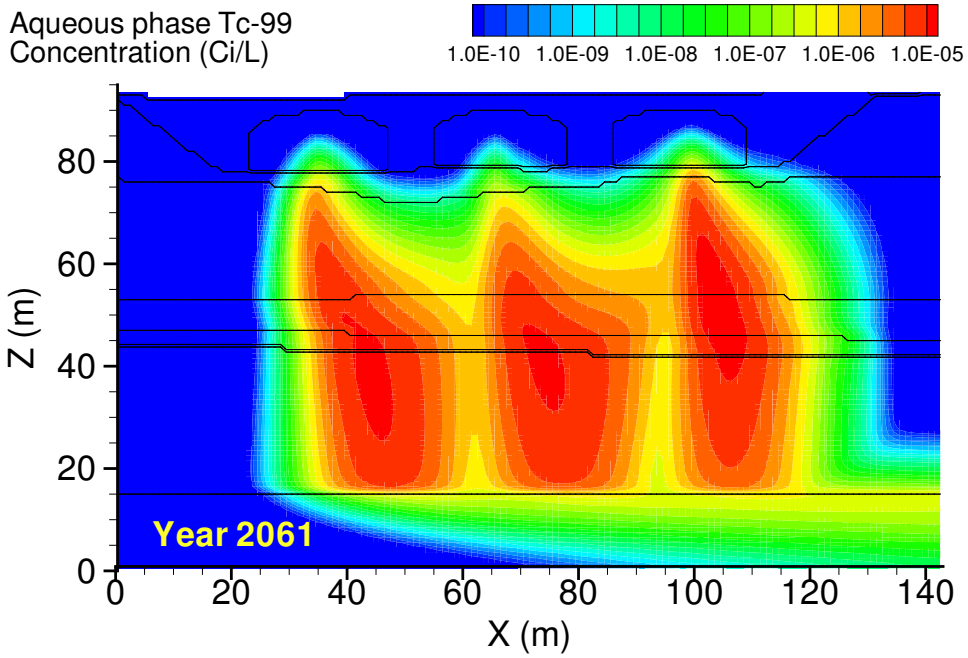

Figure A.13. Case 2v, Tc-99 aqueous concentration at year 2061, time of peak concentration of aggregated tank-specific solutes at fence line

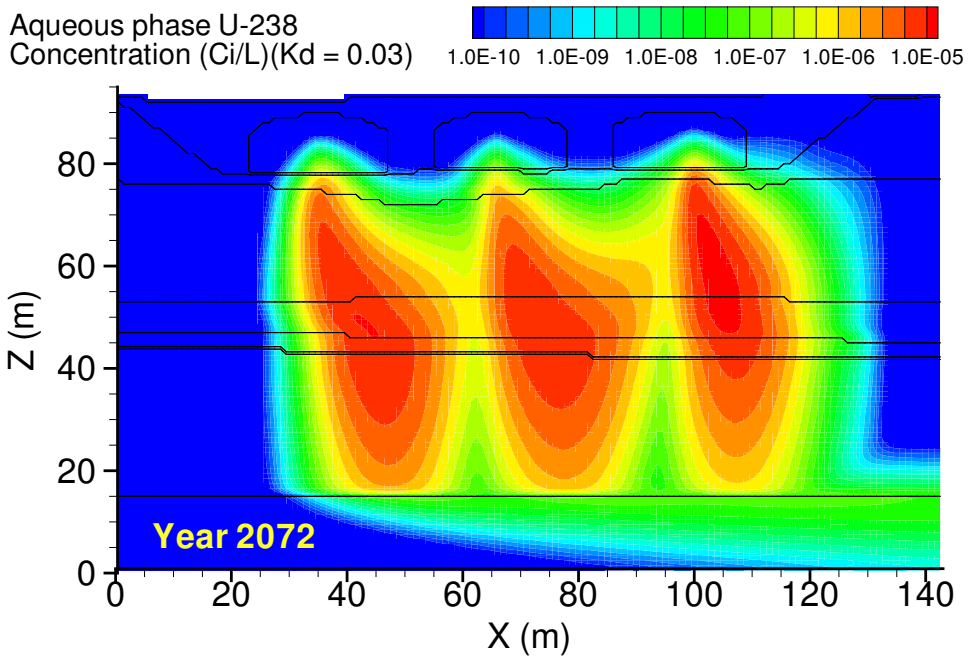

Figure A.14. Case 2v, U-238 (K_d = 0.03) aqueous concentration at year 2072, time of peak concentration of aggregated tank-specific solutes at fence line

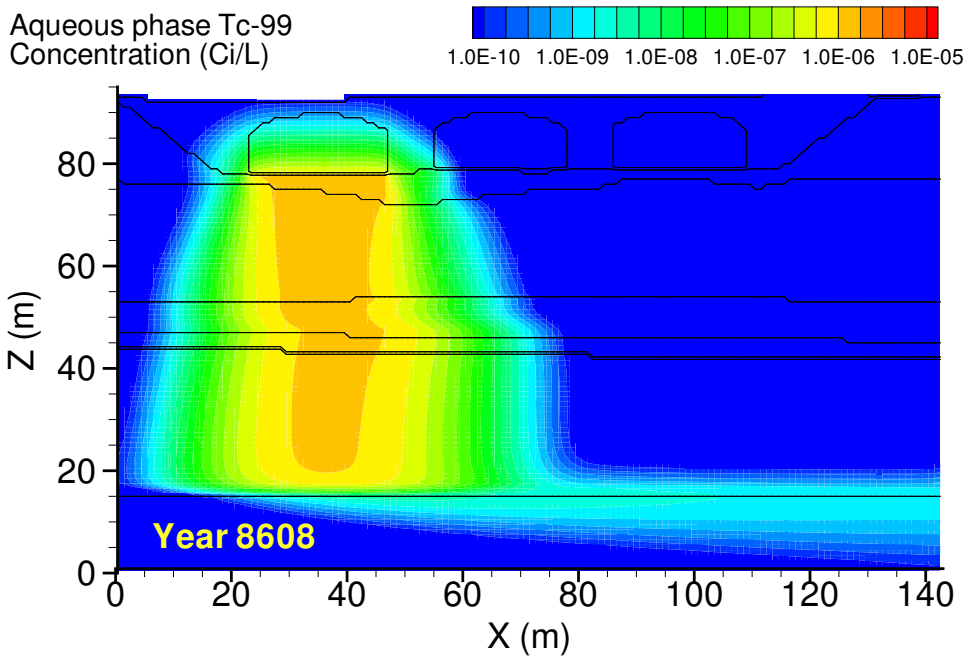

Figure A.15. Case 3, Tc-99 aqueous concentration at year 8608, time of peak concentration at fence line

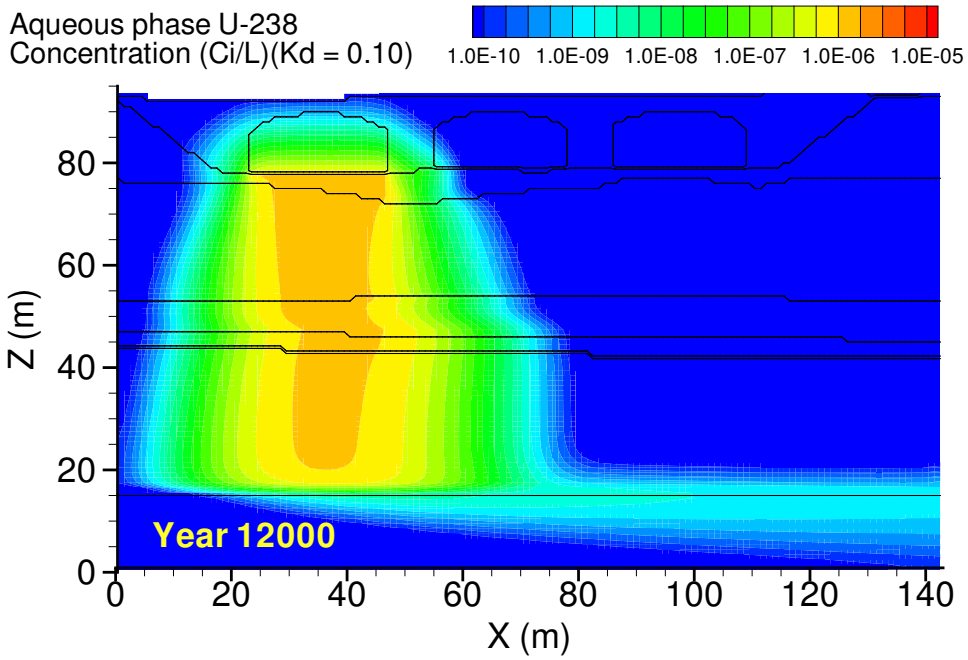

Figure A.16. Case 3, U-238 (K_d = 0.10) aqueous concentration at year 12000, time of maximum concentration at fence line

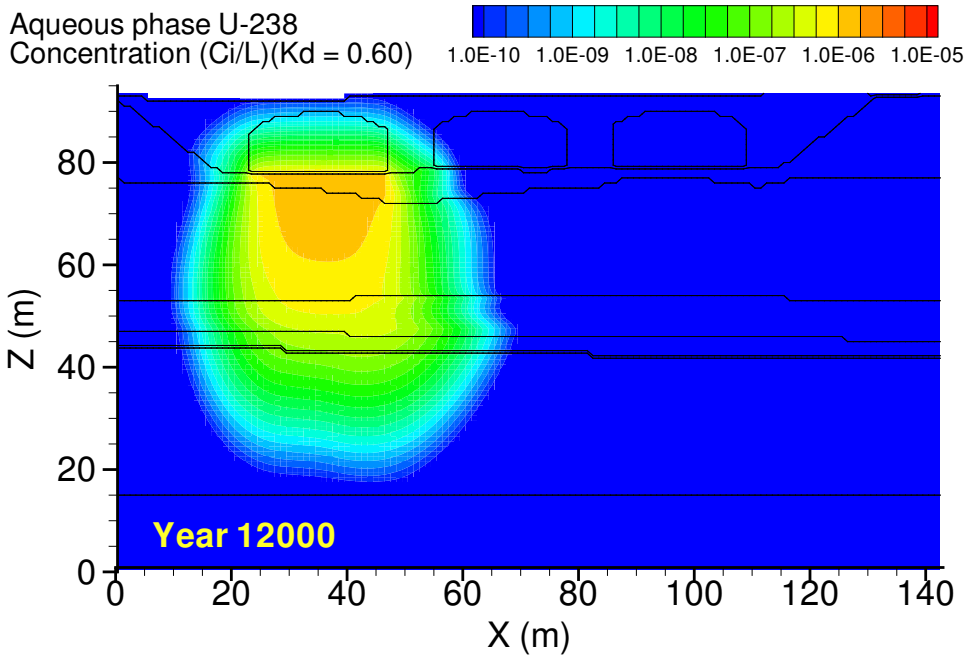

Figure A.17. Case 3, U-238 (K_d = 0.60) aqueous concentration at year 12000, time of maximum concentration at fence line

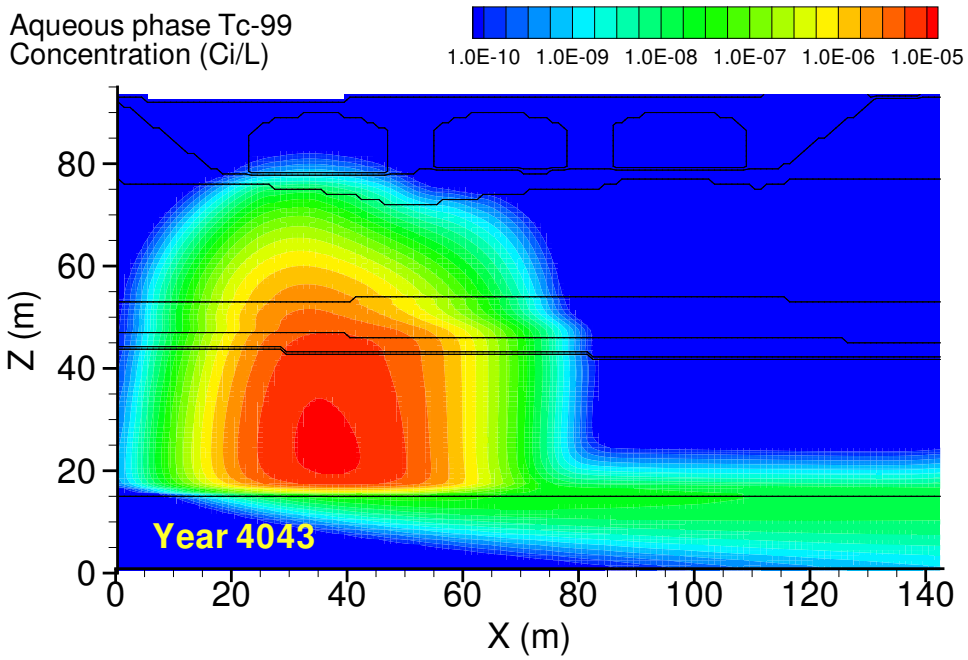

Figure A.18. Case 4, Tc-99 aqueous concentration at year 4043, time of peak concentration at fence line

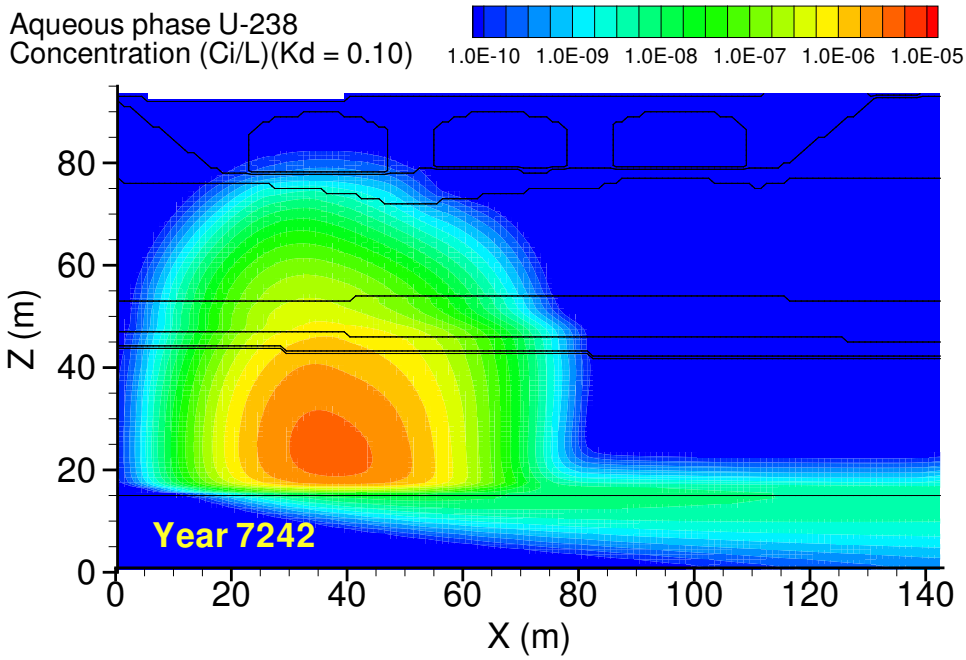

Figure A.19. Case 4, U-238 (K_d = 0.10) aqueous concentration at year 7242, time of peak concentration at fence line

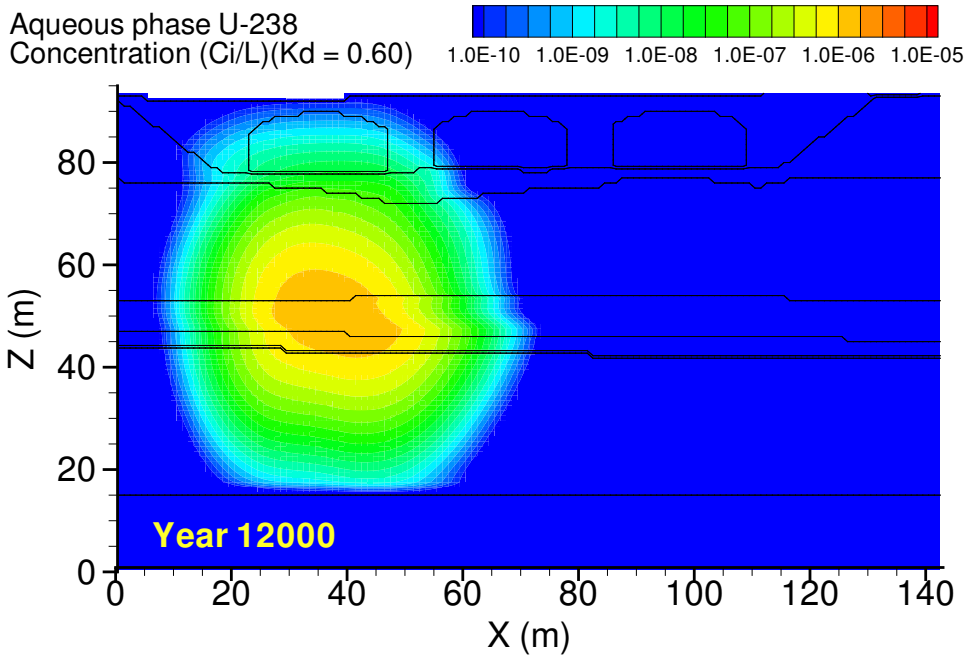

Figure A.20. Case 4, U-238 (K_d = 0.60) aqueous concentration at year 12000, time of maximum concentration at fence line

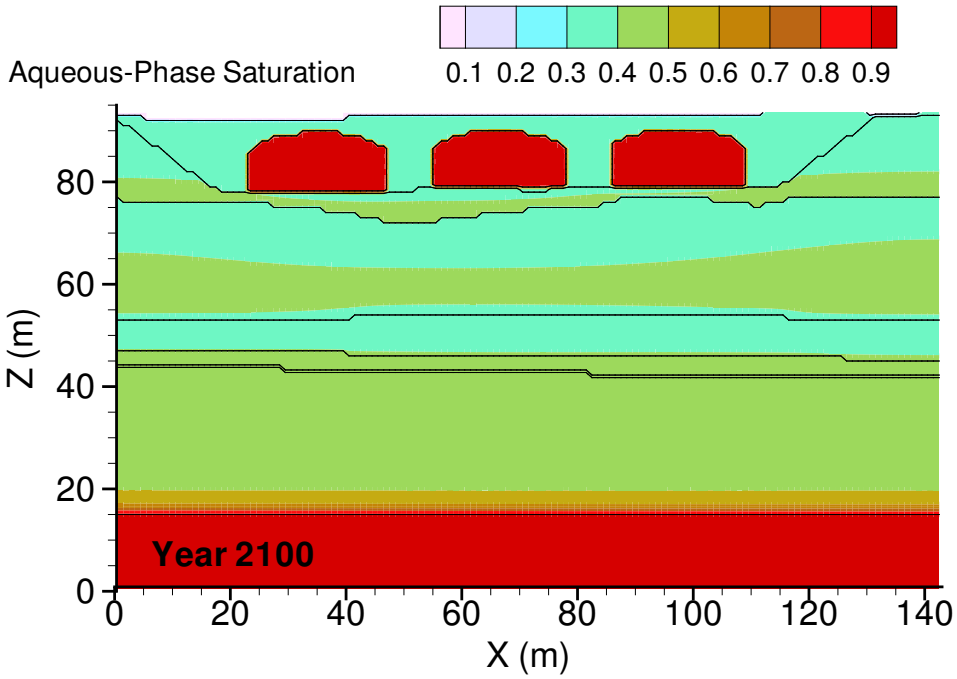

Figure A.21. Case 5, Aqueous saturation at year 2100

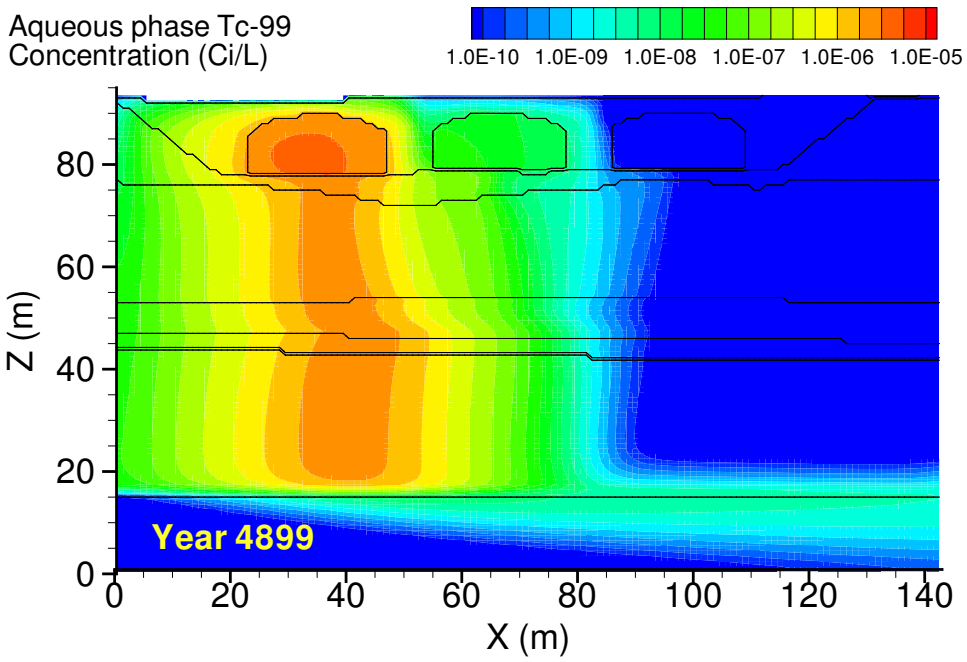

Figure A.22. Case 5, Tc-99 aqueous concentration at year 4899, time of peak concentration at fence line

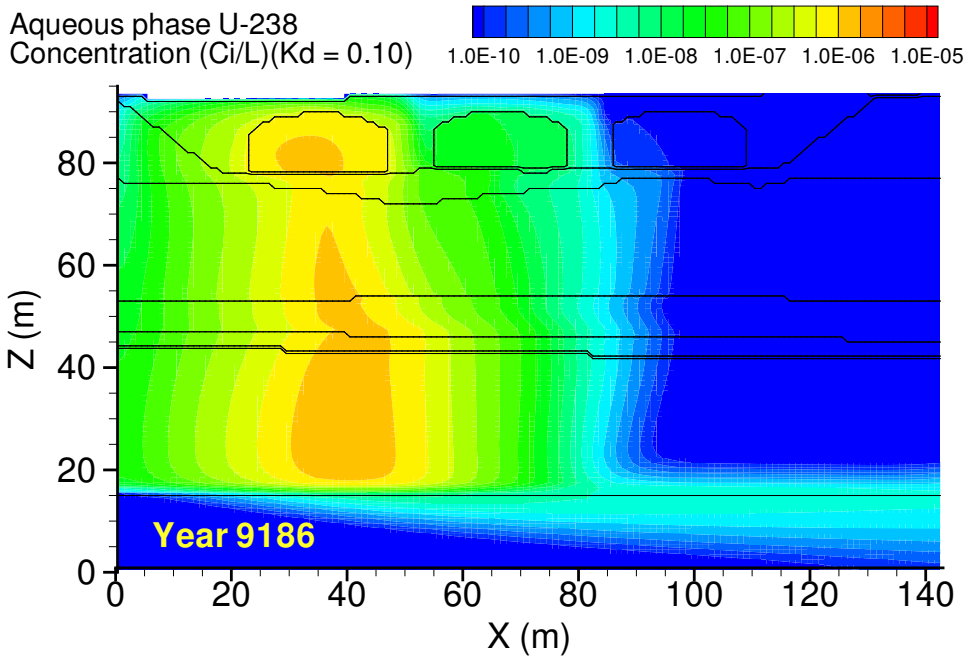

Figure A.23. Case 5, U-238 (K_d = 0.10) aqueous concentration at year 9186, time of peak concentration at fence line

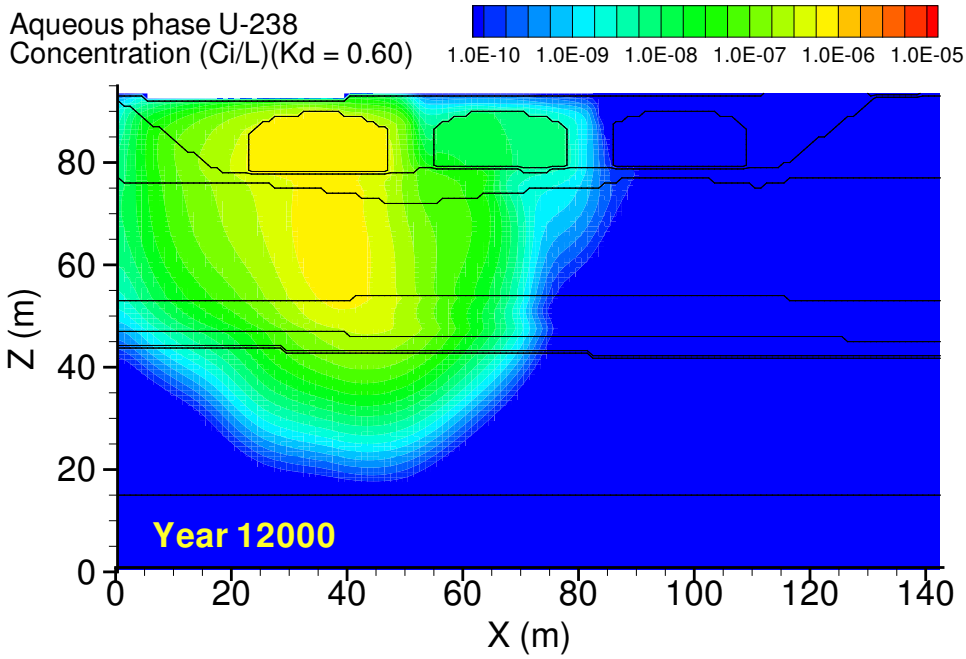

Figure A.24. Case 5, U-238 (K_d = 0.60) aqueous concentration at year 12000, time of maximum concentration at fence line

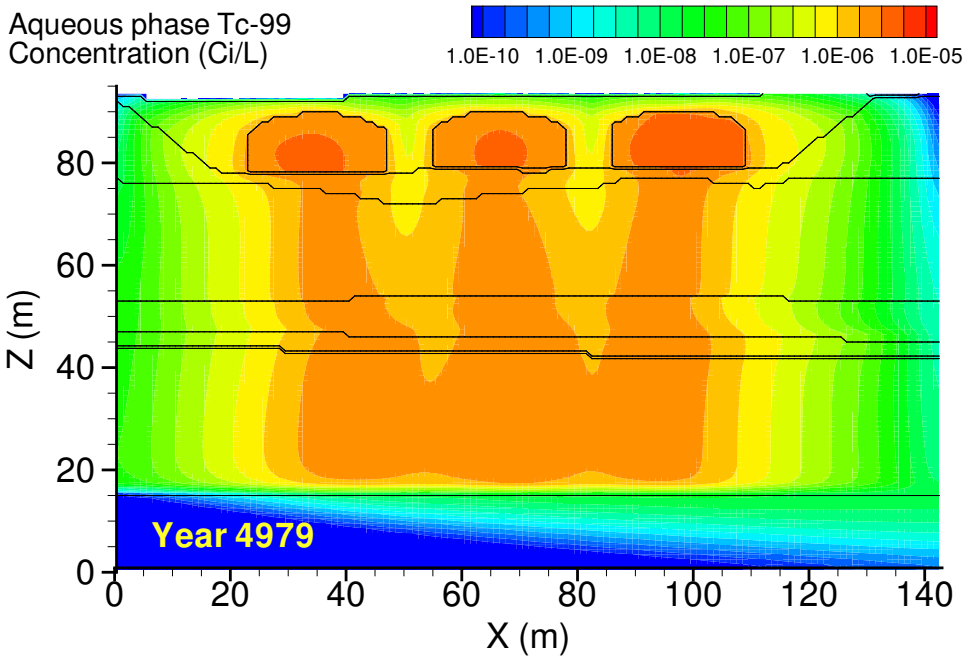

Figure A.25. Case 5v, Tc-99 aqueous concentration at year 4979, time of peak concentration of aggregated tank-specific solutes at fence line

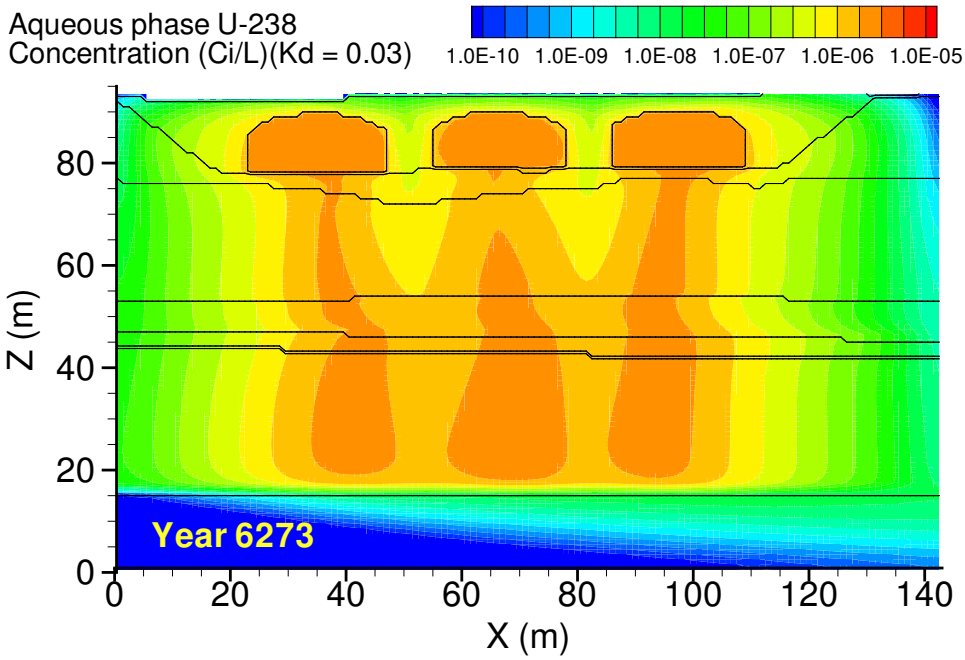

Figure A.26. Case 5v, U-238 (K_d = 0.03) aqueous concentration at year 6273, time of peak concentration of aggregated tank-specific solutes at fence line

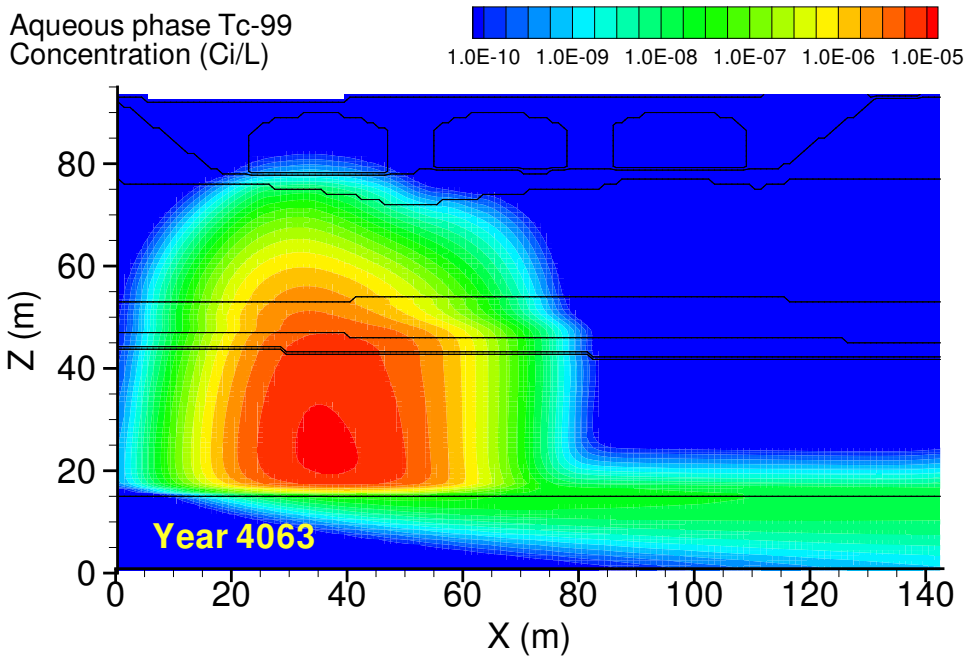

Figure A.27. Case 6, Tc-99 aqueous concentration at year 4063, time of peak concentration at fence line

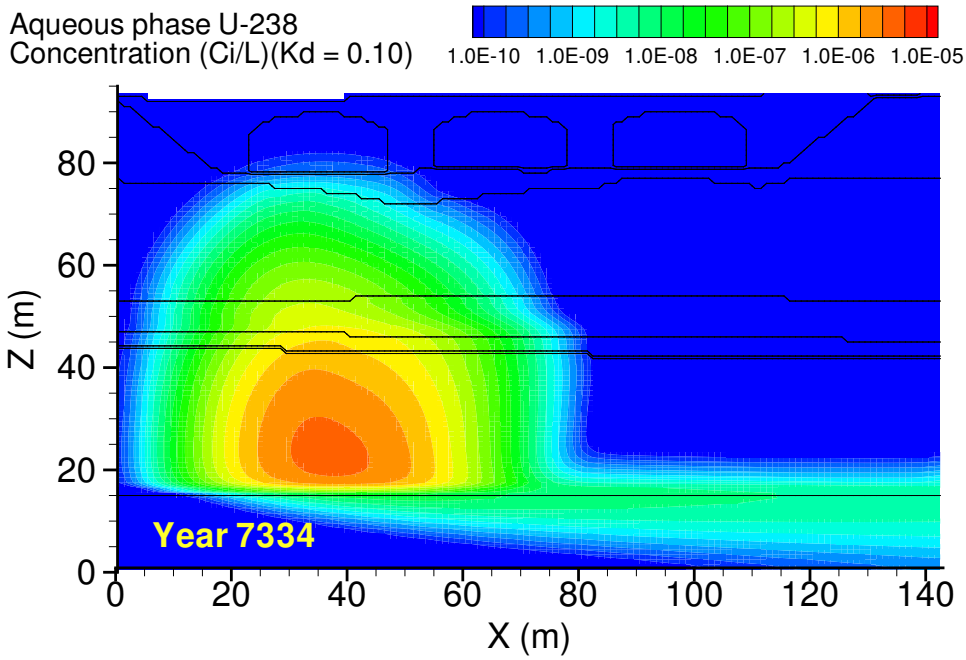

Figure A.28. Case 6, U-238 (K_d = 0.10) aqueous concentration at year 7334, time of peak concentration at fence line

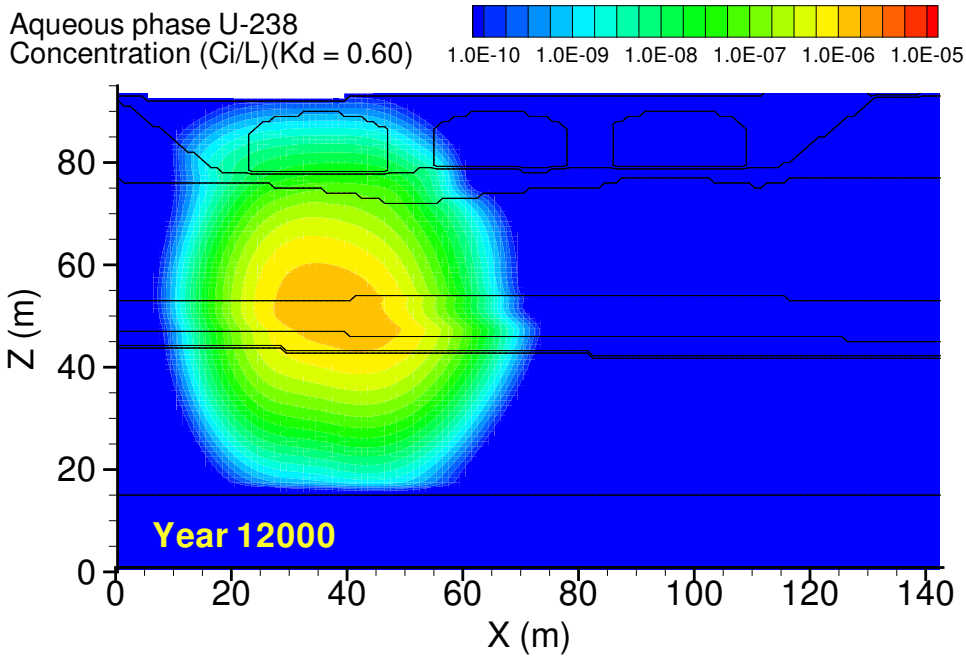

Figure A.29. Case 6, U-238 (K_d = 0.60) aqueous concentration at year 12000, time of maximum concentration at fence line

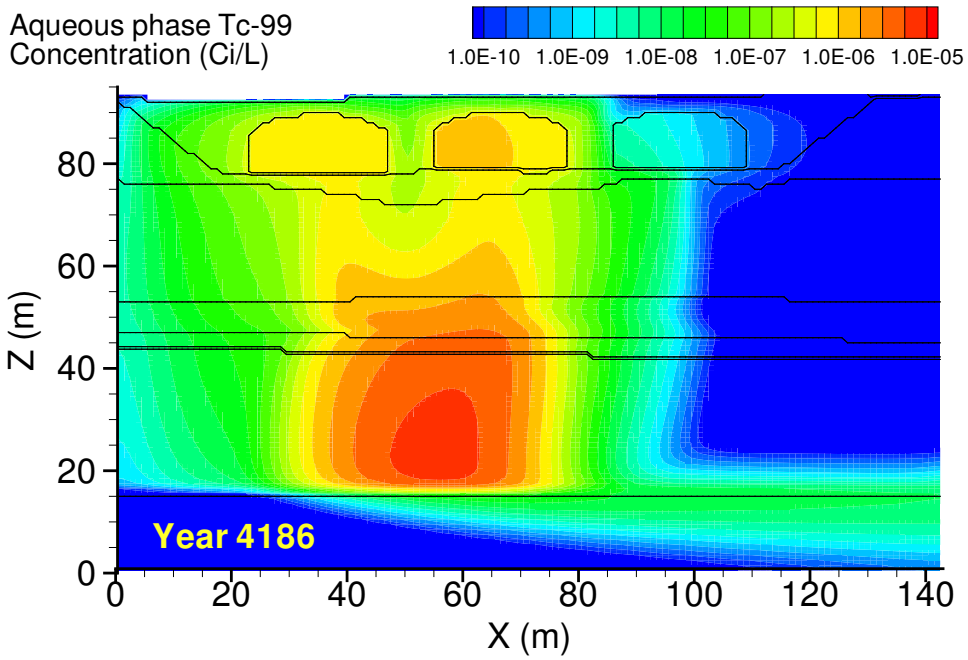

Figure A.30. Case 7, Tc-99 aqueous concentration at year 4186, time of peak concentration at fence line

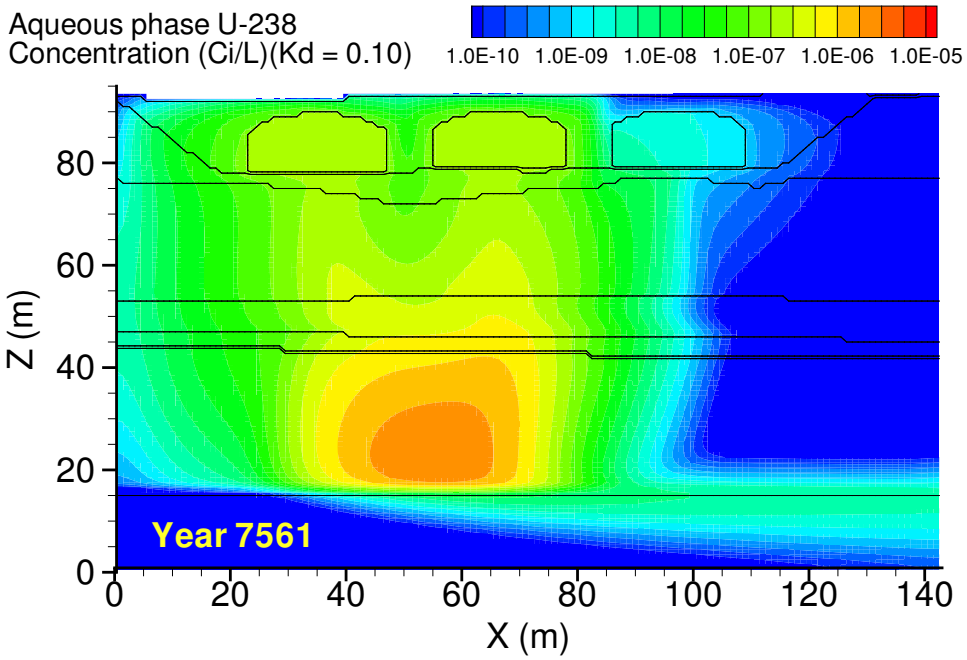

Figure A.31. Case 7, U-238 (K_d = 0.10) aqueous concentration at year 7561, time of peak concentration at fence line

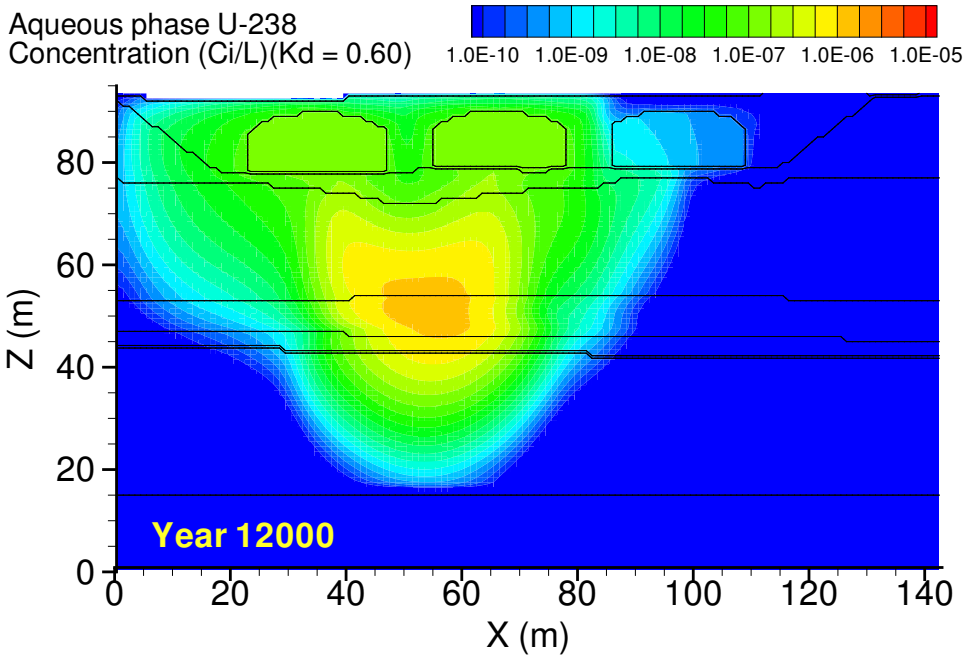

Figure A.32. Case 7, U-238 (K_d = 0.60) aqueous concentration at year 12000, time of maximum concentration at fence line

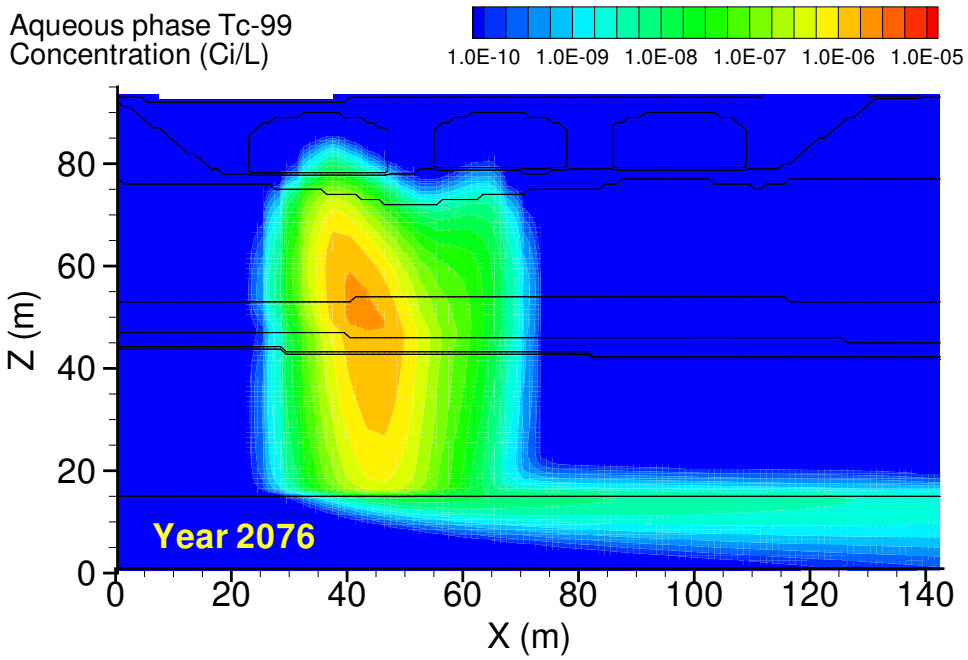

Figure A.33. Case 1-3d, Tc-99 aqueous concentration at year 2076, time of peak concentration at fence line

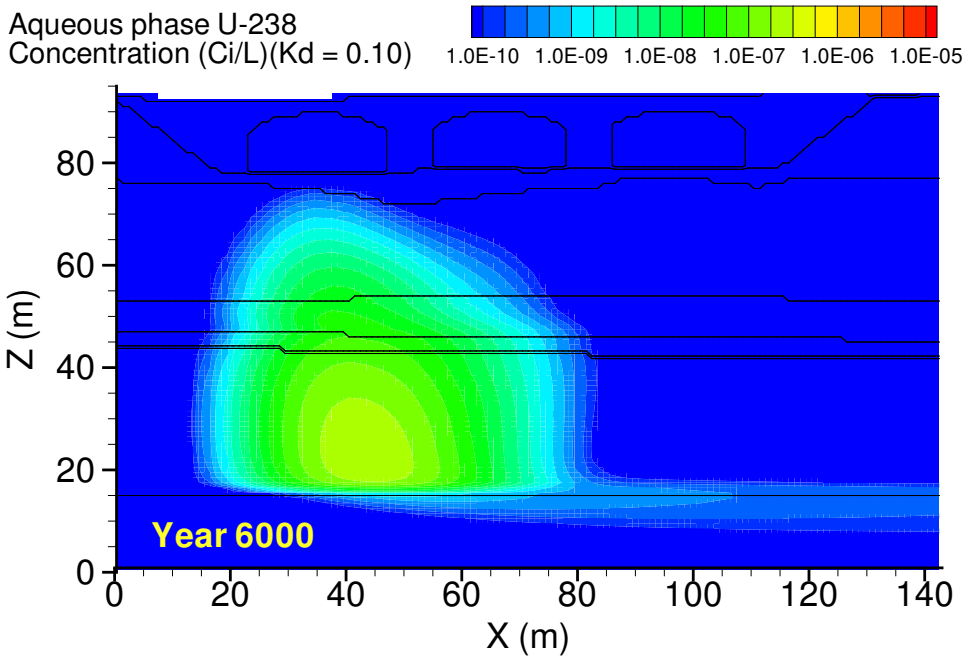

Figure A.34. Case 1-3d, U-238 (K_d = 0.10) aqueous concentration at year 6000 (actual time of peak concentration at fence line was year 5996)

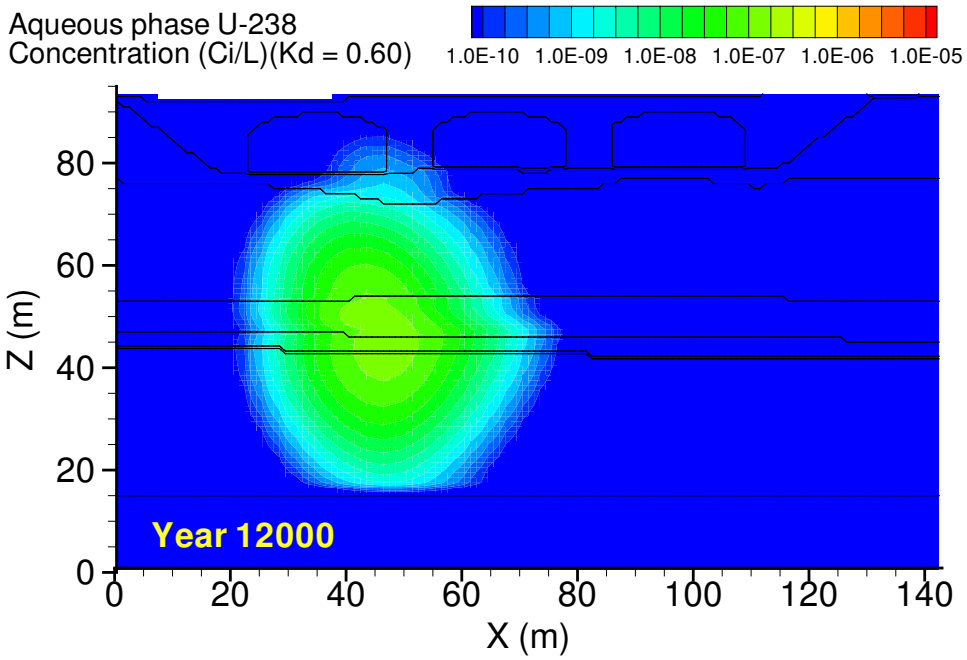

Figure A.35. Case 1-3d, U-238 (K_d = 0.60) aqueous concentration at year 12000, time of maximum concentration at fence line

Appendix B: Breakthrough Curves

(a)

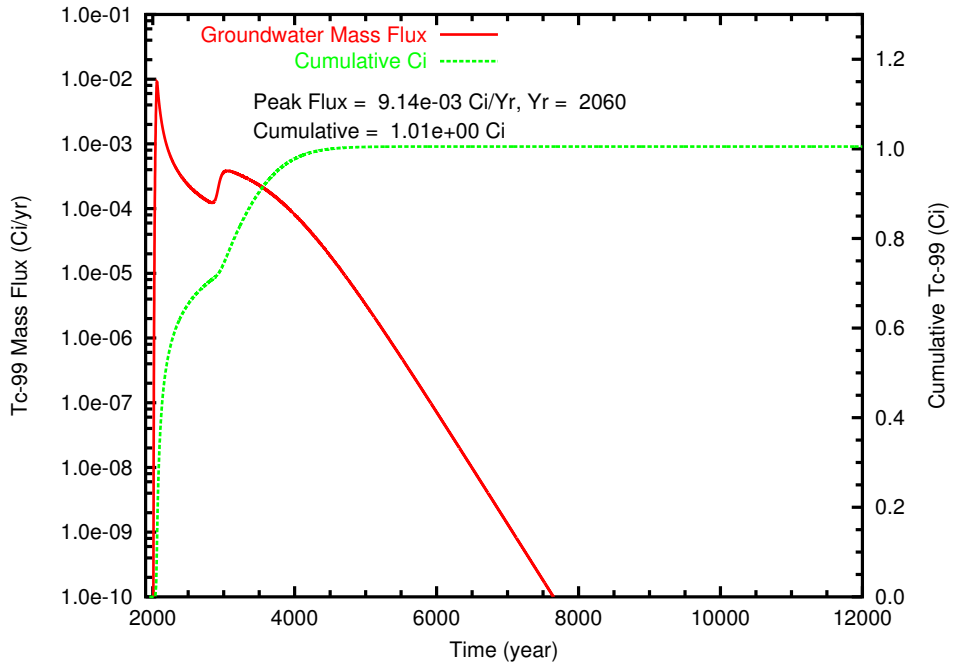

(b)

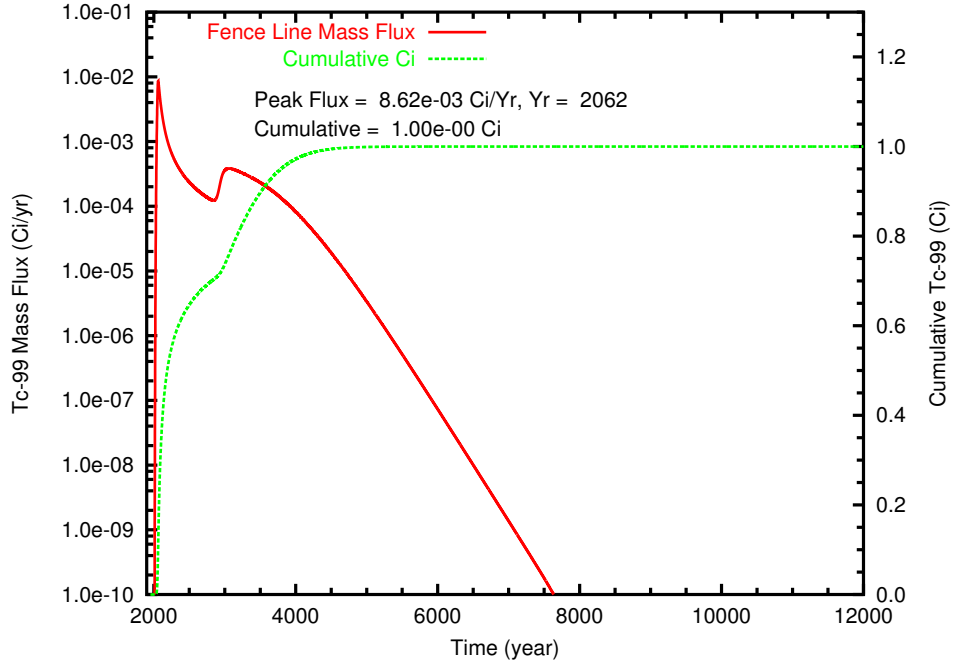

Figure B.1. Case 1, Tc-99 mass flux and cumulative mass at (a) the groundwater table and (b) the fence line

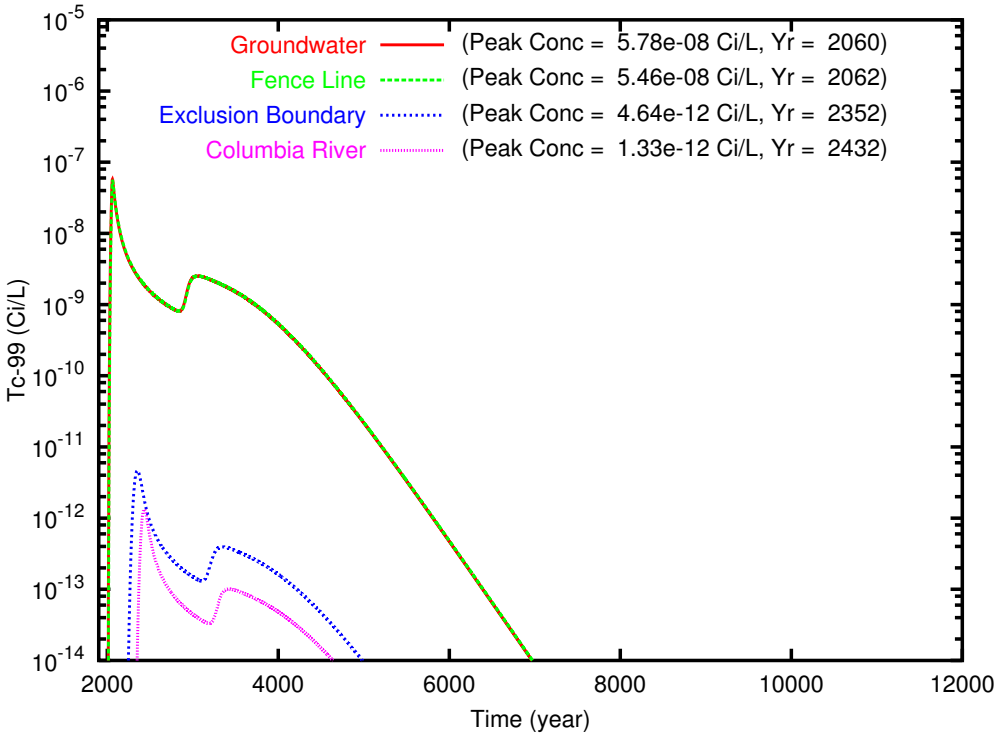

Figure B.2. Case 1, Tc-99 concentration versus time at the groundwater table and the fence line, exclusion boundary, and Columbia River compliance points

(a)

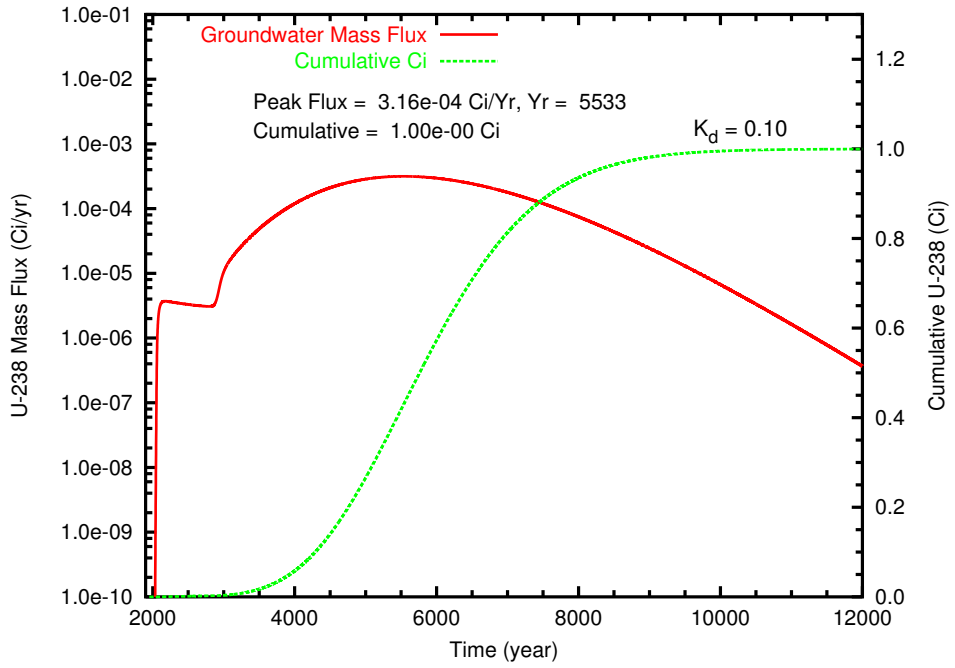

(b)

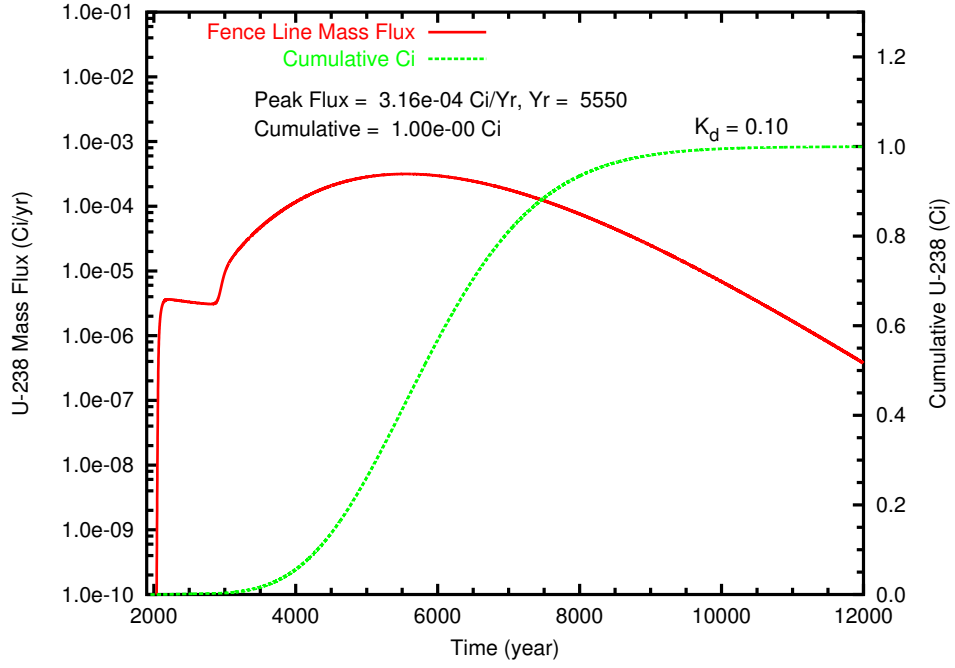

Figure B.3. Case 1, U-238 (K_d = 0.10) mass flux (Ci/L) and cumulative mass (Ci) at (a) the groundwater table and (b) the fence line

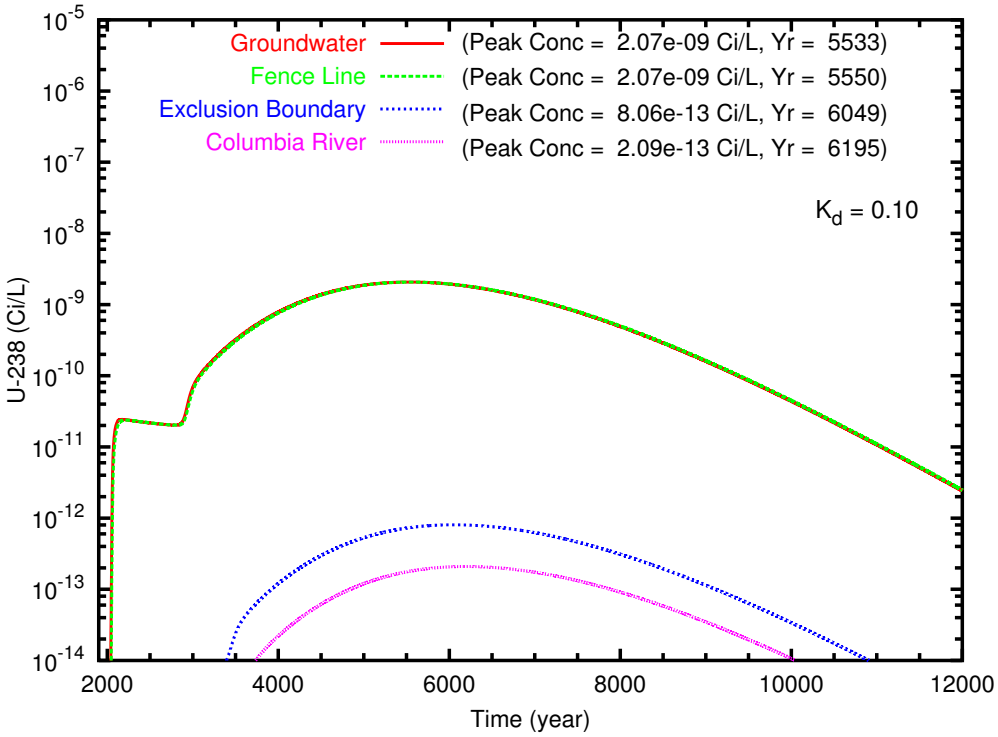

Figure B.4. Case 1, U-238 ($K_d = 0.10$) concentration versus time at the groundwater table and the fence line, exclusion boundary, and Columbia River compliance points

(a)

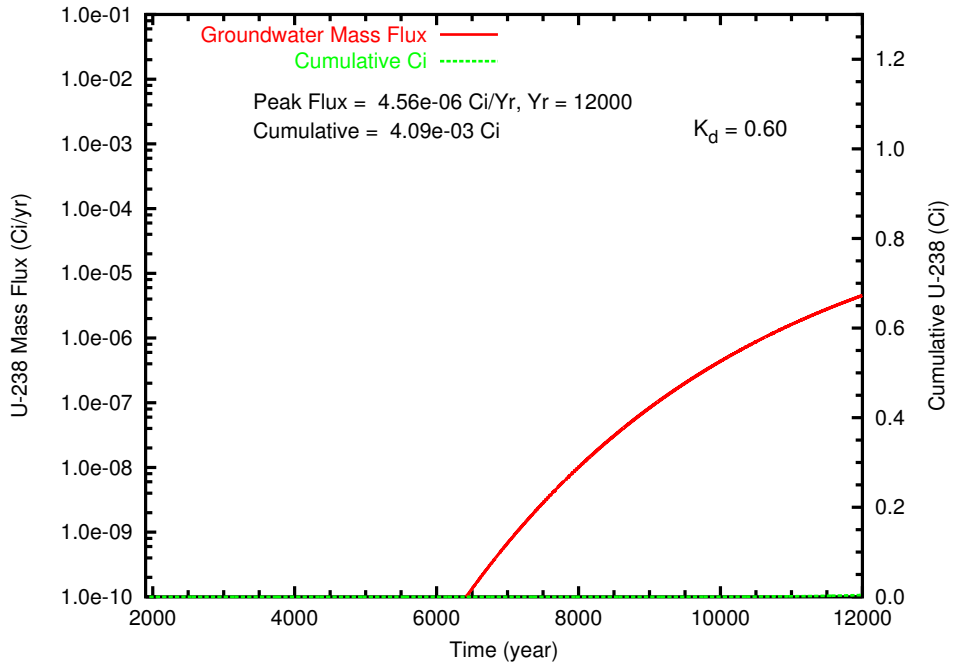

(b)

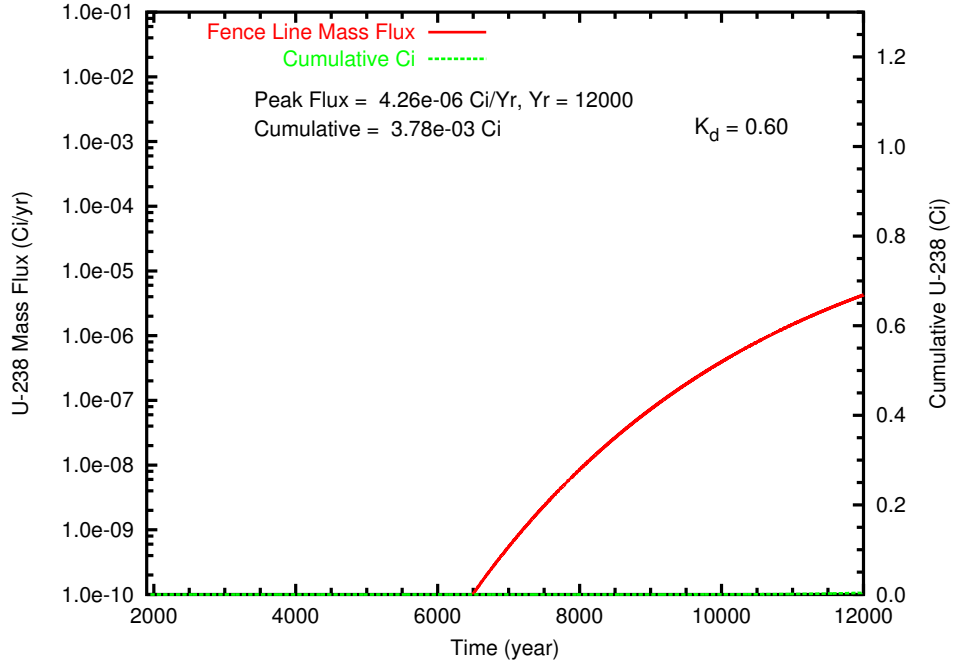

Figure B.5. Case 1, U-238 (K_d = 0.60) mass flux (Ci/L) and cumulative mass (Ci) at (a) the groundwater table and (b) the fence line

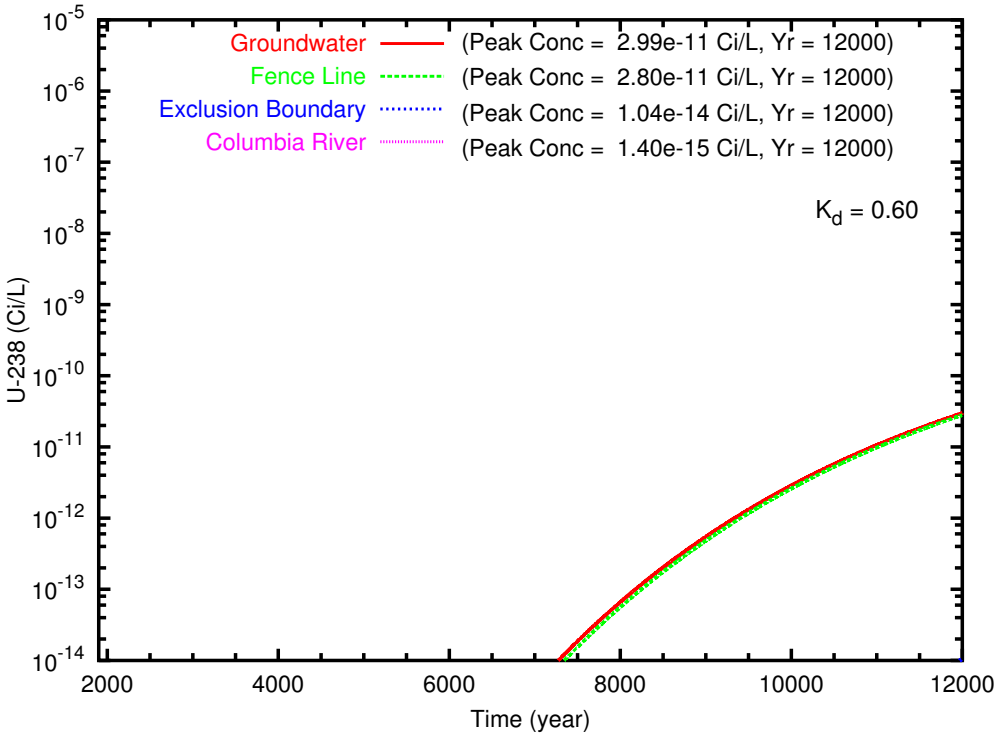

Figure B.6. Case 1, U-238 (K_d = 0.60) concentration versus time at the groundwater table and the fence line, exclusion boundary, and Columbia River compliance points

(a)

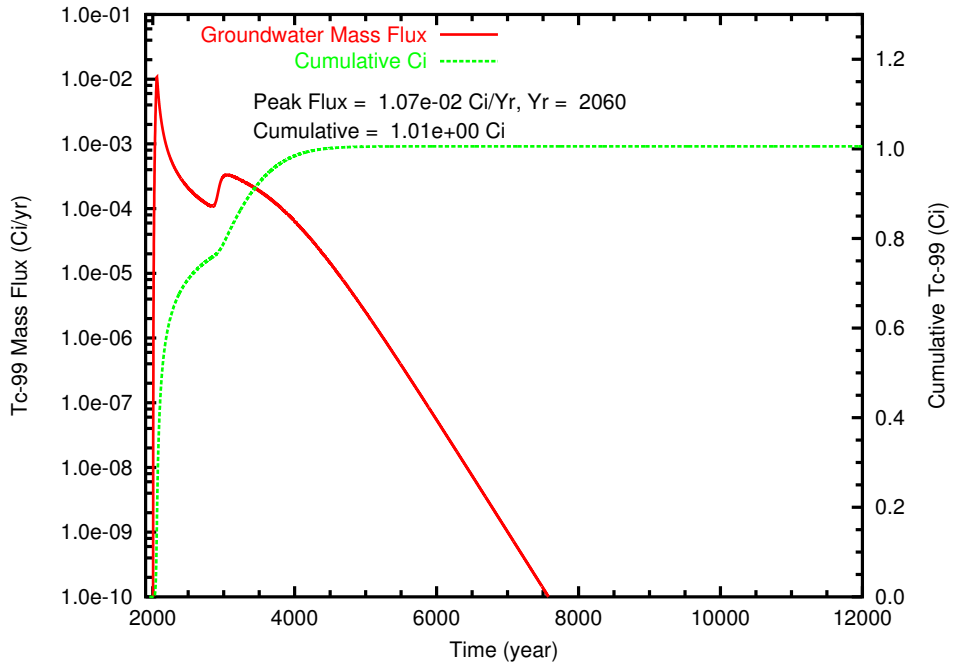

(b)

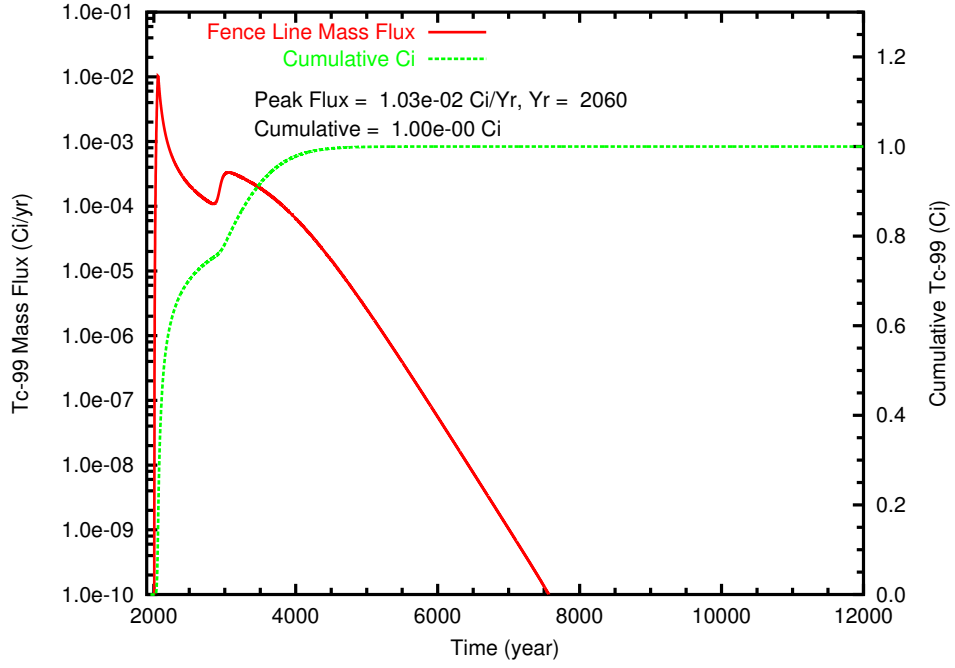

Figure B.7. Case 2, Tc-99 mass flux and cumulative mass at (a) the groundwater table and (b) the fence line

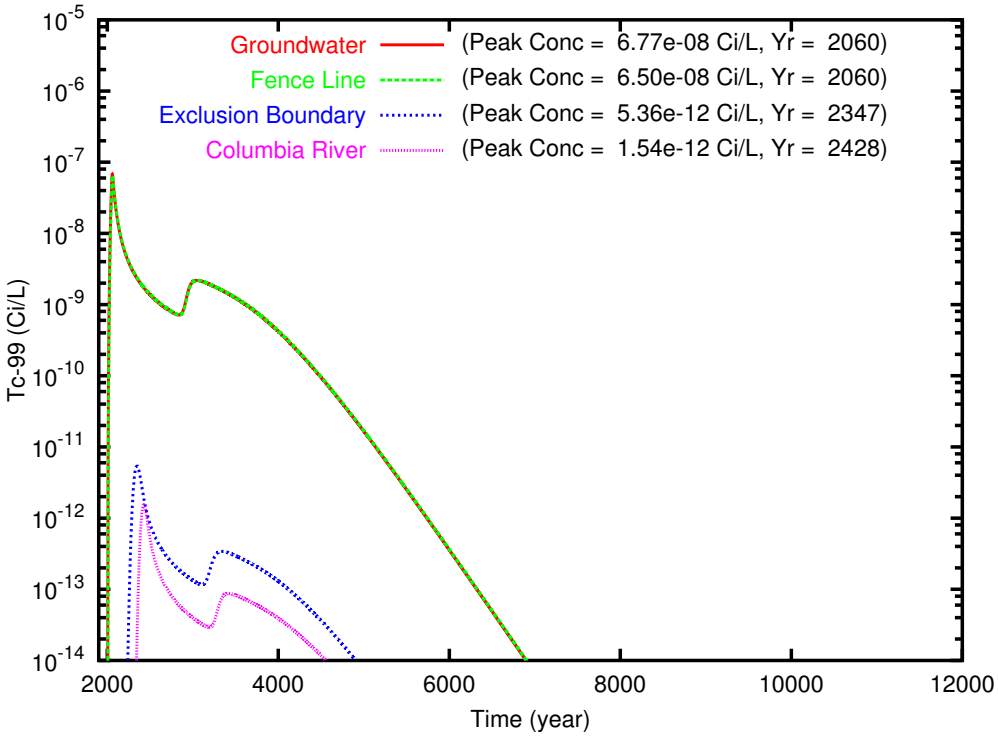

Figure B.8. Case 2, Tc-99 concentration versus time at the groundwater table and the fence line, exclusion boundary, and Columbia River compliance points

(a)

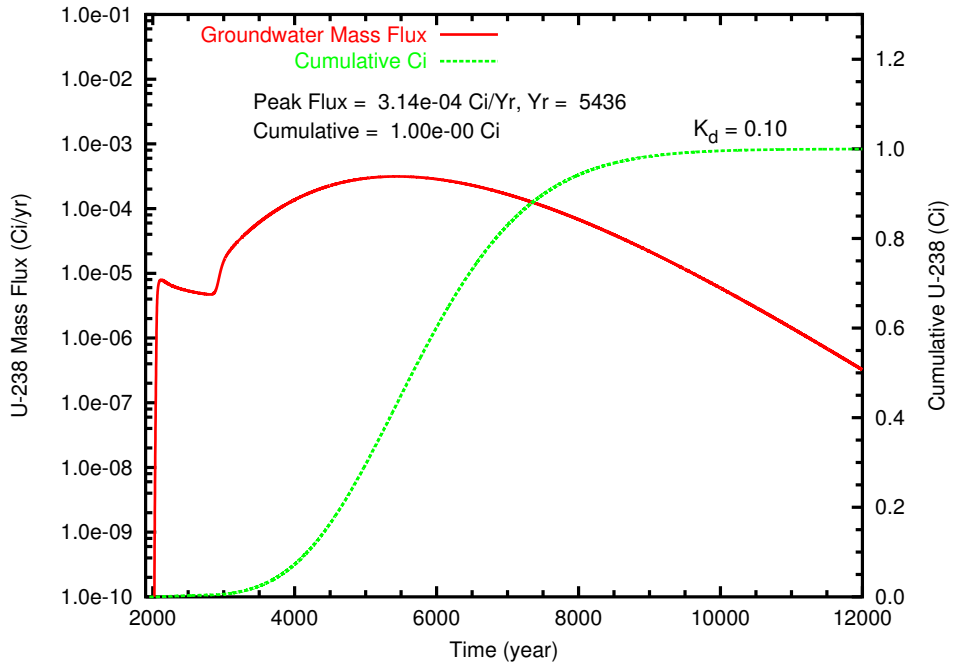

(b)

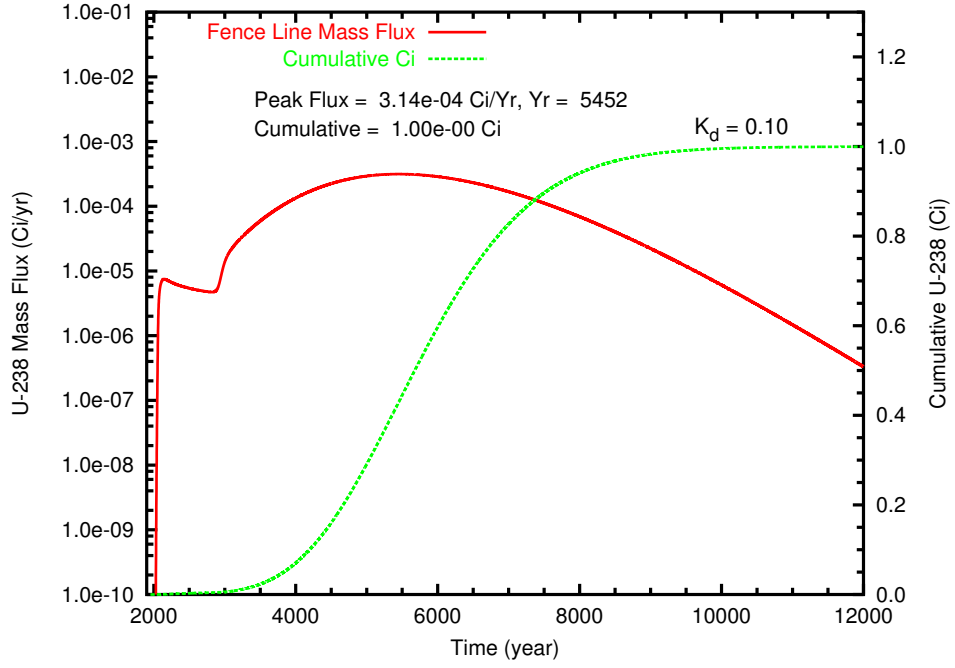

Figure B.9. Case 2, U-238 (K_d = 0.10) mass flux (Ci/L) and cumulative mass (Ci) at (a) the groundwater table and (b) the fence line

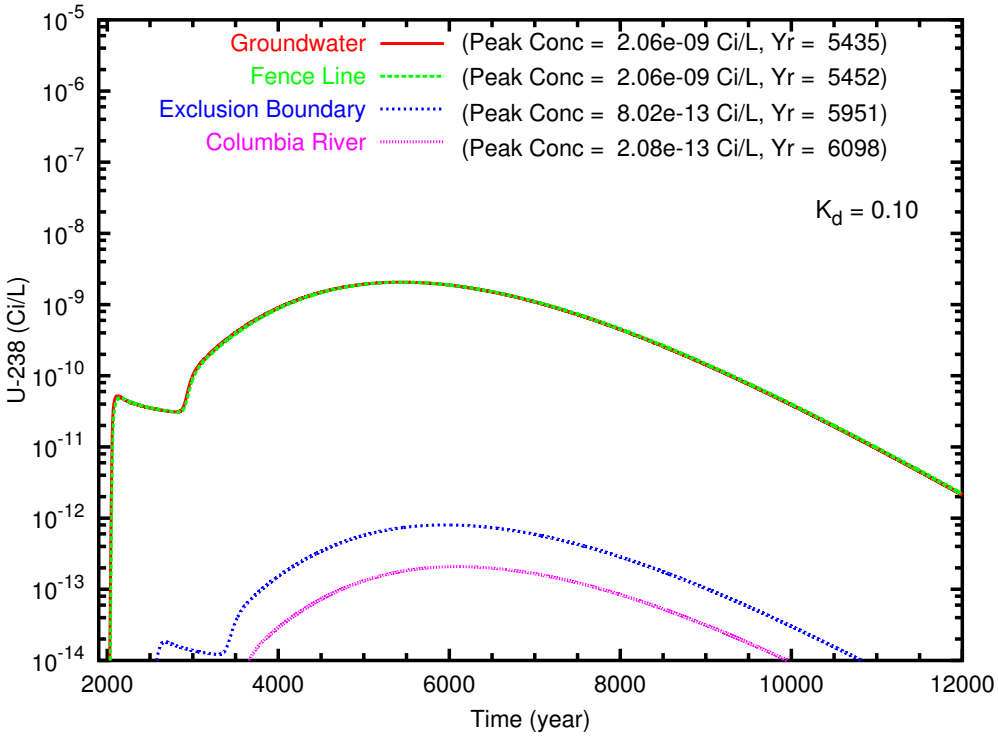

Figure B.10. Case 2, U-238 (K_d = 0.10) concentration versus time at the groundwater table and the fence line, exclusion boundary, and Columbia River compliance points

(a)

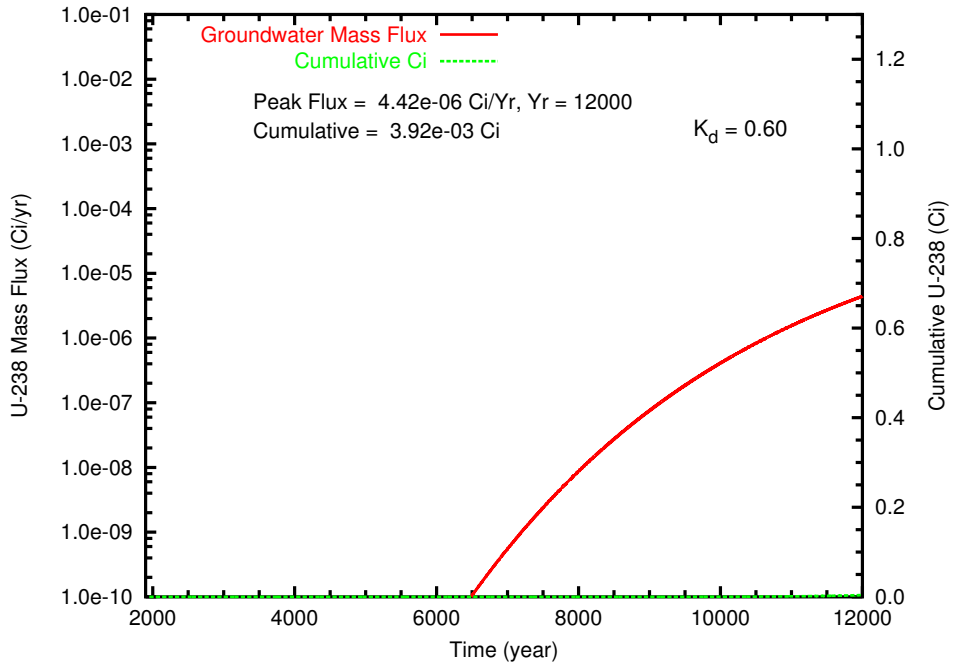

(b)

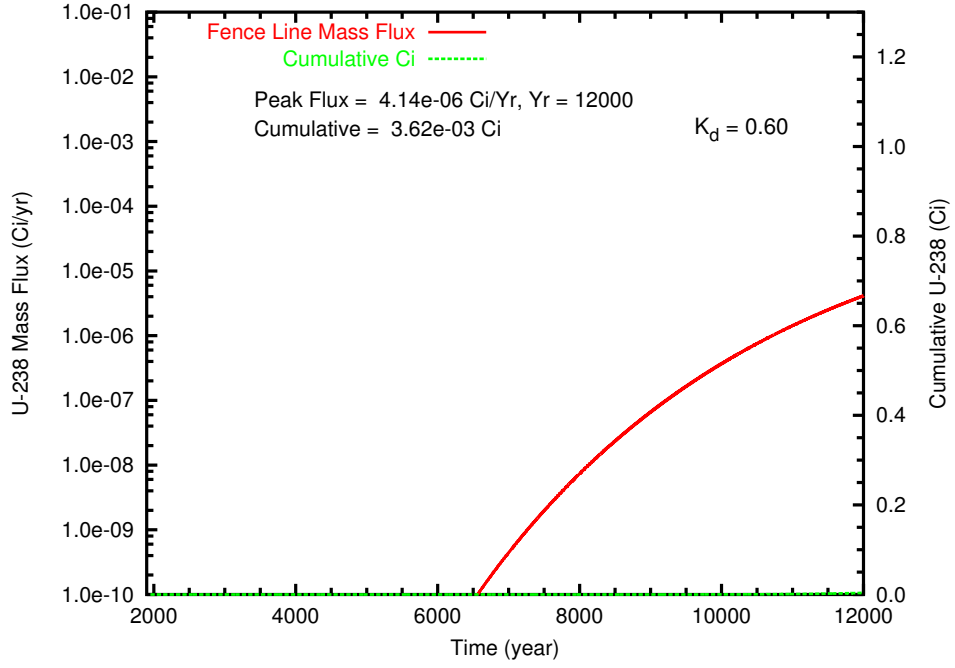

Figure B.11. Case 2, U-238 (K_d = 0.60) mass flux (Ci/L) and cumulative mass (Ci) at (a) the groundwater table and (b) the fence line

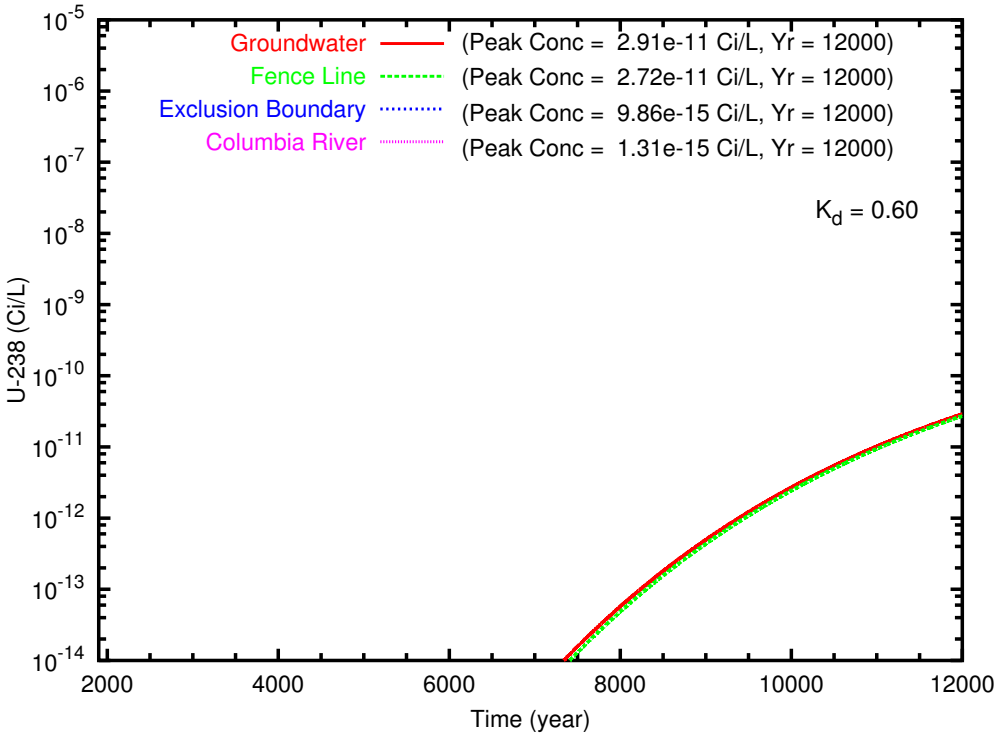

Figure B.12. Case 2, U-238 (K_d = 0.60) concentration versus time at the groundwater table and the fence line, exclusion boundary, and Columbia River compliance points

(a)

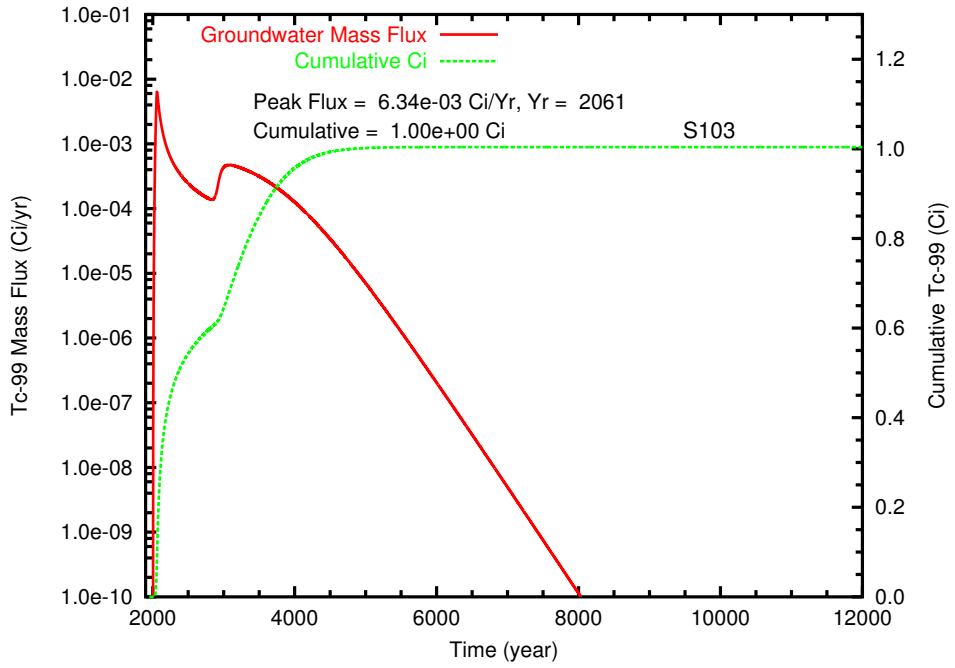

(b)

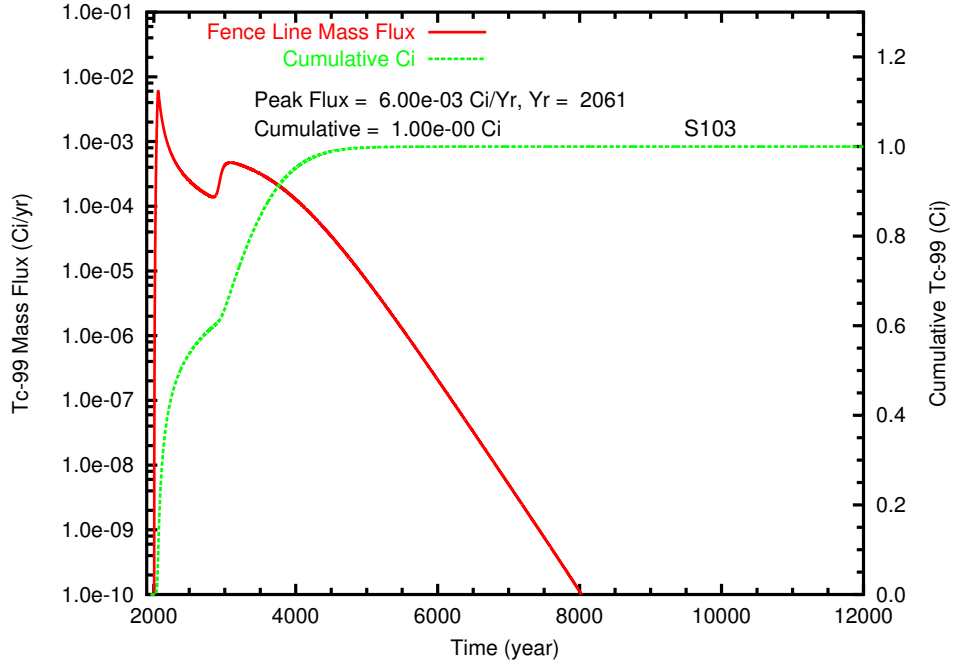

Figure B.13. Case 2v, Mass flux and cumulative mass of Tc-99 from Tank S-103 at (a) the groundwater table and (b) the fence line

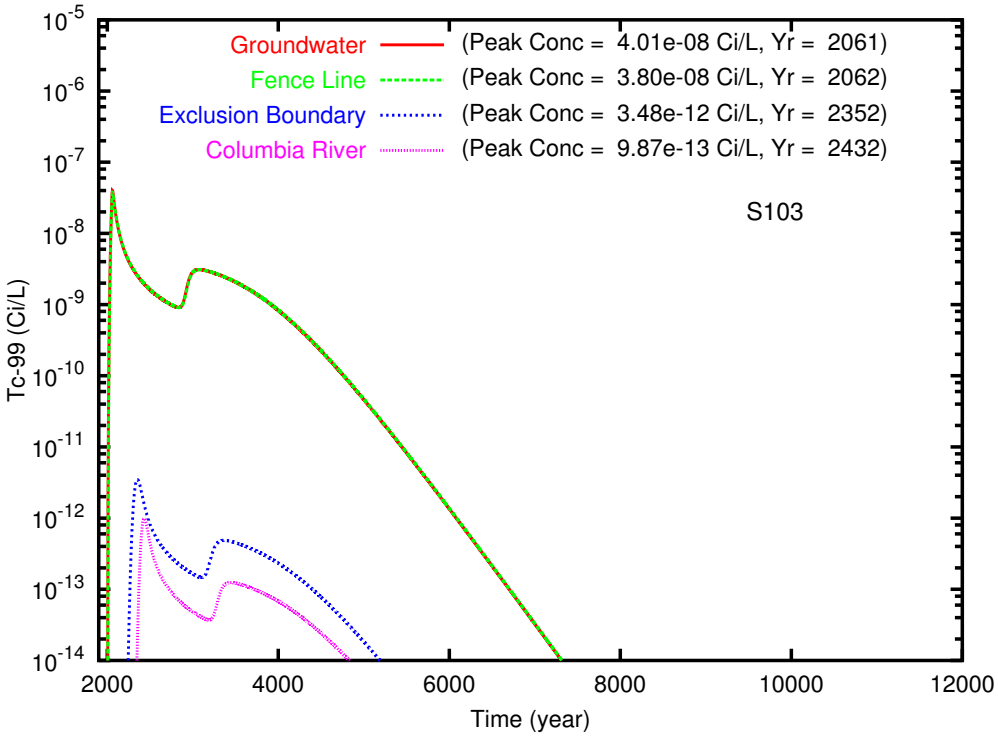

Figure B.14. Case 2v, Concentration of Tc-99 from Tank S-103 at the groundwater table and the fence line, exclusion boundary, and Columbia River compliance points

(a)

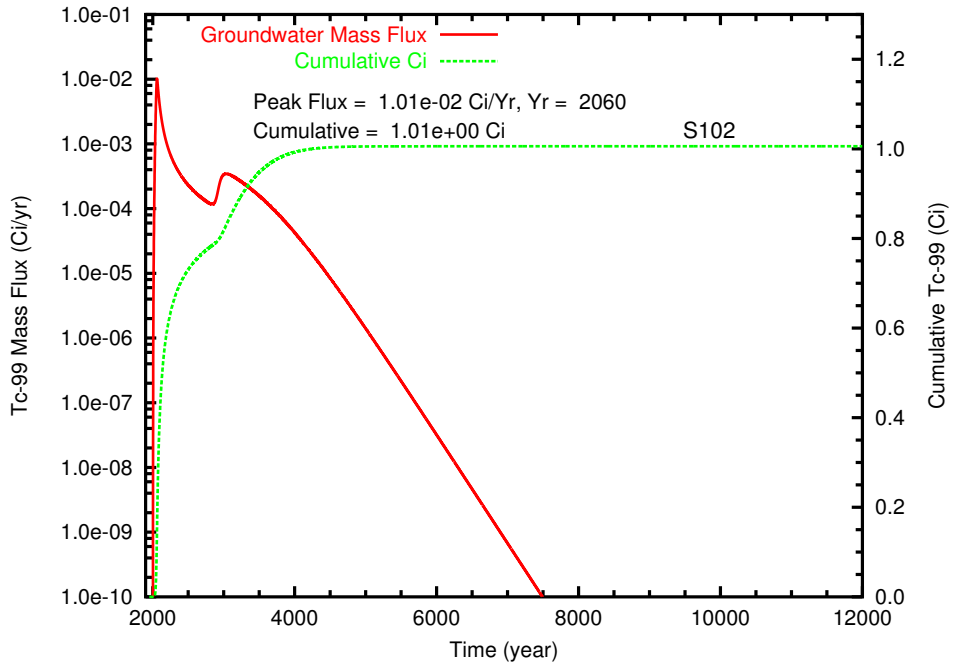

(b)

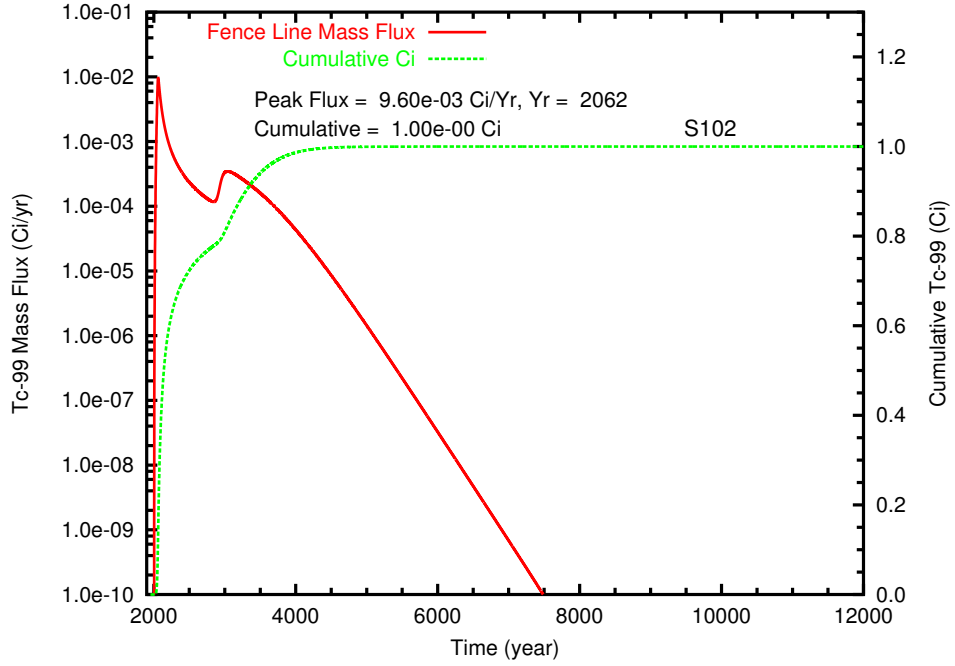

Figure B.15. Case 2v, Mass flux and cumulative mass of Tc-99 from Tank S-102 at (a) the groundwater table and (b) the fence line

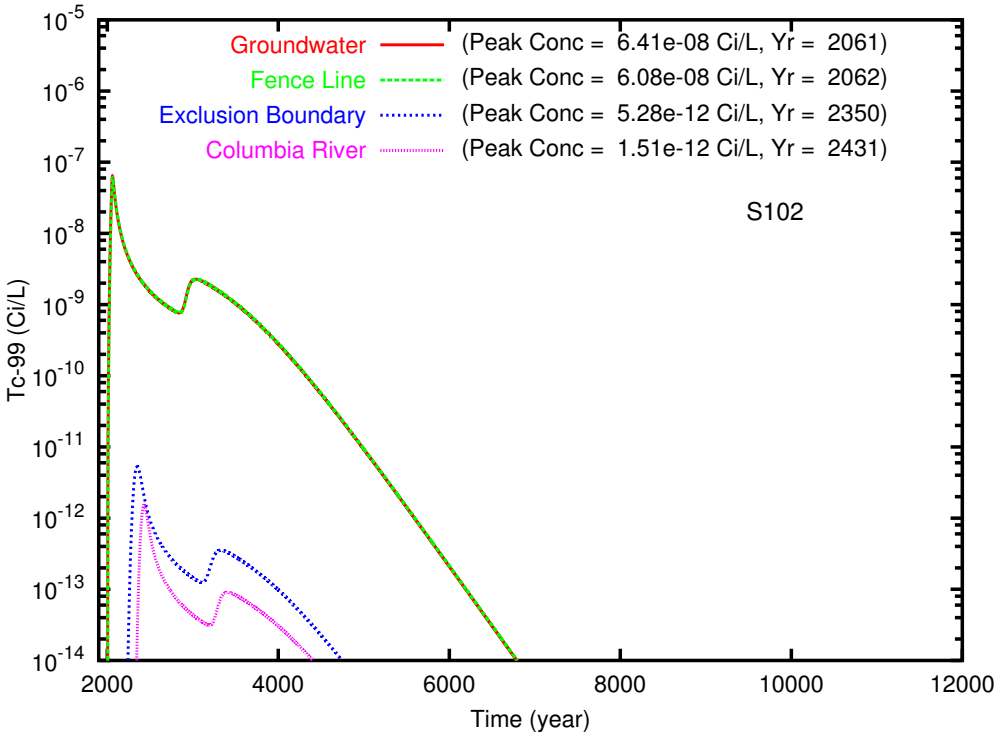

Figure B.16. Case 2v, Concentration of Tc-99 from Tank S-102 at the groundwater table and the fence line, exclusion boundary, and Columbia River compliance points

(a)

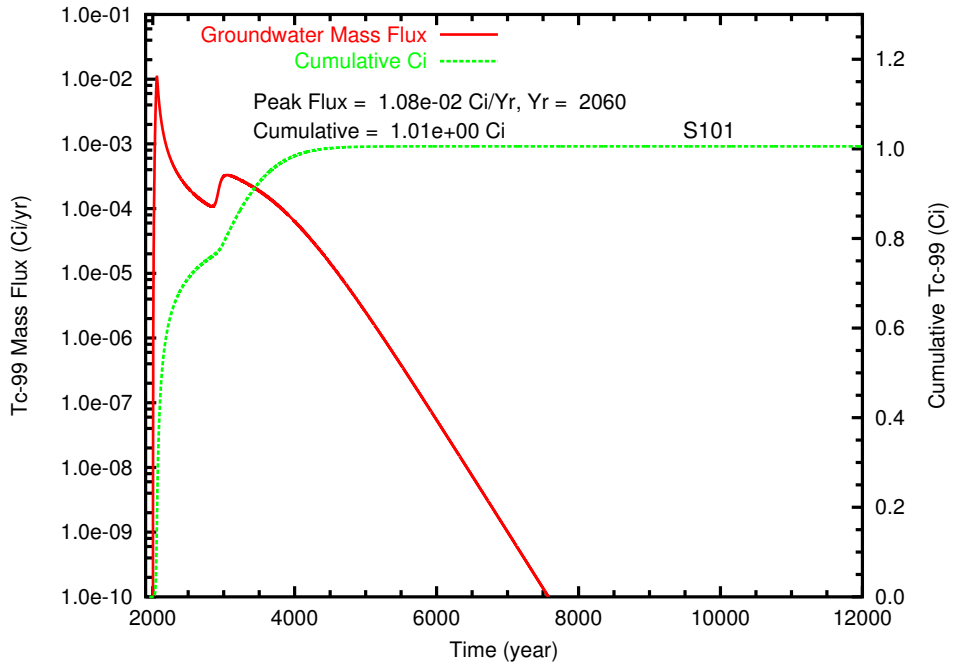

(b)

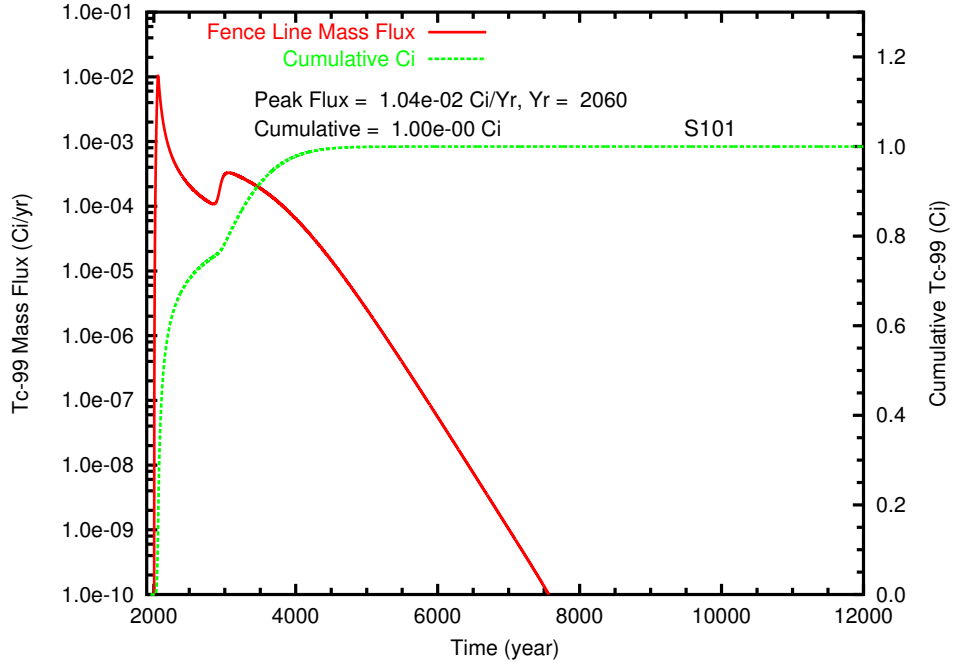

Figure B.17. Case 2v, Mass flux and cumulative mass of Tc-99 from Tank S-101 at (a) the groundwater table and (b) the fence line

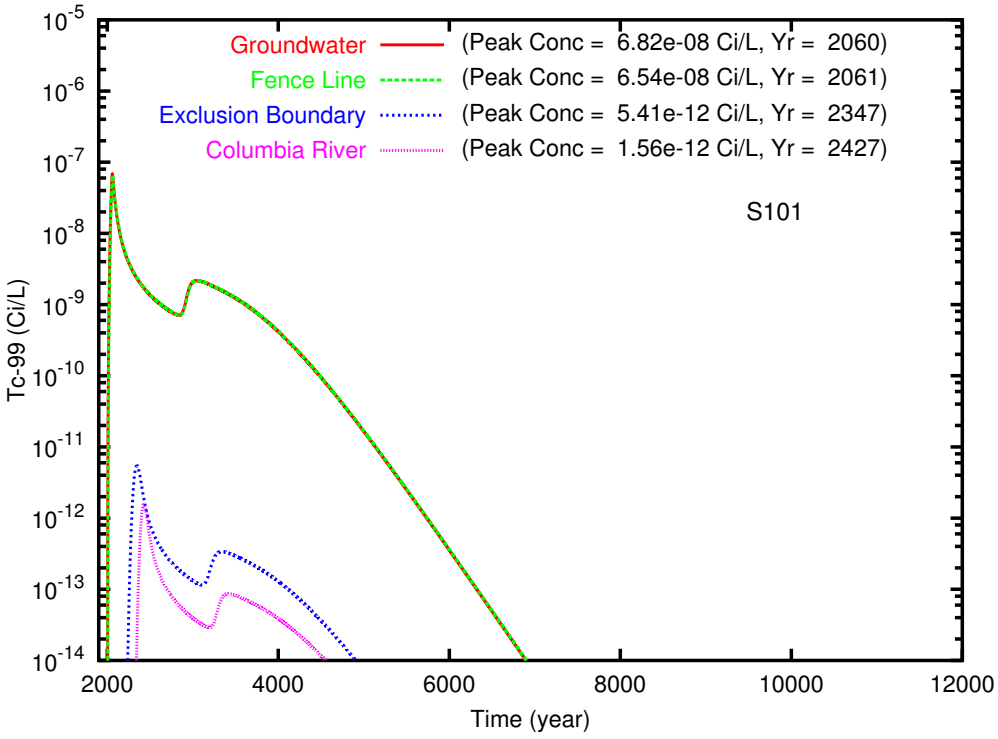

Figure B.18. Case 2v, Concentration of Tc-99 from Tank S-101 at the groundwater table and the fence line, exclusion boundary, and Columbia River compliance points

(a)

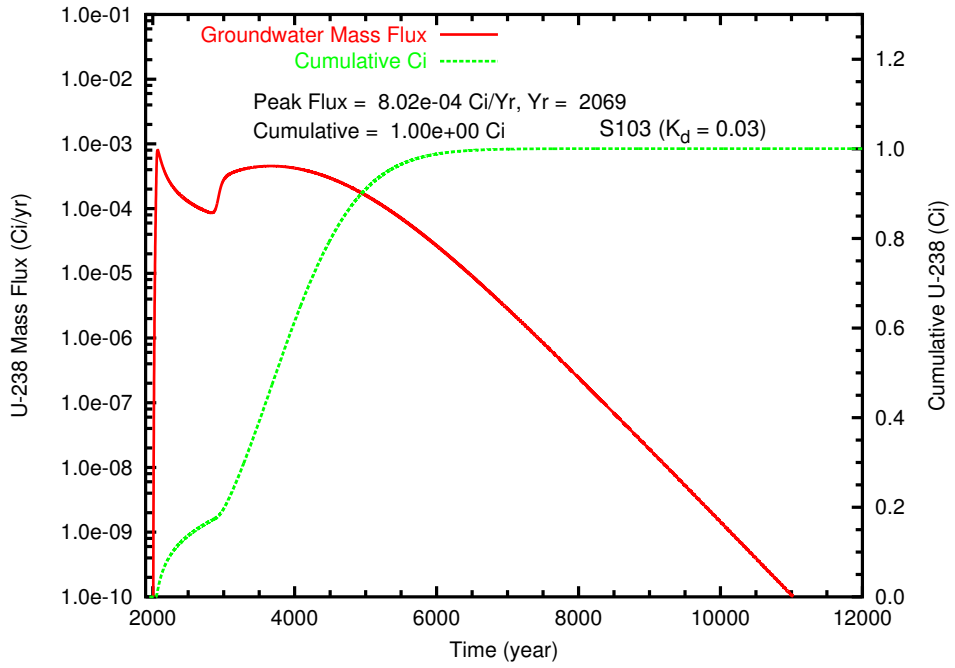

(b)

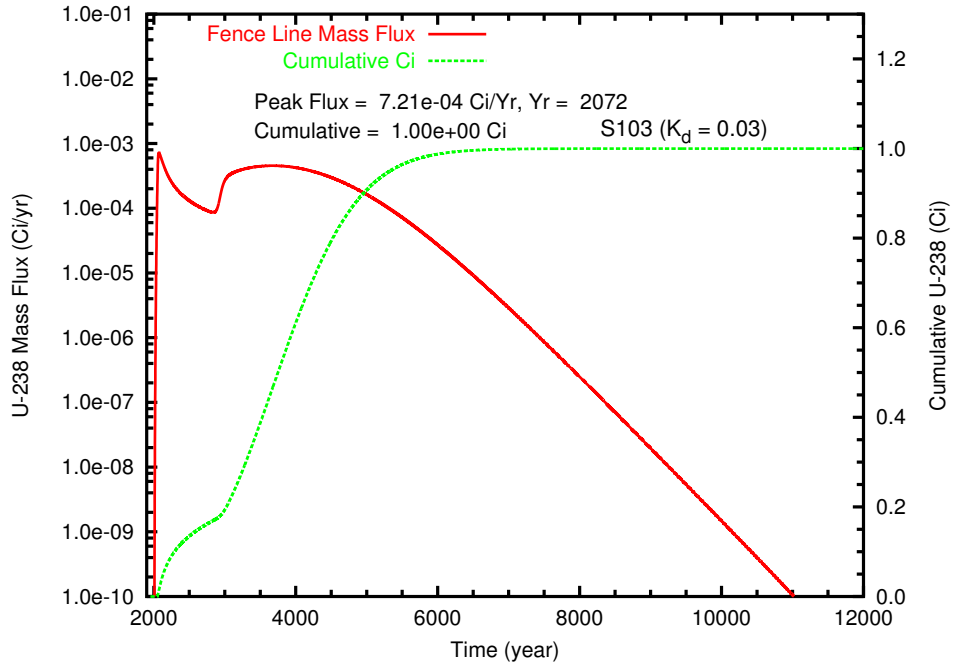

Figure B.19. Case 2v, Mass flux and cumulative mass of U-238 (K_d = 0.03) from Tank S-103 at (a) the groundwater table and (b) the fence line

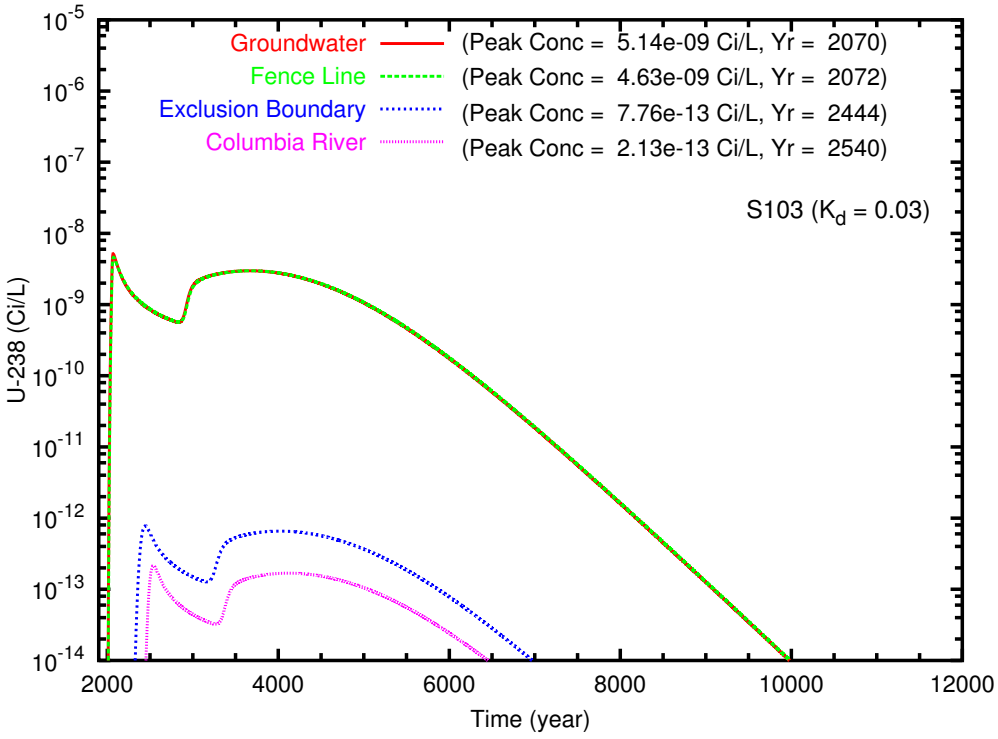

Figure B.20. Case 2v, Concentration of U-238 ($K_d = 0.03$) from Tank S-103 at the groundwater table and the fence line, exclusion boundary, and Columbia River compliance points

(a)

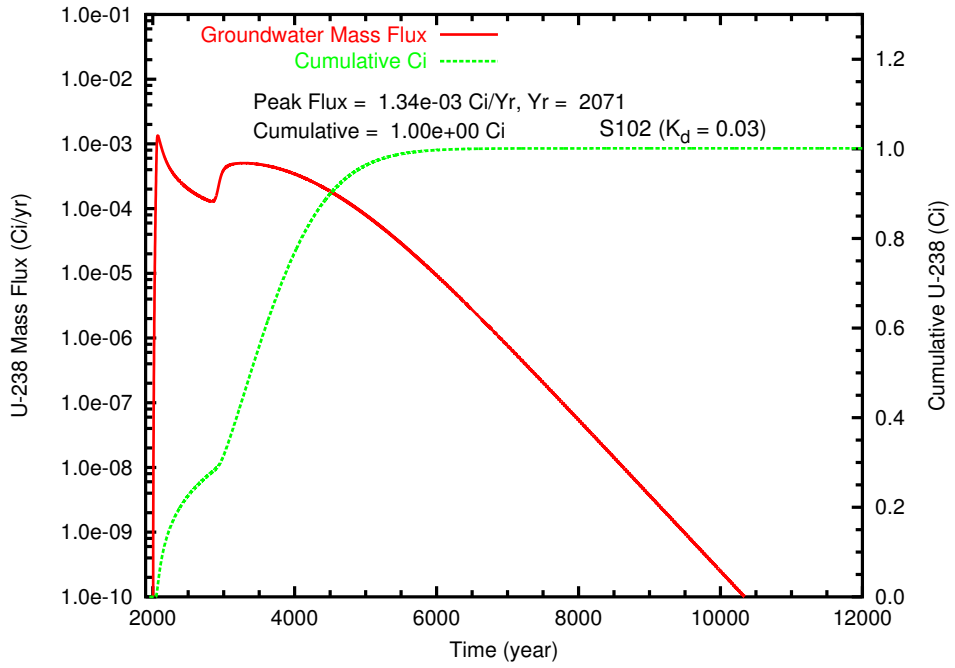

(b)

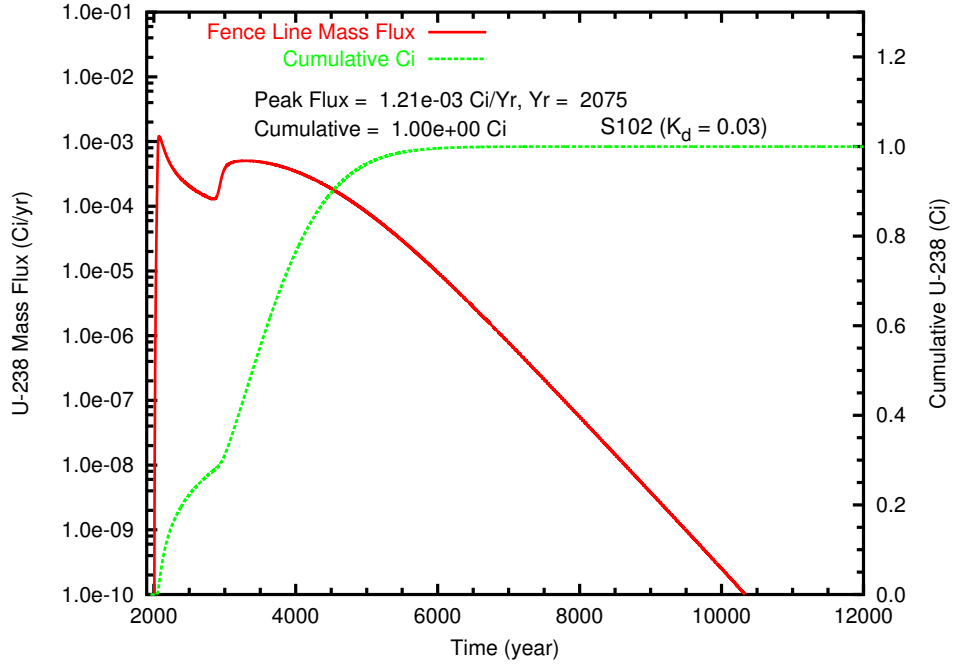

Figure B.21. Case 2v, Mass flux and cumulative mass of U-238 (K_d = 0.03) from Tank S-102 at (a) the groundwater table and (b) the fence line

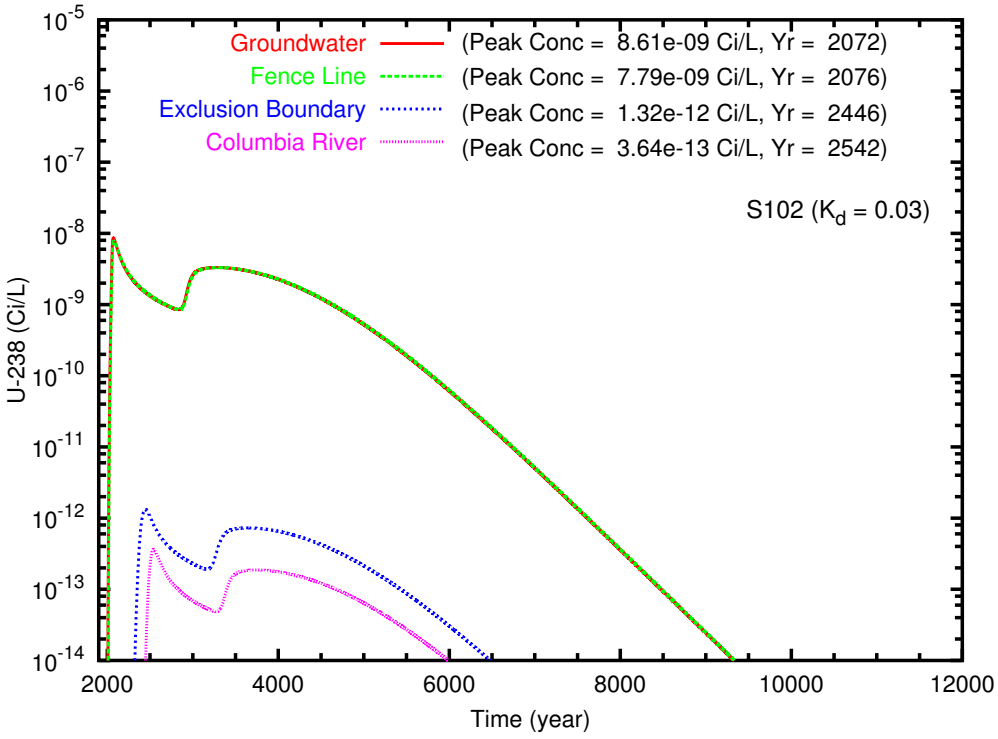

Figure B.22. Case 2v, Concentration of U-238 ($K_d = 0.03$) from Tank S-102 at the groundwater table and the fence line, exclusion boundary, and Columbia River compliance points

(a)

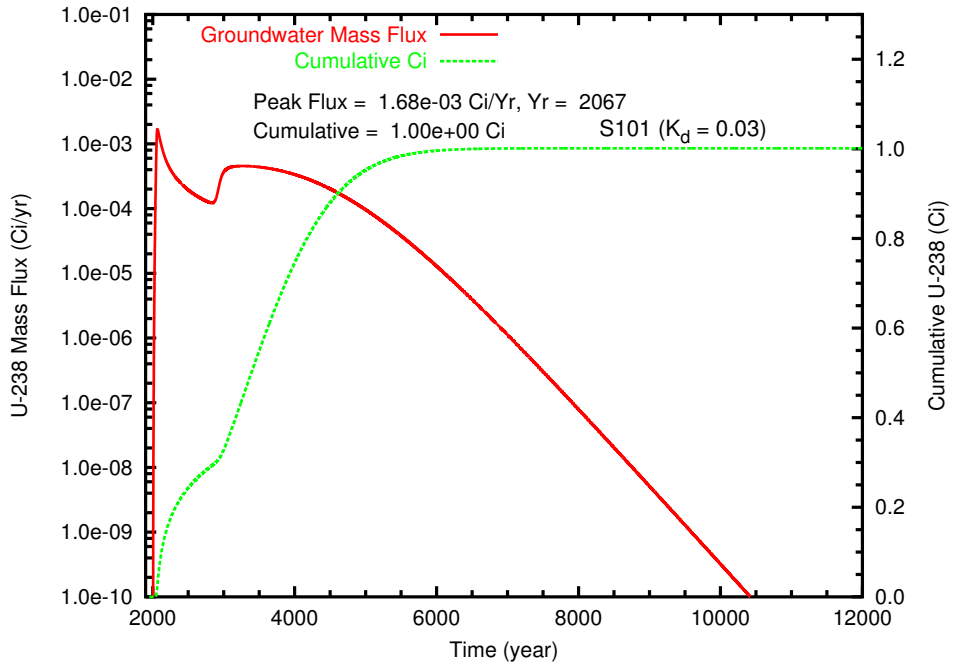

(b)

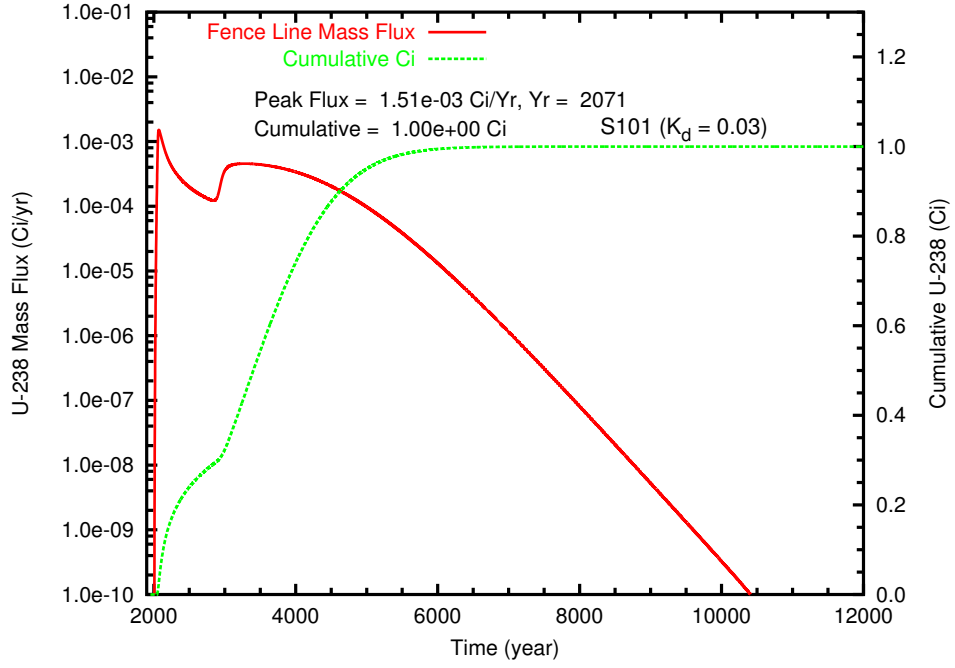

Figure B.23. Case 2v, Mass flux and cumulative mass of U-238 (K_d = 0.03) from Tank S-101 at (a) the groundwater table and (b) the fence line

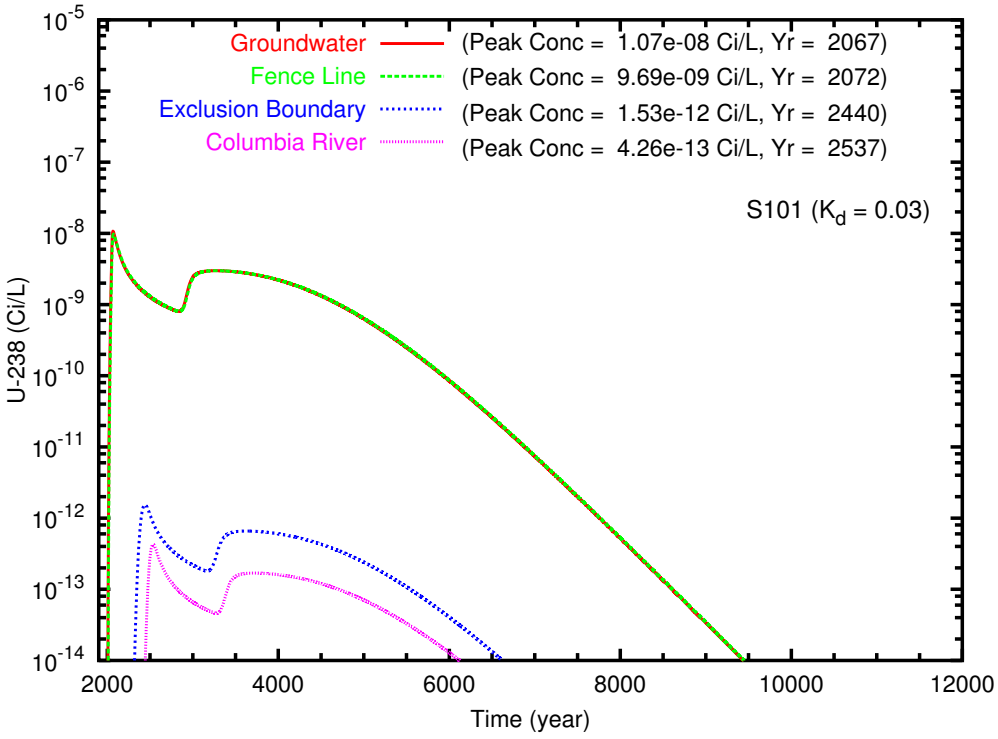

Figure B.24. Case 2v, Concentration of U-238 ($K_d = 0.03$) from Tank S-101 at the groundwater table and the fence line, exclusion boundary, and Columbia River compliance points

(a)

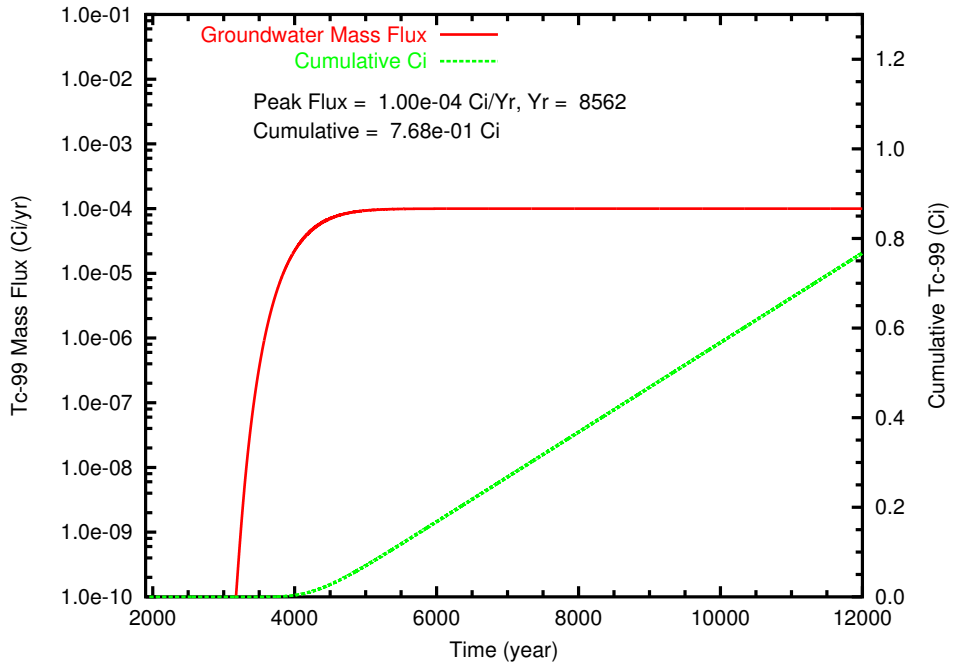

(b)

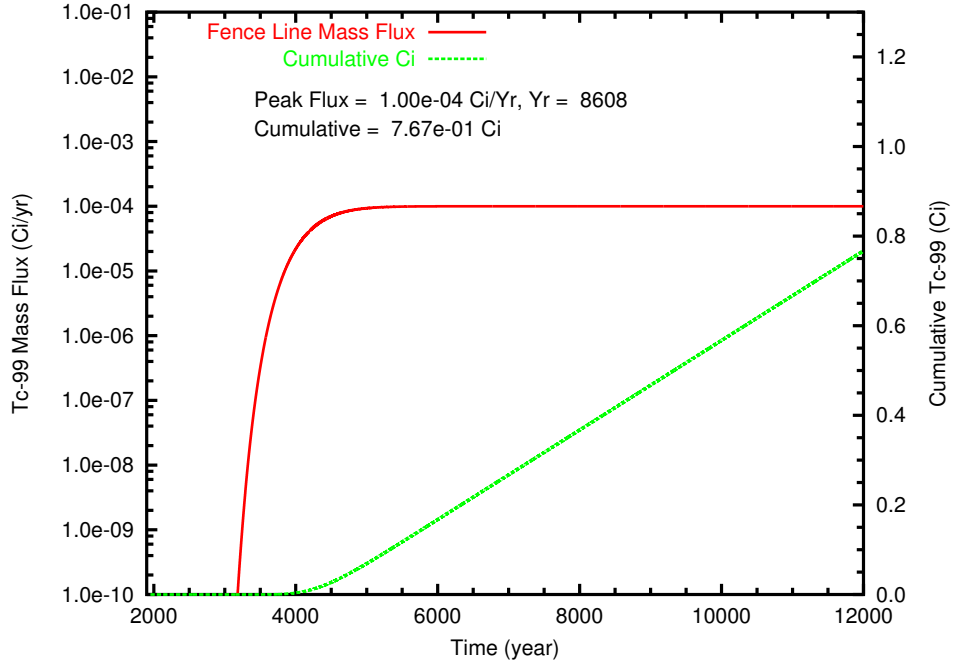

Figure B.25. Case 3, Tc-99 mass flux and cumulative mass at (a) the groundwater table and (b) the fence line

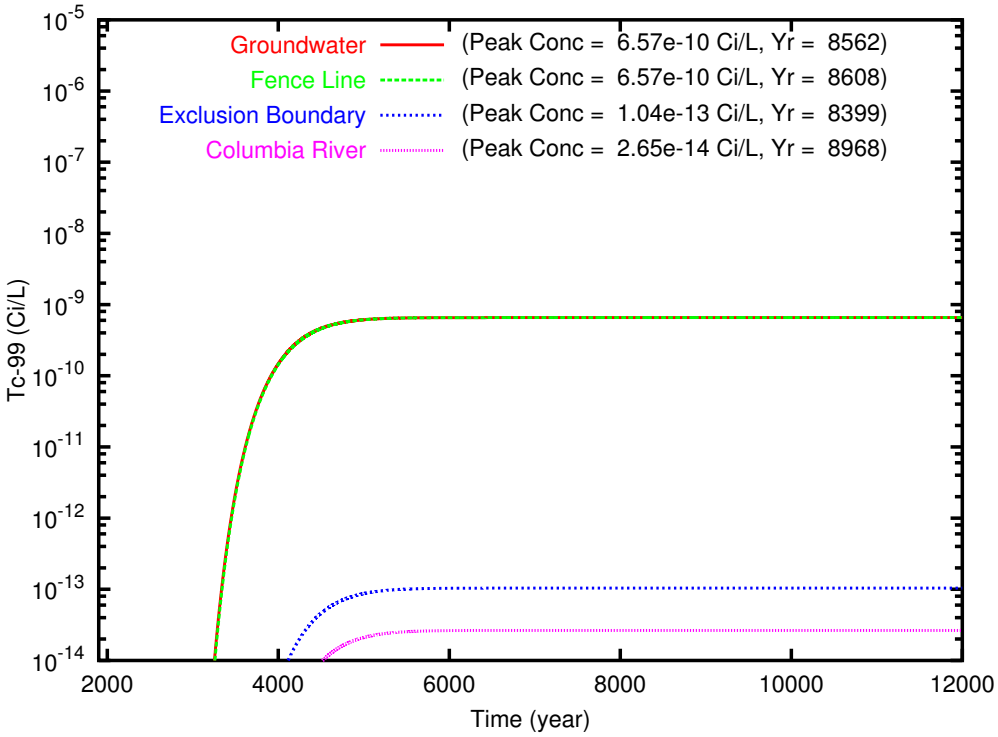

Figure B.26. Case 3, Tc-99 concentration versus time at the groundwater table and the fence line, exclusion boundary, and Columbia River compliance points

(a)

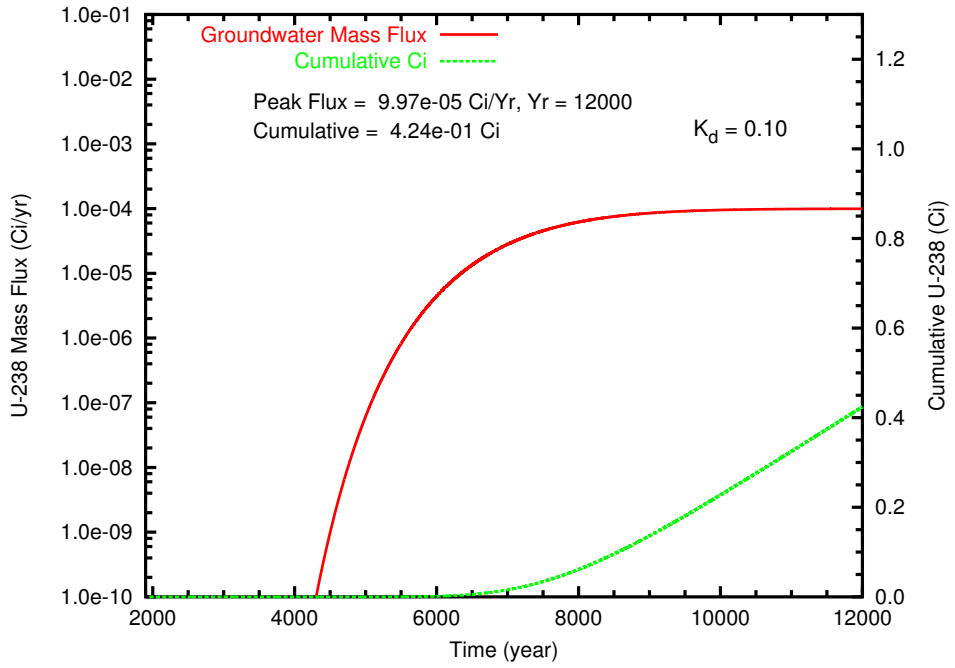

(b)

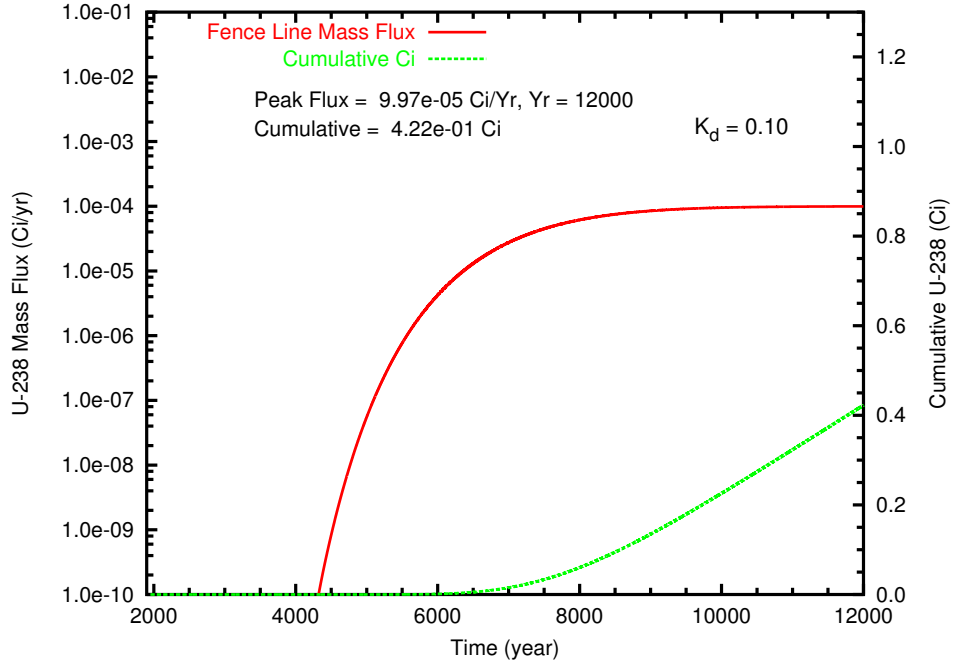

Figure B.27. Case 3, U-238 (K_d = 0.10) mass flux (Ci/L) and cumulative mass (Ci) at (a) the groundwater table and (b) the fence line

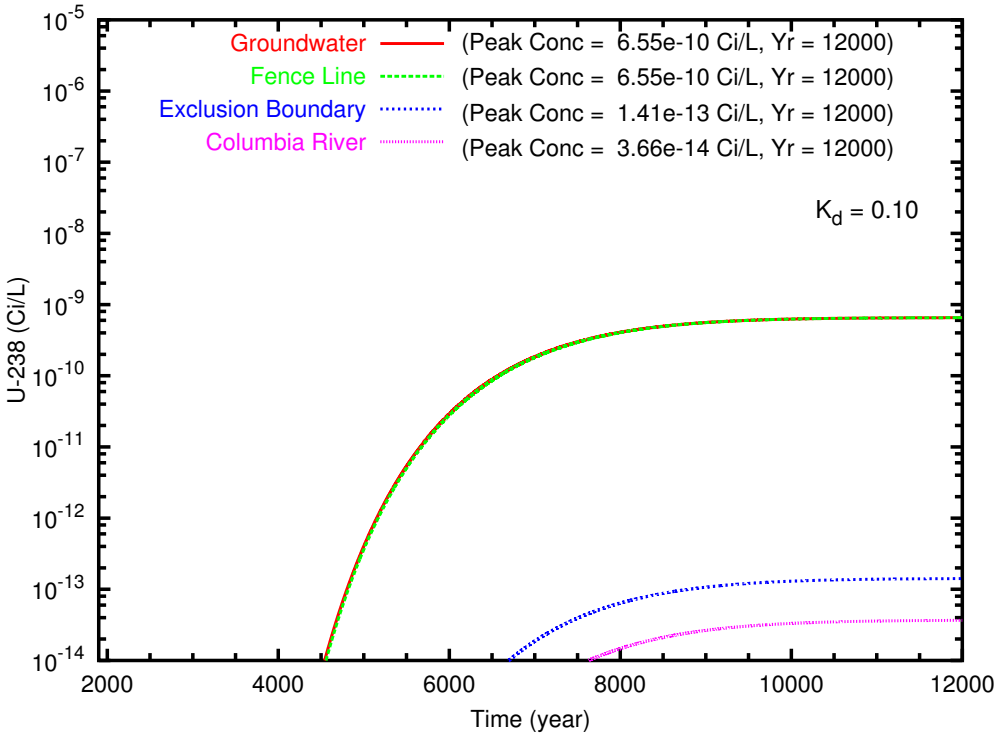

Figure B.28. Case 3, U-238 (K_d = 0.10) concentration versus time at the groundwater table and the fence line, exclusion boundary, and Columbia River compliance points

(a)

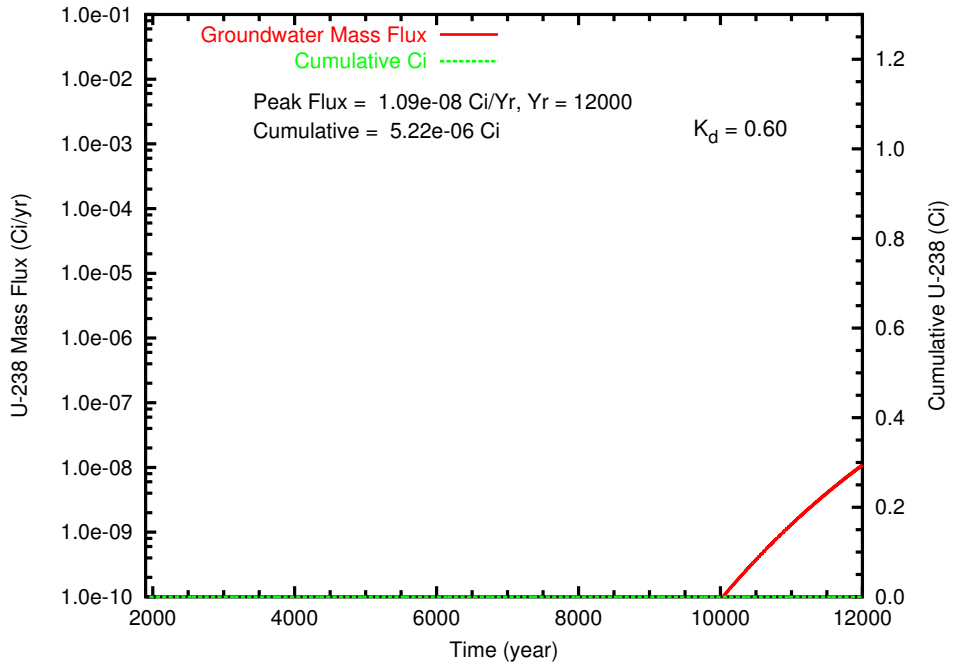

(b)

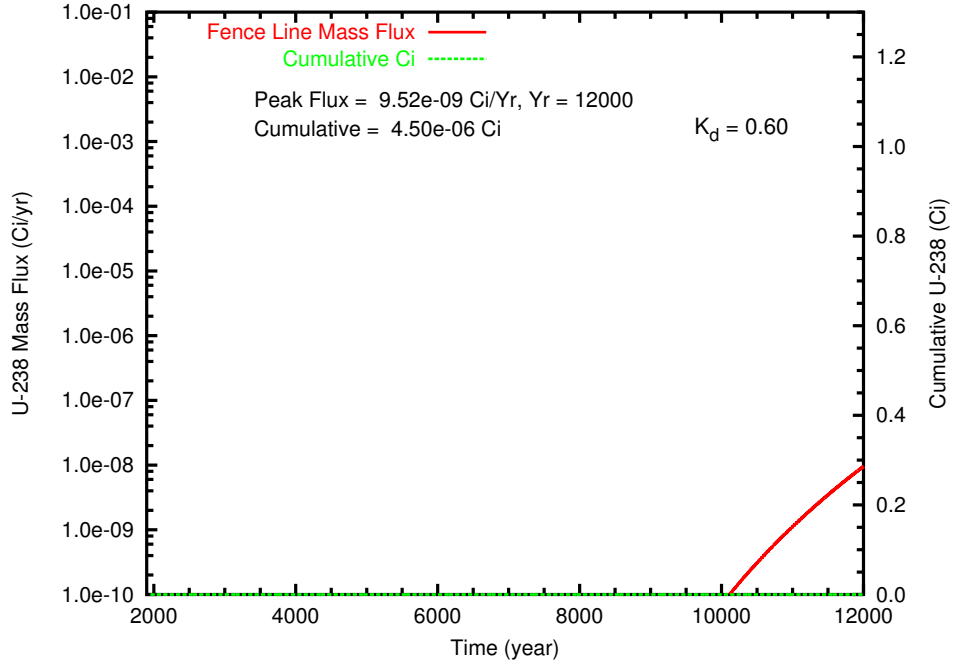

Figure B.29. Case 3, U-238 (K_d = 0.60) mass flux (Ci/L) and cumulative mass (Ci) at (a) the groundwater table and (b) the fence line

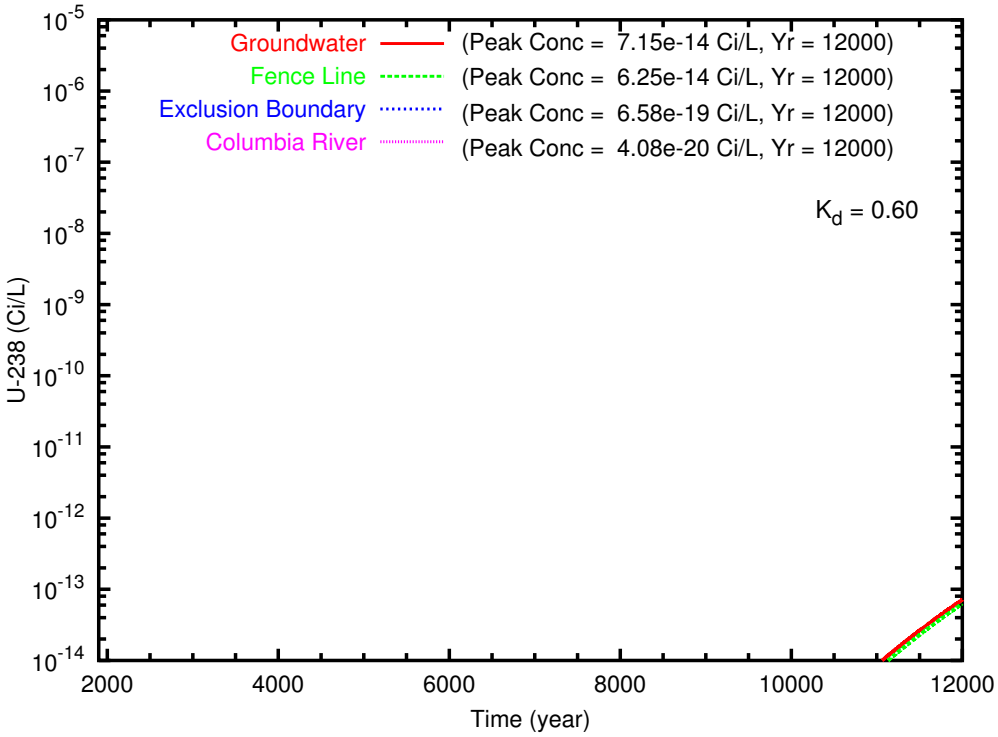

Figure B.30. Case 3, U-238 (K_d = 0.60) concentration versus time at the groundwater table and the fence line, exclusion boundary, and Columbia River compliance points

(a)

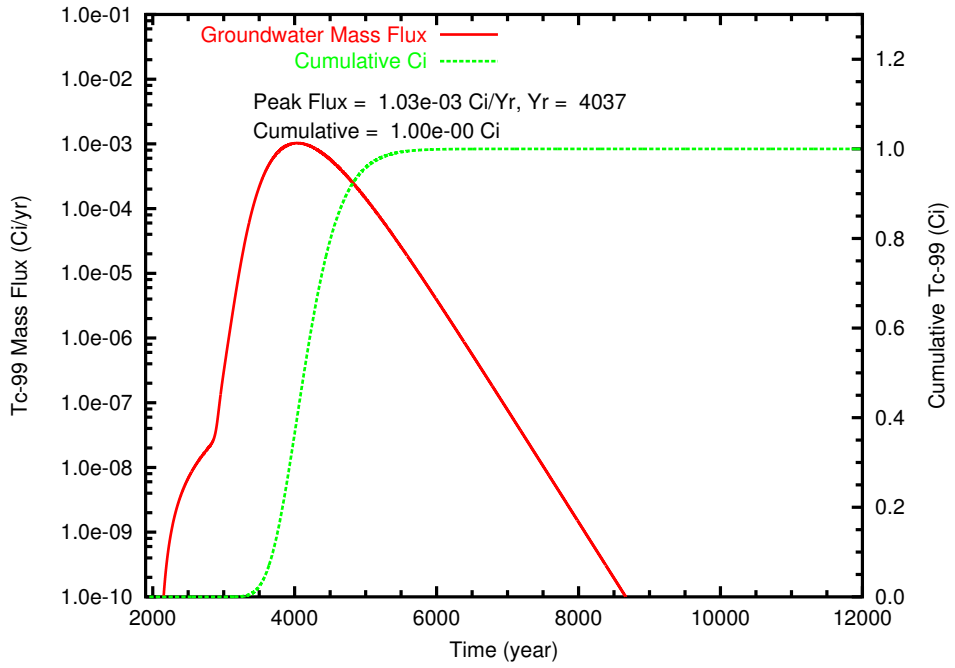

(b)

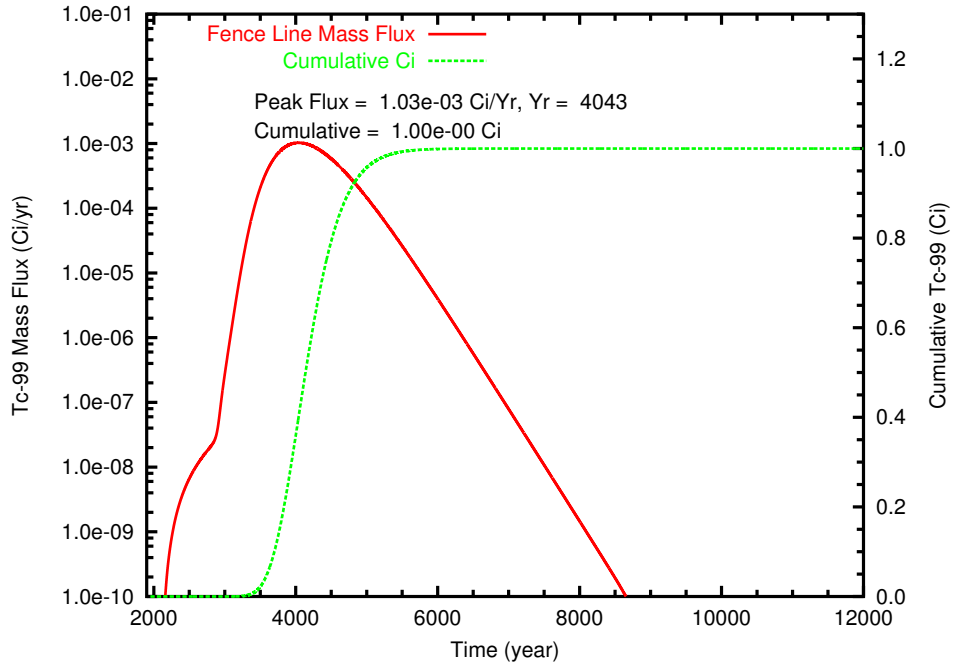

Figure B.31. Case 4, Tc-99 mass flux and cumulative mass at (a) the groundwater table and (b) the fence line

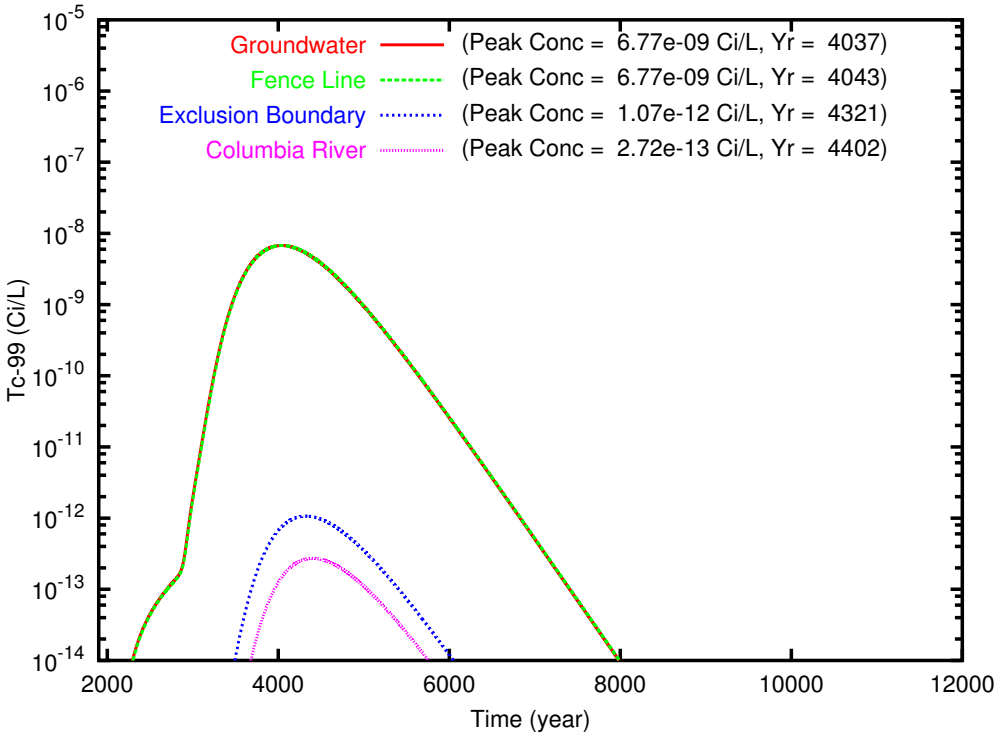

Figure B.32. Case 4, Tc-99 concentration versus time at the groundwater table and the fence line, exclusion boundary, and Columbia River compliance points

(a)

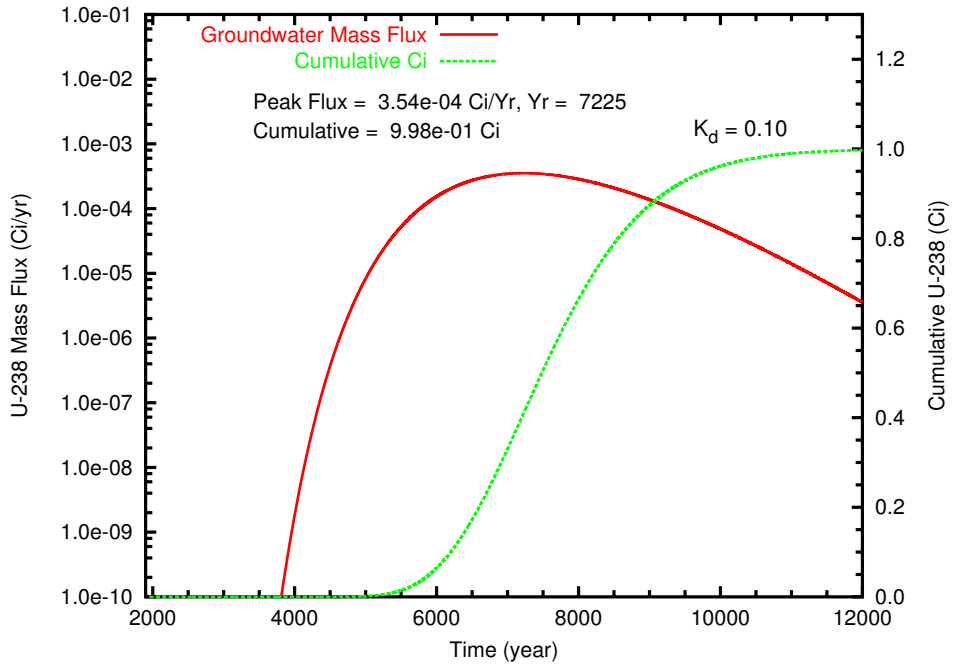

(b)

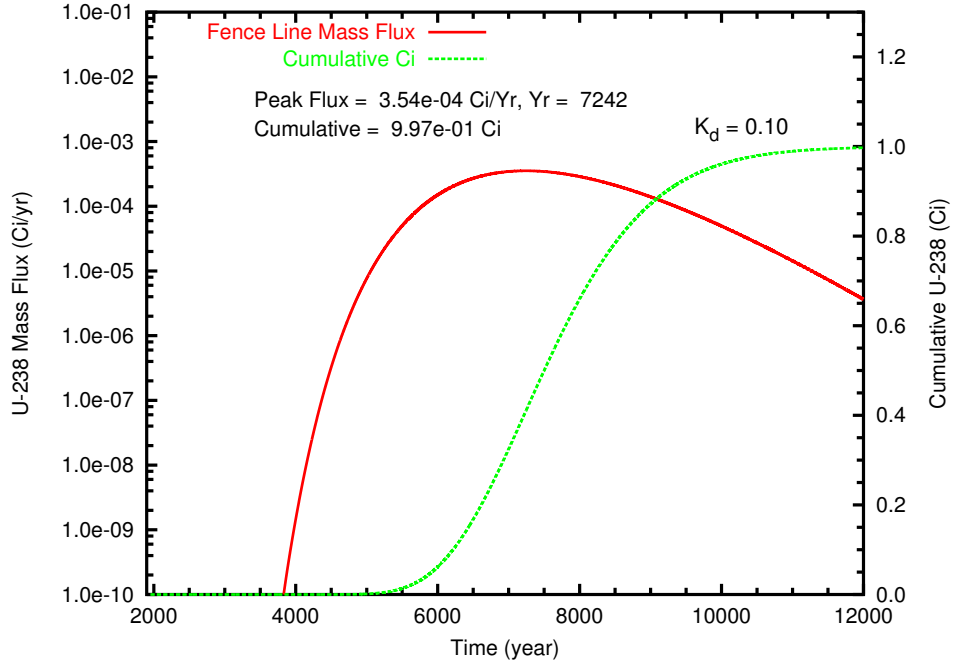

Figure B.33. Case 4, U-238 (K_d = 0.10) mass flux (Ci/L) and cumulative mass (Ci) at (a) the groundwater table and (b) the fence line

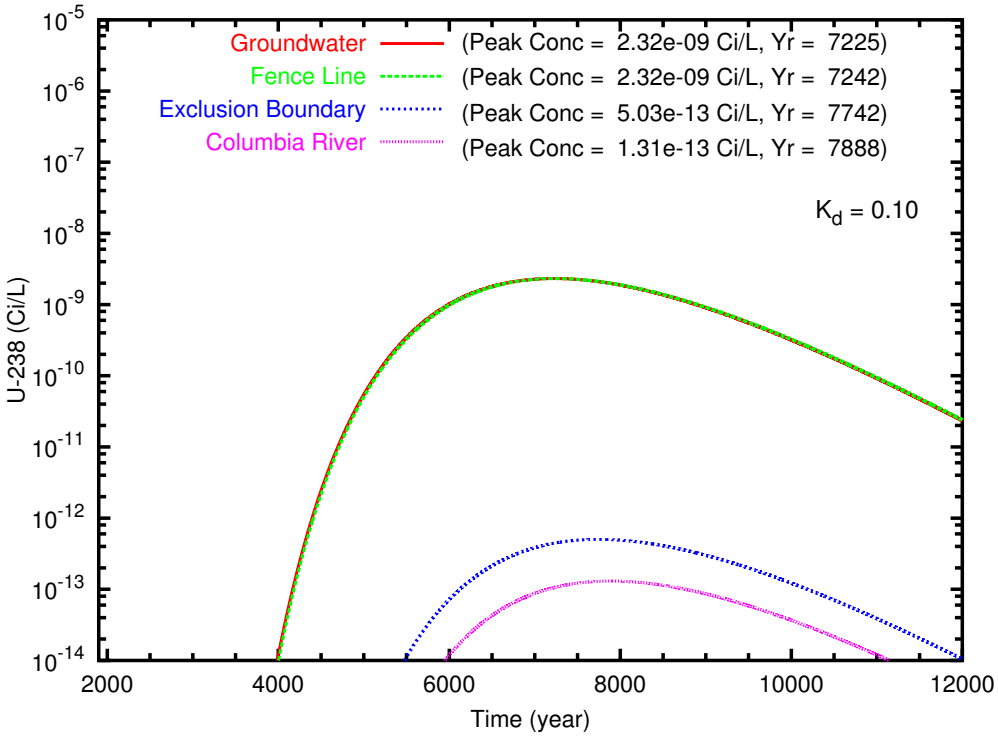

Figure B.34. Case 4, U-238 (K_d = 0.10) concentration versus time at the groundwater table and the fence line, exclusion boundary, and Columbia River compliance points

(a)

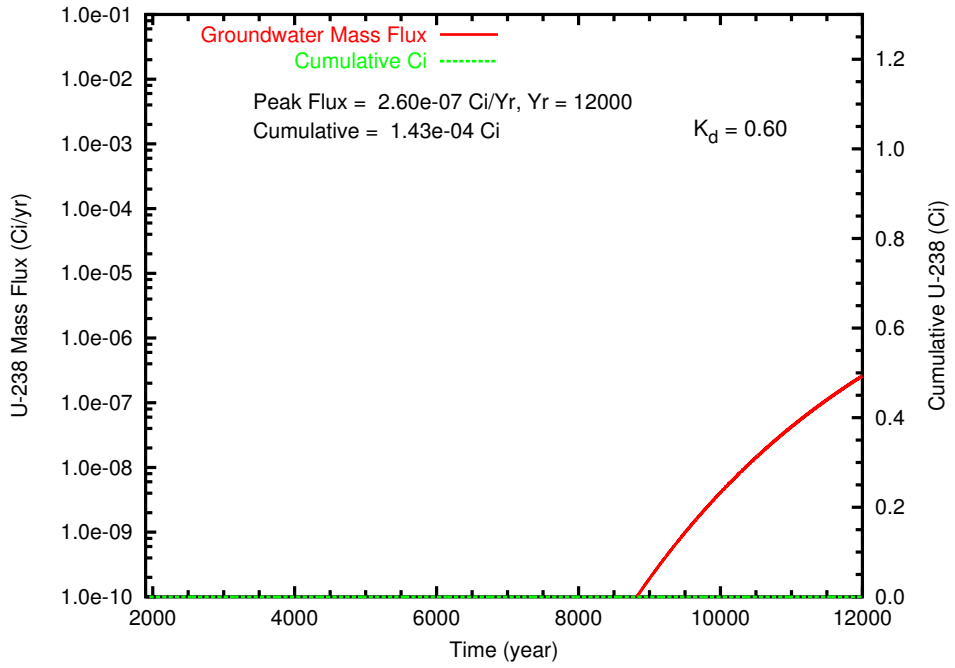

(b)

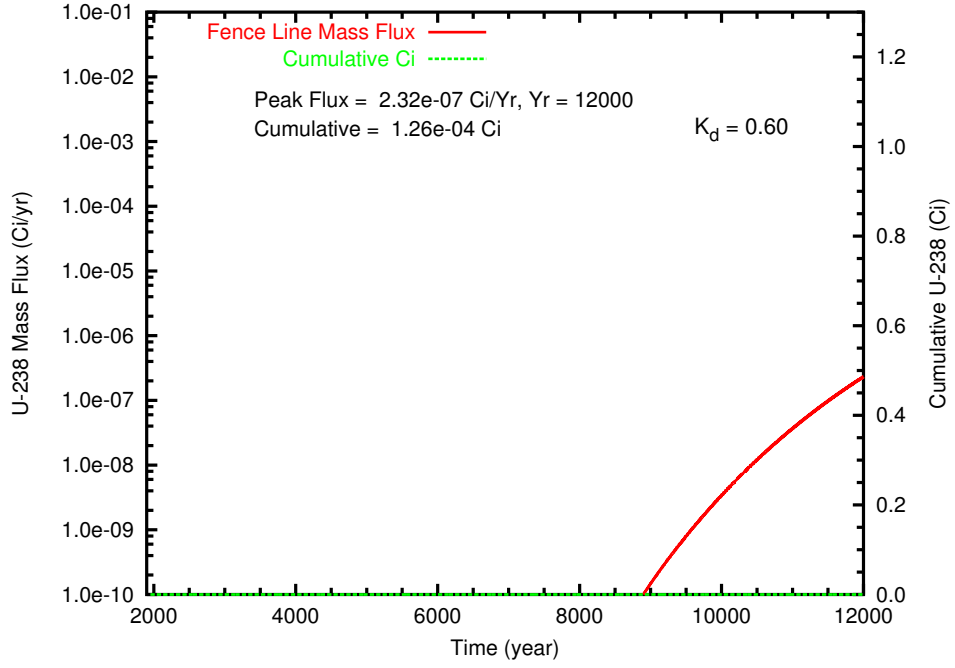

Figure B.35. Case 4, U-238 (K_d = 0.60) mass flux (Ci/L) and cumulative mass (Ci) at (a) the groundwater table and (b) the fence line

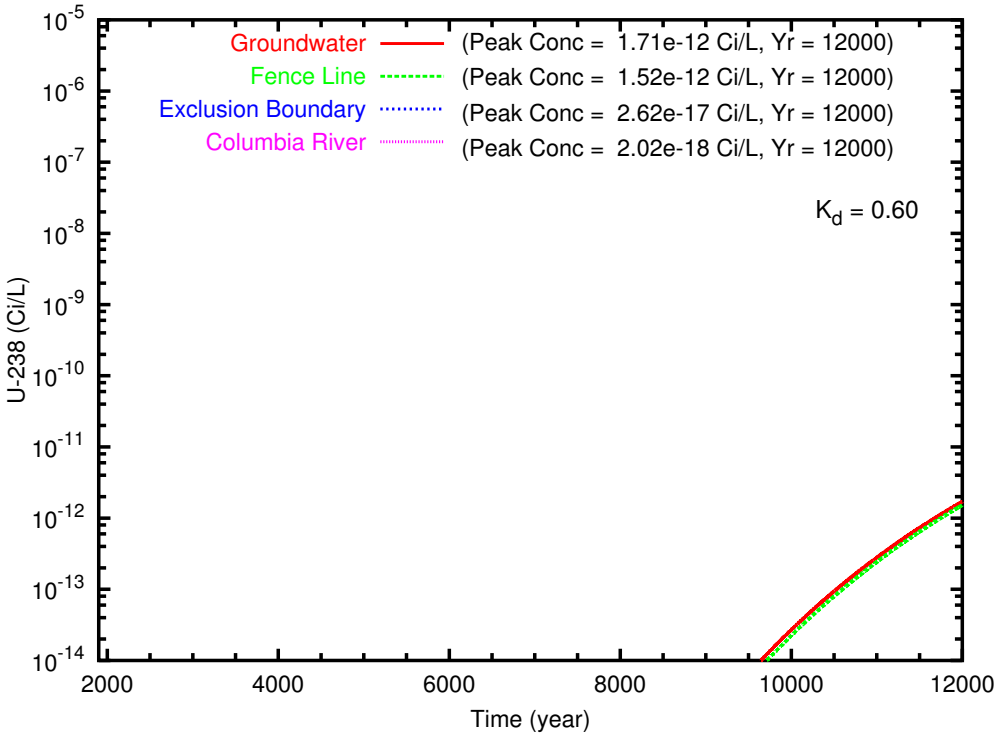

Figure B.36. Case 4, U-238 (K_d = 0.60) concentration versus time at the groundwater table and the fence line, exclusion boundary, and Columbia River compliance points

(a)

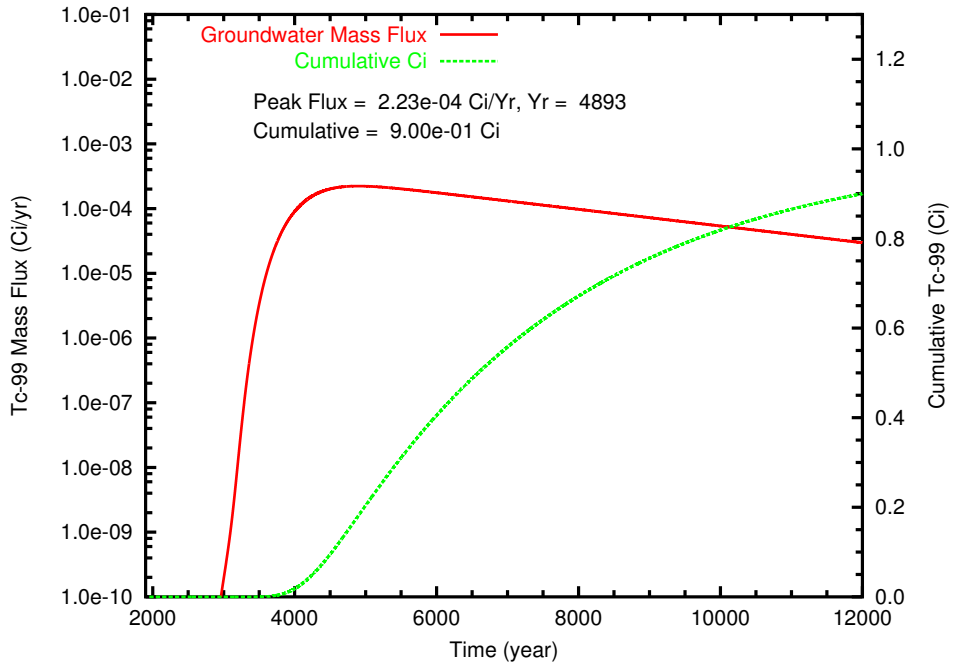

(b)

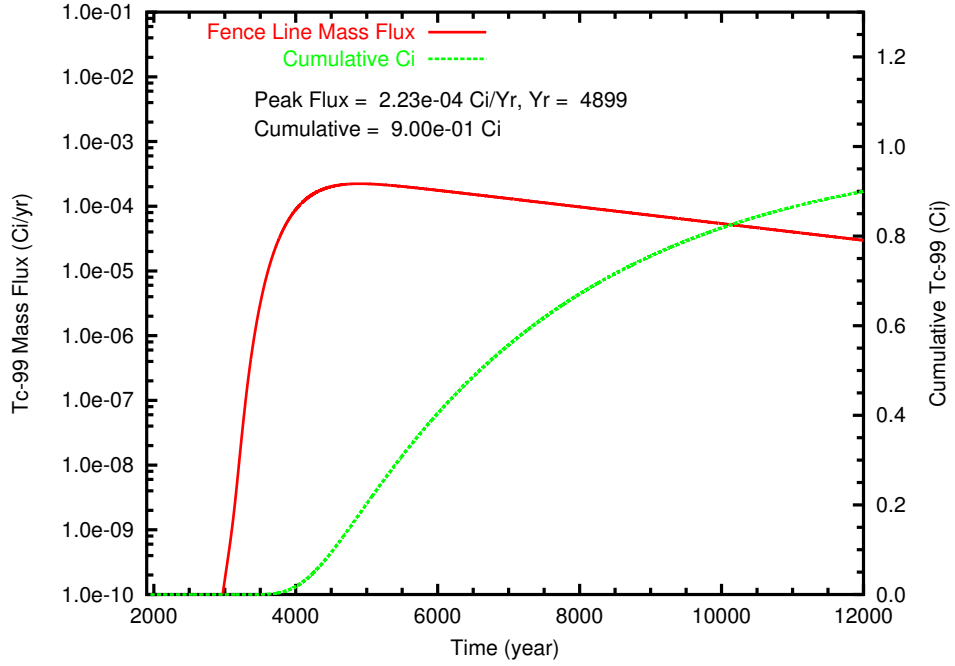

Figure B.37. Case 5, Tc-99 mass flux and cumulative mass at (a) the groundwater table and (b) the fence line

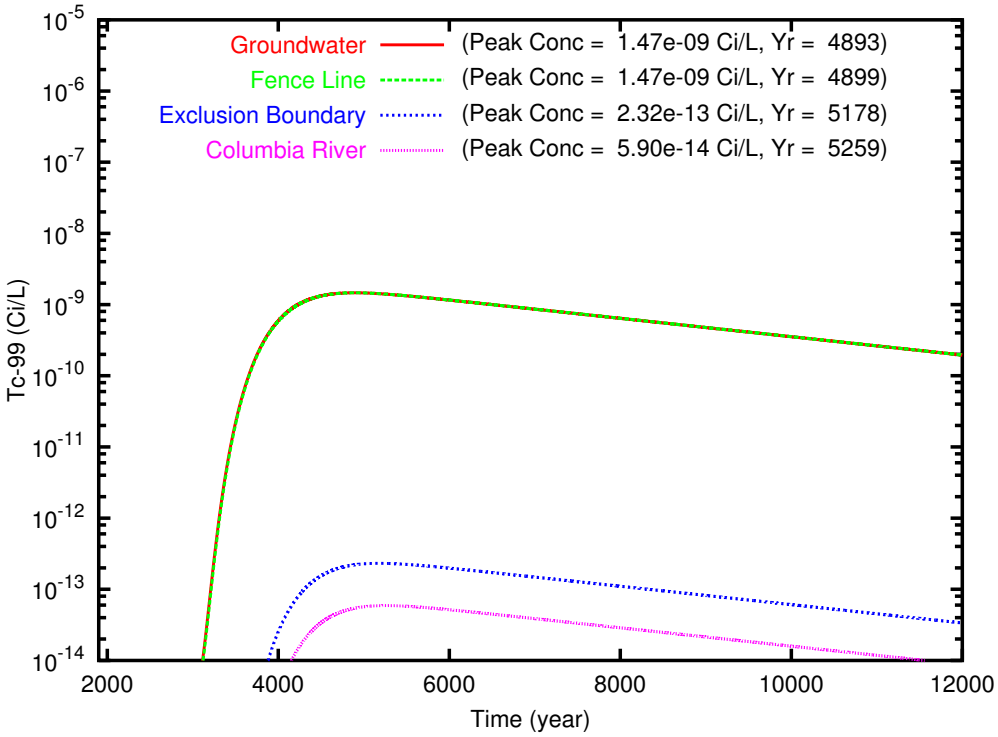

Figure B.38. Case 5, Tc-99 concentration versus time at the groundwater table and the fence line, exclusion boundary, and Columbia River compliance points

(a)

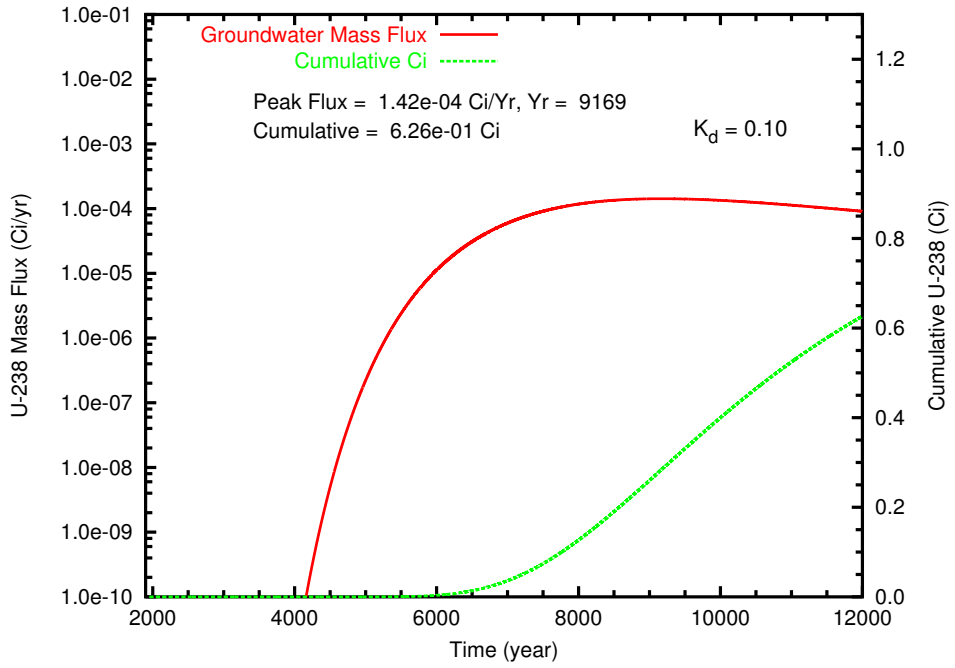

(b)

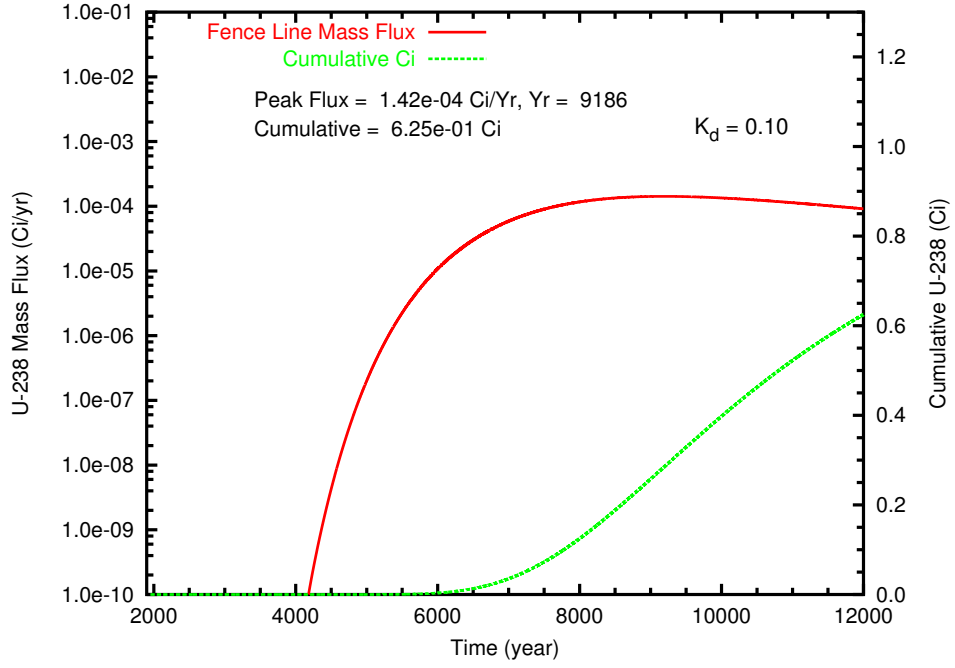

Figure B.39. Case 5, U-238 (K_d = 0.10) mass flux (Ci/L) and cumulative mass (Ci) at (a) the groundwater table and (b) the fence line

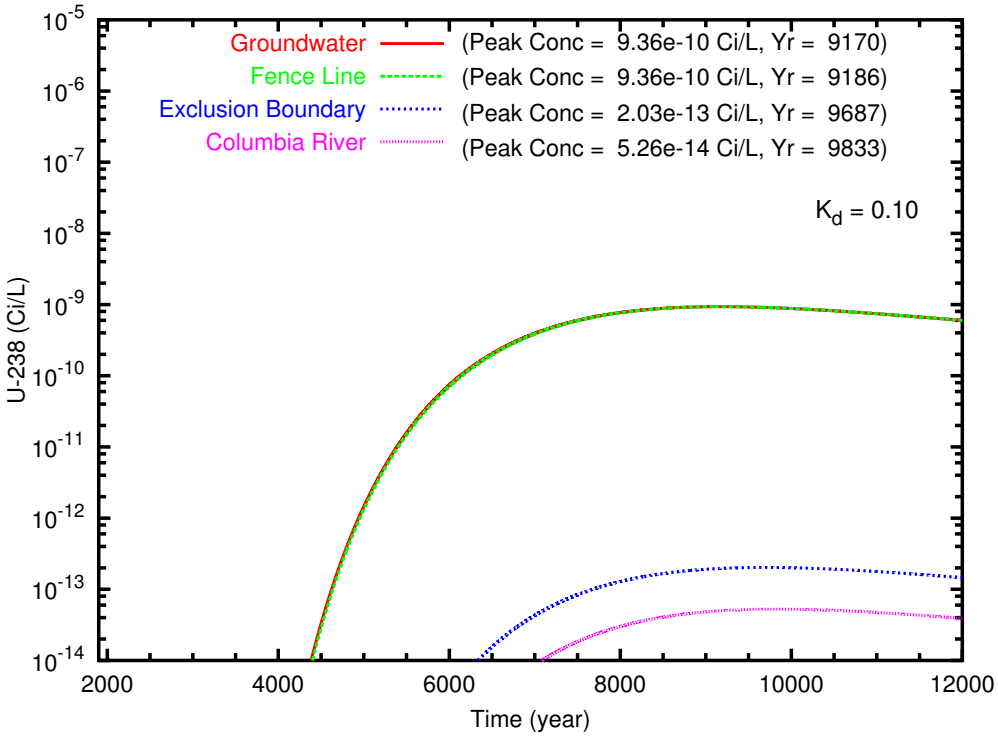

Figure B.40. Case 5, U-238 (K_d = 0.10) concentration versus time at the groundwater table and the fence line, exclusion boundary, and Columbia River compliance points

(a)

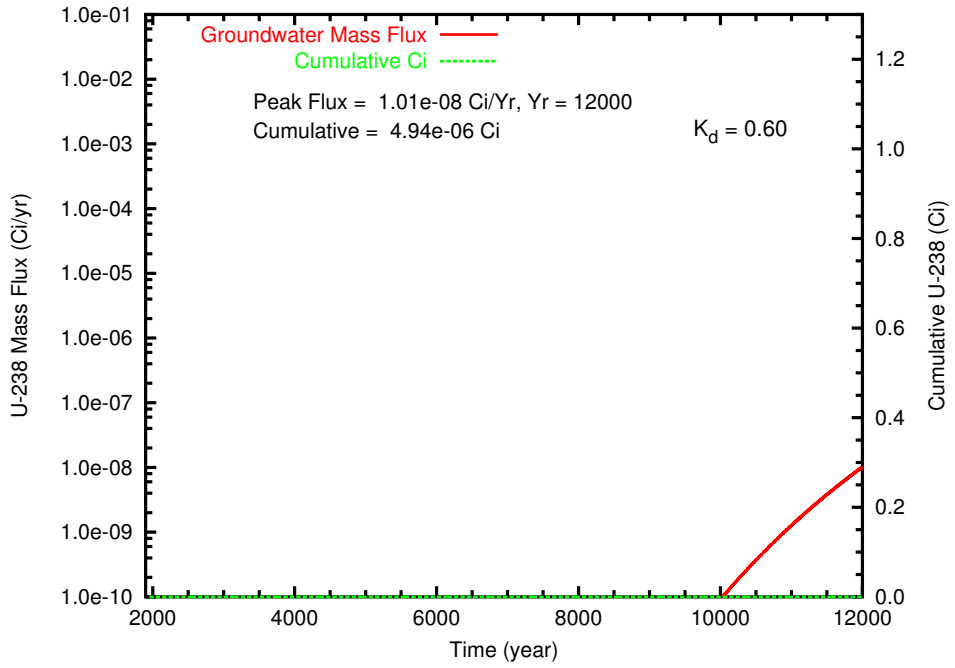

(b)

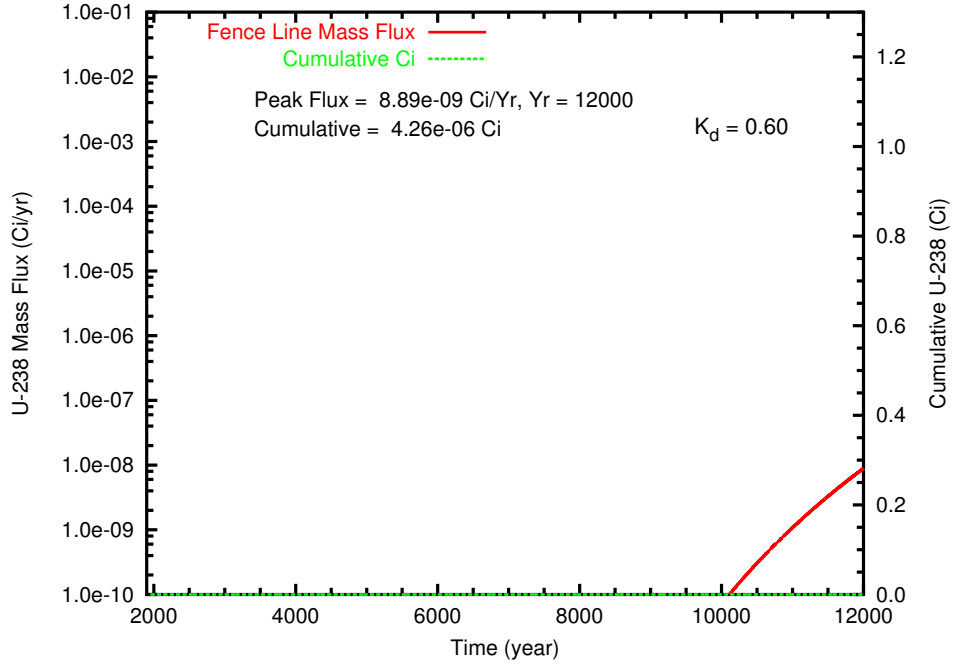

Figure B.41. Case 5, U-238 (K_d = 0.60) mass flux (Ci/L) and cumulative mass (Ci) at (a) the groundwater table and (b) the fence line

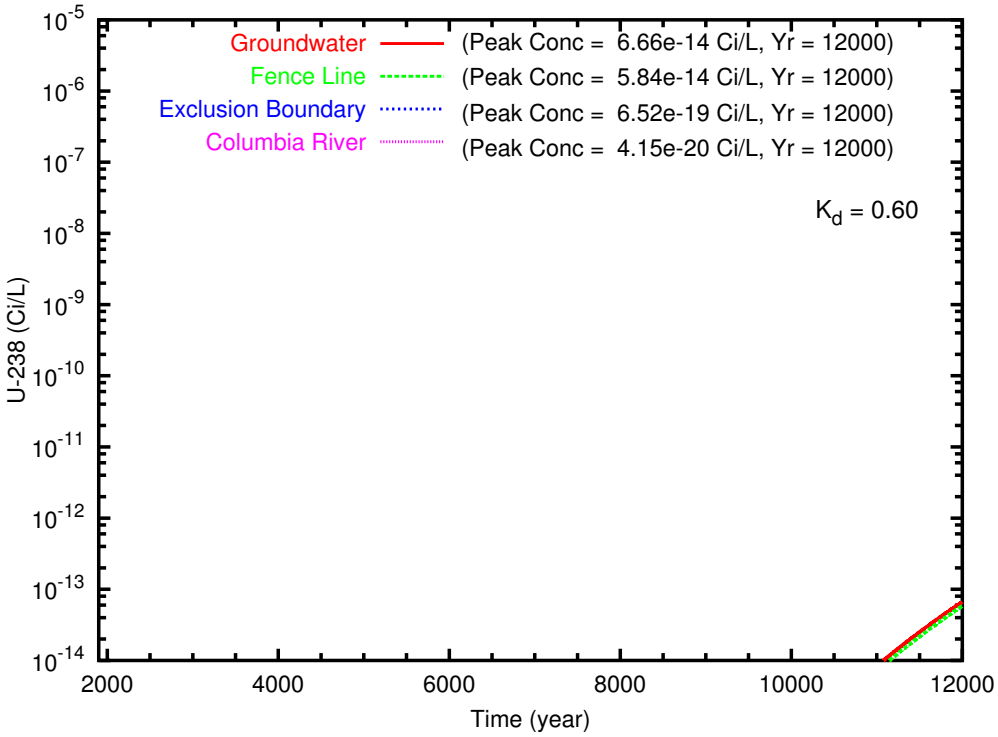

Figure B.42. Case 5, U-238 (K_d = 0.60) concentration versus time at the groundwater table and the fence line, exclusion boundary, and Columbia River compliance points

(a)

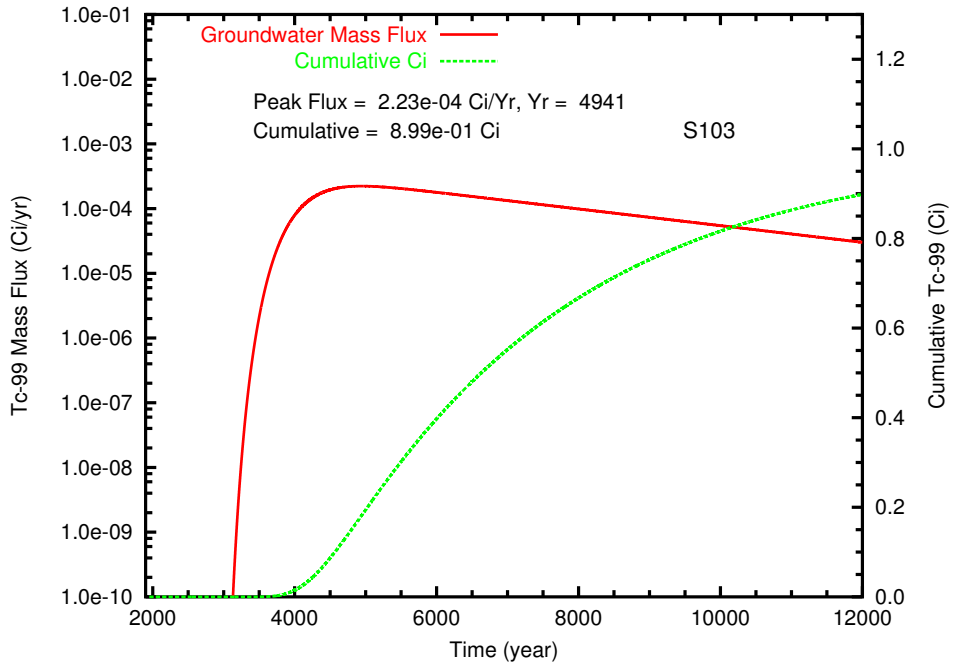

(b)

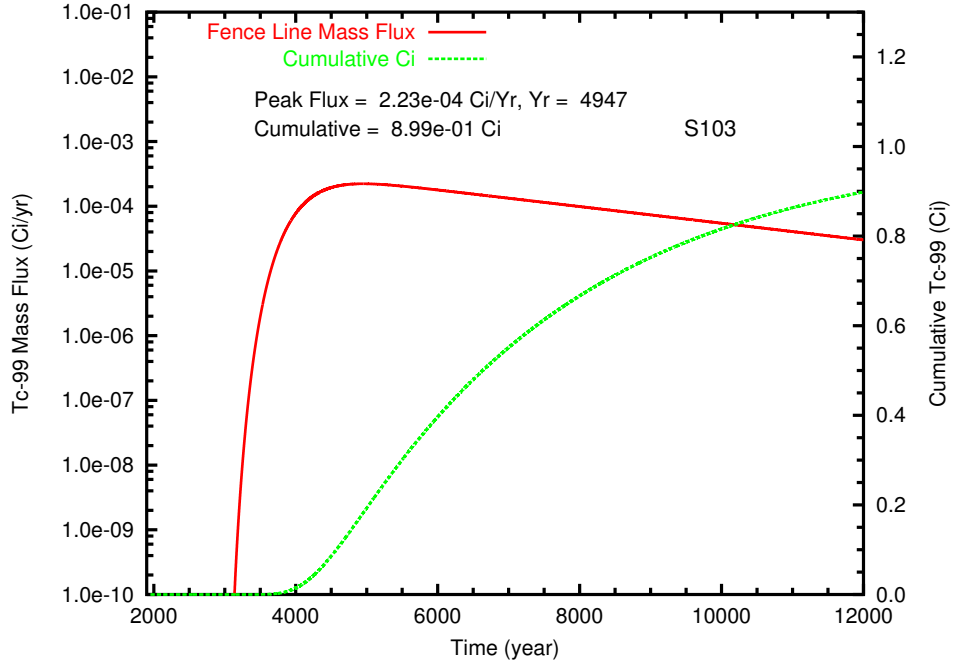

Figure B.43. Case 5v, Mass flux and cumulative mass of Tc-99 from Tank S-103 at (a) the groundwater table and (b) the fence line

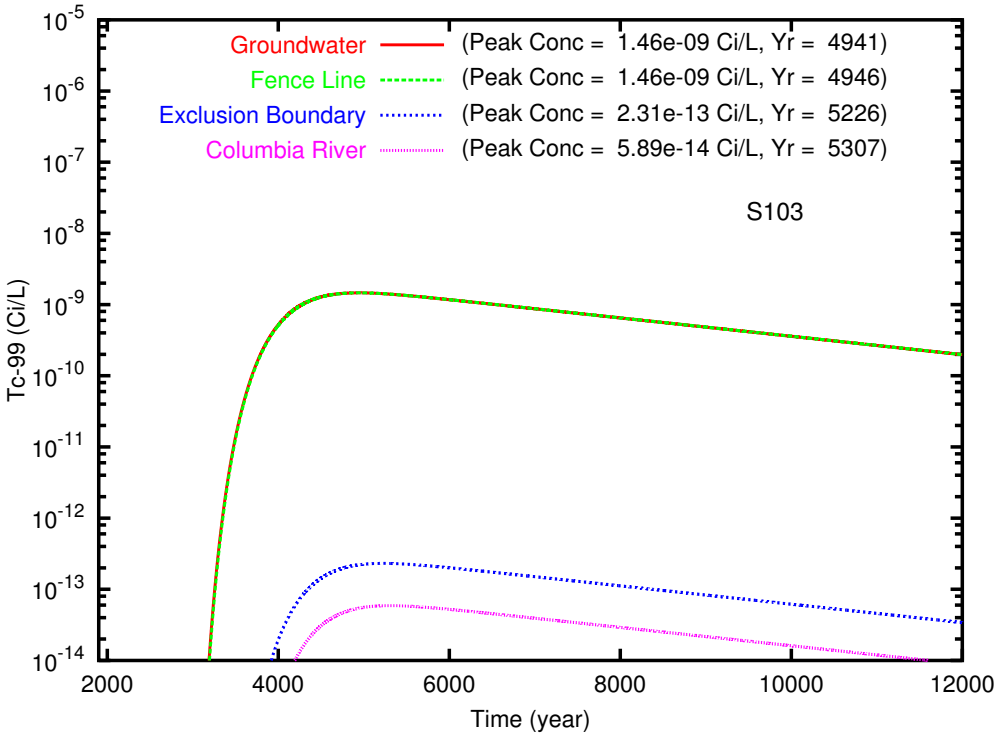

Figure B.44. Case 5v, Concentration of Tc-99 from Tank S-103 at the groundwater table and the fence line, exclusion boundary, and Columbia River compliance points

(a)

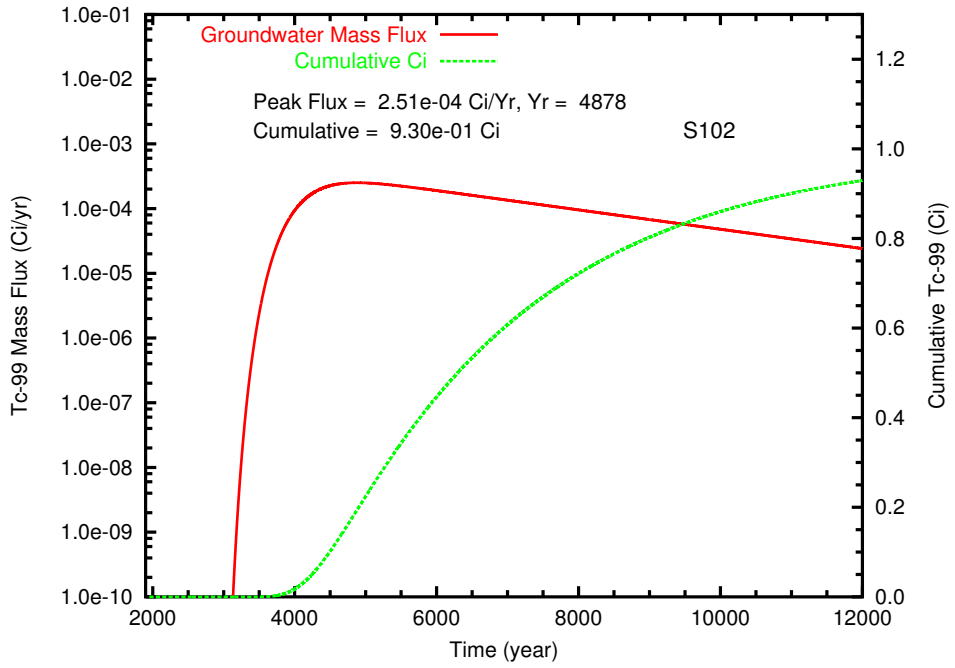

(b)

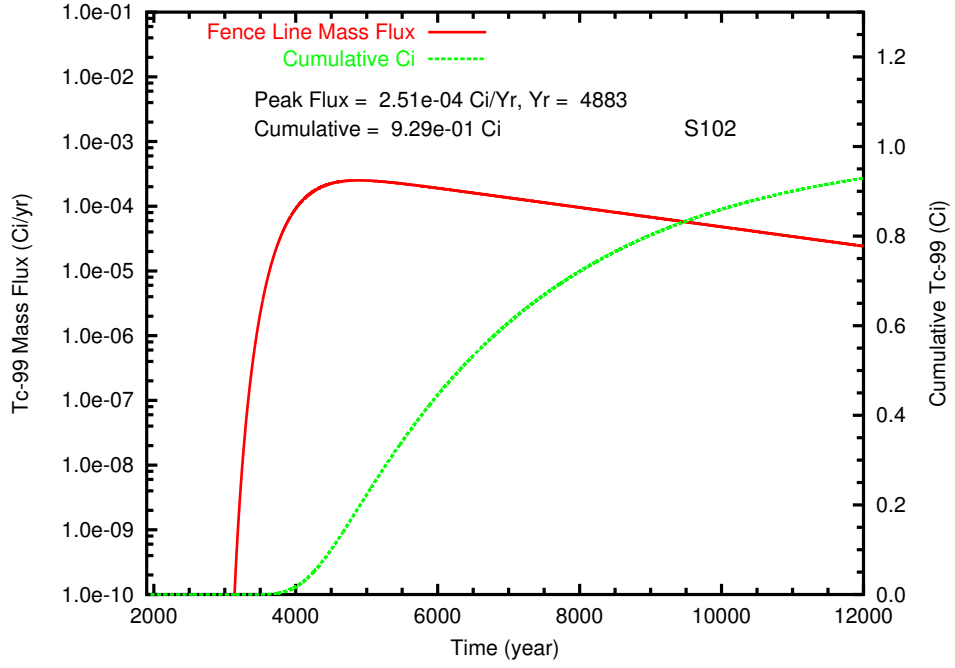

Figure B.45. Case 5v, Mass flux and cumulative mass of Tc-99 from Tank S-102 at (a) the groundwater table and (b) the fence line

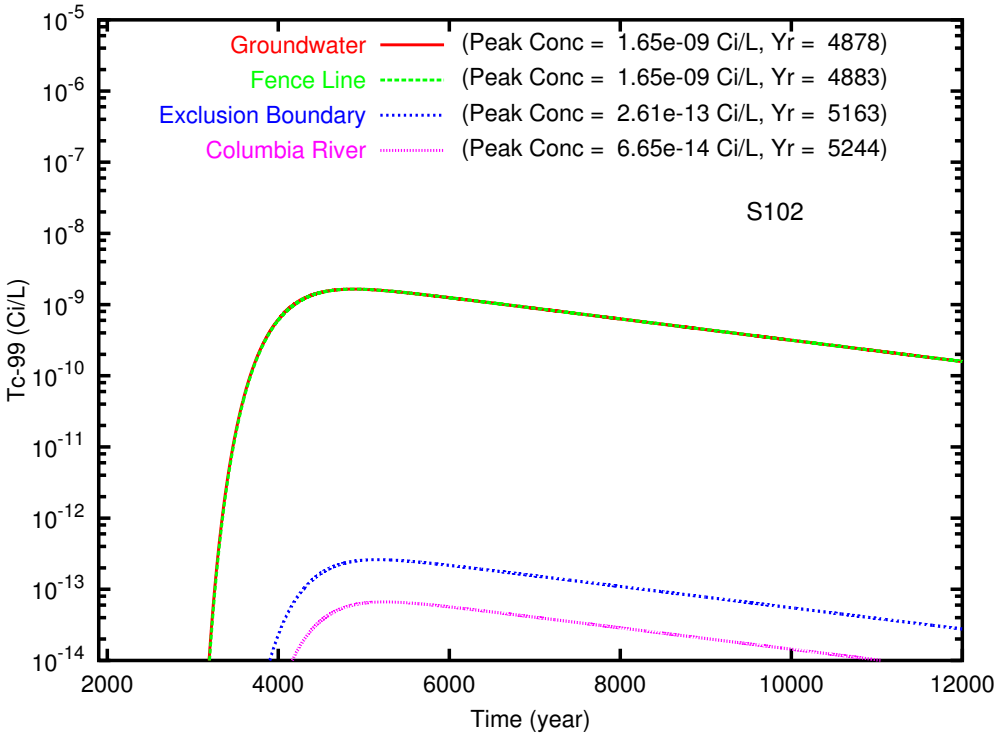

Figure B.46. Case 5v, Concentration of Tc-99 from Tank S-102 at the groundwater table and the fence line, exclusion boundary, and Columbia River compliance points

(a)

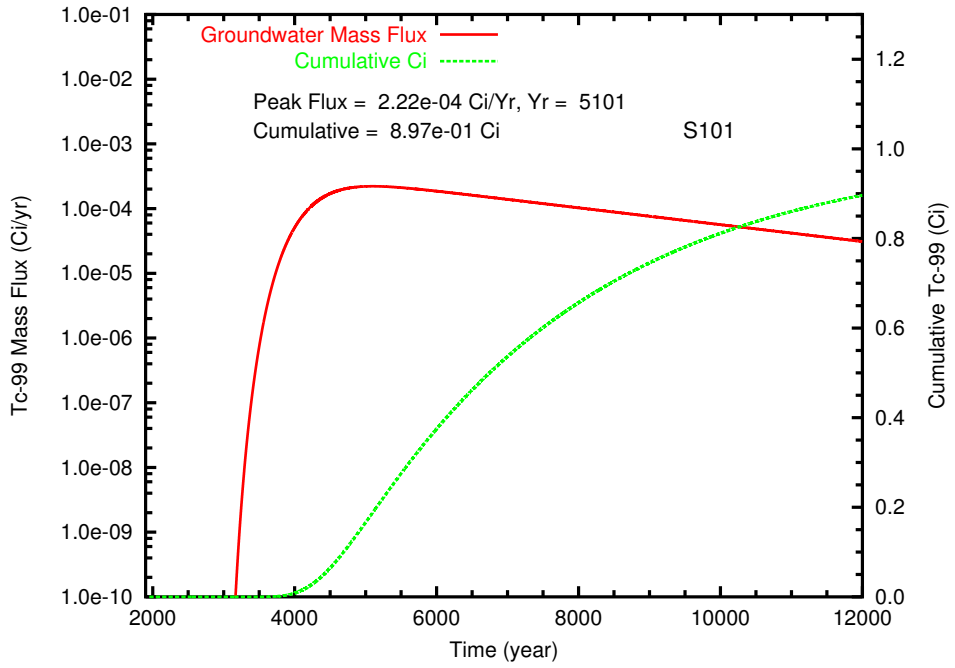

(b)

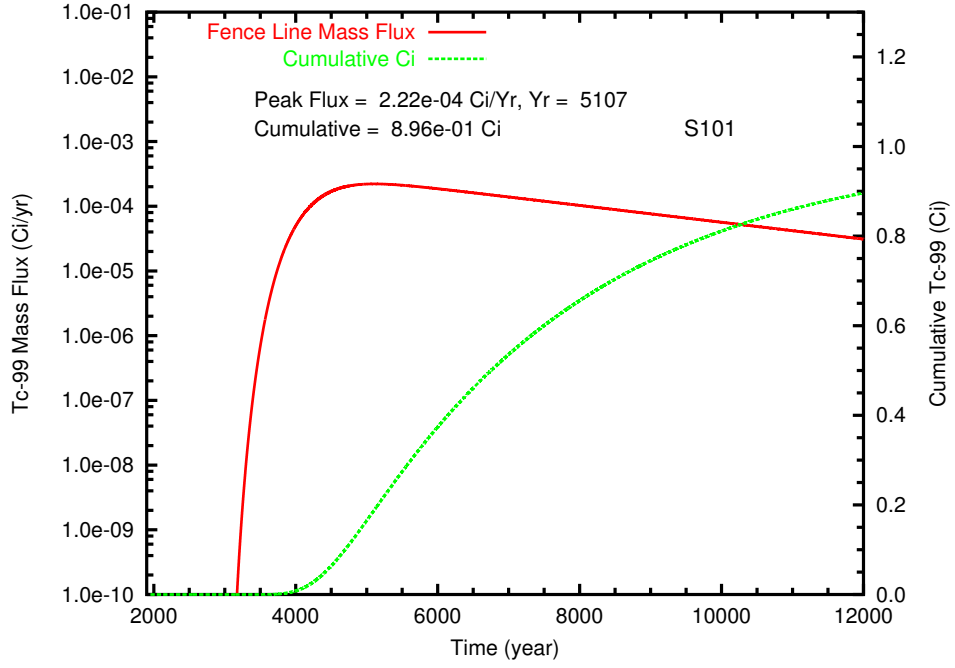

Figure B.47. Case 5v, Mass flux and cumulative mass of Tc-99 from Tank S-101 at (a) the groundwater table and (b) the fence line

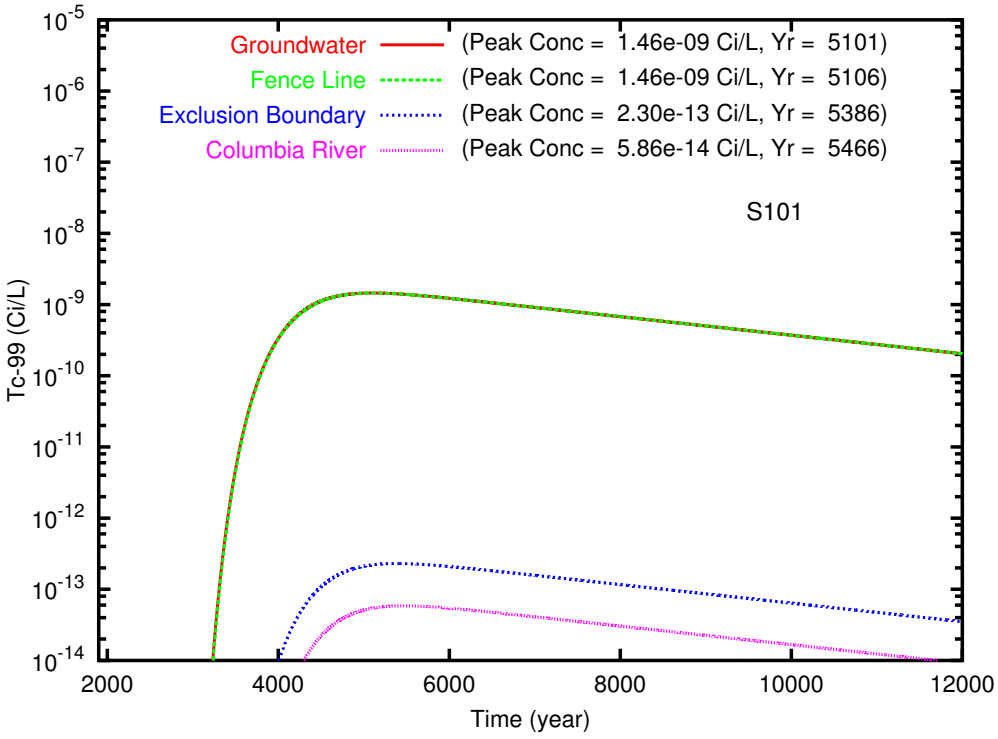

Figure B.48. Case 5v, Concentration of Tc-99 from Tank S-101 at the groundwater table and the fence line, exclusion boundary, and Columbia River compliance points

(a)

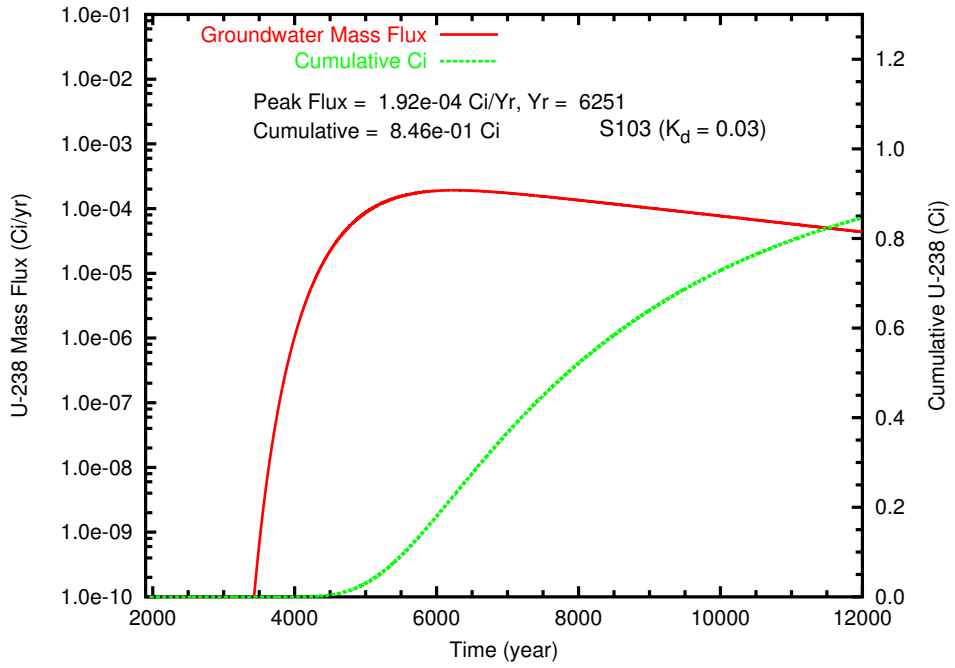

(b)

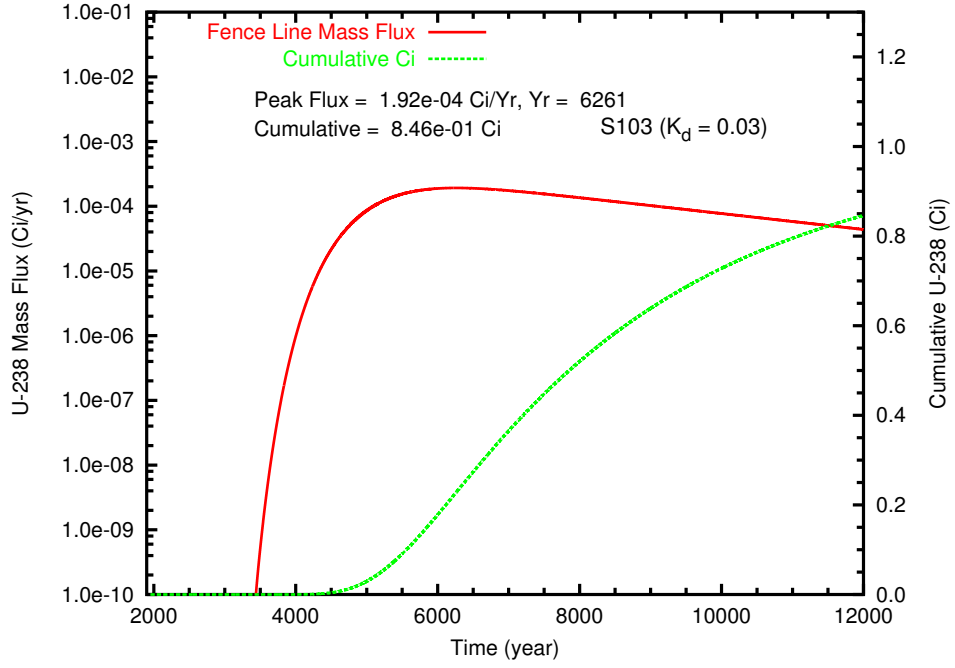

Figure B.49. Case 5v, Mass flux and cumulative mass of U-238 (K_d = 0.03) from Tank S-103 at (a) the groundwater table and (b) the fence line

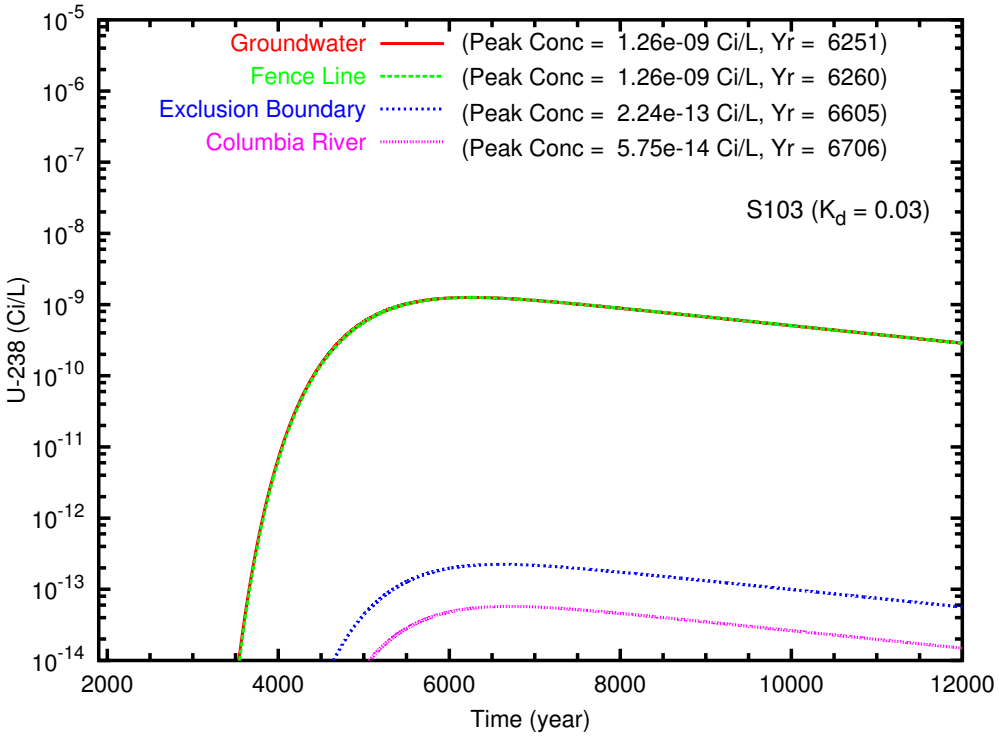

Figure B.50. Case 5v, Concentration of U-238 ($K_d = 0.03$) from Tank S-103 at the groundwater table and the fence line, exclusion boundary, and Columbia River compliance points

(a)

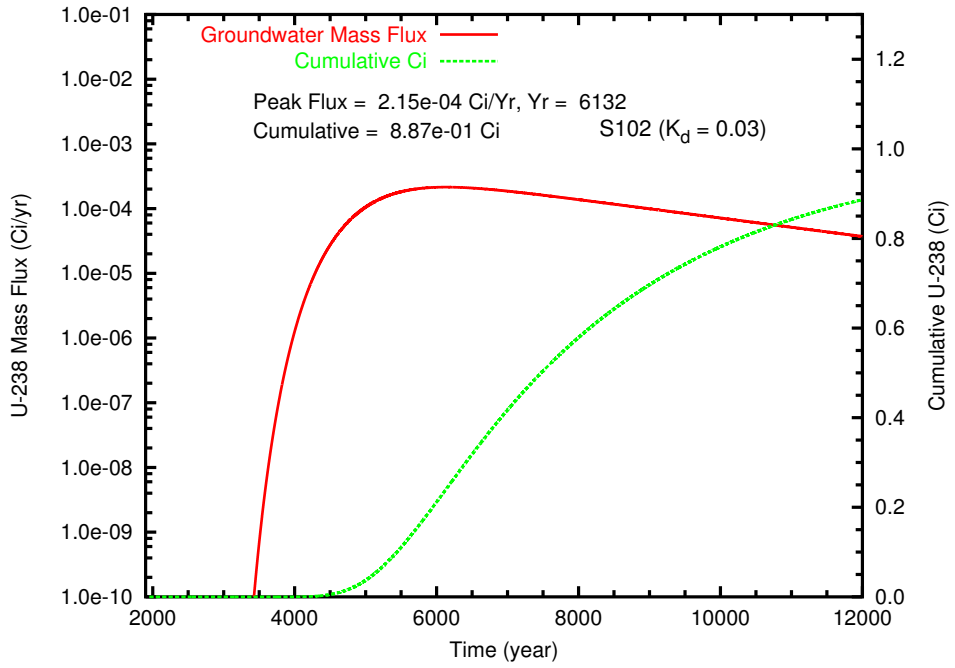

(b)

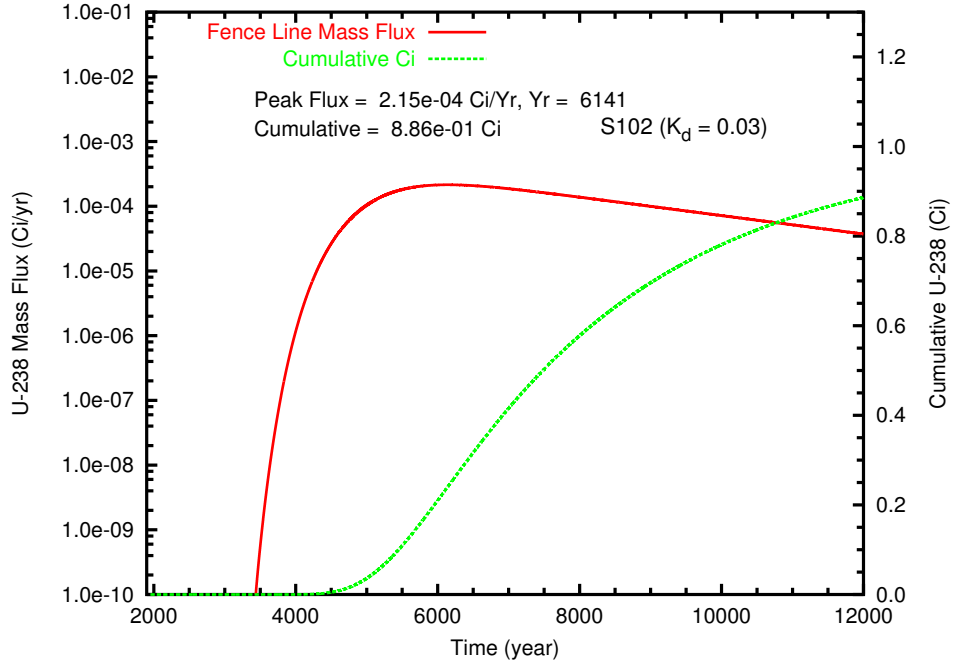

Figure B.51. Case 5v, Mass flux and cumulative mass of U-238 (K_d = 0.03) from Tank S-102 at (a) the groundwater table and (b) the fence line

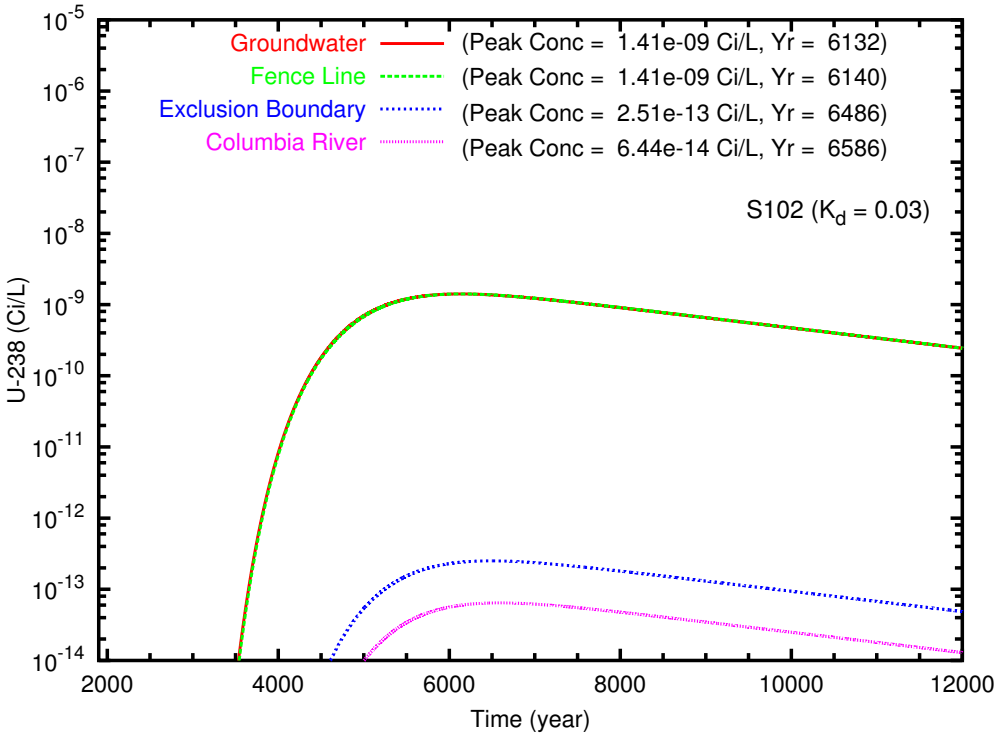

Figure B.52. Case 5v, Concentration of U-238 ($K_d = 0.03$) from Tank S-102 at the groundwater table and the fence line, exclusion boundary, and Columbia River compliance points

(a)

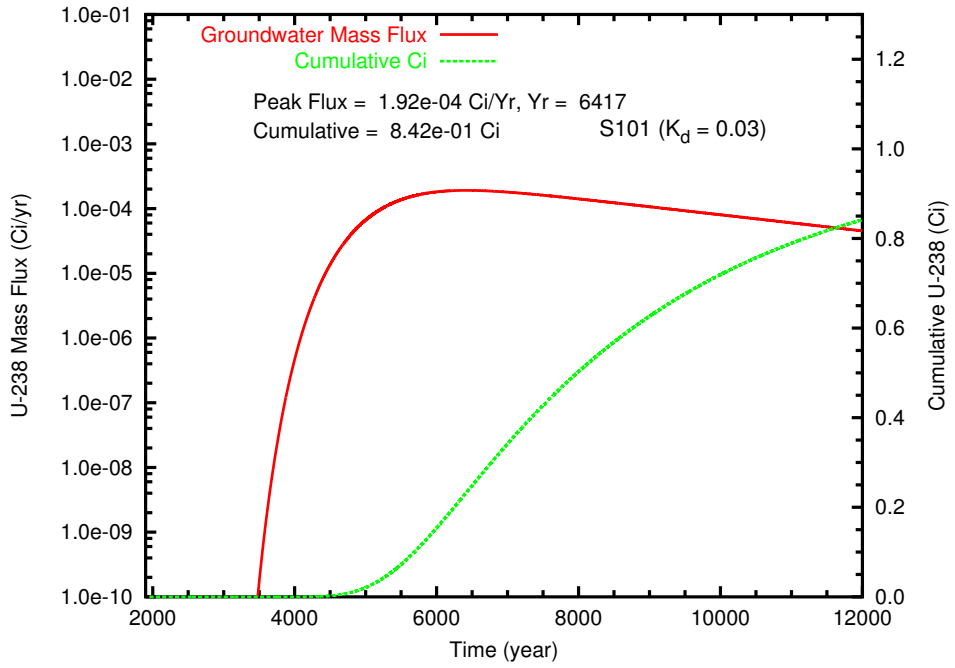

(b)

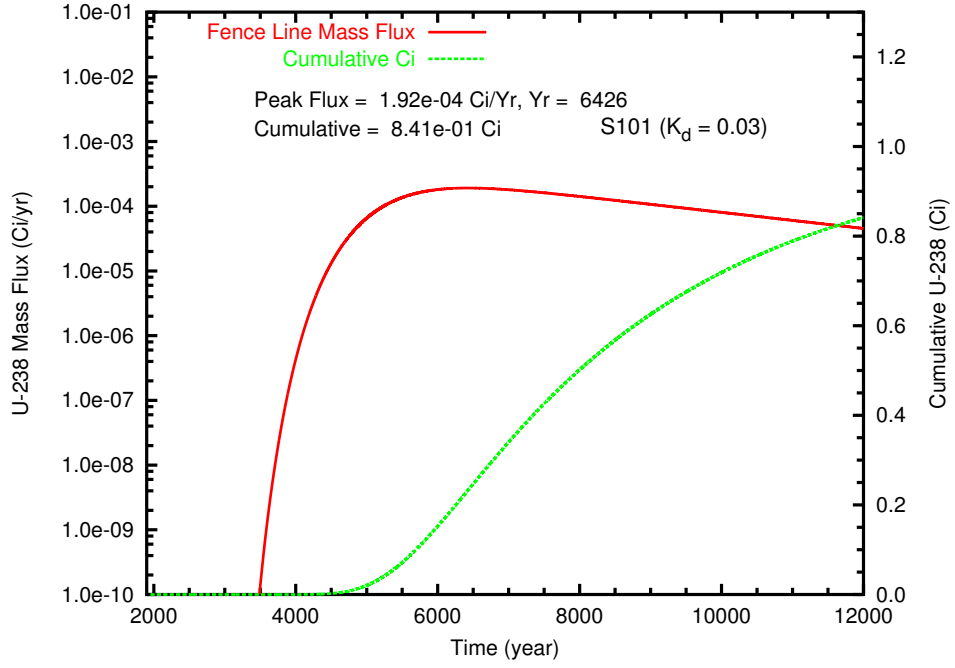

Figure B.53. Case 5v, Mass flux and cumulative mass of U-238 (K_d = 0.03) from Tank S-101 at (a) the groundwater table and (b) the fence line

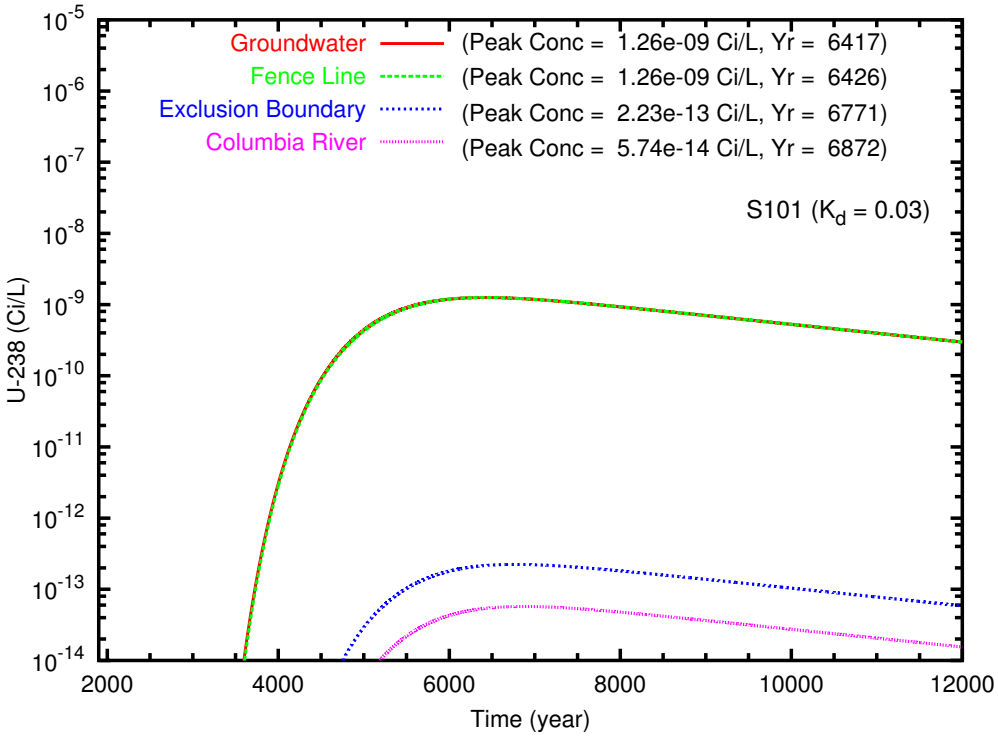

Figure B.54. Case 5v, Concentration of U-238 ($K_d = 0.03$) from Tank S-101 at the groundwater table and the fence line, exclusion boundary, and Columbia River compliance points

(a)

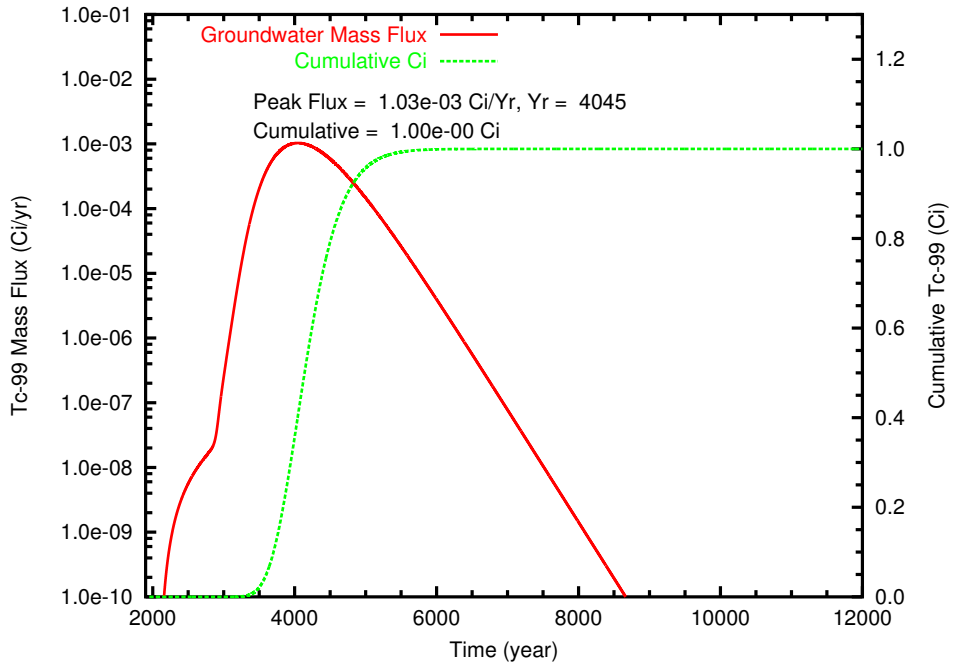

(b)

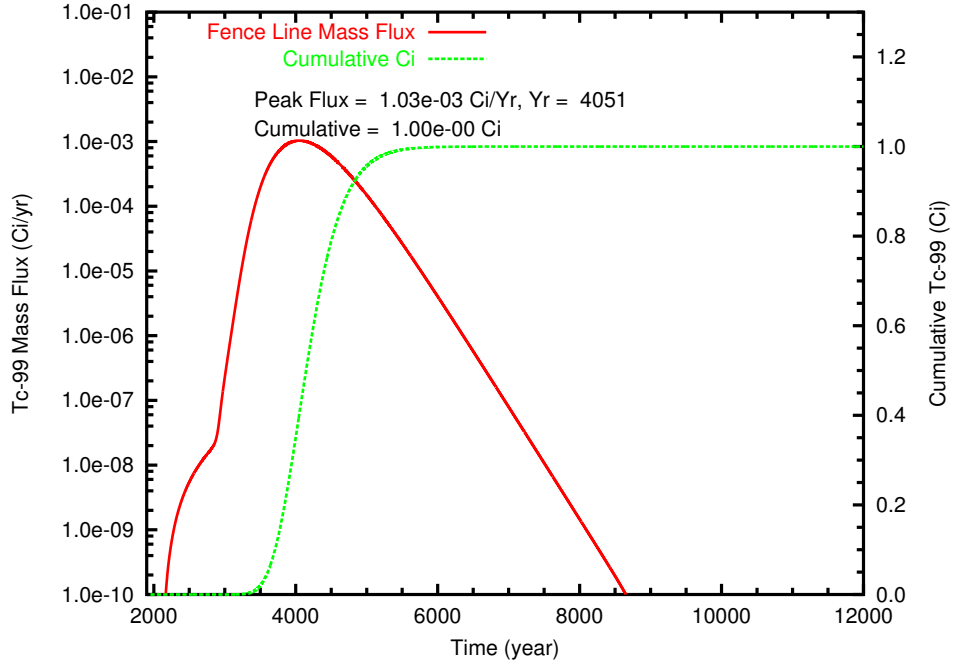

Figure B.55. Case 6, Tc-99 mass flux and cumulative mass at (a) the groundwater table and (b) the fence line

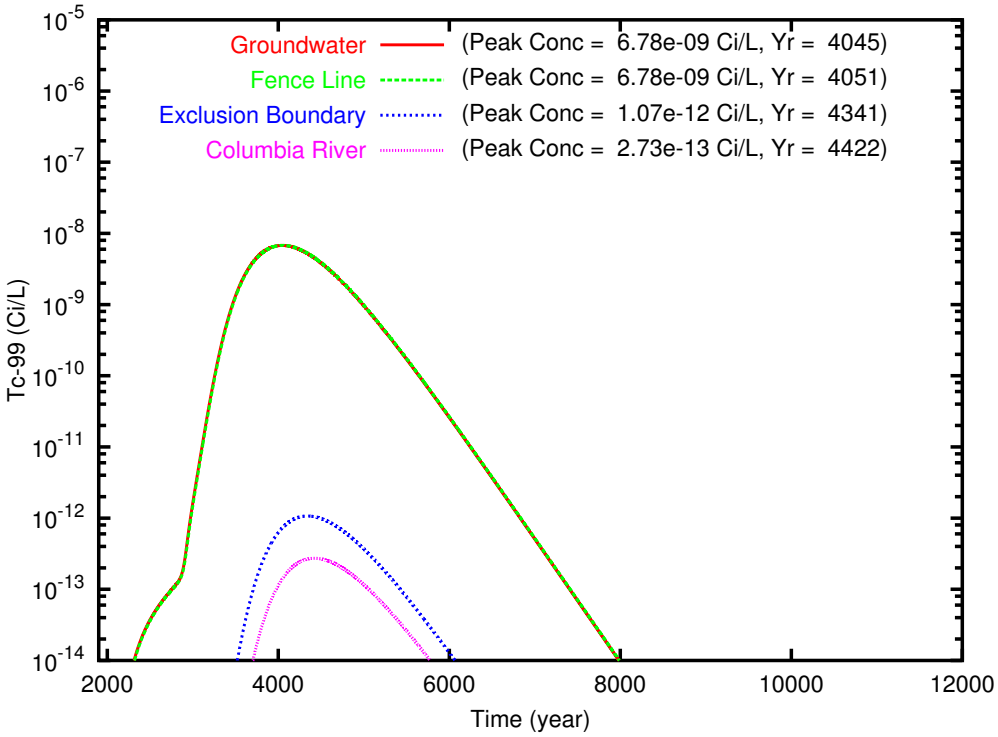

Figure B.56. Case 6, Tc-99 concentration versus time at the groundwater table and the fence line, exclusion boundary, and Columbia River compliance points

(a)

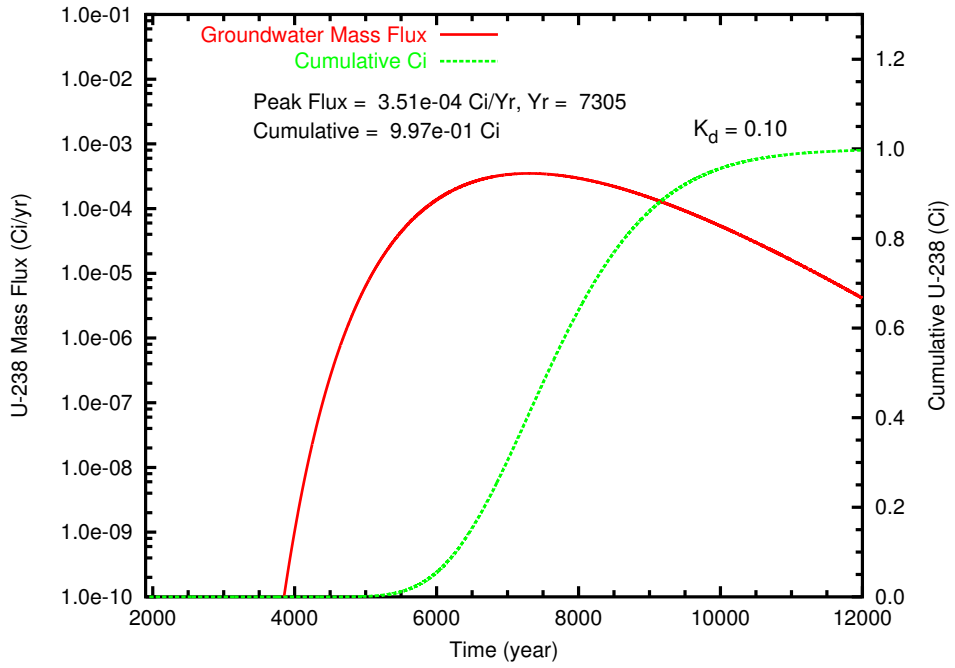

(b)

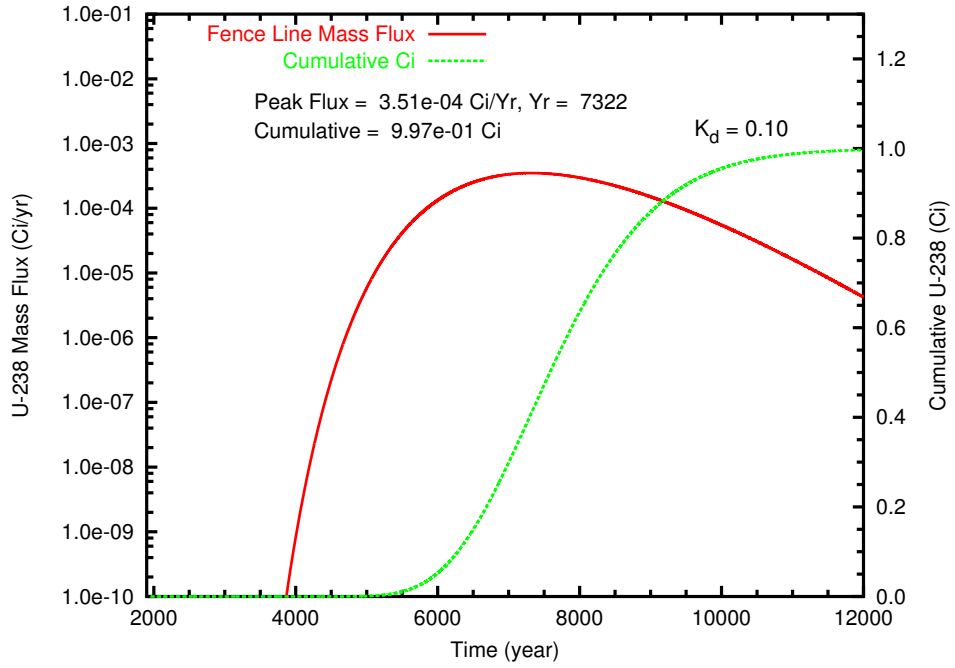

Figure B.57. Case 6, U-238 (K_d = 0.10) mass flux (Ci/L) and cumulative mass (Ci) at (a) the groundwater table and (b) the fence line

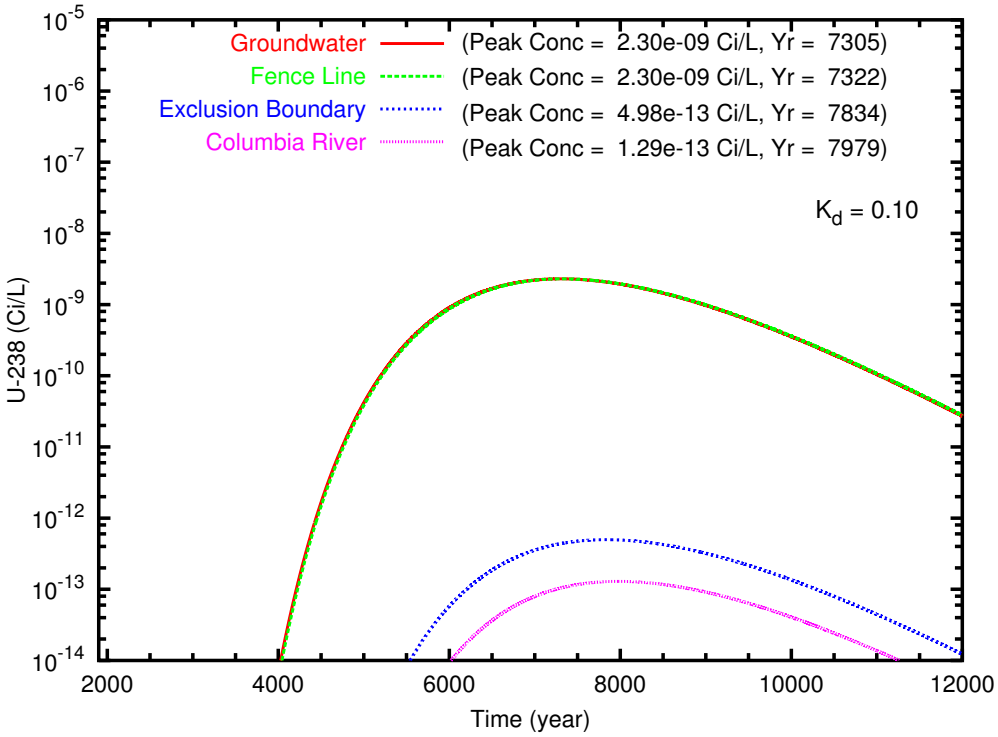

Figure B.58. Case 6, U-238 (K_d = 0.10) concentration versus time at the groundwater table and the fence line, exclusion boundary, and Columbia River compliance points

(a)

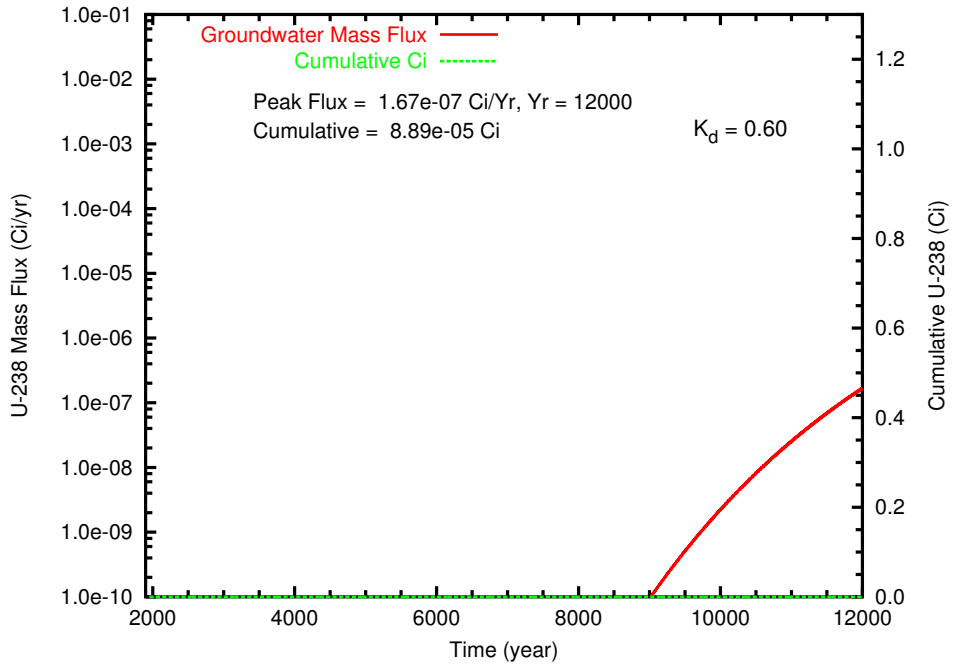

(b)

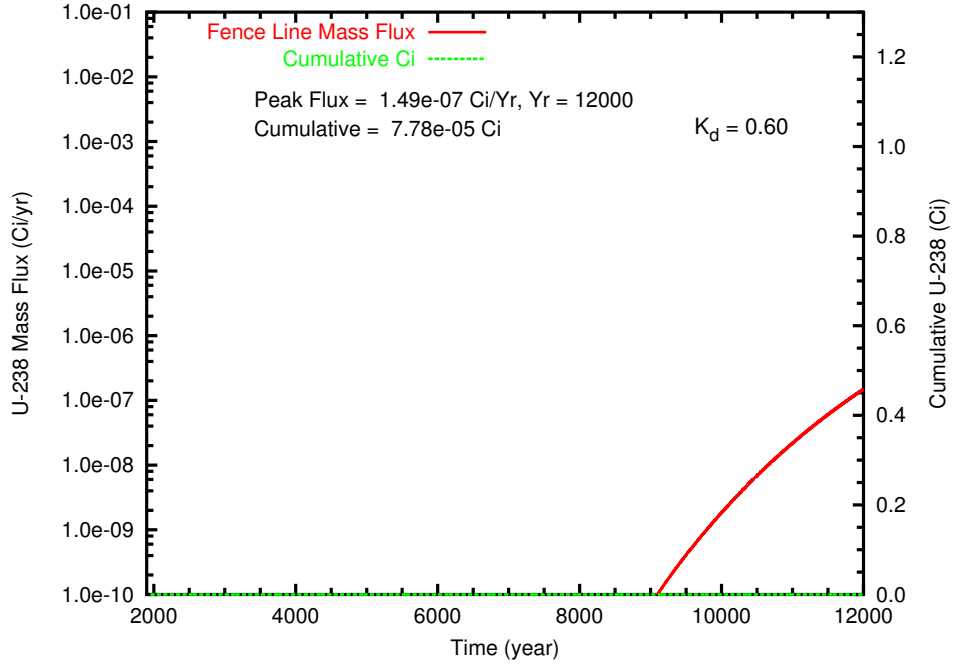

Figure B.59. Case 6, U-238 (K_d = 0.60) mass flux (Ci/L) and cumulative mass (Ci) at (a) the groundwater table and (b) the fence line

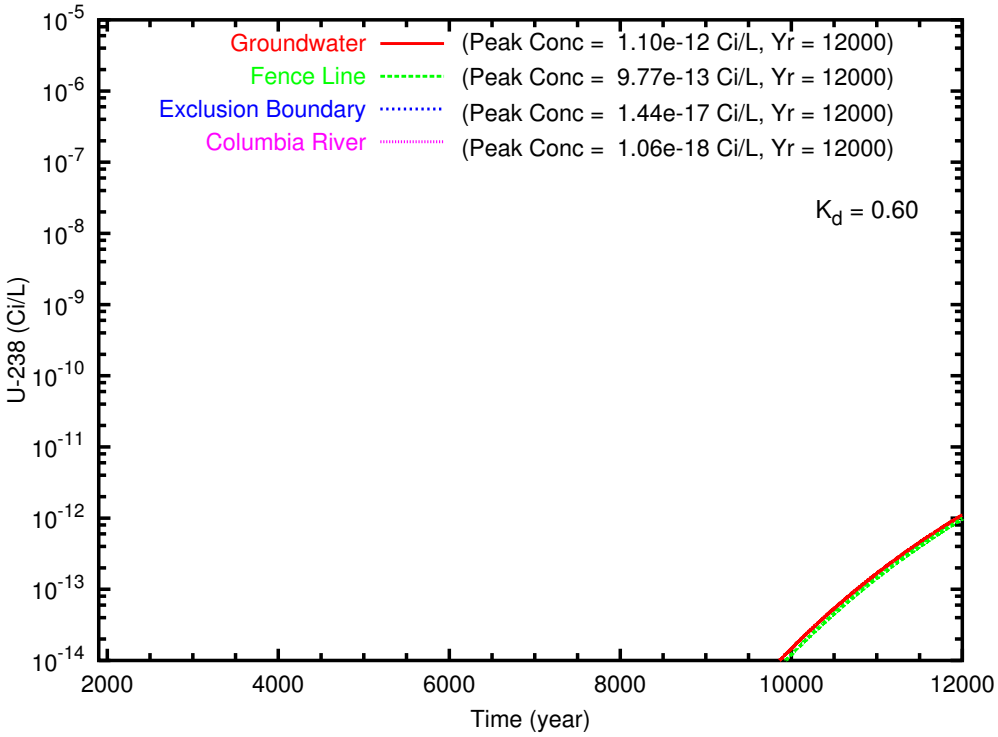

Figure B.60. Case 6, U-238 (K_d = 0.60) concentration versus time at the groundwater table and the fence line, exclusion boundary, and Columbia River compliance points

(a)

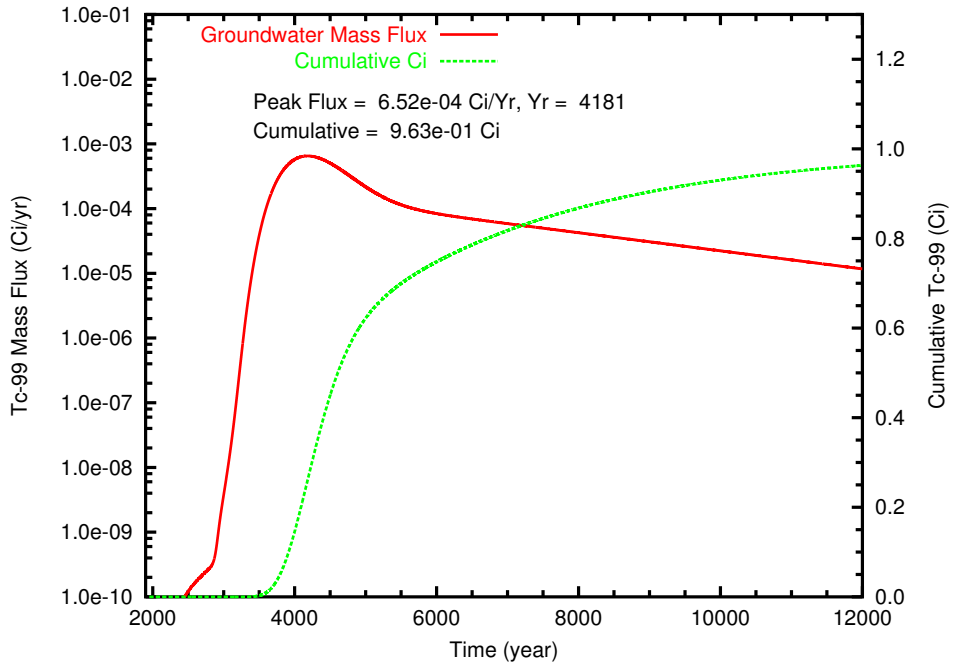

(b)

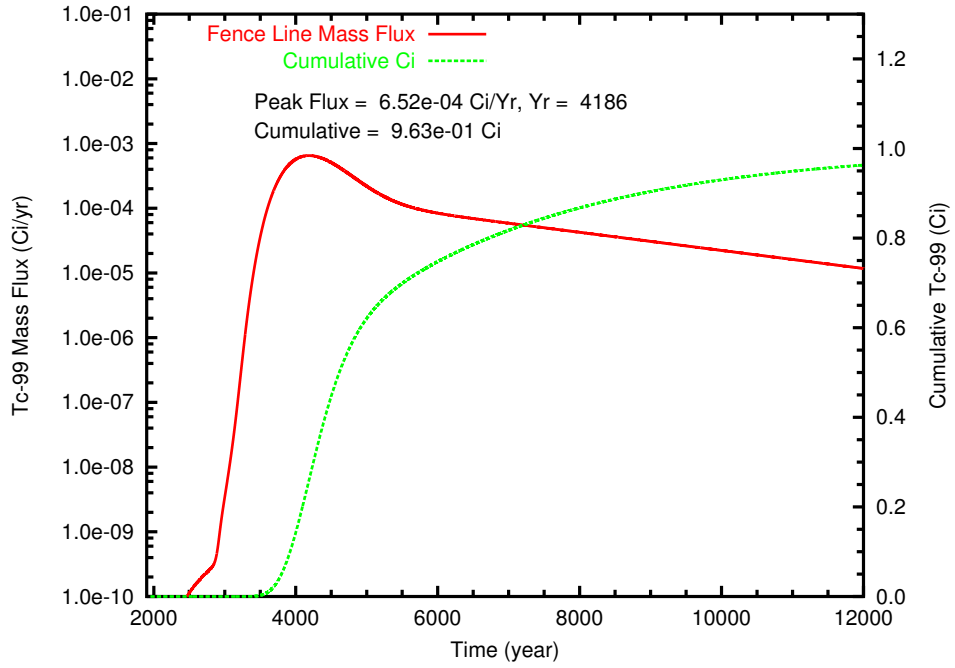

Figure B.61. Case 7, Tc-99 mass flux and cumulative mass at (a) the groundwater table and (b) the fence line

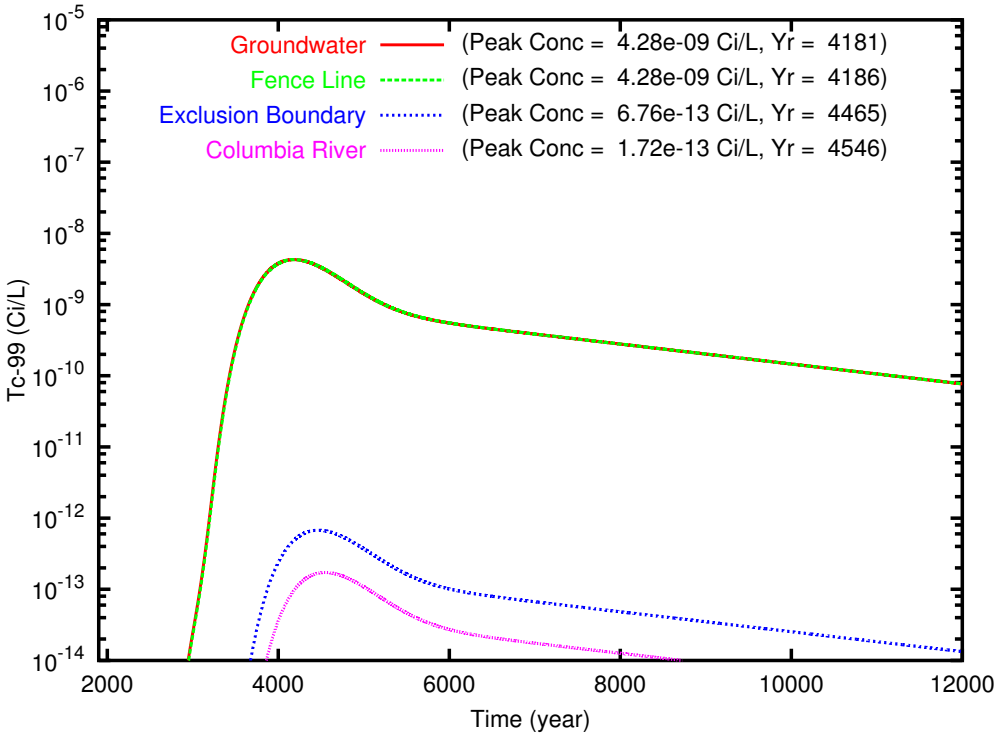

Figure B.62. Case 7, Tc-99 concentration versus time at the groundwater table and the fence line, exclusion boundary, and Columbia River compliance points

(a)

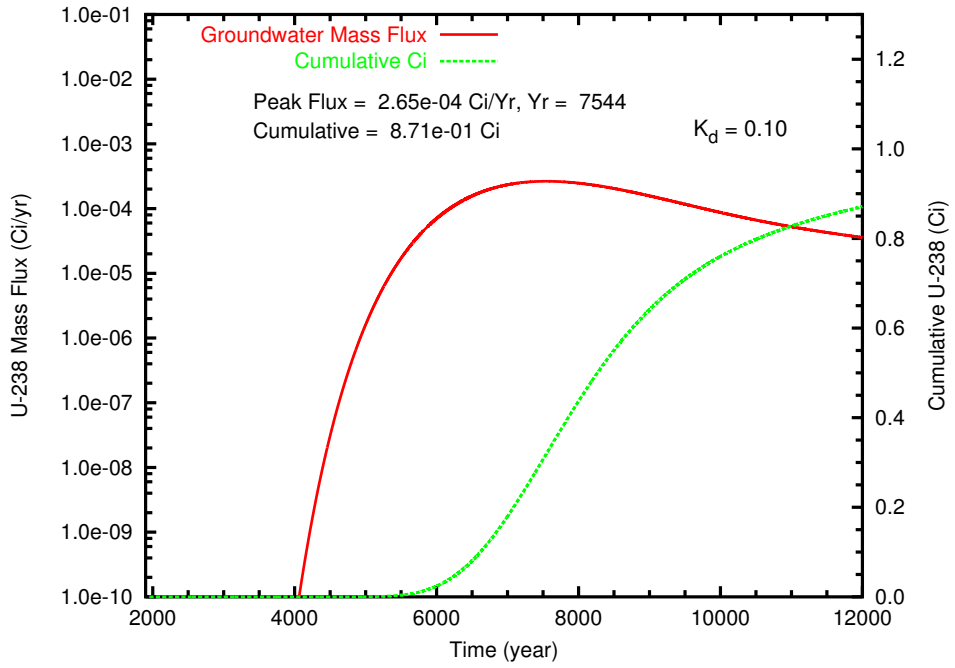

(b)

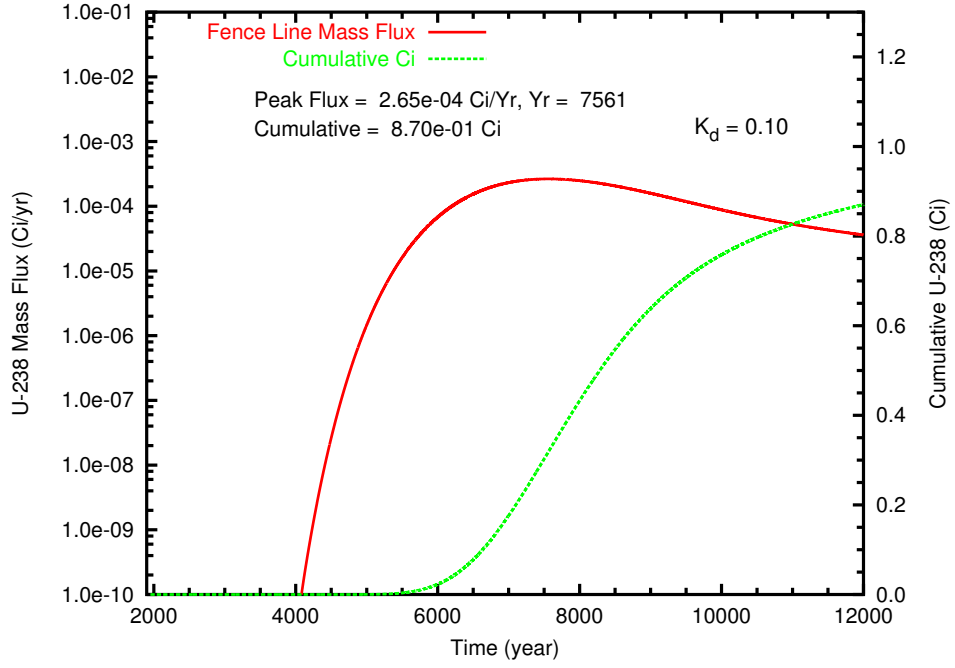

Figure B.63. Case 7, U-238 (K_d = 0.10) mass flux (Ci/L) and cumulative mass (Ci) at (a) the groundwater table and (b) the fence line

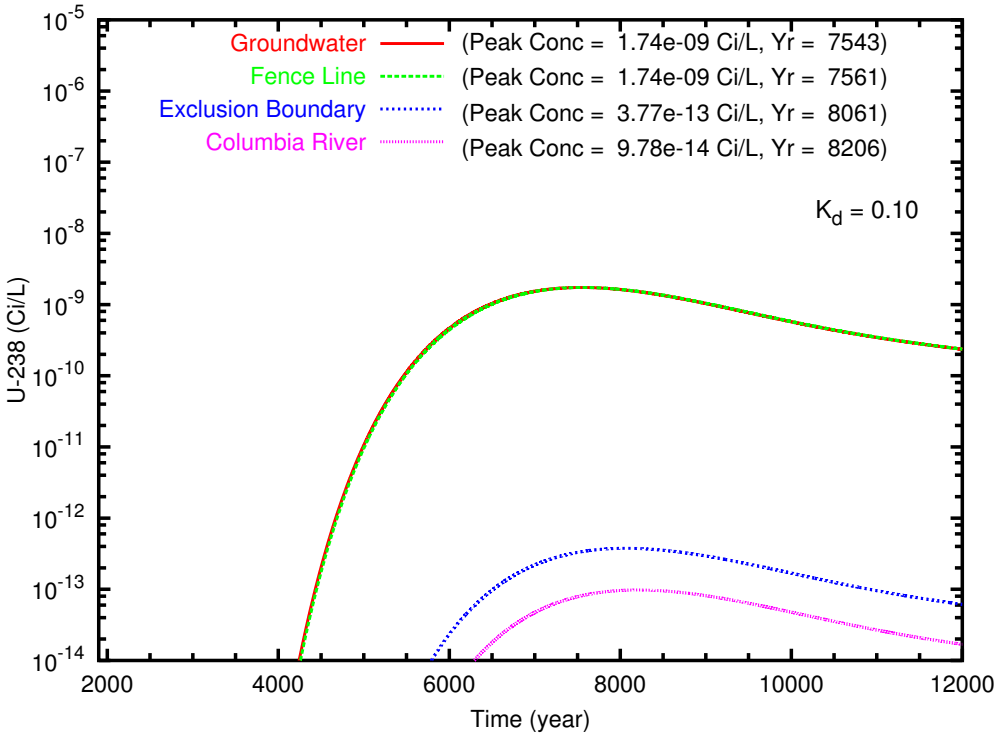

Figure B.64. Case 7, U-238 (K_d = 0.10) concentration versus time at the groundwater table and the fence line, exclusion boundary, and Columbia River compliance points

(a)

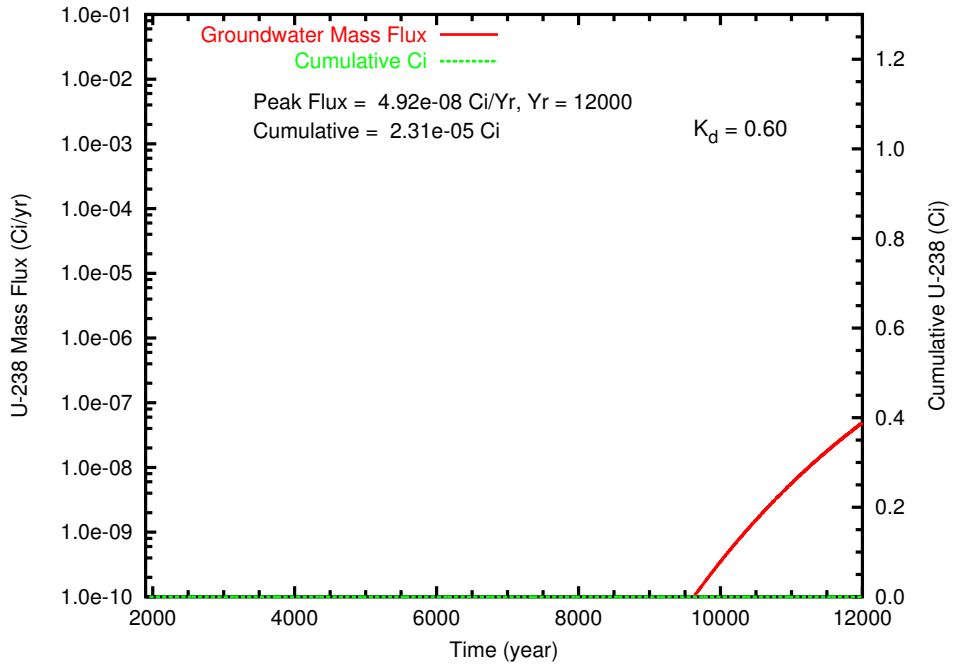

(b)

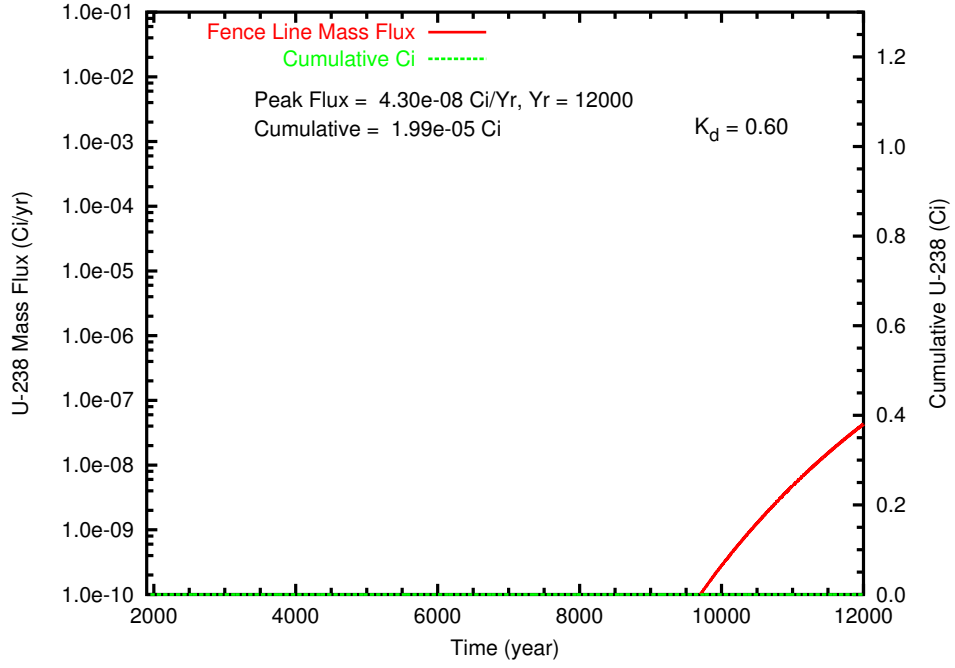

Figure B.65. Case 7, U-238 (K_d = 0.60) mass flux (Ci/L) and cumulative mass (Ci) at (a) the groundwater table and (b) the fence line

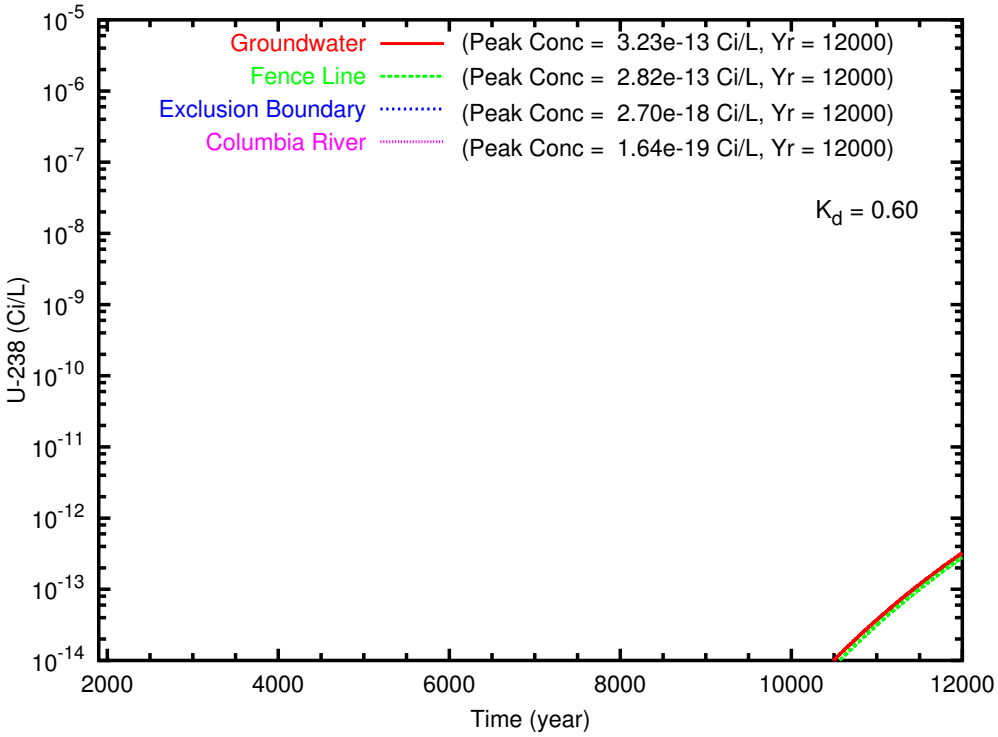

Figure B.66. Case 7, U-238 (K_d = 0.60) concentration versus time at the groundwater table and the fence line, exclusion boundary, and Columbia River compliance points

Distribution

No. of Copies

Onsite

1 Fluor Federal Services

R. Khaleel	E6-17

10 CH2M-HILL Group, Inc.

M. Connelly	E6-35

9 Pacific Northwest National Laboratory

Z.F. Zhang (3)	K9-36
V.L. Freedman	K9-36
S.R. Waichler	K9-36
M.D. White	K9-36
M.P. Bergeron	K9-36
Information Release (2)	K1-06